NUREG/CR-3746, Vol. 1
HEDL-TME 84-20

LWR PRESSURE VESSEL SURVEILLANCE DOSIMETRY IMPROVEMENT PROGRAM

SEMIANNUAL PROGRESS REPORT
OCTOBER 1983 - MARCH 1984

Hanford Engineering Development Laboratory

Prepared by
E.P. Lippincott
W.N. McElroy

Prepared for the U.S. Nuclear Regulatory Commission

NOTICE

This report was prepared as an account of work sponsored by an agency of the United States Government. Neither the United States Government nor any agency thereof, or any of their employees, makes any warranty, expressed or implied, or assumes any legal liability of responsibility for any third party's use, or the results of such use, of any information, apparatus, product or process disclosed in this report, or represents that its use by such third party would not infringe privately owned rights.

NOTICE

Availability of Reference Materials Cited in NRC Publications

Most documents cited in NRC publications will be available from one of the following sources:

1. The NRC Public Document Room, 1717 H Street, N.W.
   Washington, DC 20555
2. The NRC/GPO Sales Program, U.S. Nuclear Regulatory Commission,
   Washington, DC 20555
3. The National Technical Information Service, Springfield, VA 22161

Although the listing that follows represents the majority of documents cited in NRC publications, it is not intended to be exhaustive.

Referenced documents available for inspection and copying for a fee from the NRC Public Document Room include NRC correspondence and internal NRC memoranda; NRC Office of Inspection and Enforcement bulletins, circulars, information notices, inspection and investigation notices; Licensee Event Reports; vendor reports and correspondence; Commission papers; and applicant and licensee documents and correspondence.

The following documents in the NUREG series are available for purchase from the NRC/GPO Sales Program: formal NRC staff and contractor reports, NRC-sponsored conference proceedings, and NRC booklets and brochures. Also available are Regulatory Guides, NRC regulations in the *Code of Federal Regulations*, and *Nuclear Regulatory Commission Issuances*.

Documents available from the National Technical Information Service include NUREG series reports and technical reports prepared by other federal agencies and reports prepared by the Atomic Energy Commission, forerunner agency to the Nuclear Regulatory Commission.

Documents available from public and special technical libraries include all open literature items, such as books, journal and periodical articles, and transactions. *Federal Register* notices, federal and state legislation, and congressional reports can usually be obtained from these libraries.

Documents such as theses, dissertations, foreign reports and translations, and non-NRC conference proceedings are available for purchase from the organization sponsoring the publication cited.

Single copies of NRC draft reports are available free, to the extent of supply, upon written request to the Division of Technical Information and Document Control, U.S. Nuclear Regulatory Commission, Washington, DC 20555.

Copies of industry codes and standards used in a substantive manner in the NRC regulatory process are maintained at the NRC Library, 7920 Norfolk Avenue, Bethesda, Maryland, and are available there for reference use by the public. Codes and standards are usually copyrighted and may be purchased from the originating organization or, if they are American National Standards, from the American National Standards Institute, 1430 Broadway, New York, NY 10018.

GPO Printed copy price: $6.00

NUREG/CR--3746-Vol.1
TI85 003254

LWR PRESSURE VESSEL SURVEILLANCE DOSIMETRY IMPROVEMENT PROGRAM

SEMIANNUAL PROGRESS REPORT OCTOBER 1983 - MARCH 1984

Hanford Engineering Development Laboratory

Operated by Westinghouse Hanford Company
P.O. Box 1970, Richland, WA 99352
A Subsidiary of Westinghouse Electric Corporation

Prepared by
E.P. Lippincott
W.N. McElroy

Manuscript Completed: May 1984
Date Published: November 1984

Prepared for Division of Engineering Technology
Office of Nuclear Regulatory Research
U.S. Nuclear Regulatory Commission
Washington, DC 20555
NRC FIN No. B5988

PREVIOUS REPORTS IN LWR-PV-SDIP SERIES

NUREG/CR-0038	HEDL-TME 78-4	July 1977 - September 1977
NUREG/CR-0127	HEDL-TME 78-5	October 1977 - December 1977
NUREG/CR-0285	HEDL-TME 78-6	January 1978 - March 1978
NUREG/CR-0050	HEDL-TME 78-7	April 1978 - June 1978
NUREG/CR-0551	HEDL-TME 78-8	July 1978 - September 1978
NUREG/CR-0720	HEDL-TME 79-18	October 1978 - December 1978
NUREG/CR-1240, Vol. 1	HEDL-TME 79-41	January 1979 - March 1979
NUREG/CR-1240, Vol. 2	HEDL-TME 80-1	April 1979 - June 1979
NUREG/CR-1240, Vol. 3	HEDL-TME 80-2	July 1979 - September 1979
NUREG/CR-1240, Vol. 4	HEDL-TME 80-3	October 1979 - December 1979
NUREG/CR-1291	HEDL-SA-1949	October 1978 - December 1979*
NUREG/CR-1241, Vol. 1	HEDL-TME 80-4	January 1980 - March 1980
NUREG/CR-1241, Vol. 2	HEDL-TME 80-5	April 1980 - June 1980
NUREG/CR-1747	HEDL-TME 80-73	October 1979 - December 1980*
NUREG/CR-1241, Vol. 3	HEDL-TME 80-6	October 1980 - December 1980
NUREG/CR-2345, Vol. 1	HEDL-TME 81-33	January 1981 - March 1981
NUREG/CR-2345, Vol. 2	HEDL-TME 81-34	April 1981 - June 1981
NUREG/CP-0029	HEDL-SA-2546	October 1980 - September 1981*
NUREG/CR-2345, Vol. 4	HEDL-TME 81-36	October 1981 - December 1981
NUREG/CR-2805, Vol. 1	HEDL-TME 82-18	January 1982 - March 1982
NUREG/CR-2805, Vol. 2	HEDL-TME 82-19	April 1982 - June 1982
NUREG/CR-2805, Vol. 3	HEDL-TME 82-20	October 1981 - September 1982*
NUREG/CR-2805, Vol. 4	HEDL-TME 82-21	October 1982 - December 1982
NUREG/CR-3391, Vol. 1	HEDL-TME 83-21	January 1983 - March 1983
NUREG/CR-3391, Vol. 2	HEDL-TME 83-22	April 1983 - June 1983
NUREG/CR-3391, Vol. 3	HEDL-TME 83-23	October 1982 - September 1983*
NUREG/CR-3391, Vol. 4	**	October 1983 - December 1983

---

*Annual Reports.

**No HEDL-TME number assigned because this progress report contains only an NBS contribution on "Compendium of Benchmark Neutron Fields for Pressure Vessel Surveillance Dosimetry."

FOREWORD

The Light Water Reactor Pressure Vessel Surveillance Dosimetry Improvement Program (LWR-PV-SDIP) has been established by NRC to improve, test, verify, and standardize the physics-dosimetry-metallurgy, damage correlation, and associated reactor analysis methods, procedures and data used to predict the integrated effect of neutron exposure to LWR pressure vessels and their support structures. A vigorous research effort attacking the same measurement and analysis problems exists worldwide, and strong cooperative links between the US NRC-supported activities at HEDL, ORNL, NBS, and MEA-ENSA and those supported by CEN/SCK (Mol, Belgium), EPRI (Palo Alto, USA), KFA (Jülich, Germany), and several UK laboratories have been extended to a number of other countries and laboratories. These cooperative links are strengthened by the active membership of the scientific staff from many participating countries and laboratories in the ASTM E10 Committee on Nuclear Technology and Applications. Several subcommittees of ASTM E10 are responsible for the preparation of LWR surveillance standards.

The primary objective of this multilaboratory program is to prepare an updated and improved set of physics-dosimetry-metallurgy, damage correlation, and associated reactor analysis ASTM standards for LWR pressure vessel and support structure irradiation surveillance programs. Supporting this objective are a series of analytical and experimental validation and calibration studies in "Standard, Reference, and Controlled Environment Benchmark Fields," research reactor "Test Regions," and operating power reactor "Surveillance Positions."

These studies will establish and certify the precision and accuracy of the measurement and predictive methods recommended in the ASTM Standards and used for the assessment and control of the present and end-of-life (EOL) condition of pressure vessel and support structure steels. Consistent and accurate measurement and data analysis techniques and methods, therefore, will be developed, tested and verified along with guidelines for required neutron field calculations used to correlate changes in material properties with the characteristics of the neutron radiation field. Application of established ASTM standards is expected to permit the reporting of measured materials property changes and neutron exposures to an accuracy and precision within bounds of 10 to 30%, depending on the measured metallurgical variable and neutron environment.

The assessment of the radiation-induced degradation of material properties in a power reactor requires accurate definition of the neutron field from the outer region of the reactor core to the outer boundaries of the pressure vessel. The accuracy of measurements on neutron flux and spectrum is associated with two distinct components of LWR irradiation surveillance procedures: 1) proper application of calculational estimates of the neutron exposure at in- and ex-vessel surveillance positions, various locations in the vessel wall and ex-vessel support structures, and 2) understanding the relationship between material property changes in reactor vessels and their support structures, and in metallurgical test specimens irradiated in test reactors and at accelerated neutron flux positions in operating power reactors.

The first component requires verification and calibration experiments in a variety of neutron irradiation test facilities including LWR-PV mockups, power reactor surveillance positions, and related benchmark neutron fields. The benchmarks serve as a permanent reference measurement for neutron flux and fluence detection techniques, which are continually under development and widely applied by laboratories with different levels of capability. The second component requires a serious extrapolation of an observed neutron-induced mechanical property change from research reactor "Test Regions" and operating power reactor "Surveillance Positions" to locations inside the body of the pressure vessel wall and to ex-vessel support structures. The neutron flux at the vessel inner wall is up to one order of magnitude lower than at surveillance specimen positions and up to two orders of magnitude lower than for test reactor positions. At the vessel outer wall, the neutron flux is one order of magnitude or more lower than at the vessel inner wall. Further, the neutron spectrum at, within, and leaving the vessel is substantially different.

To meet reactor pressure vessel radiation monitoring requirements, a variety of neutron flux and fluence detectors are employed, most of which are passive. Each detector must be validated for application to the higher flux and harder neutron spectrum of the research reactor "Test Region" and to the lower flux and degraded neutron spectrum at "Surveillance Positions." Required detectors must respond to neutrons of various energies so that multigroup spectra can be determined with accuracy sufficient for adequate damage response estimates. Detectors being used, developed, and tested for the program include radiometric (RM) sensors, helium accumulation fluence monitor (HAFM) sensors, solid state track recorder (SSTR) sensors, and damage monitor (DM) sensors.

The necessity for pressure vessel mockup facilities for physics-dosimetry investigations and for irradiation of metallurgical specimens was recognized early in the formation of the NRC program. Experimental studies associated with high- and low-flux versions of a pressurized water reactor (PWR) pressure vessel mockup are in progress in the US, Belgium, France, and United Kingdom. The US low-flux version is known as the ORNL Poolside Critical Assembly (PCA) and the high-flux version is known as the Oak Ridge Research Reactor (ORR) Poolside Facility (PSF), both located at Oak Ridge, Tennessee. As specialized benchmarks, these facilities provide well-characterized neutron environments where active and passive neutron dosimetry, various types of LWR-PV and support structure neutron field calculations, and temperature-controlled metallurgical specimen exposures are brought together.

The two key low-flux pressure vessel mockups in Europe are known as the Mol-Belgium-VENUS and Winfrith-United Kingdom-NESDIP facilities. The VENUS Facility is being used for PWR core source and azimuthal lead factor studies, while NESDIP is being used for PWR cavity and azimuthal lead factor studies. A third and important low-fluence pressure vessel mockup in Europe is identified with a French PV-simulator at the periphery of the Triton reactor. It served as the irradiation facility for the DOMPAC dosimetry experiment for studying surveillance capsule perturbations and through-PV-wall radial fluence and damage profiles (gradients) for PWRs of the Fessenheim 1 type.

Results of measurement and calculational strategies outlined here will be made available for use by the nuclear industry as ASTM standards. Federal Regulations 10 CFR 50 (Cf83) already requires adherence to several ASTM standards that establish a surveillance program for each power reactor and incorporate metallurgical specimens, physics-dosimetry flux-fluence monitors, and neutron field evaluation. Revised and new standards in preparation will be carefully updated, flexible, and, above all, consistent.

CONTENTS

CONTENTS (Cont'd)

FIGURES

FIGURES (Cont'd)

FIGURES (Cont'd)

TABLES

TABLES (Cont'd)

TABLES (Cont'd)

TABLES (Cont'd)

TABLES (Cont'd)

TABLES (Cont'd)

ACRONYMS*

AOTS	Argonne Optical Track Scanner
ANL	Argonne National Laboratory
ASEM	Automated Scanning Electron Microscope
ASTM	American Society for Testing and Materials
BSR	Bulk Shielding Reactor
BWR	Boiling Water Reactor
DM	Damage Monitor
EOL	End-of-Life
ESP	Emulsion Scanning Processor
FBR	Fast Breeder Reactor
FFTF	Fast Flux Test Facility
FSAR	Final Safety Analysis Report
FWHM	Full Width, Half Maximum
HAFM	Helium Accumulation Fluence Monitor
HOTS	Hanford Optical Track Scanner
IRL	Industrial Research Laboratory
LWR	Light Water Reactor
MFR	Magnetic Fusion Reactor
MP	Midplane
NDTT	Nil Ductility Transition Temperature
NRC	Nuclear Regulatory Commission
NRE	Nuclear Research Emulsion
ORR	Oak Ridge Research Reactor (ORNL)
PCA	Poolside Critical Assembly (ORNL)
PF	Perturbation Factor
PROM	Programmable Read Only Memory
PSF	Poolside Facility (ORNL)
PV	Pressure Vessel
PVS	Pressure Vessel Simulator

ACRONYMS (Cont'd)

PWR	Pressurized Water Reactor
QA	Quality Assurance
RM	Radiometric Monitor
SDIP	Surveillance Dosimetry Improvement Program
SDMF	Simulated Dosimetry Measurement Facility
SEM	Scanning Electron Microscope
SPVC	Simulated Pressure Vessel Capsule
SRM	Standard Reference Material
SSC	Simulated Surveillance Capsule
SSTR	Solid State Track Recorder
TLD	Thermoluminescent Dosimeter
TS	Thermal Shield
TSB	Thermal Shield Back
TSF	Thermal Shield Front
UK	United Kingdom
VB	Void Box
W	Westinghouse
WRSR	Water Reactor Safety Research

*For laboratory acronyms, please see Acknowledgments.

ACKNOWLEDGMENTS

The following organizations are presently participating in the Light Water Reactor Pressure Vessel Surveillance Dosimetry Improvement Program (LWR-PV-SDIP) and will periodically contribute written reports, experimental data, or calculations.

Atomic Energy Research Establishment (AERE-H), Harwell, UK

Babcock & Wilcox Company (B&W), USA

Battelle Memorial Institute (BMI), Columbus Laboratory, USA

Brookhaven National Laboratory (BNL), USA

Centre d'Etude de l'Energie Nucleaire - Studiecentrum Voor Kernenergie (CEN/SCK), Mol, Belgium

Centre d'Etudes Nucleaires de Saclay (CEA, Saclay), Gif-sur-Yvette, France

Combustion Engineering, Inc. (CE), USA

EG&G ORTEC, USA

Electric Power Research Institute (EPRI), USA

Engineering Services Associates (ENSA), USA

Fracture Control Corporation (FCC), USA

General Electric Vallecitos Nuclear Center (GE-VNC), USA

Hanford Engineering Development Laboratory (HEDL), USA

Institüt für Kernenergetik und Energiesysteme der Universitat Stuttgart (IKE), Stuttgart, Federal Republic of Germany

IRT Corporation (IRT), USA

Italian Atomic Power Authority (ENEL), Italy

Japan Atomic Energy Research Institute (JAERI), Japan

Kernforschungsanlage Jülich Gmbh (KFA), Germany

Kraftwerk Union, Germany

Materials Engineering Associates (MEA), USA

National Bureau of Standards (NBS), USA

Oak Ridge National Laboratory (ORNL), USA

Radiation Research Associates (RRA), USA

Rockwell International Energy Systems Group (RI-ESG), USA

Rolls-Royce and Associates Limited (RRAL), Derby, UK

Science Applications Incorporated (SAI), USA

Ship Research Institute (SRI), Japan

Southwest Research Institute (SwRI), USA

University of Arkansas (UA), USA

University of California, Santa Barbara (UCSB), USA

University of Tennessee (UT), USA

University of Tokyo, Japan

Westinghouse Electric Corporation - Nuclear Technology Division (W-NTD), USA

Westinghouse Electric Corporation - Research and Development Division (W-R&D), USA

SUMMARY

HANFORD ENGINEERING DEVELOPMENT LABORATORY (HEDL)

A list of planned Nuclear Regulatory Commission (NRC) reports is presented in Table S-1. These reports address individual and combined pressurized water reactor (PWR) and boiling water reactor (BWR) physics-dosimetry-metallurgy issues. These will provide a reference base of information to support the preparation of the new set of LWR ASTM Standards (Figures S-1 and S-2).

Initial fission rate measurements using Solid-State Track Recorders (SSTRs) have been reported for the PCA 8/7 and 12/13 configurations. Additional measurements, which have been carried out in the 8/7, 12/13, and 4/12 simulated surveillance capsule (SSC) configurations, are summarized. The experimental details of these measurements are identical to those described previously. Subsequent to the reporting of the initial SSTR fission rate measurements, the optical efficiency for fission tracks in mica has been remeasured. The newer value (0.9875 ± 0.0085 tracks/fission) has been used for the more recent measurements. All previous measurements must be corrected to correspond to the newer optical efficiency values when comparisons are made with the more recent data.

Room temperature compression tests were conducted on small cylindrical compression specimens manufactured from eleven different PV steel alloys. For each of the eleven alloys, tests were performed on unirradiated control specimens and also on specimens irradiated in the SSC-1 and SSC-2 capsules of the Poolside Facility (PSF) experiment. The measured increase in yield strength correlates with copper content, but a copper saturation effect appears to be present. The irradiation-induced increase in yield strength correlates with dpa exposure, and the functional relation shows a stronger exposure dependence than usually found between Charpy shift and fluence in surveillance irradiations. In particular, the exponent of the fluence term is ∿0.45 in contrast to the ∿0.3 value found for Charpy trend curve relations derived from surveillance data. This may indicate a rate effect since the dose rate was higher than for a power reactor surveillance irradiation. A similar change in functional relationship has been found for the SSC-1 and SSC-2 Charpy data, but the scatter in the Charpy data precludes any firm conclusions. These SSC and other yield strength results are currently being used by HEDL, UCSB, S.P. Grant and S. Earp and other LWR-PV-SDIP participants to aid in refining RT_{NDT} trend curves for welds, forgings, and plates to help improve the accuracy of the prediction of the end-of-life (EOL) metallurgical condition of the PV and to further ensure the safety of PWR and BWR power plants.

A nondestructive method for determining reactor PV neutron exposure is advanced. It is based on the observation of characteristic gamma-rays emitted by activation products in the PV with a unique continuous gamma-ray spectrometer. This spectrometer views the PV through appropriate collimators to determine the absolute emission rate of these characteristic gamma-

rays, thereby ascertaining the absolute activity of given activation products in the PV. These data can then be used to deduce the spatial and angular dependence of neutron exposure at regions of interest in the PV. In addition, this method can be used to determine the concentrations of different constituents in the PV by measuring the absolute flux of characteristic gamma-rays from radioactivity induced in these constituents through neutron exposure. Since copper concentration may be a crucial variable in radiation-induced embrittlement of PVs, the ability of this method to measure copper concentrations in base metal and weldments is examined.

Results of recent Si(Li) continuous gamma-ray spectrometry in low-power LWR-PV benchmark fields are reported. Emphasis is placed on the measurement and interpretation of perturbation factors created by the introduction of the Janus probe into the LWR-PV environment. Absolute comparisons are reported between spectrometry, calculations, and thermoluminescent dosimetry (TLD).

TABLE S-1

PROGRAM DOCUMENTATION

NRC Report No.	Vol No.	Lab Report No.	LWR-PV-SDIP Program No.*	Issue Date	Editors
NUREG/CR-1861 (PCA Physics-Dosimetry)		HEDL-TME 80-87	NUREG 1-1	July 1981	WN McElroy
NUREG/CR-3295 (PSF Metallurgy)	Vol 1	MEA-2017	NUREG 13	April 1984	JR Hawthorne
	Vol 2	MEA-2017	NUREG 14	April 1984	JR Hawthorne
NUREG/CR-3318** (PCA Physics-Dosimetry)	--	HEDL-TME 84-1	NUREG 1-2	September 1984	WN McElroy
NUREG/CR-3319** (Power Reactor Physics-Dosimetry)	--	HEDL-TME 84-2	NUREG 4	October 1984	WN McElroy
NUREG/CR-3320 (PSF SSC/SPVC Experiments & Blind Test)	Vol 1	HEDL-TME 84-3	NUREG 3	February 1985	[WN McElroy]***
	Vol 2	HEDL-TME 84-4	NUREG 2	November 1984	[FBK Kam]
	Vol 3	HEDL-TME 85-XX	NUREG 5	January 1985	↓
	Vol 4	HEDL-TME 85-XX	NUREG 6-1	June 1985	
	Vol 5	CEN/SCK-XX	NUREG 6-2	September 1984	[Ph VanAsbroeck JR Hawthorne A. Fabry]
↓	Vol 6**	HEDL-TME 85-XX	NUREG 6-3	September 1986	[WN McElroy FBK Kam]
(PSF SVBC Experiments)	Vol 7	EPRI/FCC/W-NTD	NUREG 6-4	January 1985	[JS Perrin TU Marston W-NTD Staff]
↓	Vol 8	HEDL-TME 86-XX	NUREG 6-5	January 1986	[WN McElroy FBK Kam GL Guthrie JS Perrin TU Marston]
NUREG/CR-3321** (SDMF Physics-Dosimetry)	--	HEDL-TME 86-XX	NUREG 7	June 1986	[WN McElroy FBK Kam JA Grundl ED McGarry]
NUREG/CR-3322** (Test Reactor Physics-Dosimetry)	--	HEDL-TME 86-XX	NUREG 8	September 1986	[WN McElroy FBK Kam]
NUREG/CR-3323 (VENUS Physics-Dosimetry)	Vol 1	CEN/SCK-XX, Vol 1	NUREG 9-1	September 1984	[A. Fabry WN McElroy]
	Vol 2	CEN/SCK-XX, Vol 2	NUREG 9-2	September 1985	[ED McGarry]
NUREG/CR-3324 (NESDIP Physics-Dosimetry)	Vol 1	AEEW-R 1736	NUREG 10-1	January 1984	[J. Butler M. Austin WN McElroy]
	Vol 2	UKAEA-XX, Vol 2	NUREG 10-2	September 1985	
	Vol 3	UKAEA-XX, Vol 3	NUREG 10-3	September 1986	
	Vol 4	UKAEA-XX, Vol 4	NUREG 10-4	September 1987	
↓	Vol 5	UKAEA-XX, Vol 5	NUREG 10-5	September 1988	↓
NUREG/CR-3325 (Gundremmingen Physics-Dosimetry-Metallurgy)	Vol 1	W-NTD-XX	NUREG 11-1	June 1984	[A. Anderson WM McElroy R. Gold EP Lippincott GL Guthrie]
	Vol 2	HEDL-TME 85-XX	NUREG 11-2	September 1985	
	Vol 3	HEDL-TME 86-XX	NUREG 11-3	January 1986	
	Vol 4	HEDL-TME 86-XX	NUREG 11-4	September 1986	
NUREG/CR-3326** (Test Reactor Metallurgy)		HEDL-TME 87-XX	NUREG 12	September 1987	[WN McElroy FBK Kam]

*These program numbers are not to be used on final reports.
**Loose-leaf document.
***Brackets indicate same authors for all volumes, as appropriate.

NUREG/CR-1861 (Issue Date: July 1981)
PCA Experiments and Blind Test
W. N. McElroy, Editor

This document provides the results of calculations and active and passive physics-dosimetry measurements for the PCA 8/7 and 12/13 configurations [X/Y: Water gaps (in cm) from the core edge to the thermal shield (X) and from the thermal shield to the vessel wall (Y)]. The focus of the document is on an international Blind Test of transport theory methods in LWR-PV applications involving eleven laboratories, including reactor vendors.

NUREG/CR-3295
PSF Metallury

Vol. 1 (Issue Date: April 1984)
Notch Ductility and Fracture Toughness Degradation of A302-B and A533-B Reference Plate from PSF Simulated Surveillance and Through-Wall Irradiation Capsules
R. Hawthorne, Editor

Beyond scope of title, this document will support analysis of the PSF Blind Test and provide as-built documentation and final PSF A302-B and A533-B reference plate metallurgical results for SSC and SPVC.

Vol. 2 (Issue Date: April 1984)
Postirradiation Notch Ductility and Tensile Strength Determinations for PSF Simulated Surveillance and Through-Wall Specimen Capsules
R. Hawthorne, Editor

Beyond scope of title, this document will support analysis of the PSF Blind Test and provide as-built documentation and final PSF EPRI, RR&A, CEN/SCK, and KFA steel metallurgical results generated by MEA for SSC and SPVC.

NUREG/CR-3318 (Issue Date: September 1984)
PCA Dosimetry in Support of the PSF Physics-Dosimetry-Metallurgy Experiments (4/12, 4/12 SSC configurations and update of 8/7 and 12/13 configurations)
W. N. McElroy, Editor

Beyond scope of title, this loose-leaf document will support analysis of the PSF Blind Test and updates NUREG/CR-1861, "PCA Experiments and Blind Test," July 1981.

NUREG/CR-3319 (Issue Date: September 1984)
LWR Power Reactor Surveillance Physics-Dosimetry Data Base Compendium
W. N. McElroy, Editor

In loose-leaf form this document will provide new or reevaluated exposure parameter values [total, thermal, and fast (E > 1.0 MeV) fluences, dpa, etc.] for individual surveillance capsules removed from operating PWR and BWR power plants. As surveillance reports are reevaluated with FERRET-SAND, this document will be revised annually. The corresponding metallurgical data base is provided in the loose-leaf EPRI NP-2428, "Irradiated Nuclear Pressure Vessel Steel Data Base" (Ma82).

NUREG/CR-3220
PSF Physics-Dosimetry-Metallurgy Experiments:

Vol. 1 (Issue Date: February 1985)
PSF Blind Test
W. N. McElroy and F. B. K. Kam, Editors

This document will provide summary information on the comparison of measured and predicted physics-dosimetry-metallurgy results for the PSF experiment. This document will also contain summary results of each participants' final report published in NUREG/CR-3320, Vol. 6.

Vol. 2 (Issue Date: November 1984)
PSF Startup and Simulated Surveillance Capsule (SSC) Physics-Dosimetry Program
W. N. McElroy and F. B. K. Kam, Editors

Beyond scope of title, this document will support analysis of the PSF Blind Test and provide experimental conditions, as-built documentation,and final PSF physics-dosimetry results for SSC-1 and SSC-2.

Vol. 3 (Issue Date: January 1985)
PSF Simulated Pressure Vessel Capsule (SPVC) and Simulated Void Box Capsule (SVBC) Physics-Dosimetery Program
W. N. McElroy and F. B. K. Kam, Editors

Beyond scope of title, this document will support analysis of the PSF Blind Test and provide experimental conditions, as-built documentation, and final PSF physics-dosimetry results for SPVC and SVBC.

Vol. 4 (Issue Date: June 1985)
PSF Simulated Surveillance Capsules (SCC-1 and SCC-2), Simulated Pressure Vessel Capsule (SPVC) and Simulated Void Box Capsule (SVBC) Metallurgy Program
W. N. McElroy and F. B. K. Kam, Editors

Beyond scope of title, this document will support analysis of the PSF Blind Test and provide experimental conditions, as-built documentation, and final metallurgical data on measured property changes in different pressure vessel steels for SSC-1 and -2 positions, and the (SPVC) simulated PV locations at the inner surface, 1/4 T, and 1/2 T positions of the 4/12 PWR PV wall mockup. The corresponding SSC-1, SSC-2, and SPVC locations' neutron exposures are $\sim 2 \times 10^{19}$, $\sim 4 \times 10^{19}$, $\sim 4 \times 10^{19}$, $\sim 2 \times 10^{19}$, and $\sim 1 \times 10^{19}$ n/cm^2, respectively, for a $\sim$550°F irradiation temperature.

TABLE S-1 (Cont'd)

Vol. 5 (Issue Date: September 1984)
PSF Simulated Surveillance Capsule (SSC) Results-CEN/SCK/MEA
Ph. Van Asbroech, A. Fabry, and R. Hawthorne, Editors

This document, to be issued by CEN/SCK, will provide CEN/SCK/MEA metallurgical data and results from the Mol, Belgium PV steel irradiated in the SSC position for the ORR-PSF physics-dosimetry-metallurgy experiments.

Vol. 6 (Issue Date: September 1986)
PSF Blind Test Participants' Reports
W. N. McElroy and F. B. K. Kam, Editors

This document will provide a compilation of participants' final camera-ready reports on PSF physics-dosimetry-metallurgy experiments for the PSF Blind Test.

Vol. 7 (Issue Date: January 1985)
PSF Simulated Void Box Capsule (SVBC) Charpy and Tensile Metallurgical Test Results
J. S. Perrin and T. U. Marston, Editors

Beyond scope of title, this document will provide experimental conditions, as-built documentation, and final Charpy and tensile specimen measured property changes in PV support structure and reference steels for the SVBC simulated ex-vessel cavity (void box) neutron exposure of $\sim 5 \times 10^{17}$ n/cm^2 (E > 1.0 MeV)* for ~95°F irradiation temperature.

Vol. 8 (Issue Date: January 1986)
PSF Simulated Void Box Capsule (SVBC) Physics-Dosimetry-Metallurgy Program Results
W. N. McElroy, F. B. K. Kam, G. L. Guthrie, J. S. Perrin, and T. U. Marston, Editors

Beyond scope of title, this document will provide small specimen measured property changes in PV support structure and reference steels for the SVBC simulated ex-vessel cavity (void box) neutron exposure of $\sim 5 \times 10^{17}$ n/cm^2 (E > 1.0 MeV)* for ~95°F irradiation temperature. The report will analyze and summarize combined physics-dosimetry-metallurgy results of NUREG/CR-3320, Vols. 3 and 7, including an assessment of thermal neutron effects, which are expected to be small.

*This estimate is based on preliminary ORNL calculations, as yet unsubstantiated by measurements.

NUREG/CR-3321 (Issue Date: June 1986)
PSF Surveillance Dosimetry Measurement Facility (SDMF)
W. N. McElroy, F. B. K. Kam, J. Grundl, and E. D. McGarry, Editors

This loose-leaf volume will provide results to certify the accuracy of exposure parameter and perturbation effects for surveillance capsules removed from PWR and BWR power plants.

NUREG/CR-3322 (Issue Date: September 1986)
LWR Test Reactor Physics-Dosimetry Data Base Compendium
W. N. McElroy and F. B. K. Kam, Editors

This loose-leaf volume will present results from FERRET-SAND, LSL, and other least-squares-type code analyses of physics-dosimetry for US (BSR, PSF, SUNY-NSTF [Buffalo], Virginia, etc.), UK (DIDO, HERALD, etc.), Belgium (BR-2,etc.), France (Melusine, etc.), Germany (FRJ1, FRJ2, etc.), and other participating countries. It will provide needed and consistent exposure parameter values [total, thermal, and fast (E > 1.0 MeV) fluences, dpa, etc.] and uncertainties for correlating test reactor property change data with those obtained from PWR and BWR power plant surveillance capsules. NUREG/CR-3319 and -3322 will serve as reference physics-dosimetry data bases for correlating and applying power and research reactor-derived steel irradiation effects data. These latter metallurgical data are provided in EPRI NP-2428 (Ma82) and in NUREG/CR-3326.

NUREG/CR-3323
VENUS PWR Core Source and Azimuthal Lead Factor Experiments and Calculational Tests:

Vol. 1 (Issue Date: September 1984)
Preliminary Results
A. Fabry, W. N. McElroy, and E. D. McGarry, Editors

Vol. 2 (Issue Date: September 1985)
Final Results
A. Fabry, W. N. McElroy, and E. D. McGarry, Editors

These two documents, to be prepared by CEN/SCK and other participants, will provide VENUS-derived reference physics-dosimetry data on active, passive, and calculational dosimetry studies involving CEN/SCK, HEDL, NBS, ORNL, and other LWR program participants.

NUREG/CR-3324
NESDIP PWR Cavity and Azimuthal Lead Factor Experiments and Calculational Tests:

Vol. 1 (Issue Date: April 1984)
PCA Replica Results: Preliminary Results
J. Butler, M. Austin, and W. N. McElroy, Editors

Vol. 2 (Issue Date: September 1985)
PCA Replica Results: Final Results
J. Butler, M. Austin, and W. N. McElroy, Editors

These two documents, to be prepared by Winfrith-RR&A and other participants, will provide NESDIP-PCA replica-derived reference physics-dosimetry data on active, passive, and calculational dosimetry studies involving Winfrith, CEN/SCK, HEDL, NBS, and other LWR program participants.

Vol. 3 (Issue Date: September 1986)
Zero- and Twenty-Centimeter Cavity Results
J. Butler, M. Austin, and W. N. McElroy, Editors

This document will provide NESDIP zero- and twenty-centimeter cavity-derived reference physics-dosimetry data on active, passive, and calculational dosimetry studies involving Winfrith, RR&A, HEDL, ORNL, NBS, CEN/SCK, and other LWR program participants.

Vol. 4 (Issue Date: September 1987)
Hundred-Centimeter Cavity Results
J. Butler, M. Austin, and W. N. McElroy, Editors

This document will provide NESDIP hundred-centimeter cavity-derived reference physics-dosimetry data on active, passive, and calculational dosimetry studies involving Winfrith, RR&A, HEDL, ORNL, NBS, CEN/SCK, and other LWR program participants. Results of zero-centimeter cavity studies will also be discussed and reported, as appropriate.

Vol. 5 (Issue Date: September 1988)
Other Configuration Cavity Results
J. Butler, M. Austin, and W. N. McElroy, Editors

This document will provide NESDIP "other" configuration cavity-derived results similar to those indicated for Vols. 3 and 4, above.

NUREG/CR-3325
Gundremmingen Physics-Dosimetry-Metallurgy Program:

These documents will provide results that support the NRC fracture mechanics analysis of pressure vessel base metal using Charpy, tensile, compact tension, and full-wall thickness metallurgical specimens for Gundremmingen. HEDL compression and micro-hardness metallurgical and dosimetry specimens will be obtained as a function of distance through the PV wall. Previous surveillance capsule and cavity physic-dosimetry-metallurgy results will be correlated with new in-wall vessel results. Appropriate PSF results will be used to help NRC obtain the best possible overall data correlations.

Vol. 1 (Issue Date: June 1984)
Reactor Physics Calculational and Preliminary Dosimetry Results
W. N. McElroy and R. Gold, Editors

This document will provide the results of the W-NTD physics calculations and comparisons to previously available reactor cavity, concrete wall/steel liner, and surveillance capsule results. The calculations will provide information on both neutron and gamma components of the radiation field as well as best estimates of PV wall temperature profiles during full-power operation.

Vol. 2 (Issue Date: September 1985)
Program Description
W. N. McElroy and R. Gold, Editors

This document will provide relevant as-built and operated plant reference information and trepan metallurgical and dosimetry specimen experimental conditions, locations, etc. Information on previous reactor cavity and surveillance capsule physics-dosimetry-metallurgy results will be discussed and referenced, as well as results of radiometric [Si(Li)] and [Ge(Li)] measurements on PV wall trepans, concrete wall/steel liner trepans, PV wall, and other components, as appropriate.

Vol. 3 (Issue Date: January 1986)
Final Physics-Dosimetry Results
W. N. McElroy and R. Gold, Editors

This document will provide the final results of estimated surveillance capsule and PV (r,θ,z) wall neutron exposure parameter values [total, thermal, and fast ($E > 1.0$ MeV) fluences, dpa, etc.]; all in support of the data analysis of the trepan and surveillance capsule metallurgical specimens results.

Vol. 4 (Issue Date: September 1986)
Final Metallurgical and Data Correlation Results
W. N. McElroy and R. Gold, Editors

This document will provide the final results of the physics-dosimetry-metallurgy data correlation studies performed by HEDL/W-NTD of the surveillance capsule and PV wall metallurgical results. As appropriate, the results will be used to help in developing improved trend curves for future revisions of the E706 (IIF), E900, ΔNTT versus fluence and Reg. Guide 1.99 trend curves. The physics-dosimetry results will, similarly, be used to help in the final 1987 and 1988 revisions of the set of 21 LWR ASTM standards.

NUREG/CR-3326 (Issue Date: September 1987)
LWR Test Reactor Irradiated Nuclear Pressure Vessel and Support Structure Steel Data Base Compendium
W. N. McElroy and F. B. K. Kam, Editors

This loose-leaf volume will present data and results for selected metallurgical experiments performed in the US (BSR, PSF, SUNY-NSTF [Buffalo], Virginia, etc.), UK (DIDO, HERALD, etc.), Belgium (BR-2, etc.), France (Melusine, etc.), Germany (FRJ1, FRJ2, etc.), and other participating countries. It will provide needed and consistent Charpy, upper shelf energy, tensile, compact tension, compression, hardness, etc. property change values and uncertainties. With NUREG/CR-3322 physics-dosimetry data, NUREG/CR-3326 provides: 1) a more precisely defined and representative research reactor physics-dosimetry-metallurgy data base, 2) a better understanding of the mechanisms causing neutron damage, and 3) tested and verified exposure data and physical damage correlation models, all of which are needed to support the preparation and acceptance of the ASTM E706(IE) Damage Correlation and ASTM E706(IIF) ΔNDTT with fluence standards and future revisions of Reg. Guide 1.99.

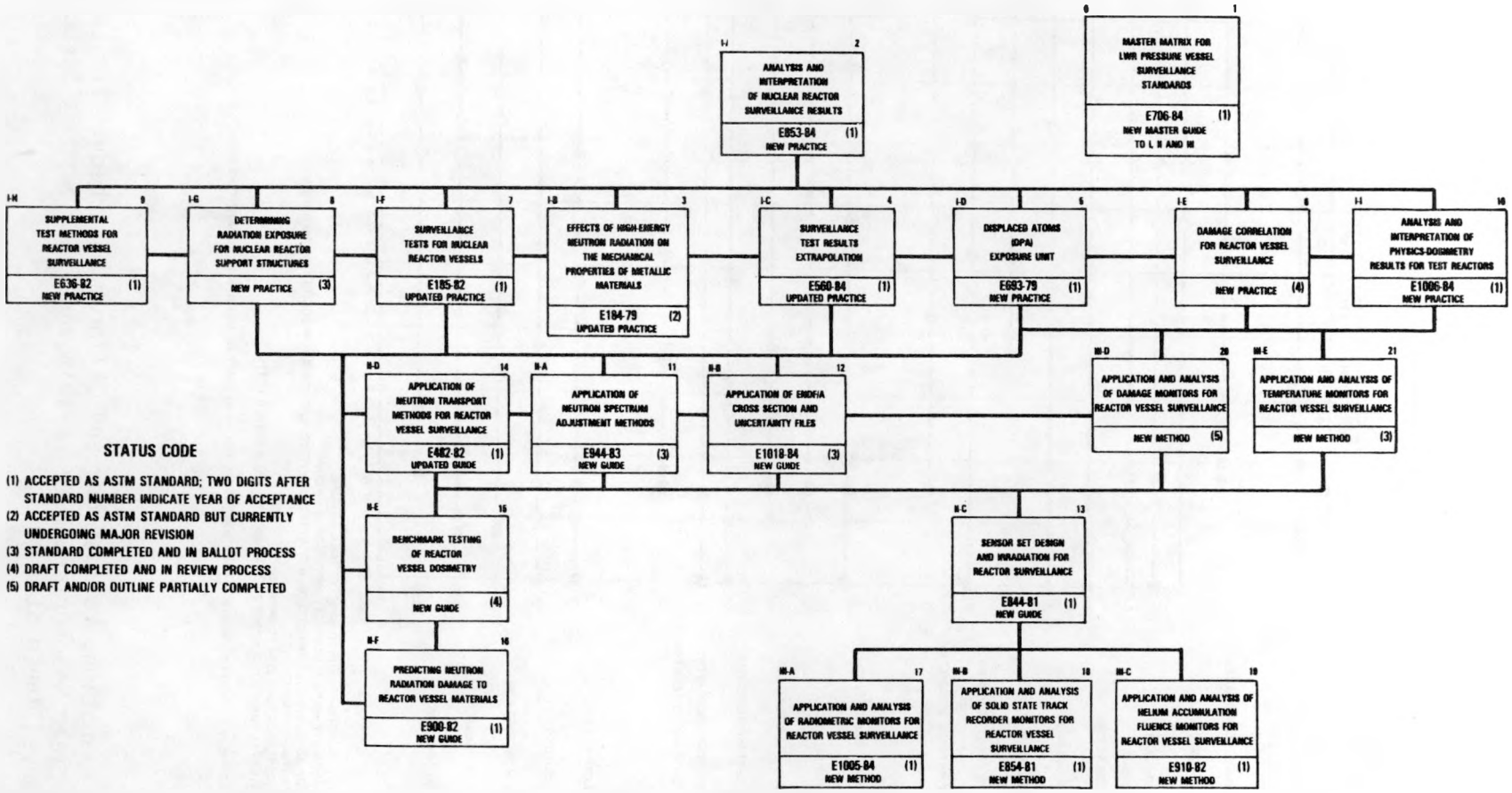

ASTM STANDARDS FOR SURVEILLANCE OF LWR NUCLEAR REACTOR PRESSURE VESSELS AND SUPPORT STRUCTURES.

HEDL 8407-057

FIGURE S-1. ASTM Standards for Surveillance of LWR Nuclear Reactor Pressure Vessels and Their Support Structures.

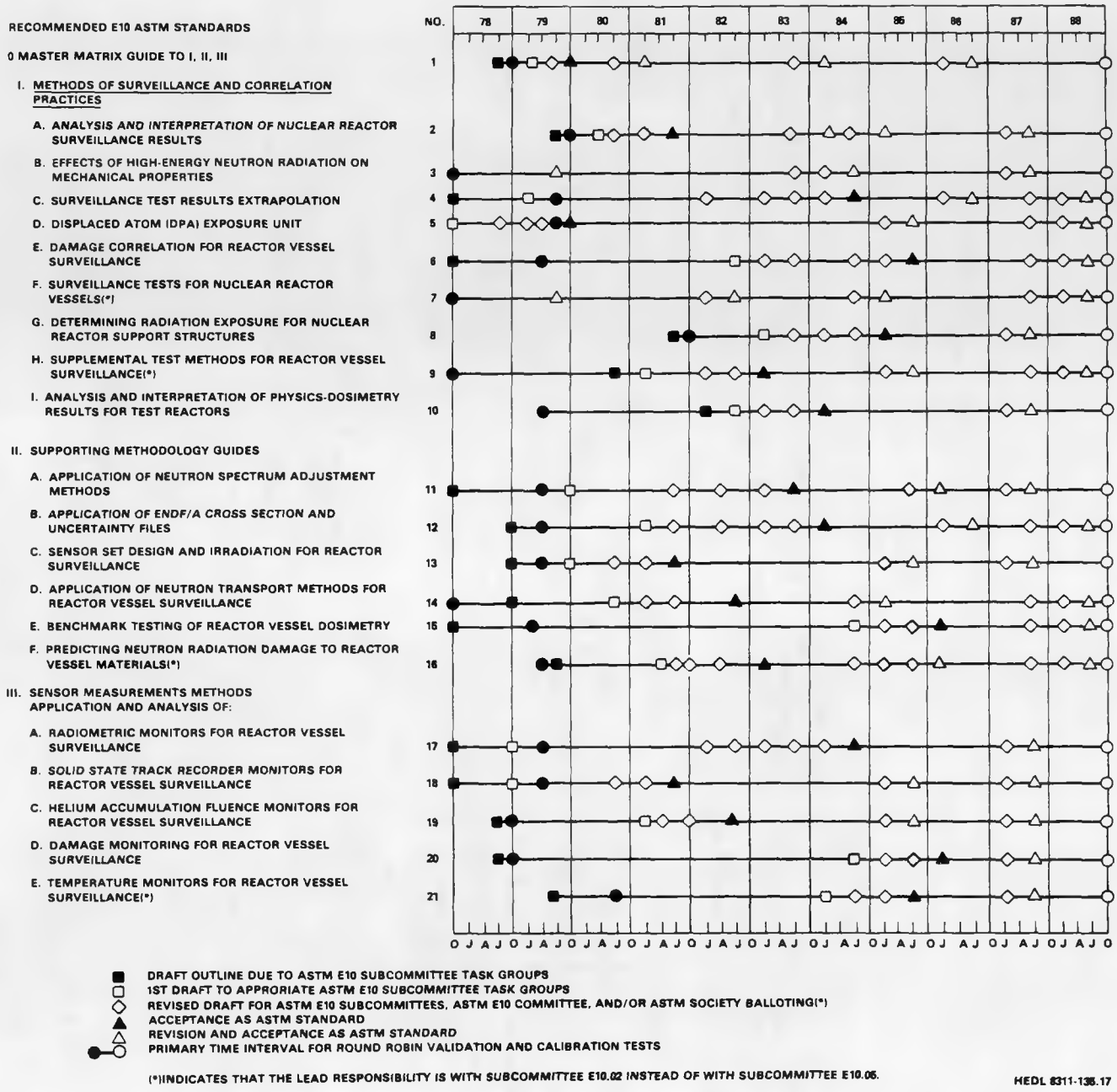

FIGURE S-2. Preparation, Validation, and Calibration Schedule for LWR Nuclear Reactor Pressure Vessels and Their Support Structure Surveillance Standards.

HANFORD ENGINEERING DEVELOPMENT LABORATORY

(HEDL)

A. SOLID STATE TRACK RECORDER FISSION RATE MEASUREMENTS AT THE PCA

F. H. Ruddy, J. H. Roberts, R. Gold and C. C. Preston (HEDL)

Objective

To obtain absolute fission rate measurements in the PCA 8/7, 12/13 and 4/12 SSC configurations.

Initial fission rate measurements using Solid State Track Recorders (SSTRs) have been reported for the PCA 8/7 and 12/13 configurations (Mc81). Additional measurements, which have been carried out in the 8/7, 12/13, and 4/12 SSC configurations, are summarized in Table HEDL-1. The experimental details of these measurements are identical to those described previously in (Ru81). Subsequent to the reporting of the initial SSTR fission rate measurements, the optical efficiency for fission tracks in mica has been remeasured (Ro83a). The newer value (0.9875 ± 0.0085 tracks/fission) has been used for the more recent measurements. All previous measurements must be corrected to correspond to the newer optical efficiency values when comparisons are made with the more recent data.

Accomplishments and Status

PCA 12/13 Configuration -- In November 1981, fission rates were measured for all seven radial locations simultaneously in separate runs for ^{237}Np and ^{238}U. These data represent the only Poolside Critical Assembly (PCA) radial traverses where relative fission rates can be obtained without power normalization uncertainties for the seven radial locations. The SSTR fission rates measured in the PCA for ^{237}Np and ^{238}U are listed as a function of radial position for the 12/13 configuration in Table HEDL-2. These data are plotted in Figure HEDL-1 for ^{237}Np and Figure HEDL-2 for ^{238}U. These fission rates display an exponential decrease as a function of distance within the Pressure Vessel Simulator (PVS) block that is characteristic of threshold reactions. The departure of the ^{237}Np fission rates in Figure HEDL-1 from exponential behavior in the water locations is influenced by contributions to the fission rate from subthreshold fission. The cross section for neutron-induced ^{237}Np fission shows resonances in the epithermal energy range, and the relative number of epithermal neutrons increases as the core is approached.

In the case of the ^{238}U data plotted in Figure HEDL-2, a straight line with a slope slightly less than the slope in the PVS is obtained in the water positions. These lines intersect at the PVS-H_2O boundary. The contribution to the measured fission rate from ^{235}U in the ^{238}U foils is appreciable in the water positions. A 14.6% correction was required in the pressure vessel front (PVF) position, and a 30% correction was required at the TSB location. The thermal fission correction resulted in an overall uncertainty of 15% for the thermal shield back (TSB) ^{238}U fission rate.

TABLE HEDL-1

SCHEDULE OF PCA SSTR MEASUREMENTS

Run Number	Date	Configuration	Isotope	Positions*
PCA37	01/14/81	4/12 SSC	^{237}Np	SSC (+75 mm, MP, -75 mm), 1/4 T (+150 mm, MP, -130 mm), 1/2 T (MP)
PCA38	01/14/81	4/12 SSC	^{238}U	SSC (+75 mm, MP, -75 mm), 1/4 T (+75 mm, MP, -75 mm), 1/2 T (MP), 3/4 T (MP)
PCA39	10/15/81	8/7	^{238}U	1/4 T, 1/2 T, 3/4 T, VB (all MP)
PCA40	10/15/81	8/7	^{237}Np	1/4 T, 1/2 T, 3/4 T, VB (all MP)
PCA42	10/16/81	12/13	^{238}U	1/4 T, 1/2 T, 3/4 T, VB (all MP)
PCA43	10/16/81	12/13	^{237}Np	1/4 T, 1/2 T, 3/4 T, VB (all MP)
PCA51	11/18/81	12/13	^{238}U	TSF, TSB, PVF, 1/4 T, 1/2 T, 3/4 T, VB (all MP)
PCA52	11/18/81	12/13	^{237}Np	TSF, TSB, PVF, 1/4 T, 1/2 T, 3/4 T, VB (all MP)
PCA53	11/19/81	12/13	^{235}U	TSF, TSB, PVF, 1/4 T, 1/2 T, 3/4 T, VB (all MP)
PCA54	11/19/81	12/13	^{238}U	TSF, TSB, PVF (all +75 mm, MP, -75 mm)

*1/4 T, 1/2 T and 3/4 T refer to depths in a PVS of total thickness T. The other acronyms are defined as follows: Simulated Surveillance Capsule (SSC), Thermal Shield Front (TSF), Thermal Shield Back (TSB), Pressure Vessel Front (PVF), Void Box (VB), and Midplane (MP).

TABLE HEDL-2

SSTR FISSION RATES MEASURED IN THE PCA 12/13 CONFIGURATION

Location	Distance from Core (cm)*	Fission Rate** (fissions per atom per core neutron) ^{237}Np	Fission Rate** (fissions per atom per core neutron) ^{238}U
TSF	12.0	7.90×10^{-30} (±3.3%)	---
TSB	23.8	7.47×10^{-31} (±3.3%)	---
PVF	29.7	3.10×10^{-31} (±3.3%)	6.48×10^{-32} (±4.1%)
1/4 T	39.5	1.18×10^{-31} (±3.6%)	1.75×10^{-32} (±2.7%)
1/2 T	44.7	6.19×10^{-32} (±5.4%)	7.50×10^{-33} (±2.7%)
3/4 T	50.1	3.32×10^{-32} (±3.3%)	3.23×10^{-33} (±2.7%)
VB	59.1	9.70×10^{-33} (±3.4%)	9.70×10^{-34} (±2.7%)

*Distance from inner face of core aluminum simulator (or window).
**All SSTR fission rates were calculated using the newly measured value for the mica optical efficiency (0.9875 ± 0.0085 tracks/fission).

Although this point has been plotted in Figure HEDL-2, it has been omitted from Table HEDL-2 because of its large uncertainty. In the thermal shield front (TSF) position, the ^{238}U fission rate could not be accurately measured even with ^{238}U deposits containing as little as 6 ppm ^{235}U because of the extremely high thermal-to-fast-neutron ratio at this location.

The relative uncertainties (1σ) have been obtained by combining the sources of error tabulated in (Fa81) in quadrature. Uncertainties in power normalization do not enter into the calculation of the relative uncertainties, since a single run was used for ^{238}U or ^{237}Np. To obtain the absolute uncertainties from the relative uncertainties of Table HEDL-2, the 4.1% uncertainty in the absolute power normalization must be combined in quadrature with the tabulated values. The absolute uncertainties in these data are generally 5% (1σ) or less.

Note that the November 1981, SSTR fission rates for ^{237}Np were 15% lower than the SSTR fission rates measured in October 1978, which are tabulated in (Ru81). This difference must be due to a mispositioning of the PCA 12/13 configuration during the earlier measurements, as a 15% error is far too large to be accounted for by any other experimental error. Additional ^{237}Np and ^{238}U 12/13 fission rates are available from the October 1981 runs, and these data are contained in Table HEDL-3. The fission rates measured in November 1981 and the ratios of the fission rates are shown for comparison. In general, the agreement between the two sets of data is excellent, indicating that the measurements are reproducible within the quoted experimental uncertainties.

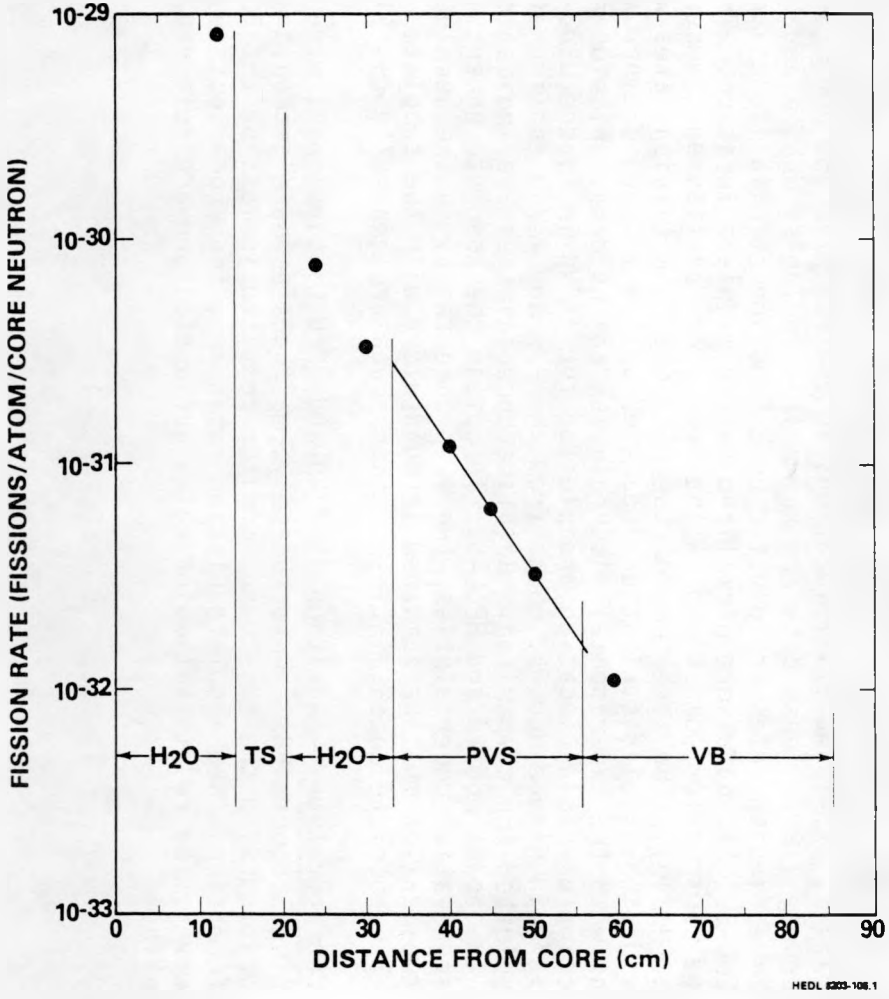

FIGURE HEDL-1. Radial Fission Rate Distribution for ^{237}Np in the PCA 12/13 Configuration. Neg P12736-1

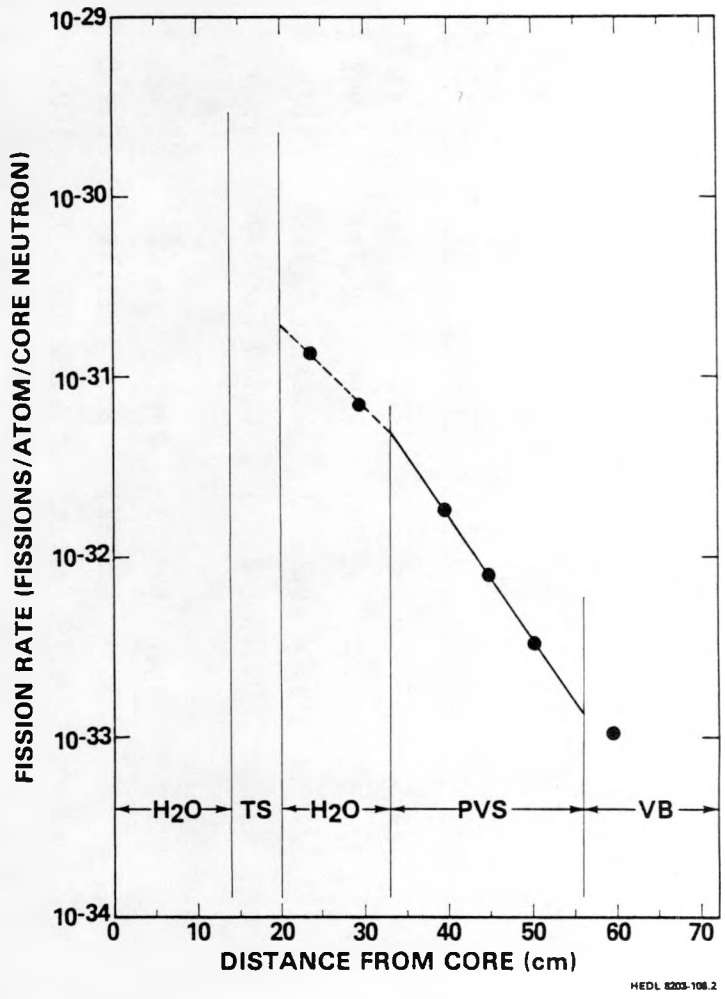

FIGURE HEDL-2. Radial Fission Rate Distribution for ^{238}U in the PCA 12/13 Configuration. Neg P12736-2

TABLE HEDL-3

RATIOS OF DUPLICATE PCA 12/13 SSTR FISSION RATE MEASUREMENTS

Isotope	Location	Fission Rate [(fissions per atom per core neutron) x 10^{33}] October 1981	November 1981	Oct 1981/Nov 1981
^{238}U	1/4 T	17.4 (±2.7%)	17.5 (±2.7%)	0.992 (±3.6%)
	1/2 T	7.44 (±2.7%)	7.50 (±2.7%)	0.992 (±3.6%)
	3/4 T	3.24 (±2.7%)	3.23 (±2.7%)	1.01 (±3.6%)
	VB	0.970 (±2.7%)	0.970 (±2.7%)	1.00 (±3.6%)
^{237}Np	1/4 T	116.0 (±3.3%)	118.0 (±3.6%)	0.983 (±4.7%)
	3/4 T	32.3 (±3.3%)	33.2 (±3.3%)	0.970 (±4.5%)
	VB	9.79 (±3.3%)	9.70 (±3.4%)	1.01 (±4.6%)
			Average	0.994 (±1.45%)

PCA 4/12 SSC Configuration -- ^{237}Np and ^{238}U fission rates were measured in the SSC, 1/4-T, 1/2-T and 3/4-T locations in the PCA 4/12 SSC configuration during January 1981. These data are summarized in Tables HEDL-4 and HEDL-5. The relative fission rates are plotted as a function of axial location in Figure HEDL-3. All data were normalized to the midplane location. The solid line plotted for comparison is the result of Mol fission chamber traverses (Mc81b). The agreement of the relative SSTR fission rates with the shape of the axial distribution indicated by the fission chamber is consistent with the experimental uncertainties of the data. Fission rates as a function of radial location are plotted for ^{237}Np in Figure HEDL-4 and for ^{238}U in Figure HEDL-5. Data from the 8/7 and 12/13 configurations are also plotted for comparison. Relative uncertainties are indicated for the data in Tables HEDL-4 and HEDL-5. To obtain the absolute uncertainties from these relative uncertainties, the 4.1% uncertainty in the absolute power normalization must be combined in quadrature with the tabulated values. The absolute uncertainties in these data are generally <5% (1σ).

PCA 8/7 Configuration -- Additional ^{237}Np and ^{238}U fission rates were measured during October 1981. Unfortunately, malfunctioning electronic equipment associated with the run-to-run monitor resulted in loss of the PCA power information. New absolute fission rates are, therefore, not available; however, the relative fission rates are useful and are referred to subsequently.

TABLE HEDL-4

PCA ^{237}Np FISSION RATES

PCA Configuration	Axial Location (mm)	Fission Rate (fissions per atom per core neutron) SSC Position	1/4 T Position	1/2 T Position
4/12 SSC	+150	---	5.08 E-31 (±2.6%)	---
	+75	8.16 E-30 (±2.6%)	---	---
	0	8.48 E-30 (±2.6%)	6.25 E-31 (±2.6%)	3.44 E-31 (±2.6%)
	-75	8.42 E-30 (±2.6%)	---	---
	-130	---	5.52 E-31 (±2.6%)	---

TABLE HEDL-5

PCA ^{238}U FISSION RATES

PCA Configuration	Axial Location (mm)	Fission Rate (fissions per atom per core neutron) SSC Position	1/4 T Position	1/2 T Position	3/4 T Position
4/12 SSC	+75	1.04 E-30 (±2.6%)	5.89 E-32 (±2.4%)	---	---
	0	1.15 E-30 (±2.6%)	6.60 E-32 (±2.4%)	2.99 E-32 (±2.4%)	1.29 E-32 (±2.4%)
	-75	1.11 E-30 (±2.6%)	6.51 E-32 (±2.4%)	---	---

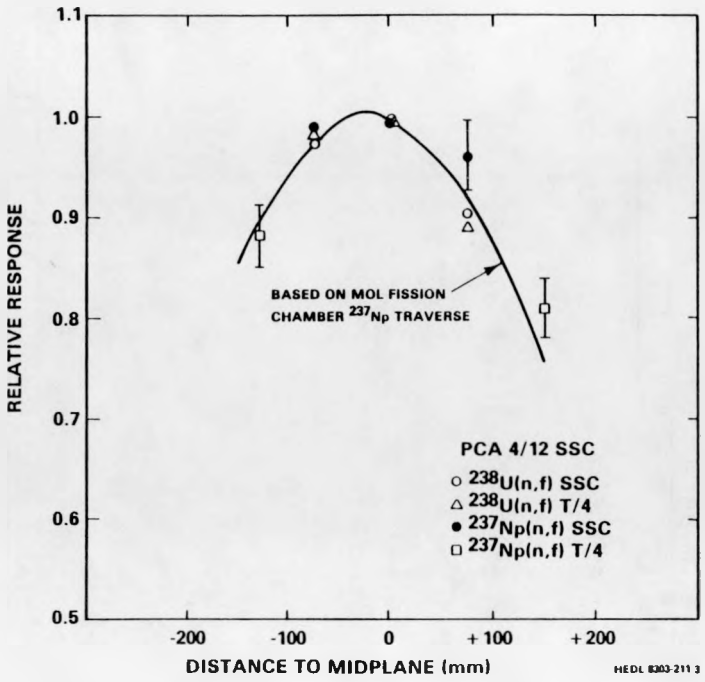

FIGURE HEDL-3. Axial Distributions of the ^{237}Np and ^{238}U Fission Rates in the PCA 4/12 Configuration. Neg 831925-1

General Data Trends

The data plotted in Figures HEDL-4 and HEDL-5 show that the slopes of the attenuation in the PVS block appear to be independent of configuration. This fact, which was first noted in (Mc81b), is further substantiated by the data in Table HEDL-6. Here all fission rates have been normalized to one at the 1/4-T location, and the 1/2-T and 3/4-T relative fission rate values are seen to be independent of configuration. The small standard deviations of the means of the relative reaction rates for each location indicate that the precision of the SSTR results is within the quoted uncertainties.

As a further check on the consistency of the SSTR reaction rates, ratios were taken for equivalent locations in the different configurations. These data are contained in Table HEDL-7. For the PVS block, the reaction rate ratios are independent of location. Again, the standard deviations of the means are consistent with the experimental uncertainties of the data.

The relative reaction rate data of Tables HEDL-6 and HEDL-7, as well as the data of Table HEDL-3 indicate that all the PCA SSTR reaction rate measurements are self-consistent on a relative basis and that the measurements are reproducible within the stated experimental uncertainties on an absolute basis. Fission rate measurements made with SSTR can be compared with the corresponding measurements made with fission chambers.

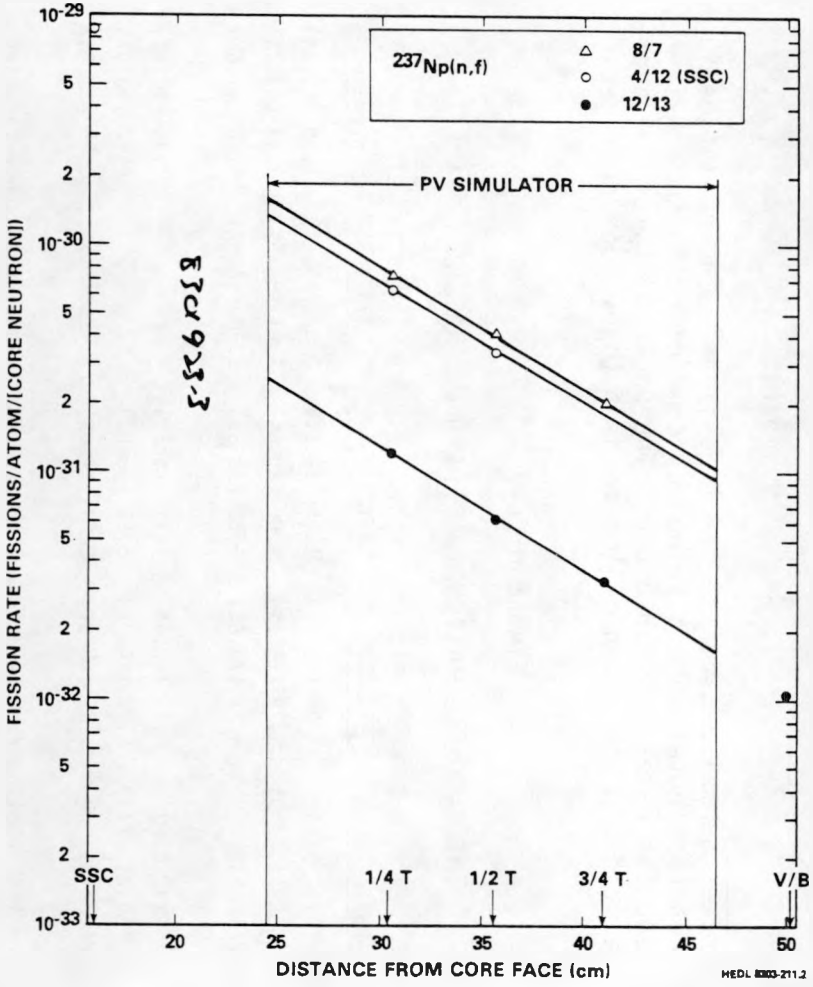

FIGURE HEDL-4. Radial Fission Rate Distributions for ^{237}NP in the PCA 8/7, 4/12 SSC, and 12/13 Configuratiion. Neg 8301923-3

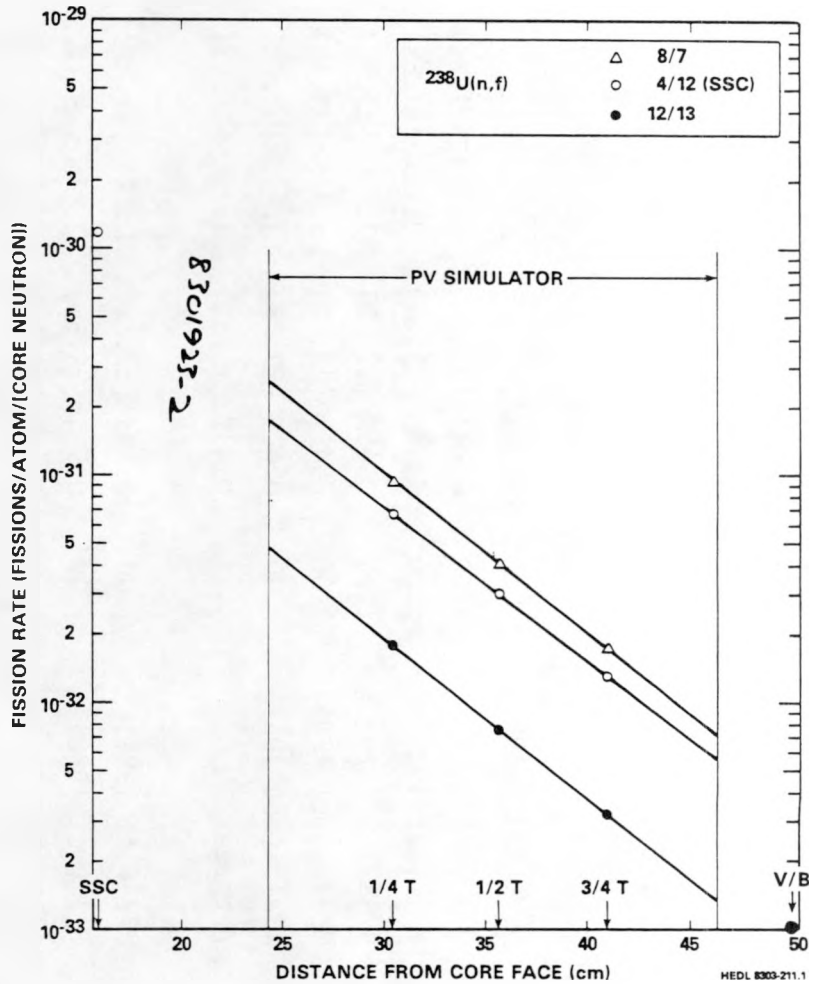

FIGURE HEDL-5. Radial Fission Rate Distributions for ^{238}U in the PCA 8/7, 4/12 SSC, and 12/13 Configurations. Neg 8301923-2

TABLE HEDL-6

RELATIVE REACTION RATES IN THE PCA PRESSURE VESSEL SIMULATOR

Isotope	Configuration	Location 1/4 T*	1/2 T	3/4 T
^{238}U	8/7 (Oct 1981)	1.00	0.442 (±3.7%)	0.193 (±3.7%)
	8/7 (Oct 1978)	1.00	0.443 (±3.8%)	0.187 (±3.6%)
	4/12 SSC	1.00	0.454 (±3.2%)	0.196 (±3.2%)
	12/13 (Oct 1981)	1.00	0.427 (±3.7%)	0.187 (±3.7%)
	12/13 (Nov 1981)	1.00	0.429 (±3.7%)	0.185 (±3.7%)
	Average	--	0.439 (±2.5%)	0.190 (±2.5%)
^{237}Np	8/7 (Oct 1981)	1.00	0.593 (±3.7%)	0.275 (±3.7%)
	8/7 (Oct 1978)	1.00	0.564 (±3.5%)	0.275 (±5.1%)
	4/12 SSC	1.00	0.549 (±3.5%)	---
	12/13 (Oct 1981)	1.00	---	0.278 (±3.7%)
	12/13 (Nov 1981)	1.00	0.524 (±6.4%)	0.281 (±4.7%)
	Average	--	0.558 (±5.2%)	0.277 (±1.0%)

*Reaction rates normalized to the 1/4 T position. Uncertainties in relative reaction rates were obtained by combining the uncertainties of reaction rates in quadrature. The uncertainty of the average is the standard deviation of the mean of the values averaged.

TABLE HEDL-7

INTER-CONFIGURATION REACTION RATE RATIOS

Isotope	Ratio	Location 1/4 T	1/2 T	3/4 T	Average
^{238}U	(8/7)/(4/12 SSC)	1.38 (±3.4%)	1.35 (±3.6%)	1.32 (±3.4%)	1.35 (±2.2%)
	(4/12 SSC)/(12/13)	3.78 (±3.5%)	3.99 (±3.5%)	4.01 (±3.5%)	3.93 (±3.2%)
	(8/7)/(12/13)	5.22 (±3.6%)	5.39 (±3.8%)	5.30 (±3.6%)	5.30 (±1.6%)
^{237}Np	(8/7)/(4/12 SSC)	1.14 (±5.3%)	1.17 (±5.9%)	---	1.16 (±1.8%)
	(4/12 SSC)/(12/13)	5.30 (±4.3%)	5.55 (±6.0%)	---	5.42 (±3.3%)
	(8/7)/(12/13)	6.06 (±5.8%)	6.51 (±7.6%)	5.92 (±5.5%)	6.16 (±5.0%)

*Uncertainties on the reaction rate ratios were obtained by combining the uncertainties of the reaction rates in quadrature. The uncertainty of the average is the standard deviation of the mean of the ratios averaged.

At present, pending the result of benchmark irradiations of the SSTR fissionable deposits, the SSTR results are reported as absolute fission rates. The fission chamber results, on the other hand, have been benchmark referenced, and the fission chamber results are reported as fission equivalent fluxes. In order to make direct comparisons between the SSTR and fission chamber results, the fission chamber data from (Mc81b) were converted into the corresponding reaction rates. These comparisons are contained in Tables HEDL-8 through HEDL-11.

For the PCA 12/13 configuration, the data of Tables HEDL-8 and HEDL-9 indicate that the SSTR results are lower than the fission chamber results by ~10%. The overall mean of the fission rate ratios from Table HEDL-8 is 0.902 ± 0.023 and from Table HEDL-9 is 0.896 ± 0.023. The mean of the eleven fission rate ratio values from both tables is 0.899 ± 0.022. The magnitude of the standard deviation of this mean (2.4%) is consistent with the experimental uncertainties, indicating good relative precision of the SSTR and fission chamber data but an absolute discrepancy (10%) that is not consistent with the quoted experimental uncertainties on the absolute fission rates.

The data for the PCA 8/7 configuration are contained in Table HEDL-9. The overall mean of these six fission rate ratios is 0.902 ± 0.023. Again, the relative precision is good, but an absolute 10% discrepancy exists between the SSTR and fission chamber data.

The data for the PCA 4/12 SSC configuration are contained in Table HEDL-11. The overall mean of these five fission rate ratios is 0.896 ± 0.034. Once again, the relative precision is consistent with the experimental uncertainties, but a 10% discrepancy in magnitude exists.

The similarity of the discrepancy for all three configurations suggests that the discrepancy is configuration-independent. The mean of all the fission rate ratios tabulated in Tables HEDL-8 through HEDL-11 is 0.897 ± 0.025.

In order to detect any reaction-dependent difference in the discrepancy, the fission rates have been ratioed separately for ^{237}Np and ^{238}U in Table HEDL-12. The discrepancy is consistently larger for ^{238}U (11%) than for ^{237}Np, (9%), and the ratio of the average discrepancy for ^{237}Np divided by that for ^{238}U is 1.024 ± 0.011. Although there is a great deal of overlap in the distributions of the individual SSTR/fission chamber ratios for ^{237}Np and ^{238}U, the difference appears to be real.

Although both the SSTR and fission chamber data sets are internally consistent and have good relative precision, an average 10% absolute bias exists between the two sets of data. A possible explanation for this bias is the fact that the void introduced by the fission chamber causes some uncertainty as to the effective position of the fission rate measurement. The fact that the fission chamber measurements are consistently higher would indicate that the fission chamber measurements correspond to a position closer to the core side of the void rather than the assigned central position (Mc81b).

TABLE HEDL-8

COMPARISON OF SSTR AND FISSION CHAMBER MEASURED FISSION RATES
FOR THE PCA 12/13 CONFIGURATION FOR NOVEMBER 1981

Isotope	Location	Fission Rate [(fissions per atom per core neutron) x 10^{32}] Fission Chamber		SSTR		SSTR/ Fission Chamber Ratio*
^{237}Np	1/4 T	12.55	(±2.9%)	11.8	(±3.6%)	0.940 ± 0.043
	1/2 T	7.045	(±3.1%)	6.19	(±5.4%)	0.879 ± 0.055
	3/4 T	3.690	(±3.1%)	3.32	(±3.3%)	0.900 ± 0.041
					Average	0.906 ± 0.031
^{238}U	1/4 T	1.943	(±3.0%)	1.75	(±2.7%)	0.901 ± 0.036
	1/2 T	0.8536	(±3.1%)	0.750	(±2.7%)	0.879 ± 0.036
	3/4 T	0.3546	(±3.1%)	0.323	(±2.7%)	0.911 ± 0.037
					Average	0.897 ± 0.016

*The uncertainties on individual ratios were obtained by combining the uncertainties on the SSTR and fission chamber measurements in quadrature. The uncertainty on the average is the standard deviation of the mean of the three ratios.

TABLE HEDL-9

COMPARISON OF SSTR AND FISSION CHAMBER MEASURED FISSION RATES
FOR THE PCA 12/13 CONFIGURATION FOR OCTOBER 1981

Isotope	Location	Fission Rate [(fissions per atom per core neutron) x 10^{32}] Fission Chamber		SSTR		SSTR/ Fission Chamber Ratio*
^{237}Np	1/4 T	12.55	(±2.9%)	11.6	(±3.3%)	0.924 ± 0.037
	3/4 T	3.690	(±3.1%)	3.23	(±3.3%)	0.875 ± 0.040
					Average	0.899 ± 0.035
^{238}U	1/4 T	1.943	(±3.0%)	1.74	(±2.7%)	0.896 ± 0.037
	1/2 T	0.8536	(±3.1%)	0.744	(±2.7%)	0.872 ± 0.036
	3/4 T	0.3546	(±3.1%)	0.324	(±2.7%)	0.914 ± 0.021
					Average	0.894 ± 0.021

*See footnote for Table HEDL-8.

TABLE HEDL-10

COMPARISON OF SSTR AND FISSION CHAMBER MEASURED FISSION RATES
FOR THE PCA 8/7 CONFIGURATION

Isotope	Location	Fission Rate [(fissions per atom per core neutron) x 10^{31}] Fission Chamber	SSTR	SSTR/ Fission Chamber Ratio*
^{237}Np	1/4 T	7.789 (±2.9%)	7.15 (±4.6%)	0.918 ± 0.050
	1/2 T	4.321 (±2.9%)	4.03 (±5.4%)	0.933 ± 0.057
	3/4 T	2.282 (±2.9%)	1.97 (±4.4%)	0.863 ± 0.045
			Average	0.905 ± 0.037
^{238}U	1/4 T	1.050 (±2.8%)	0.913 (±2.6%)	0.870 ± 0.033
	1/2 T	0.4575 (±3.0%)	0.404 (±2.9%)	0.883 ± 0.037
	3/4 T	0.1899 (±3.0%)	0.171 (±2.7%)	0.900 ± 0.036
			Average	0.884 ± 0.016

*See footnote for Table HEDL-8.

TABLE HEDL-11

COMPARISON OF SSTR AND FISSION CHAMBER MEASURED FISSION RATES
FOR THE PCA 4/12 SSC CONFIGURATION

Isotope	Location	Fission Rate [(fissions per atom per core neutron) x 10^{31}] Fission Chamber	SSTR	SSTR/ Fission Chamber Ratio*
^{237}Np	1/4 T	6.826 (±1.7%)	6.26 (±2.6%)	0.917 ± 0.031
	1/2 T	3.765 (±1.9%)	3.44 (±2.6%)	0.914 ± 0.029
			Average	0.915 ± 0.002
^{238}U	1/4 T	0.7845 (±1.8%)	0.660 (±2.4%)	0.841 ± 0.025
	1/2 T	0.3392 (±2.3%)	0.300 (±2.4%)	0.884 ± 0.029
	3/4 T	0.1409 (±2.6%)	0.130 (±2.4%)	0.923 ± 0.033
			Average	0.883 ± 0.041

*See footnote for Table HEDL-8.

TABLE HEDL-12

COMPARISON OF SSTR AND FISSION CHAMBER MEASURED FISSION RATES FOR ^{237}Np and ^{238}U

Configuration	SSTR/Fission Chamber Ratio ^{237}Np	SSTR/Fission Chamber Ratio ^{238}U
8/7	0.905 ± 0.037	0.884 ± 0.016
12/13 (Nov 81)	0.906 ± 0.031	0.897 ± 0.016
12/13 (Oct 81)	0.899 ± 0.035	0.894 ± 0.021
4/12 SSC	0.915 ± 0.002	0.883 ± 0.041
Average	0.908 ± 0.006	0.887 ± 0.007

In order to bypass absolute discrepancies and investigate the relative precision of the SSTR and fission chamber measurements, reaction rate ratios may be compared. Data were presented (see Table HEDL-6) to show that the relative reaction rates in the PVS 1/4-T, 1/2-T and 3/4-T locations are independent of PCA configuration for both ^{237}Np and ^{238}U. This was also demonstrated (Mc81b) using the data of Table 2.3.7 of that work. In order to compare the SSTR and fission chamber reaction rate slopes within the PVS block, data were taken from (Mc81b) and converted to the same form as Table HEDL-6 by normalizing to 1.00 at the 1/4-T location. These fission chamber relative fission rates averaged over the 8/7, 12/13, 4/12 SSC, 8/12 and 4/9 PCA configurations are compared with the average SSTR relative reaction rates in Table HEDL-13. Agreement for the 1/2-T location is excellent, being well within 1% for both ^{238}U and ^{237}Np. Since the discrepancy is in opposite directions for the two isotopes, the overall swing of 10% is beyond what can be accounted for by experimental uncertainty.

In order to investigate this discrepancy in the PVS gradients, all available PCA SSTR, fission chamber (Mc81b), and radiometric (Fa81a) threshold integral reaction rate data have been correlated in terms of an exponential attenuation formalism. The ratio between the 1/2-T and 1/4-T reaction rates R_F is assumed to depend on distance as follows:

$$R_F = \exp -\left(\frac{(\ln 2)S_F}{(S_{1/2})_F}\right) \qquad (1)$$

where:

S_F = Distance between 1/4-T and 1/2-T locations (5.2 cm)

TABLE HEDL-13

COMPARISON OF SSTR AND FISSION CHAMBER RELATIVE FISSION RATES IN THE PVS BLOCK

Isotope	Method of Measurement	Location 1/2 T	Location 3/4 T
^{237}Np	Fission Chamber	0.555 (±1.1%)	0.291 (±1.4%)
	SSTR	0.558 (±5.2%)	0.277 (±1.0%)
	Fission Chamber/SSTR	0.995	1.05
^{238}U	Fission Chamber	0.436 (±0.51%)	0.181 (±1.3%)
	SSTR	0.439 (±2.5%)	0.190 (±2.5%)
	Fission Chamber/SSTR	0.993	0.953

$(S_{1/2})_F$ = Effective half-thickness in front half of PVS block

R_F = Average ratio of 1/2-T and 1/4-T reaction rates (see Table HEDL-6)

Similar quantities R_B, S_B (5.4 cm), and $(S_{1/2})_B$ can be determined for the back half of the PVS block using the 3/4 T-to-1/2 T reaction rate ratio. The ratio of the two effective half-thicknesses $(S_{1/2})_F/(S_{1/2})_B$ is a measure of the expected departure of the attenuation in the PVS block from a true exponential stopping law. This ratio was plotted as a function of effective threshold energy (Zi79) for the available integral reaction rate data in Figure HEDL-6. As expected, ratios close to one are found for reactions with higher threshold energy, indicating that an exponential attenuation model is obeyed more closely for higher threshold energies.

At lower energies, the SSTR ^{237}Np(n,f) ratio at an effective threshold of 0.575 MeV and the radiometric ^{103}Rh(n,n') ratio (Fa81a) at an effective threshold of 0.760 MeV indicate departures from pure exponential attenuation. The ^{237}Np(n,f) fission chamber data appear to be inconsistent with both the ^{237}Np(n,f) SSTR data and the ^{103}Rh(n,n') radiometric data. Although the reason for this discrepancy is unknown at this time, it probably has the same cause as the discrepancies noted in Table HEDL-13.

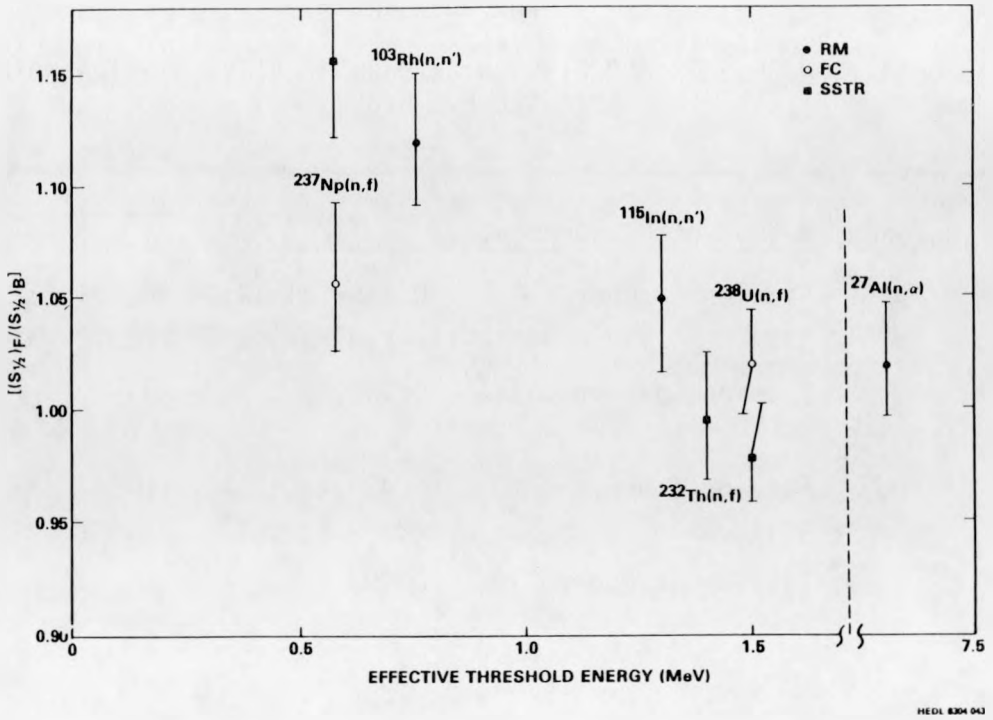

FIGURE HEDL-6. Front-to-Back Ratios of the Effective Half-Thicknesses for Integral Reaction Rates in the PVS Block as a Function of Effective Threshold Energy. Neg 8302506-1

Conclusions

Final SSTR fission rates were presented for the PCA 8/17, 12/13, and 4/12 SSC configurations. These measurements were found to be reproducible and self-consistent both on an intra- and inter-configuration basis. On an absolute basis, a constant 10% discrepancy exists between the SSTR fission rates and the National Bureau of Standards (NBS) fission chamber fission rates. Attempts to resolve this discrepancy involve:

- Benchmark referencing irradiations of the SSTR foils. These irradiations are nearing completion and will enable reporting of the SSTR data as fission equivalent fluxes. Fission chamber measurements are already reported on this basis.
- Re-investigation of the perturbation effect caused by the introduction of a fission chamber void. Measurements have been carried out at PCA to measure radiometric as well as SSTR fission rates both inside the NBS fission chamber and in a void free environment. Analysis of these measurements is now in progress.

With the few exceptions noted, the relative precision of the SSTR and fission chamber measurements is consistent with the experimental uncertainties. The apparent discrepancy between the attenuation of the SSTR and fission chamber $^{237}Np(n,f)$ fission rates in the PVS block may be resolved by:

- Investigating additional integral reaction rate data (SSTR, fission chamber, and radiometric) from PCA and NESDIP PVS irradiations.
- Making use of Poolside Facility (PSF) and Simulated Dosimetry Measurement Facility (SDMF) reaction rate data (SSTR and radiometric) from the PVS block. Particularly important in this regard will be the results of the $^{93}Nb(n,n')$ irradiations planned for the fourth SDMF test. The threshold for this reaction is less than that for $^{237}Np(n,f)$ and would be a useful addition to Figure HEDL-6.
- Using available nuclear emulsions scanned in the integral mode to define integral reaction rates with thresholds corresponding to less than 0.5 MeV.

Expected Accomplishments

Results of the recent radiometric SSTR fission chamber comparison at PCA will be available and the effect of the fission chamber void will be evaluated.

Preliminary NESDIP and VENUS SSTR fission rates will be reported.

B. EMBRITTLEMENT OF COMPRESSION SPECIMENS IRRADIATED IN THE SSC-1 AND SSC-2 CAPSULES OF THE PSF EXPERIMENT

G. L. Guthrie (HEDL), K. Carlson and G. R. Odette (UCSB)

Objective

The immediate objective of this work is to measure the irradiation-induced increase in the room temperature yield strength of specimens made from pressure vessel (PV) steel alloy material and irradiated in the SSC-1 and SSC-2 capsules of the PSF experiment. The ultimate objective is to provide knowledge that can be used to predict fracture toughness at points inside the PV wall of an operating power plant. Another important objective by LWR-PV-SDIP participants is to use these and other tensile specimen results to help evaluate candidate models for changes in the yield strength of low alloy steel used in nuclear reactor vessels. The intent is to provide auxiliary information for model and trend curve development even through they are not necessarily proportional to radiation embrittlement damage.

Summary

Room temperature compression tests were conducted on small cylindrical compression specimens manufactured from eleven different PV steel alloys. For each of the eleven alloys, tests were performed on unirradiated control specimens and also on specimens irradiated in the SSC-1 and SSC-2 capsules of the Poolside Facility (PSF) experiment. The measured increase in yield strength correlates with copper content, but a copper saturation effect appears to be present. The irradiation-induced increase in yield strength correlates with dpa exposure, and the functional relation shows a stronger exposure dependence than usually found between Charpy shift and fluence in surveillance irradiations. In particular, the exponent of the fluence term is ∿0.45 in contrast to the ∿0.3 value found for Charpy trend curve relations derived from surveillance data. This may indicate a rate effect since the dose rate was higher than for a power reactor surveillance irradiation. A similar change in functional relationship has been found for the SSC-1 and SSC-2 Charpy data, but the scatter in the Charpy data precludes any firm conclusions. These SSC and other yield strength results are currently being used by HEDL, UCSB, S.P. Grant and S. Earp (Gr84) and other LWR-PV-SDIP participants to aid in refining RT_{NDT} trend curves for welds, forgings, and plates to help improve the accuracy of the prediction of the EOL metallurgical condition of the PV and to further ensure the safety of PWR and BWR power plants.

Accomplishments and Status

This report is a follow-up and extension of a previous report (Ca81) in the same LWR-PV-SDIP series. The earlier work was a report on the compression test results from the cylindrical compression specimens irradiated in the SSC-1 capsule of the PSF. The present report gives the results of measurements on specimens from the SSC-2 experiment and combines the two sets of data in the analysis.

The specimens consisted of small solid cylinders manufactured in two sizes. One size, referred to as Electric Power Research Institute (EPRI) cylinders was 0.157 inches in diameter and 0.392 inches long. The other size, referred to as Naval Research Laboratory (NRL) cylinders, was 0.250 inches in diameter and 0.410 inches long. The specimens were irradiated in the SSC-1 and SSC-2 capsules in the PSF experiment and tested in a subpress compression fixture discussed in a previous report (Mc81a). Unirradiated control specimens were also tested to determine the irradiation-induced increase in the 0.2% offset yield strength. The two irradiations produced exposures of $\sim 2.69 \times 10^{19}$ n/cm^2 (E > 1 MeV) for the center of the SSC-1 capsule and approximately twice that amount for the center of the SSC-2 capsule. The corresponding dpa exposures were 0.0403 dpa for the SSC-1 capsule and approximately twice that amount for the SSC-2. The SSC-1 exposure values quoted above are the result of preliminary unpublished work by R. L. Simons. The irradiation was conducted in holders described in (Mc80a).

The individual compression specimens cylinder did not receive identical neutron exposures because of the variation of the neutron field as a function of position within the capsule. This variation has been accounted for in the analysis.

The PSF irradiation is more completely described in (Mc82a). However, the SSC-1 and SSC-2 capsules were irradiated sequentially in time at a location intended to simulate the surveillance position in an operating PWR. The SSC-1 irradiation was for ~45 days (3842106 s), and the SSC-2 irradiation was for approximately twice that length of time (7761860 s). The flux was $\sim 6 \times 10^{12}$ n/cm^2/s (E > 1.0 MeV) in the PSF SSC location compared to $\sim 6 \times 10^{10}$ n/cm^2/s for the surveillance capsule of a four-loop Westinghouse PWR. Thus, there is some question of a rate effect.

The eleven alloys were received from two sources. Most of the material was collected by R. Wullaert of Fracture Control Corporation (FCC) with the help of G. R. Odette of the University of California at Santa Barbara (UCSB) working under EPRI funding in a cooperative effort with HEDL. Some of the material was supplied to HEDL by J. R. Hawthorne of NRL. The materials are described in Table HEDL-14. The chemical compositions are given in Table HEDL-15. Table HEDL-16 gives the sample ID code, Ni and Cu content, 0.2% offset yield strength, yield strength increase, and dpa exposure for each specimen.

An attempt has been made to fit the data to equations of the type

$$\Delta(\sigma_y) = f_1 \text{ (chem)} \cdot f_2 \text{ (neutron dose)} \qquad (1)$$

using dpa as the dose parameter. To judge the success of the fitting procedure, a first crude fit was accomplished using $\Delta\sigma_y = c$, where c is the average shift. This resulted in a standard deviation of 8.83 KSI.

TABLE HEDL-14

DESCRIPTION OF COMPRESSION CYLINDER SPECIMENS

HEDL Material* Description	Source and Source Code	Dimensions	Irradiation Locations	Material Description
BG 1	EPRI 2bE			A508-2 Forging. 1/4-T depth. EPRI received from B&W.
BG 2	EPRI EP24			Hi Cu-Hi Shelf. Linde 0091 weld on A533B-1 base. EPRI/West/NRL Source.
BG 3	EPRI 1bA			Originally from NRL. Surface of HSST-02 A533B plate.
BG 4	EPRI NP 933-1-150 Heat Code 1mQ			EPRI archive. E8018-03 electrode 1 mQMMA weld on an SA533B-1 base. Weld by Combustion Engineering (CE), plate and weld given to EPRI.
BG 5	EPRI 1bA			Originally from NRL. Broken halves of 1TCT specimens differ from BG 3 in that it is in the 1/4-T location. HSST-02 A533B plate.
BG 6	EPRI 4bA			Originally from NRL. Broken halves of 1TCT specimens A302B ASTM heat, samples from 1/4-T positions.
BG 7	EPRI 7bB			A537-2 material sent to EPRI from General Atomic. Manufactured by Lukens. Broken halves of 1TCT specimens.
27 N	NRL 27N	0.175 in. diam. x 0.392 in. long cylinder	Located in Charpy carriers Fig (21)** in LRI, LR2 & RR1 positions in SCC-1, SCC-2, 0 T, 1/4 T, 1/2 T & VB.	A533B plate, cross rolled, 0.13% Cu, 1/4-T position.
29 N	NRL 29N			A533B plate, cross rolled, 0.03% Cu, 1/4-T position.
3 PT	NRL-3PT	0.250 in. diam. x 0.410 in. long cylinder	Located in block holes (Fig 21)** 38A, 38F, 39A, 36F, 36E, 37F of SSC-1, SSC-2, 0 T, 1/4 T, & 1/2 T	HSST-03 A533B plate. 1/4-T location cut directly from plate.
F 23	NRL-F23			ASTM Reference heat. 1/4-T location cut directly from A302B plate.

*Accumulation of materials was done principally by Fracture Control Corporation (R. Wullaert).
**See Reference (Ca81).

TABLE HEDL-15

COMPRESSION CYLINDER CHEMISTRY (wt%)

HEDL Designation	C	Mn	P	S	Si	Ni	Cr	Mo	V	Cu	NDT (°C)	RT_{NDT} (°C)	Upper Shelf (J)
BG 1	0.23	0.73	0.007	0.009	0.31	0.65	0.41	0.59	0.054	0.04	-7	-7	182.
BG 2	0.11	1.57	0.007	0.011	0.23	0.64	0.02	0.48	0.005	0.36	---	---	---
BG 3	0.23	1.55	0.009	0.014	0.2	0.67	0.04	0.53	0.003	0.16	-30	-15	144.
BG 4	0.1	1.11	0.007	0.01	0.4	1.06	0.01	0.34	0.006	0.02	-57	-57	212.
BG 5	0.23	1.55	0.009	0.014	0.2	0.67	0.04	0.53	0.003	0.16	---	---	---
BG 6	0.23	1.47	0.013	0.024	0.26	0.17	0.05	0.52	0.004	0.2	-18	---	61.
BG 7	0.21	1.25	0.007	0.007	0.170	0.210	0.250	0.08	0.005	0.12	---	---	138.
27 N	0.18	1.29	0.008	0.008	0.20	0.56	0.06	0.51	---	0.13	---	---	---
29 N	0.18	1.27	0.008	0.007	0.20	0.55	0.06	0.52	---	0.03	---	---	---
3 PT	0.20	1.26	0.011	0.018	0.25	0.56	0.10	0.45	---	0.10	---	---	---
F 23	0.23	1.47	0.013	0.024	0.26	0.17	0.05	0.52	0.004	0.20	---	---	---

TABLE HEDL-16

COMPRESSION CYLINDER SPECIMENS

Specimen ID	Neutron Exposure (10^{-2} dpa)	Cu (wt%)	Nu (wt%)	Irradiated 0.2% Offset Ys (KSI)	Alloy	Unirradiated Control Ys (KSI)	Shift in Ys (KSI)
BU	5.362	0.36	0.64	106.004	BG2	79.099	26.905
BR	5.475	0.36	0.64	107.788	BG2	79.099	28.689
ER	2.560	0.16	0.67	92.389	BG3	77.319	15.070
EN	2.625	0.16	0.67	93.773	BG3	77.319	16.454
FF	5.302	0.16	0.67	107.925	BG3	77.319	30.606
EV	5.171	0.16	0.67	108.560	BG3	77.319	31.241
EU	5.237	0.16	0.67	106.274	BG3	77.319	28.955
FV	2.498	0.02	1.06	74.100	BG4	69.898	4.202
FU	2.528	0.02	1.06	74.938	BG4	69.898	5.040
HVB	4.303	0.20	0.17	88.014	F23	68.010	20.004
HVL	4.388	0.20	0.17	87.197	F23	68.010	19.187
HU1	8.600	0.20	0.17	95.748	F23	68.010	27.738
HXB	8.691	0.20	0.17	99.200	F23	68.010	31.190
HTR	4.338	0.10	0.56	80.318	3PT	66.005	14.313
HUX	4.402	0.10	0.56	78.839	3PT	66.005	12.834
HR4	8.855	0.10	0.56	90.655	3PT	66.005	24.650
HT6	8.763	0.10	0.56	90.655	3PT	66.005	24.650
NT	2.563	0.13	0.56	82.648	27N	66.510	16.138
NX	5.177	0.13	0.56	87.702	27N	66.510	21.192
NV	5.223	0.13	0.56	87.002	27N	66.510	20.492
NR	2.586	0.13	0.56	77.520	27N	66.510	11.010
F2	5.046	0.02	1.06	74.736	BG4	69.898	4.838
F1	5.106	0.02	1.06	77.680	BG4	69.898	7.782
J4	2.415	0.16	0.67	89.280	BG5	68.382	20.898
J5	2.444	0.16	0.67	87.770	BG5	68.382	19.388
J6	4.832	0.16	0.67	101.631	BG5	68.382	33.249
J7	4.878	0.16	0.67	102.528	BG5	68.382	34.146
KO	2.489	0.20	0.17	86.264	BG6	67.884	18.380
LA	2.512	0.20	0.17	84.793	BG6	67.884	16.909
LK	5.074	0.20	0.17	95.440	BG6	67.884	27.556
LB	4.982	0.20	0.17	93.021	BG6	67.884	25.137
MU	2.586	0.12	0.21	78.731	BG7	62.315	16.416
MT	2.563	0.12	0.21	77.346	BG7	62.315	15.031
MV	5.137	0.12	0.21	82.438	BG7	62.315	20.123
M1	5.177	0.12	0.21	83.105	BG7	62.315	20.790
AE	2.381	0.04	0.65	76.415	BG1	70.844	5.571
AF	4.930	0.04	0.65	80.167	BG1	70.844	9.323
AK	4.809	0.04	0.65	77.761	BG1	70.844	6.917
AB	2.412	0.04	0.65	72.317	BG1	70.844	1.473
BP	2.655	0.36	0.64	102.528	BG2	79.099	23.429
BL	2.711	0.36	0.64	102.911	BG2	79.099	23.812
PV	2.503	0.03	0.55	75.195	29N	67.453	7.742
P1	2.472	0.03	0.55	75.965	29N	67.453	8.512
P3	5.056	0.03	0.55	77.741	29N	67.453	10.288
P5	4.993	0.03	0.55	78.018	29N	67.453	10.565

Previous work by G. R. Odette (Od83a) has shown that there is a proportionality relationship between irradiation-induced increase in yield strength and irradiation-induced shift in 41-J Charpy transition temperature. In the present study, the restricted quantity of the data seemed to advise against attempting separate analyses for weld and plate specimens. Consequently, the weld and plate data were combined. In view of the observation by Odette (Od83a) cited above, a statistical fit was attempted using

$$\Delta\sigma_y = \chi(1) \cdot f_{ctc}\ (\text{chemistry, dose}) \qquad (2)$$

where f_{ctc} is a Charpy trend curve formula previously developed (Gu82c) using combined plate and weld data from surveillance irradiations, and $\chi(1)$ is an adjustable parameter. The fit thus obtained was very little improved over the result obtained using a single average. Subsequent attempts using more flexibility in the exposure exponent gave minor improvements. Analysis of the residuals showed that the original (Charpy curve) fluence exponent was too low for application to the SSC yield strength data. Further attempts at statistical fits involved using linear combinations of Cu and Ni contents in the chemical factor of Eq. (1). No great benefit was obtained by including the nickel content as an independent variable. When a simple function linear in copper was used as the chemistry factor, analysis of the residuals indicated a copper saturation effect.

Consequently, the functions

$$\Delta\sigma_y = [\chi(1) + \chi(2)\ \ Cu] * [dpa\ **\ \chi(3)] \qquad (3)$$

and

$$\Delta\sigma_y = [\chi(1) + \chi(2) \cdot Cu^{0.25}] * [dpa\ **\ \chi(3)] \qquad (4)$$

were used in fitting procedures, where ** denotes exponentation, and $\chi(1)$, $\chi(2)$ and $\chi(3)$ are adjustable parameters. The resultant standard deviations were 4.28 and 4.02 KSI, respectively. The exposure exponents were 0.462 ± 0.08 and 0.45 ± 0.07 for the two cases. This is noticeably higher than the (0.25 - 0.30) values found in Charpy surveillance studies. The flux rate in the SSC position of the PSF was $\sim 6 \times 10^{12}$ n/cm²/s compared to $\sim 6 \times 10^{10}$ n/cm²/s for the PWR surveillance capsules. To check the possibility of a rate effect, the Charpy data of J. R. Hawthorne was plotted and shifts were determined for the 41-J transition temperature. This was done on a crude basis with no consideration being given to the variation of flux with position in the capsule. The resultant shifts were fitted to separate functions of the type

$$\Delta T = A \cdot (\phi t)^N \qquad (5)$$

for each of the six Charpy specimen alloys of the PSF. The six values of N were averaged and produced N = 0.46, but with an uncertainty much larger than for the exponent found in the compression study. The high value of the exponent "N" from the preliminary PSF SSC Charpy data analysis precludes

ruling out a rate effect as at least a partial explanation of the high value of the dose exponent in the compression test formulas. The copper saturation effect is consistent with the result already noted in the previous report (Ca81) on the SSC-1 specimens. It is also consistent with results of Charpy trend curve studies (Gu83). The effect of nickel was less than expected.

Expected Future Accomplishments

Testing and analysis of remaining compression specimens from the 0-T, 1/4-T, and 1/2-T positions will be performed in the next six month period. It is expected that these new SPVC in-vessel-wall yield strength results will be combined with the previous SSC-1 and SSC-2 (as well as other) results and will be used by HEDL, UCSB, S. P. Grant and S. L. Earp (Gr84) and other LWR-PV-SDIP participants to aid in refining RT_{NDT} trend curves for welds, forgings, and plates to help improve the accuracy of the prediction of the EOL metallurgical condition of the PV and to further ensure the safety of PWR and BWR power plants.

C. NONDESTRUCTIVE DETERMINATION OF REACTOR PRESSURE VESSEL NEUTRON EXPOSURE AND TRACE CONSTITUENTS

R. Gold, W. N. McElroy and J. P. McNeece (HEDL), and B. J. Kaiser (GE)

Objective

To develop an independent method of measuring the neutron exposure of light water reactor (LWR) pressure vessels (PV). A new neutron dosimetry method that complements and extends conventional passive neutron dosimetry for PV surveillance in LWR power plants has been developed and is being evaluated. This new method is expected to improve the accuracy of LWR-PV neutron exposure determinations, especially for power plants that have not generated adequate surveillance data throughout their operating lifetime.

Summary

A nondestructive method for determinating reactor PV neutron exposure is advanced. It is based on the observation of characteristic gamma-rays emitted by activation products in the PV with a unique continuous gamma-ray spectrometer. This spectrometer views the PV through appropriate collimators to determine the absolute emission rate of these characteristic gamma-rays, thereby ascertaining the absolute activity of given activation products in the PV. These data can then be used to deduce the spatial and angular dependence of neutron exposure at regions of interest in the PV. In addition, this method can be used to determine the concentrations of different constituents in the PV by measuring the absolute flux of characteristic gamma-rays from radioactivity induced in these constituents through neutron exposure. Since copper concentration may be a crucial variable in radiation-induced embrittlement of PVs, the ability of this method to measure copper concentrations in base metal and weldments is examined.

Accomplishments and Status

Introduction

Neutron-induced radiation damage experienced by the pressure vessel of a power reactor can be a controlling factor in defining the effective life of plant operation. As a consequence, methods of quantifying the neutron exposure fluence of reactor PVs are of worldwide interest. Therefore, a new nondestructive method of reactor PV neutron dosimetry based on the observation of characteristic gamma-rays emitted by activation products in the PV with a unique Si(Li) Compton continuous gamma-ray spectrometer is advanced.

The ability to measure complex gamma-ray continua in reactor environments through Compton recoil gamma-ray spectrometry is well established (Go80d, Go81c,Go82b). On this basis, the general applicability of continuous gamma-ray spectrometry for neutron dosimetry has already been described in (Go78b). This method is based upon the complementarity of the components of a mixed radiation field (Go70a). Neutron and gamma-ray components possess a

strong interrelationship, particularly for mixed radiation fields in reactor environments. This interrelationship is manifested through the existence of intense gamma-ray peaks that lie above the gamma continuum at characteristic and identifiable gamma-ray energies.

Actually, in-situ continua in reactor environments possess many peaks observed above the general level of the continuum. Furthermore, each of these peaks can be analyzed separately to determine absolute activity concentrations within the pressure vessel. Since these different peaks arise from neutron reactions with the constituent isotopes of the pressure vessel, a potential to produce considerably more information exists. For example, peaks in Si(Li)-observed gamma continua arise from different neutron reaction cross sections so that absolute Si(Li) gamma-ray data can be used the same way radiometric dosimetry data are analyzed with unfolding or least-squares adjustment codes to infer neutron energy spectral information. On the other hand, some of these peaks can be analyzed to determine the concentration levels of different PV constituents. Of particular interest are those constituents which may play a significant role in the neutron-induced embrittlement of PVs, such as copper.

Reactor Pressure Vessel Neutron Dosimetry -- Recent work for Three Mile Island Unit 2 (TMI-2) reactor recovery (Go83b,Mc83c) has demonstrated that this unique Si(Li) Compton gamma-ray spectrometer can be operated in very intense gamma fields. In fact, these efforts demonstrated that fields of up to roughly 2000 R/h could be accommodated, with shielded collimators of appropriate design. In LWR-PV neutron dosimetry, measurements could be conducted on both sides of the PV, depending on accessibility. For example, on the core side of the PV, the shielded Compton spectrometer could be placed in a corner fuel assembly location to measure the maximum exposure experienced by the PV. Measurements on the other side, i.e., in the reactor cavity, would have the advantage of reduced background. Owing to count rate limitations, measurements on the core side of the PV would have to be carried out with the reactor shut down. In the reactor cavity, however, measurements may be possible at low reactor power depending on the collimator size that can be used within the spatial constraints of the cavity.

The general configuration for such reactor cavity measurements is shown in Figure HEDL-7. Here the Si(Li) Compton spectrometer views the PV through a collimator shield, which possesses an aperture of diameter d_1 and a length x_1. The absolute flux intensity of a characteristic gamma-ray observed at energy ε_0, $I_1(\varepsilon_0)$, is given by

$$I_1(\varepsilon_0) = \int_0^T A(s)e^{-\mu(\varepsilon_0)s}\Omega(s)ds \quad . \tag{1}$$

where A(s) is the absolute activity per unit volume, including appropriate branching ratios, at a depth s in the PV. The depth variable s is measured from the outer surface of the PV as shown in Figure HEDL-7.

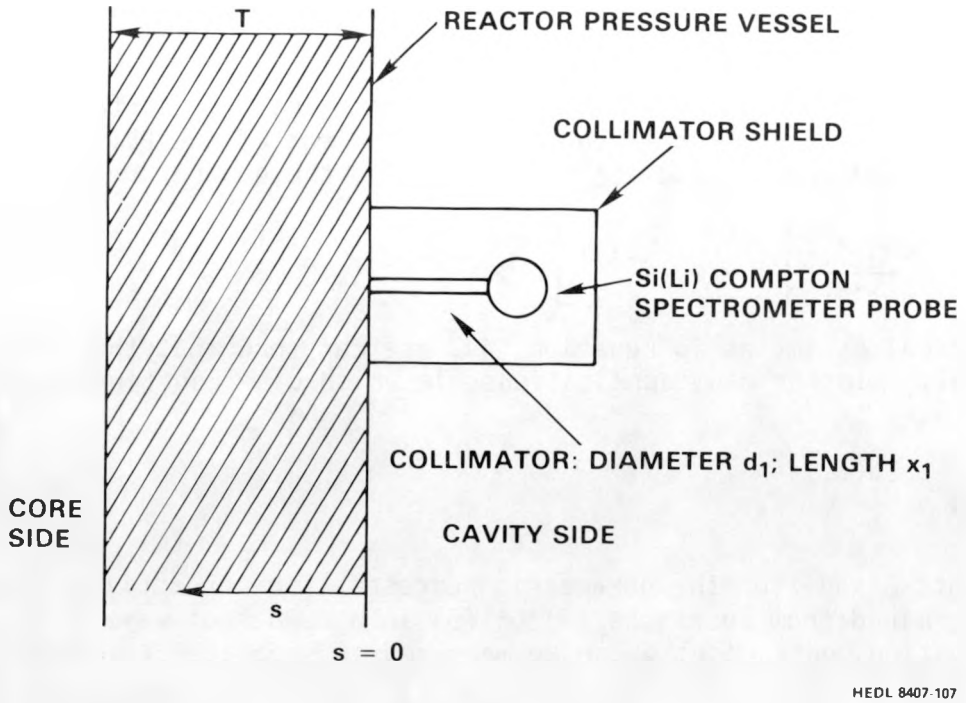

FIGURE HEDL-7. Overhead View of Reactor Cavity Measurements with Continuous Gamma-Ray Spectrometer.

At a depth s, $\Omega(s)$ is the solid angle projected through the collimator aperture and $\mu(\varepsilon_0)$ is the attenuation coefficient of the PV for gamma-rays of energy ε_0. The solid angle $\Omega(s)$ is given by

$$\Omega(s) = \frac{1}{4\pi} \int \frac{dA}{r^2} = \frac{1}{4\pi} \int_0^{\alpha_1} r d\theta \int_0^{2\pi} \frac{r \sin \theta d\phi}{r^2},$$

where $\alpha_1 = \tan^{-1} (d/2x_1)$ is the half angle of the collimator, so that

$$\Omega(s) = \frac{1 - \cos \alpha_1}{2} \qquad (2)$$

Since $\Omega(s)$ is independent of s and is a function of only the collimator property α_1, it can be identified as $\Omega(\alpha_1)$. Use of the geometric solid angle is an assumption to be explored in greater detail in future work, which will describe the very first application of this method in the BR-3 reactor at the CEN/SCK laboratory in Mol, Belgium.

The spatial dependence of the activity density A(s) has been shown to possess exponential behavior (Mc81), so that to a reasonable approximation one can write

$$A(s) = Ce^{\lambda s} \quad . \tag{3}$$

where C is a constant, i.e., C = A(o), that represents the surface activity density and λ is the neutron attenuation coefficient of the PV. Using Equations (2) and (3) in Equation (1), one finds the quadrature result

$$I_1(\varepsilon_o) = \frac{C\Omega(\alpha_1)}{(\mu-\lambda)}\left[1 - e^{-(\mu-\lambda)T}\right] \quad . \tag{4}$$

Using numerical estimates in Equation (4), one can show that the exponential term is negligible for many applications, in which case Equation (4) reduces simply to

$$I_1(\varepsilon_o) = \frac{C\Omega(\alpha_1)}{\mu-\lambda} \quad . \tag{5}$$

The constants C and λ of the parametric representation of activity density can be determined from Equations (4) or (5) in a number of ways. The neutron attenuation coefficient λ can be measured in separate PV benchmark field calibration experiments, such as the LWR-PV mockups studied in the pool critical assembly (PCA) (Mc81). Using the value of λ, Equation (4) or (5) can be solved directly for C. On the other hand, both parameters, C and λ, can be regarded as unknown, in which event an additional measurement is required.

Consider, therefore, a second measurement with a different collimator of solid angle $\Omega(\alpha_2)$, which makes an angle θ with respect to the normal of the PV surface. Using the above results, it can be shown for this case that

$$I_2(\varepsilon_o) = \frac{C\Omega(\alpha_2)}{(\mu-\lambda_2)}\left[1 - e^{-(\mu-\lambda_2)T_2}\right] \quad , \tag{6}$$

where $\lambda_2 = \lambda \cos\theta$, (7a)

and $T_2 = T/\cos\theta$. (7b)

Since $\lambda_2 \leq \lambda$, the exponential term can be neglected for many applications so that

$$I_2(\varepsilon_o) = \frac{C\Omega(\alpha_2)}{\mu-\lambda_2} \quad . \tag{8}$$

Taking the ratio of Equation (5) by Equation (8), one can write

$$\frac{\mu-\lambda_2}{\mu-\lambda} = \delta \quad , \tag{9a}$$

where $\delta = \left[\frac{I_1(\varepsilon_0)}{I_2(\varepsilon_0)}\right]\left[\frac{\Omega(\alpha_2)}{\Omega(\alpha_1)}\right]$. (9b)

The constant δ can be determined in terms of the Si(Li) gamma-ray spectrometer results, $I_1(\varepsilon_0)$ and $I_2(\varepsilon_0)$, obtained with the two different collimators. Consequently, use of Equation (7a) in Equation (9a) provides a relation that can be solved for λ. One finds

$$\lambda = \mu\left(\frac{\delta - 1}{\delta - \cos\theta}\right) \quad . \tag{10}$$

This value of λ can then be used in Equation (5) or Equation (8) to determination C.

The more general result, which follows from Equations (4) and (6), is

$$\left(\frac{\mu-\lambda_2}{\mu-\lambda}\right)\left[\frac{1 - e^{-(\mu-\lambda)T}}{1 - e^{-(\mu-\lambda_2)T_2}}\right] = \delta \quad , \tag{11}$$

where δ is again the constant given in Equation (9b). Equation (11) is a transcendental relation that can be solved for λ iteratively. In fact, the iterative process would start with the approximate solution given by Equation (10). Having determined λ iteratively, Equations (4) or (6) can be used to find C.

An additional point that must be stressed is the advantage of reduced background that arises for measurements conducted at an angle θ with respect to the normal to the PV surface. Here the angle θ can be chosen so that the collimated spectrometer no longer directly views leakage radiation from the core that penetrates through the PV. Consequently, measurements can be carried out with two different collimators which make angles θ_1 and θ_2, respectively, with respect to the normal to the PV surface. Under these conditions:

$$I_1(\varepsilon_0) = \frac{C\omega(\alpha_1)}{\mu-\lambda_1}\left[1 - e^{-(\mu-\lambda_1)T_1}\right], \tag{12}$$

and $$I_2(\varepsilon_0) = \frac{C\omega(\alpha_2)}{\mu-\lambda_2}\left[1 - e^{-(\mu-\lambda_2)T_2}\right], \tag{13}$$

Using these results, Equations (10) and (11) generalize to

$$\lambda = \mu\left(\frac{\delta - 1}{\delta\cos\theta_1 - \cos\theta_2}\right) \quad , \tag{14}$$

$$\text{and} \quad \left(\frac{\mu-\lambda_2}{\mu-\lambda_1}\right)\left[\frac{1 - e^{-(\mu-\lambda_1)T_1}}{1 - e^{-(\mu-\lambda_2)T_2}}\right] = \delta, \tag{15}$$

respectively. Here δ is again given by Equation (9b) and

$$\begin{aligned} \lambda_1 &= \lambda \cos \theta_1 \\ \lambda_2 &= \lambda \cos \theta_2 \\ T_1 &= T/\cos \theta_1 \\ T_2 &= T/\cos \theta_2 \end{aligned} \tag{16}$$

One can easily show that Equations (14) and (15) obey the correct limiting condition for $\theta_1 \to 0$, reducing to Equations (10) and (11), respectively. As before, the solution of λ given by Equation (14) can be used in the approximations obtained from Equations (12) or (13); i.e., when the exponential term is neglected in these equations, to provide C. In an analogous manner, the more general result can be obtained by using the iterative solution of λ, found from Equation (15), in either Equation (12) or (13) to provide C.

It must be noted that limitations on accessibility do exist for the collimated Si(Li) spectrometer. For certain reactor designs, the reactor cavity is too small to permit insertion of the collimated spectrometer. On the core side, the thermal shield, pad, or barrel may lie between the collimated spectrometer and the PV. In this case, the method is actually applied to the specific configuration viewed by the collimator. Often the collimated Si(Li) spectrometer can be inserted into reactor instrument tubes to allow a view of the PV. In fact, for the very first application of this method in the BR-3 reactor, the Si(Li) spectrometer was located in an instrument tube. The advantage of viewing the bare PV surface lies in the direct quantification of activity within the PV, so that neutron dosimetry for the PV can be performed without the need for extrapolation.

Advantages

- This method is nondestructive.
- This method can be applied to very localized regions of the PV. For example, neutron exposure of PV weldments can be mapped as a function of position.
- Direct observation of steel-induced PV radioactivities eliminates the need for extrapolating of data such as is required in customary PV surveillance work.

Measurement of Reactor PV Constituent Concentrations -- The concentration of copper is a crucial variable governing radiation-induced embrittlement of PV steels (Mc84). Hence, copper concentration is a critical factor in end-of-

life determinations for nuclear power PVs. Copper concentration is not only important in PV base metals, but is of particular significance in PV weldments. Consequently, copper concentration is used to illustrate this method of measuring PV constituent concentrations.

Owing to constraints that arise from the gamma-ray field intensity and limited spatial access, it will be assumed that measurements must be conducted with the reactor shut down. To determine such PV copper concentrations, measurements would have to begin soon after power reactor shutdown. Two radionuclides are produced by neutron capture on natural copper, namely copper-64 and copper-66. While the short half-life of copper-66, only 5.1 min., makes this radionuclide impractical to use in this application, copper-64 possesses a 12.7-h half-life and consequently can be used for PV observations. With advance preparations made inside reactor containment, it should take only a few hours after shutdown to set up the collimated Si(Li) Compton spectrometer for measurement of PV gamma spectra.

Two candidate gamma-rays in the copper-64 decay exist, namely the 1.346-MeV transition from the low intensity electron capture branch (0.6%) and annihilation radiation at 0.511 MeV from the position decay branch (19%). The analysis given above for peak intensities above the general level of the gamma continuum is applicable for these two gamma-rays from copper-64. In this analysis, the absolute activity per unit volume A(s), at a given depth s in the PV, is quantified in the exponential form given in Equation (3), where C and λ are determined by the measurements.

Gamma-ray peaks due to the decay of iron-59 will exist in the very same spectral measurements. The iron-59 radionuclide (45.5- day half-life) is produced by neutron capture on natural iron, whereas iron-58 exists at a level of 0.3%. Two candidate peaks from iron-59 exist, namely the transition at 1.292 MeV (45%) and the transition at 1.099-MeV (53%). Again, following the same analysis given above, the iron-59 activity per unit volume A(s) can be quantified. Consequently, copper-64 activity per unit volume can be written

$$A_1(s) = C_1 d^{\lambda s} \quad , \tag{17}$$

and for the iron-59 activity per unit volume

$$A_2(s) = C_2 e^{\lambda s} \quad , \tag{18}$$

The copper-64 and iron-59 activities per unit volume at a depth s can be simply expressed in terms of the thermal neutron flux, $\phi_{th}(s)$, [$n/cm^2 \cdot s$)] at depth s:

$$A_1(s) = \phi_{th}(s) \cdot \sigma_1 \cdot \rho_1 \cdot e^{-\lambda_1 t_d} \cdot \left(1-e^{-\lambda_1 t_x}\right), \tag{19}$$

and

$$A_2(s) = \phi_{th}(s) \cdot \sigma_2 \cdot \rho_2 \cdot e^{-\lambda_2 t_d} \cdot \left(1-e^{-\lambda_2 t_x}\right). \quad (20)$$

where:

λ_1 is the copper-64 decay constant

λ_2 is the iron-59 decay constant

σ_1 is the copper-63 thermal neutron capture cross section

σ_2 is the iron-58 thermal neutron capture cross section

ρ_1 is the copper-63 concentration (at./cm^3)

ρ_2 is the iron-58 concentration (at./cm^3)

t_x is the duration time of the irradiation

t_d is the elapsed time since reactor shutdown

All these parameters are known except for the copper-63 concentration ρ_1. Hence, taking the ratio of Equation (19) to Equation (20), can be written

$$\rho_1/\rho_2 = K \quad , \quad (21)$$

where K is expressed in terms of known parameters as

$$K = \frac{A_1(s)e^{\lambda_1 t_d}\left(1-e^{-\lambda_2 t_x}\right)\sigma_2}{A_2(s)e^{\lambda_2 t_d}\left(1-e^{-\lambda_1 t_x}\right)\sigma_1} \quad (22)$$

Thus, the copper concentration can be simply obtained from the ρ_1/ρ_2 ratio by using the known percent abundances of copper-63 and iron-58 in natural copper and iron, respectively.

The copper concentration of the base metal can often be determined from archive PV specimens, so that only the copper concentration of PV weldments is desired for certain power reactors. In this case, the analysis given above can be used to show that only relative gamma spectra observations are necessary between PV base metal and PV weldments. Consequently, one can write

$$(\rho_1/\rho_2)_{weld} = \frac{(I_1/I_2)_{weld}}{(I_1/I_2)_{base\ metal}} \cdot (\rho_1/\rho_2)_{base\ metal}, \quad (23)$$

where I_1 and I_2 are the observed peak intensities of the copper-64 and iron-59 gamma-rays, respectively, so that (I_1/I_2) weld is the ratio of these intensities obtained observing the weld, whereas (I_1/I_2) base metal is the ratio of these intensities obtained observing the base metal.

Hence, if the copper concentration is known for the base metal, then only relative Si(Li) gamma spectra observations are needed between the base metal and weldment to determine the copper concentration of the weldment.

Interferences and background can arise in PV gamma spectra observed with the collimated Si(Li) Compton spectrometer that could make the detection of copper-64 very difficult. Additional radionuclides are produced that possess gamma-ray transitions close to the gamma-ray energies emitted by either copper-64 or iron-59. For example, cobalt-58 can be produced by an (n,p) reaction on nickel-58. Since cobalt-58 is a positron emitter, annihilation radiation would be produced at 0.511 MeV from the cobalt-58 decay just as it is produced in the decay of copper-64. However, the $^{58}Ni(n,p)^{58}Co$ reaction cross section is very small relative to the $^{63}Cu(n,\gamma)$ cross section, and the cobalt-58 half-life is 70.8 days, which is considerably longer than the 12.7-h half-life of copper-64. Hence, the background annihilation component from cobalt-58 will be small relative to the copper-64 annihilation gamma peak.

In general, the time-dependent decay of the different radionuclides contributing to a given gamma peak can be used to separate signal from background. For example, that component of peak intensity at the annihilation energy possessing a 12.7-h half-life can be determined by measuring time-dependent PV gamma spectra. Sequential gamma spectra measurements over a time period of a few days should serve to isolate the 12.7-h decay component uniquely attributed to copper-64.

Another example of background is the production of cobalt-60 in the PV by neutron capture on trace concentrations of natural cobalt, i.e., cobalt-59. The cobalt-60 decay possesses gamma-ray transitions at 1.173 MeV (100%) and 1.332 MeV (100%). Since the energy resolution of the Si(Li) spectrometer is about 30 keV (FWHM), the 1.332-meV gamma-ray from cobalt-60 would interfere with the 1.346-MeV transition of copper-64, and to a lesser extent with the 1.292-MeV transition of iron-59. Fortunately, cobalt-60 has a half-life of 5.27 yr so that time-dependent measurements can be used to separate signal from background, should the need arise.

Another general method for isolating background contributions exists based on the observation of additional peaks in the gamma spectrum that are emitted by the very same background-producing radionuclide. If such a peak can be identified, then the absolute activity of the background radionuclide can be quantified. Knowledge of the decay scheme of this background radionuclide together with the absolute activity of the background radionuclide provide the means to determine the background contribution to the peak intensity in question. For example, cobalt-58 possesses a gamma transition at 0.8108 MeV (99%). Consequently, if the cobalt-58 decay is contributing to the annihilation peak at 0.511 MeV, then a peak in the gamma spectrum should be

observed at 0.8108 MeV. Hence, observation of this peak at 0.8108 MeV with the collimated Si(Li) spectrometer can be used to identify the absolute activity per unit volume of cobalt-58. This absolute cobalt-58 activity, together with a knowledge of the cobalt-58 decay scheme, will permit evaluation of the background component at the 0.511-MeV annihilation gamma-ray energy.

In spite of the much higher specific activity of copper-64, extracting copper-64 data from a continuous gamma-ray spectra may still be difficult. In view of the importance attributed to copper in the radiation-induced embrittlement of PVs, further investigation of this method is warranted. Realistic field tests should be conducted to evaluate the actual capabilities and limitations of this method. For some applications, particularly for measurements that might be made on the PV inside surface, the differences between thermal and fast neutron-induced activations in Cu and Fe would have to be considered. Generally, this should involve only a small correction to the thermal neutron-induced events.

Advantages

- This method is nondestructive.
- Copper concentrations of base metal and weldments can be determined locally as a function of spatial position on the PV surface. The exact location of a weld of interest need not be known, since the change in gamma spectra between the base metal and weldment can be used to locate the collimated spectrometer at the weld.
- If the copper concentration of the base metal is known, then only relative gamma spectra measurements between base metal and weldment are needed to determine the copper concentration of the weldment.
- Copper concentrations are determined without the need to quantify the thermal neutron exposure flux ϕ_{th}.

Expected Future Accomplishments

A summary presentation of the results of the first field test of this new nondestructive method for the determination of the neutron exposure for the Mol, Belgium BR-3 reactor will be included in the next progress report. As appropriate, information on plans to use and further test the method for its direct applicability for B&W, CE, and W PWRs (with different size ex-vessel cavities) will be reported.

D. CHARACTERIZATION OF GAMMA-RAY SPECTRA AND ENERGY DEPOSITION IN LIGHT WATER REACTOR-PRESSURE VESSEL ENVIRONMENTS

R. Gold and J. P. McNeece (HEDL), and B. J. Kaiser (GE)

Objective

To meet the needs of the Light Water Reactor-Pressure Vessel (LWR-PV) Surveillance Dosimetry Improvement Program (SDIP), continuous gamma-ray spectrometry has been carried out in simulated LWR-PV environments. These in-situ observations provide gamma-ray spectra, dose, and heating rates needed to:

- Benchmark industry-wide reactor physics computational tools, e.g., independently, the gamma-ray spectrometry measurements provide absolute data for comparison with calculations.
- Assess radial, azimuthal, and axial contributions of gamma heating to the temperature attained within surveillance capsules, the PV wall, and other components of commercial LWR power reactors (Ra82a).
- Design, control, and analyze high-power metallurgical irradiation tests.
- Interpret fission neutron dosimetry in LWR-PV environments, where non-negligible photofission contributions can arise.

Summary

Results of recent Si(Li) continuous gamma-ray spectrometry in low power LWR-PV benchmark fields are reported. Emphasis is placed on the measurement and interpretation of perturbation factors created by the introduction of the Janus probe into the LWR-PV environment. Absolute comparisons are reported between spectrometry, calculations, and thermoluminescent dosimetry (TLD).

Accomplishments and Status

Introduction

Since the inception of continuous, Compton recoil gamma-ray spectrometry (Go68a,Go70a,Si68), rather than being static, this method has evolved and improved. Earliest efforts were directed toward in-situ observation of gamma-ray continua in reactors (Go70b,Si69). Almost simultaneously, the significance of this method for gamma-ray dosimetry was recognized (Go70). It was, therefore, not surprising that after these initial reactor experiments, applications arose in gamma-ray dosimetry (Go70d,St71), health

physics (Go71a), and environmental science (Go71c,Go72a,Go73). An environmental survey of the Experimental Breeder Reactor II (EBR-II) was conducted with these techniques (Go74). This method has been applied in reactor environments in Europe (Ko75,Ji78), and recognition of the general need for gamma-heating data (Go78a) led to spectrometry measurements in fast breeder reactor environments. Compton recoil gamma-ray spectrometry was actually the first experiment performed in the Fast Flux Test Facility (FFTF) at startup (Go80b). Efforts to characterize the gamma-ray field in LWR-PV environments have already been reported (Go80d,Go82b). Consequently, recent gamma-ray spectrometry efforts conducted in three LWR-PV-SDIP benchmark fields, namely the Poolside Critical Assembly (PCA) in Oak Ridge National Laboratory (ORNL) (USA), VENUS in CEN/SCK (Belgium), and NESDIP in Atomic Energy Establishment Winfrith (AEEW) (UK), will be summarized here.

A significant outgrowth of these collaborative efforts was the recognition and subsequent quantification of the perturbation factor (PF) created by the Janus probe. It was conjectured that the PF arises from the void or semi-voided regions introduced by the Janus probe into the gamma-ray intensity gradient that exists in the PV block. Initial analysis of the 1981 work performed in the 4/12 SSC configuration at the PCA has already been presented that confirms the existence of such PF. Since the significance of this PF is now clearly established, recent follow-on PF measurements at NESDIP will be elaborated upon here.

Perburtation Factor (PF) Measurements at NESDIP -- Two different gamma-ray dosimetry methods were used at NESDIP to measure Janus probe perturbation factors, namely, ionization chambers (IC) and thermoluminescence dosimetry (TLD). Both techniques were implemented using a "dummy" Janus probe. Measurements are first carried out at a given location by incorporating the miniature IC or TLD in the "dummy" Janus probe. Measurements are then repeated at this location with the channel completely back-filled with appropriate material so as to eliminate voids. The PF is defined by the ratio

$$PF = \dot{D}_p / \dot{D}_u \qquad (1)$$

where $\dot{D}_p$ is the perturbed dose rate observed in the presence of the "dummy" Janus probe and $\dot{D}_u$ is the unperturbed dose rate observed in the back-filled channel.

Special miniature ICs were developed at HEDL specifically for PF measurements in the PV block, and these were employed in the earlier PF measurements conducted in the PCA (Go82b). The PF measurements with TLD were carried out in collaboration with T. A. Lewis and colleagues of the Berkeley Nuclear Laboratories (UK), who used beryllium-oxide (BeO) TLD (Le83). The results of these PF measurements at NESDIP, which were performed only for the 12/13 configuration, are compared to the earlier PF observations obtained in the 4/12 SSC configuration at the PCA in Table HEDL-17.

TABLE HEDL-17

JANUS PROBE PERTURBATION FACTORS

Location	PCA - 4/12 SSC IC	NESDIP - 12/13 TLD	NESDIP - 12/13 IC
A2	--	1.12	--
1/4 T	1.16	1.30	1.27
1/2 T	1.14	1.24*	--
3/4 T	1.11	1.18	--
VB	--	0.90	--

*Since the 1/2-T location is not readily available at NESDIP, this value was obtained by linear interpolation of the 1/4-T and 3/4-T results.

Due to the limitations of the miniature IC design as well as NESTOR power operation, IC measurements could be carried out only for the 1/4-T location of the 12/13 configuration at NESDIP. The gamma-ray intensity levels that could be attained at the 3/4-T and VB locations were too low to provide reliable readings. Moreover, it is well to note that the design of these miniature ICs restricts applicability for PF measurements to the PV block. In view of the restricted nature of the IC results for the 12/13 configuration, the BeO TLD results, which represent a consistent set of PF for the 12/13 configuration, are recommended for use at this time. Nevertheless, it is important to stress that the IC and TLD results agree within experimental uncertainty at the 1/4-T location of the 12/13 configuration.

PF results shown in Table HEDL-17 vary with both configuration and location. In order to understand this behavior, it is instructive to examine the spatial dependence of dose rates within the PV block. Figure HEDL-8 compares (uncorrected) finite-size dose rates for the 4/12 SSC and 12/13 configurations. It is clear from Figure HEDL-8 that the 12/13 configuration gamma data possesses a larger gradient. In light of the results in Table HEDL-17, one finds that, when the Janus probe is used in a field possessing a larger gradient, the PFs are, in turn, larger.

This conclusion is also supported by the PF result for the A2 water position of the 12/13 configuration. This PF result, namely 1.12, is essentially as low as any result obtained within the PV block for either the 12/13 or 4/12 SSC configuration. However, it is well known that water is a rather poor attenuator of gamma radiation compared with the iron medium of the PV. Hence, gamma-ray intensity gradients at water locations are generally less than those in the PV block, and the corresponding Janus probe PF is indeed lower. Consequently, these overall PF results confirm the original conjecture that Janus probe PF stem from the introduction of voids or semi-voided regions into a gamma field possessing an intensity gradient.

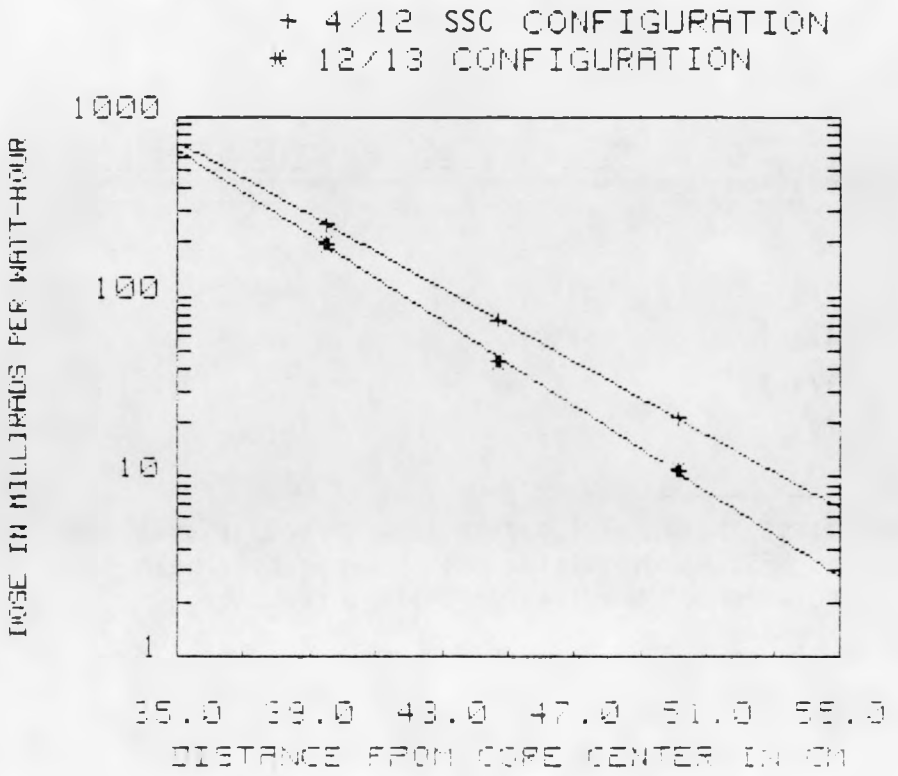

FIGURE HEDL-8. Comparison of the Spatial Behavior of the Finite-Size Dose Rate, $\dot{D}_{FS}$, for the 4/12 SSC and 12/13 Configurations. (The smooth lines are linear least-squares fits of the logarithm of the experimental data.)

The existence of a PF less than unity for the VB location of the 12/13 location can also be qualitatively explained. Comparison of the Janus probe with a point detector for measurements in a void reveals that the probe must produce some attenuation of gamma radiation in the solid angle that the probe subtends at the Si(Li) sensitive volume. Consequently in a void, one must expect that the perturbed dose rate $\dot{D}_p$ would be less than the unperturbed dose rate $\dot{D}_u$. Hence an observed PF of less than unity for the VB location of the 12/13 configuration is in accord with very simple physical considerations.

Gamma-Ray Spectra and Dose Rates in the PCA -- The PFs provided in Table HEDL-17 have been used to correct both gamma-ray spectra and dose rates measured with the Janus probe in LWR-PV configurations studied in the PCA. However, from a rigorous viewpoint, the PF considered here are dose PF. Consequently, use of dose PF for spectral adjustments must obviously be justified. Such a justification can be made by examining spectral ratios obtained from Janus probe spectral measurements conducted at different locations of the same LWR-PV configuration. On this basis, it can be shown

that the dose PF can be used for spectral adjustment without compromising experimental accuracy. This justification will be more fully delineated in the forthcoming LWR-PV-SDIP NUREG report (NUREG/CR-3318).

Figures HEDL-9, -10, and -11 compare Janus probe spectral measurements with calculations for the 1/4-T, 1/2-T, and 3/4-T locations of the 12/13 configuration, respectively. All measured gamma-ray spectra have been corrected for background as well as for the perturbation introduced by the Janus probe. Calculations for the 12/13 configuration have been performed by ORNL (Ma84) and CEN/SCK (Ma82). These spectral comparisons are absolute and possess conventional units, i.e., gamma-rays/cm^2•MeV•s), at 1 watt of PCA power.

For the 12/13 configuration, ORNL calculations are roughly a factor of two lower than experimental gamma-ray spectra, whereas CEN/SCK calculations occupy an intermediate position. Comparisons between theory (Ma82) and experiment for the 4/12 SSC configuration exhibit the same general trends. It is surprising to see that comparisons between theory and experiment generally improve with increasing penetration into the PV. However, calculations generally decrease more rapidly than experimental results with increasing gamma-ray energy.

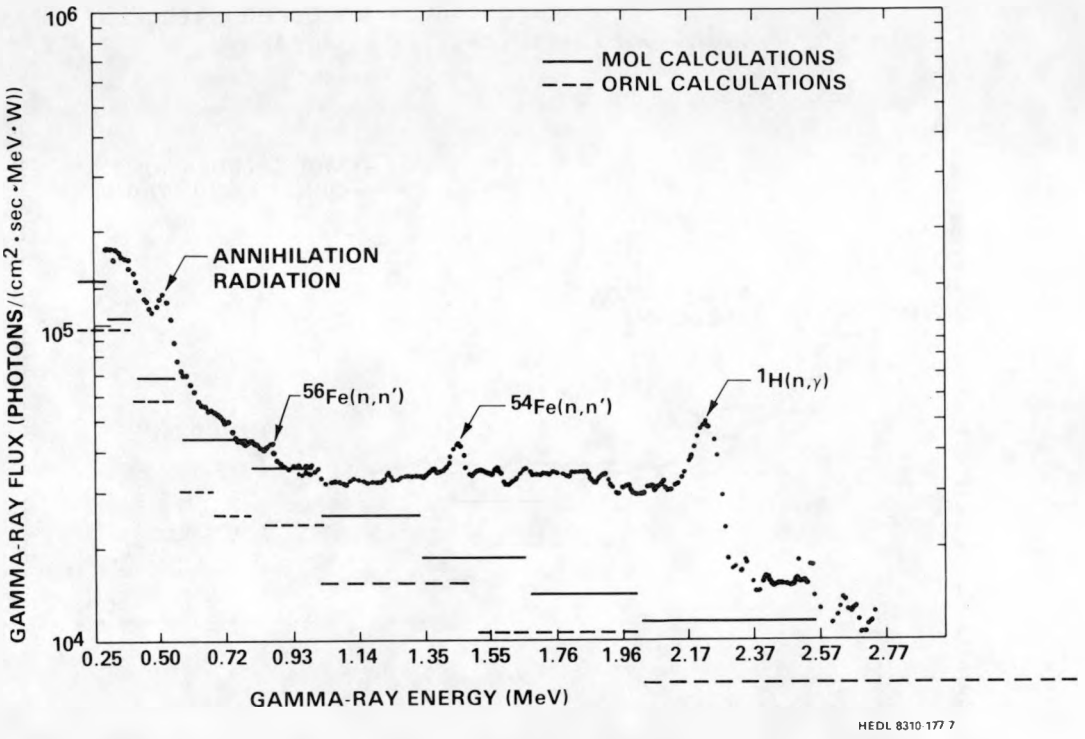

FIGURE HEDL-9. Low-Energy Gamma-Ray Continuum for the 1/4-T Location of the 12/13 Configuration as Compared with CEN/SCK and ORNL Calculational Results. Neg 8307649-7

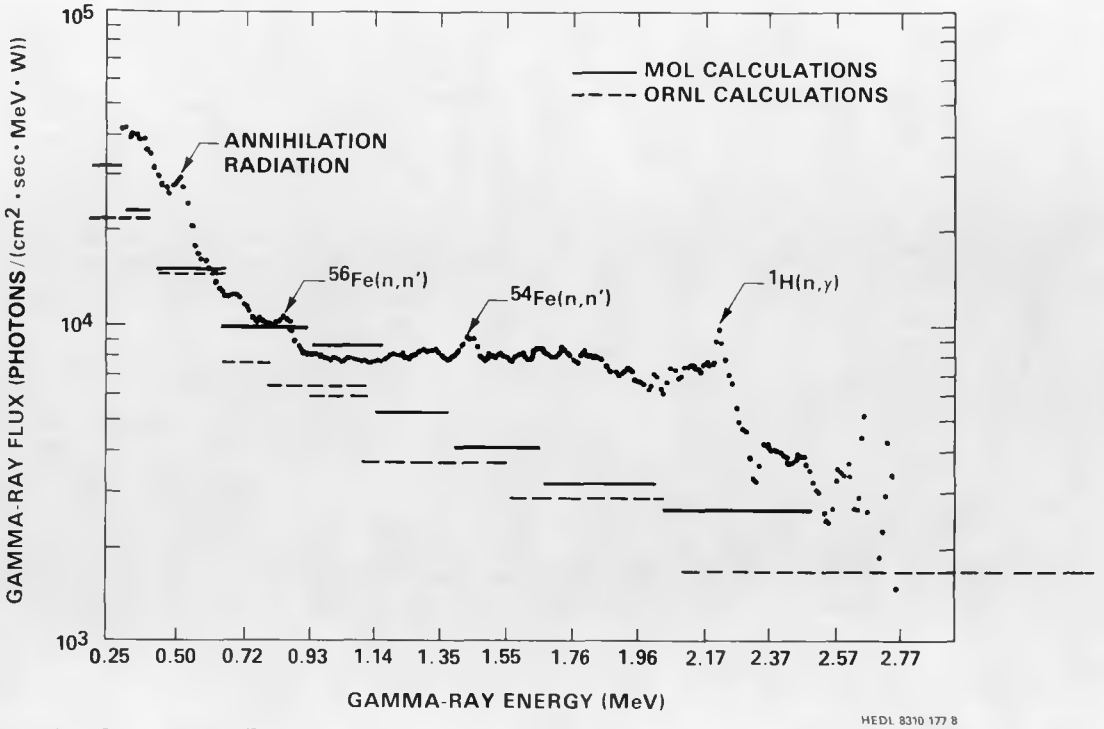

FIGURE HEDL-10. Low-Energy Gamma-Ray Continuum for the 1/2-T Location of the 12/13 Configuration as Compared with CEN/SCK and ORNL Calculational Results. Neg 8307469-8

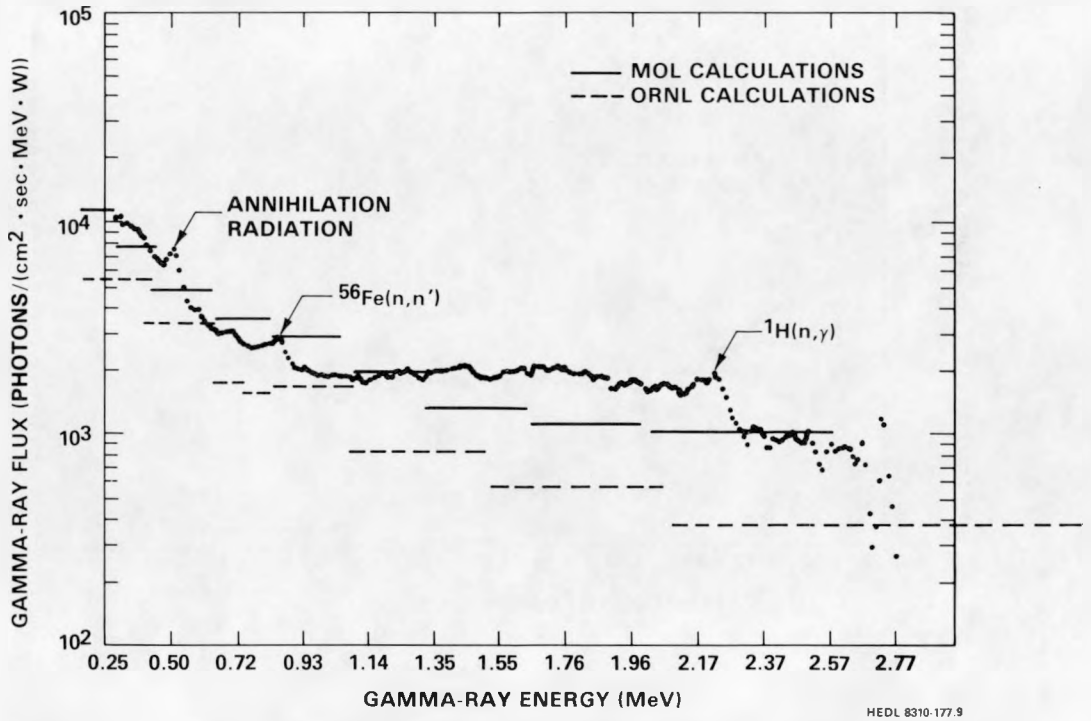

FIGURE HEDL-11. Low-Energy Gamma-Ray Continuum for the 3/4-T Location of the 12/13 Configuration as Compared with CEN/SCK and ORNL Calculational Results. Neg 8307469-9

Infinite medium dose rates D_{IM} observed with the Janus probe in the 1981 PCA experiments are enumerated in Table HEDL-18. These results have been corrected for Janus probe field perturbation, which varies with both configuration and location (see Table HEDL-17). These dose rates can be taken as infinite medium dose rates in steel. It has already been shown that the difference between infinite medium dose rates for silicon and iron is negligible (Ka81).

Table HEDL-19 presents a comparison of experimental and calculated gamma-ray dose rates for the 4/12 SSC configuration. In addition to the $\dot{D}_{IM}$ results from the 1981 Janus probe experiments, this table presents results obtained by the CEN/SCK group (Fa81,Fa81b,Ma82), who performed both TLD measurements and calculations.

TABLE HEDL-18

INFINITE MEDIUM DOSE RATES* OBSERVED IN THE 1981 PCA EXPERIMENTS

	Configuration		
Location	4/12 SSC	12/13	4/12
1/4 T	220	152	490***
1/2 T	65.4	35.6	---
3/4 T	19.1	9.24	---
VB	11.0**	2.56	---

*Dose rates in mrad/h at 1-watt PCA power were corrected for Janus probe field perturbation.
**A perturbation factor of 0.9 has been applied corresponding to that obtained at the VB location in the 12/13 configuration.
***A perturbation factor of 1.16 has been applied corresponding to that obtained at the 1/4-T location in the 4/12 configuration.

TABLE HEDL-19

GAMMA-RAY DOSE RATES* FOR THE 4/12 SSC CONFIGURATION

	Experiment		Calculation		
Location	TLD	$\dot{D}_{IM}$	CEN/SCK	$\dot{D}_{IM}$/TLD	$\dot{D}_{IM}$/CAL
1/4 T	255	220	210	0.86	1.05
1/2 T	68	65.4	52	0.96	1.26
3/4 T	21.5	19.1	19.1	0.89	1.00
VB	11.5	11.0	2.2	0.96	5.05

*Dose rates in mrad/h at 1-watt PCA power.

Using the results from all four locations of the 4/12 SSC configuration given in Table HEDL-19, one finds a $\dot{D}_{IM}$/TLD average ratio of 0.92. Consequently, the Si(Li) and TLD methods agree within experimental uncertainty. Comparison of these experimental results with calculations does not show consistent agreement. The extremely low calculational result at the VB location might be due to inadequate modeling of the actual geometric configuration used in the PCA.

Expected Accomplishments

Work is in progress to extend the applicability of continuous gamma-ray spectrometry beyond 3 MeV. While the original intent with the Janus probe was to cover the energy region up to 6 MeV, statistical limitations may not permit extension throughout this entire energy region. These extended efforts with the Janus probe will be applied to produce final gamma-ray spectrometry results for the LWR-PV benchmark fields in PCA, VENUS, and NESDIP. Spectrometry results will also be obtained for the standard gamma-ray fields measured at CEN/SCK, Mol, Belgium.

OAK RIDGE NATIONAL LABORATORY

(ORNL)

OAK RIDGE NATIONAL LABORATORY

LIGHT WATER REACTOR PRESSURE VESSEL SIMULATION (LWR-PVS) PROGRAM

F. B. K. Kam

The LWR-PVS program has two major tasks; the first task is concerned primarily with well-defined reproducible benchmark experiments, and the second task deals with ASTM Standards activities.

During this report period, the following work is presented:

- Calculated activities and spectral fluences for the PSF two-year metallurgical irradiation experiment.
- Power distribution calculations for the VENUS PWR engineering mockup using DOT IV (Rh79) and comparison with measurements from CEN/SCK.
- Babcock & Wilcox SDMF perturbation experiment.
- Fourth SDMF experiment.
- Determination of damage exposure parameter values in the PSF metallurgical irradiation experiment.
- Neutronics calculations for the Pool Critical Assembly 4/12 SSC and 4/12 configurations.
- Statistical evaluation of the Charpy test results in the ORR-PSF metallurgical irradiation experiment using the CV81 procedure - preliminary results.
- ASTM Standards activities.

A. BENCHMARK EXPERIMENTS

Objectives

The objective of the benchmark experiments is to validate, by means of advanced statistical procedures, current methodologies and data bases which are used to predict radiation damage in reactor pressure vessels (RPV).

A.1 CALCULATED ACTIVITIES AND SPECTRAL FLUENCES FOR THE PSF TWO-YEAR IRRADIATION EXPERIMENT

R. E. Maerker
B. A. Worley

Summary

The neutron source calculations and the neutron transport calculations from the core to the irradiation capsules are summarized. Forty-six fuel cycles are calculated using the VENTURE code (Vo77) to obtain three-dimensional (3-D) fission source densities for the two-year irradiation period. The data are on a 9-track magnetic tape which permits easy access to other participants in the program. Rolls Royce and Associates, Ltd. has been given a copy of the tape so that they can perform a 3-D Monte Carlo calculation of the PSF experiment.

A neutron transport calculation of the reaction rates and spectral fluences in the irradiation capsules are presented and the results compared with the available experimental data at the time the calculations were completed. More recent measurements may not be included. The comparisons of calculated-to-measured data agree to within 5 to 15% which is consistent with the PCA benchmark results (Mc81b).

Accomplishments and Status

Since some HEDL dosimetry measurements in the two-year irradiation experiment disagreed by approximately 10 to 20% with ECN and CEN/SCK measurements performed earlier for the startup experiment, it is of interest to investigate analytically the cause of this disagreement. If due to differences in the measurement techniques between HEDL and the Europeans, that is one thing, and leads to its own worries and re-evaluation of measurement uncertainties; if due to differences in the source distributions (i.e., cycle-to-cycle variations) or differences in the geometry of the two experiments, this should be verified and the original startup calculations replaced by more rigorous ones that take these differences into account. A further consideration is the choice of the startup experiment as an important benchmark in the LEPRICON adjustment procedure, and the certainty that the startup calculations and use of ECN measurements are consistent with the additional information provided by the two-year experiment. A final consideration is that, because of the large number of calculations involved, probably no one else will perform them, and hence these calculations will be the only ones to be used in the analysis of the blind test metallurgical benchmark experiment that the two-year irradiation sequence was set up to represent.

The results of a simpler calculation of the startup experiment than the one originally performed were presented August 8, 1983 (Wi82). The method adopted for this simpler calculation was based on the validated results of further calculations that showed there was no effect of streaming around the finite simulated surveillance capsule (SSC) on the near-centerline fluxes in the SSC

or the simulated pressure vessel capsule (SPVC). Furthermore, the presence of the horizontal voids such as the 1-in. cable storing void in the SSC and the 1/4-in. voids in the SPVC does not affect the near-centerline fluxes. Thus, the three-dimensional flux synthesis procedure involved using three calculations - DOT XY, DOT YZ, and ANISN Y, in which the revised geometry assumed the SSC to be infinitely high and wide, and with the horizontal voids only affecting the YZ flux profiles at axial distances greater than about $\pm$13 cm from the horizontal midplane 5.08 cm below the reactor centerline. This simplified method was used in all the transport calculations employed in the two-year analysis as well. The discovery of the simpler method, which is just as accurate and less subject to data-manipulation error, allowed the present analysis to be performed efficiently and accurately.

The history of the two-year irradiation is presented in Table ORNL-1, where the data originally supplied was altered slightly to include the effects of setback in the duration of each cycle. Thus, the column headed "Δtup" is simply t(retracted)-t(inserted), the column headed "setback" is the difference between Δtup and the "Delta-t" column in the original data which did not include setback, and the column headed "average power including setback" replaces the "average power" column in the original data. In this way, we have included the effects of setback, though small, into the time history of the irradiation. The k_{eff} values in Table ORNL-1 are those calculated using VENTURE and a modified VIPOR in which the axial partially burned fuel profile correlations were normalized whenever they went negative. It should be noted that only a middle-of-cycle VENTURE calculation was made for each cycle, the assumption being that the departure of the within-cycle source variation from linearity about the middle-of-cycle distribution is small compared to the cycle-to-cycle variation. The data and times in Table ORNL-1 were assumed to include the $\pm$1 hour adjustments from changing to daylight saving time and back to standard time. These adjustments were assumed to have occurred on October 26, 1980; April 26 and October 25, 1981; and April 25, 1982, all at 2 AM. No leap days occurred during the irradiation, so that the total elapsed time between the first insertion of the experiment and the last retraction was:

1980: 10.433+24(31+30+31+31+30+31+30+31)+1 = 5891.43 hours,
1981: 24(365) = 8760.00 hours, and
1982: 24(31+28+31+30+31)+24(22)-1 = 4151.00 hours

for a total of 18,802.43 hours. This agrees within 0.22 hours $\simeq$13 min. of the retraction time in cycle 161C relative to the insertion time in cycle 153B. This difference is completely negligible and not worth the trouble of tracing. The irradiation consisted of 52 fuel cycles of which all but a few (155G, 155H, 156A, and 156B) had VENTURE calculations performed for them. In addition to these four, VENTURE source distributions were not used for cycles 154H and 155D because they were late in being calculated and nominal distributions were used instead. The effect of using nominal source distributions for these six cycles instead of calculated ones should result in an estimated maximum uncertainty in the calculated fluences in the SPVC and simulated void box capsule (SVBC) locations (the only locations these cycles affect) of 2.4%, with

TABLE ORNL-1

IRRADIATION HISTORY AND CYCLE PARAMETERS

Cycle	k_{eff}	Time and Date Inserted		Time and Date Retracted		Down Time After Previous Irradiation Δt_d (hours)	t(inserted) (hours)	t(retracted) (hours)	Δtup (hours)	Setback Δt_s (hours)	Average Power Including Setback (MW)
						Start irradiation of SSC-1, SPVC, and SVBC					
153B	1.0242	4/30/80	13:34	5/8/80	7:00		0.0	185.43	185.43	1.00	29.822
153C	1.0251	5/8/80	16:43	5/14/80	13:30	9.72	195.14	335.90	140.76	0	29.800
153C	1.0251	5/16/80	9:57	5/21/80	2:17	44.45	380.35	492.68	112.33	0	29.957
153D	1.0162	5/22/80	10:49	6/6/80	24:00	32.53	525.21	898.39	373.18	2.55	29.657
153F	1.0224	6/12/80	9:20	6/23/80	12:55	129.33	1027.72	1295.30	267.58	0.43	29.377
						End irradiation of SSC-1					
153G	1.0042	6/27/80	18:30	7/5/80	3:30	101.58	1396.88	1573.88	177.00	2.32	28.855
153G	1.0042	7/7/80	13:55	7/8/80	9:40	58.42	1632.30	1652.05	19.75	0.18	29.058
153G	1.0042	7/8/80	15:18	7/13/80	8:00	5.63	1657.68	1770.38	112.70	1.01	29.565
154A	1.0047	7/18/80	17:00	7/18/80	18:32	129.00	1899.38	1900.70	1.32	0.82	3.712
154A	1.0047	7/18/80	22:50	7/21/80	4:26	4.30	1905.00	1958.60	53.60	1.26	28.319
154A	1.0047	7/22/80	10:05	7/31/80	7:00	29.65	1988.25	2201.17	212.92	13.39	28.200
154B	1.0066	7/31/80	18:20	8/12/80	19:02	11.33	2212.50	2501.20	288.70	0.33	30.335
154C	1.0019	8/15/80	14:48	8/15/80	16:07	67.77	2568.97	2570.29	1.32	0.05	28.977
154D	1.0024	8/21/80	10:55	8/26/80	16:00	138.80	2709.09	2834.17	125.08	0.39	28.849
154E	1.0016	8/27/80	14:30	9/1/80	3:29	22.50	2856.67	2965.62	108.95	0	29.799
154E	1.0016	9/3/80	9:53	9/9/80	8:00	54.40	3020.02	3162.14	142.12	0.57	30.031
154F	1.0007	9/10/80	11:22	9/23/80	4:00	27.37	3189.51	3494.14	304.63	1.73	29.471
154G	0.9993	9/23/80	13:52	10/5/80	21:32	9.87	3504.01	3799.68	295.67	0.44	29.909
154H	1.0190	10/7/80	13:46	10/17/80	17:50	40.23	3839.91	4083.95	244.04	0	29.905
154I	0.9858	10/21/80	12:48	10/29/80	4:00	90.97	4174.92	4359.05	184.13	1.00	29.486
154J	0.9890	10/29/80	18:47	11/8/80	8:00	14.78	4373.83	4603.05	229.22	0.29	29.223
155B	0.9983	12/3/80	14:51	12/9/80	0:26	606.85	5209.90	5339.48	129.58	0.90	28.786
155C	0.9920	12/10/80	12:54	12/18/80	5:15	36.47	5375.95	5560.30	184.35	0	28.247
155D	0.9936	12/18/80	17:46	12/30/80	8:00	12.52	5572.82	5851.59	278.77	0.54	27.832
155E	0.9891	12/30/80	16:11	1/7/81	8:00	8.18	5859.77	6043.59	183.82	0.29	26.823
155F	0.9922	1/7/81	21:55	1/15/81	4:00	13.92	6057.51	6231.59	174.08	0.22	27.115
155G		1/16/81	11:41	1/19/81	20:22	31.68	6263.27	6343.95	80.68	0.21	30.066
155H		1/21/81	9:02	1/22/81	7:16	36.67	6380.62	6402.85	22.23	0.89	29.311
155H		1/22/81	16:18	2/2/81	8:00	9.03	6411.88	6667.58	255.70	0.61	30.346
156A		2/9/81	13:35	2/24/81	8:00	173.58	6841.16	7195.58	354.42	2.92	27.279
156B		2/24/81	15:00	3/13/81	8:04	7.00	7202.58	7603.65	401.07	2.19	27.223
156B		3/13/81	8:47	3/16/81	3:00	0.72	7604.37	7670.59	66.22	0.61	27.168
156C	1.0052	3/19/81	10:13	3/30/81	22:40	79.22	7749.81	8026.26	276.45	0	30.447
156C	1.0052	3/31/81	11:33	4/2/81	4:00	12.88	8039.14	8079.59	40.45	1.08	29.598
156D	1.0076	4/2/81	16:10	4/19/81	8:00	12.17	8091.76	8491.60	399.84	0	30.290
157A	1.0021	4/27/81	11:12	5/11/81	3:12	194.20	8585.80	9013.80	328.00	2.50	30.174
157B	1.0184	5/11/81	17:24	5/27/81	4:00	14.20	9028.00	9398.60	370.60	0	30.335

TABLE ORNL-1 CONTINUED

Cycle	k_{eff}	Time and date inserted		Time and date retracted		Down time after previous irradiation Δt_d (hours)	t(inserted) (hours)	t(retracted) (hours)	Δtup (hours)	setback Δt_s (hours)	Average power including setback (MW)
						Start irradiation of SSC-2					
157C	1.0166	5/29/81	11:39	5/29/81	20:45	55.65	9454.25	9463.35	9.10	0	30.048
157C	1.0166	6/1/81	11:49	6/9/81	8:10	63.07	9526.42	9714.77	188.35	0.94	29.997
157D	1.0127	6/10/81	8:15	6/23/81	4:23	24.08	9738.85	10046.98	308.13	0	30.352
157E	0.9756	6/25/81	12:20	7/10/81	12:00	55.95	10102.93	10462.60	359.67	0	30.044
158C	1.0018	7/22/81	13:47	8/6/81	6:30	289.78	10752.38	11105.10	352.72	0.15	27.082
158D	0.9997	8/7/81	19:05	8/20/81	4:00	36.58	11141.68	11438.61	296.93	0	27.008
158E	1.0101	8/21/81	15:17	8/30/81	24:00	35.28	11473.89	11698.61	224.72	0	30.354
158F	1.0076	9/2/81	19:01	9/8/81	16:52	67.02	11765.63	11907.48	141.85	0.22	30.136
158G	1.0274	9/11/81	8:17	9/25/81	2:00	63.42	11970.90	12300.62	329.72	0	30.260
						End irradiation of SSC-2					
158H	1.0126	9/25/81	23:10	10/13/81	3:20	21.17	12321.79	12733.96	412.17	0.12	30.180
158I	1.0206	10/13/81	20:30	10/23/81	3:00	17.17	12751.13	12973.63	222.50	0.57	30.174
158J	1.0142	10/23/81	13:28	10/26/81	20:13	10.47	12984.10	13063.85	79.75	0.12	29.819
158J	1.0142	10/27/81	9:41	11/4/81	4:00	13.47	13077.32	13263.64	186.32	1.43	30.267
158K	1.0173	11/4/81	16:10	11/15/81	8:00	12.17	13275.81	13531.64	255.83	0.09	30.311
159A	1.0156	11/24/81	14:12	12/12/81	6:00	222.20	13753.84	14177.64	423.80	0	30.287
159B	1.0037	12/18/81	9:47	12/28/81	13:20	147.78	14325.42	14568.97	243.55	0.43	30.009
159C	1.0054	12/31/81	21:21	1/6/82	8:36	80.02	14648.99	14780.24	131.25	0.71	29.794
159C	1.0054	1/6/82	14:18	1/14/82	3:00	5.70	14785.94	14966.64	180.70	0.37	30.234
159D	1.0121	1/21/82	15:36	2/1/82	2:58	180.60	15147.24	15398.61	251.37	0	30.256
159E	1.0025	2/1/82	16:56	2/7/82	8:00	13.97	15412.58	15547.65	135.07	0	30.126
160A	1.0020	2/12/82	17:33	2/18/82	9:00	129.55	15677.20	15812.65	135.45	0.07	29.987
160B	1.0064	2/18/82	18:59	3/8/82	8:20	9.98	15822.63	16243.98	421.35	0.14	30.173
160C	1.0175	3/9/82	15:33	3/25/82	3:00	31.22	16275.20	16646.65	371.45	1.44	30.113
160D	1.0166	3/26/82	18:55	4/5/82	3:00	39.92	16686.57	16910.65	224.08	0.34	30.223
160E	1.0108	4/5/82	18:40	4/16/82	15:05	15.67	16926.32	17186.74	260.42	0.69	29.856
161B	1.0149	4/29/82	17:42	5/24/82	3:30	313.62	17500.36	18086.16	585.80	0.88	30.062
161C	1.0223	5/27/82	22:28	6/22/82	24:00	90.97	18177.13	18802.66	625.53	1.73	30.116
						End irradiation of SPVC and SVBC					

somewhat smaller values for the calculated dosimeter activities. Hence, no significant uncertainty is introduced into the analysis by the cavalier treatment of these six cycles.

The three-dimensional calculated fission source densities using the VENTURE code are stored on tape X19802 for possible use by other calculators interested in using their own transport codes to determine spectral fluence profiles in the experiment. A detailed description of the information on this tape is given in the appendix.

The sequence of calculations in the VENTURE-DOT method is shown in Fig. ORNL-1, where the introduction of the source combining procedure over groups of cycles allows one to perform a single DOT calculation (actually two, an XY and a YZ) for a group of cycles, rather than for each individual cycle, thus cutting down significantly the cost and time of the analysis. The source combining should not include too many cycles at a time or the variation from cycle to cycle, if significant, would be almost lost with the time dependence of the source which affects the dosimeter EOI activities. For this type of analysis, where as much of the (unknown) source-time variation should be retained as possible within the limiting framework of the costly DOT calculations, it was decided to do little or no combining of cycles near the end of an irradiation period (i.e., cycles active immediately prior to the removals of the SSC-1, the SSC-2, and the SPVC and SVBC), to allow a more accurate calculation of the shorter-lived dosimeter activities at the end of irradiation. For the longer-lived activities as well as for the shorter-lived ones several half-lives removed in time, the cycle sources may be combined in ever-increasing groups of cycles. For the fluence calculation no decay complications need to be considered, so that if it were not for the dosimetry considerations, all the cycle sources active during a given irradiation period (i.e., SSC-1, SSC-2, and SPVC + SVBC exposures) could be combined and only one pair of DOT calculations performed. The combining was based on weighing each cycle by its average power (each VENTURE calculation was normalized to 30 MW), duration, and calculated k_{eff}:

$$\bar{S} = 1.0225\left[\sum_{i=1}^{L}\left(\frac{S_i}{k_{eff}}\right)\left(\frac{\bar{P}_i}{30}\right)\Delta tup(i)\right] \Big/ \left[t_L(\text{retracted}) - t_1(\text{inserted})\right] \qquad (1)$$

In Eq. (1), the symbols S and S_i represent the combined and individual cycle sources as function of either x and y, y and z, or y, depending on which transport calculation is to be made. The factor 1.0225 represents a renormalization of the VENTURE neutron source to reflect updated information on (ν/K); the denominator represents the total time integral that the group of cycles represents the core source, and includes the down time between each cycle $\Delta t_d(i)$. We are thus replacing L different sources, each active for $\Delta tup(i)$, by a single reduced source of duration $\Sigma[\Delta tup(i) + \Delta t_d(i)] = t_L(\text{retracted}) - t_1(\text{inserted})$. If one chooses the group of cycles such that $\Delta t_d(i) \ll \Delta tup(i)$ for all i in the group, the decay can be very accurately calculated as coming from a constant source S extending over the period represented by the denominator of Eq. (1). If a particularly large down time

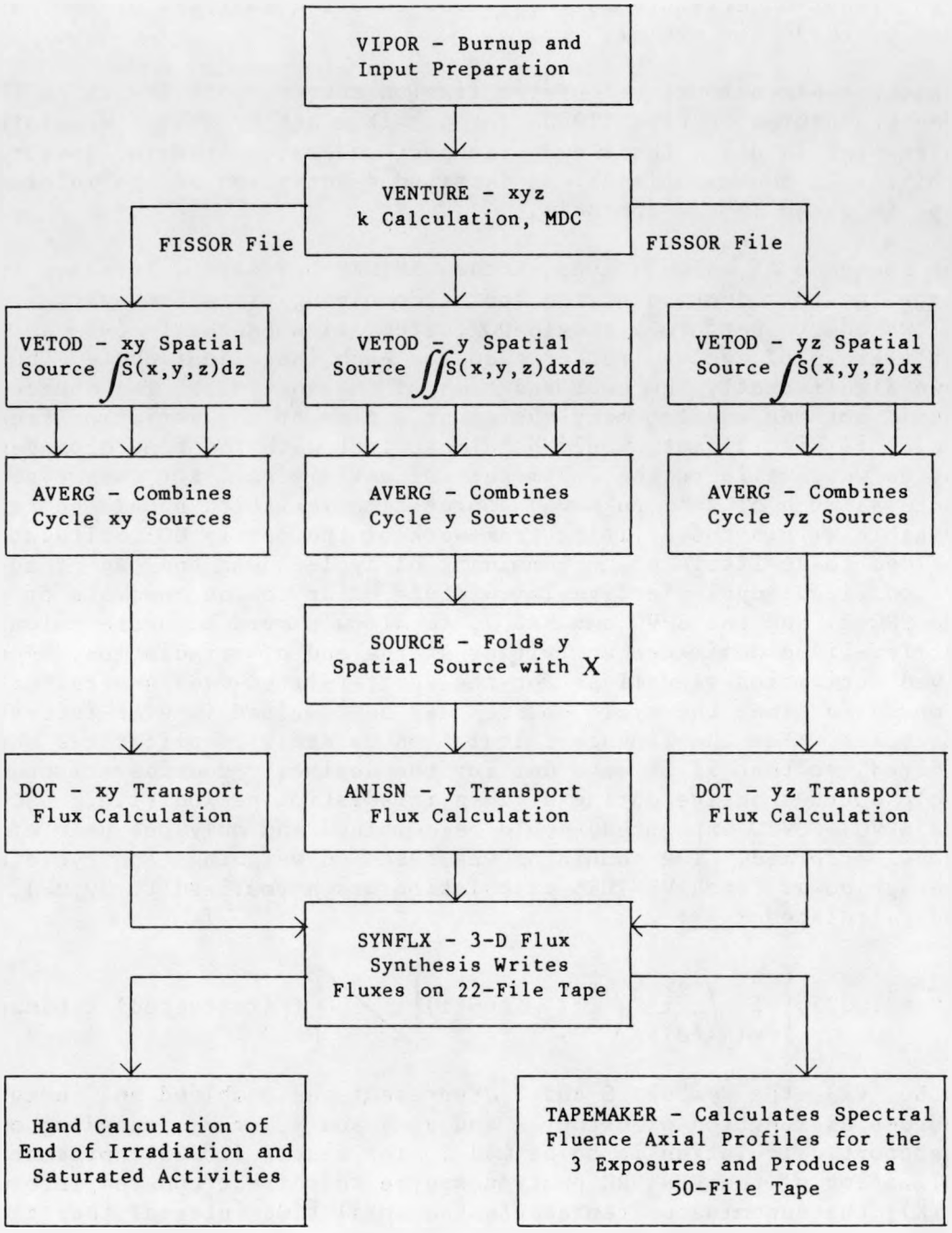

FIGURE ORNL-1. Sequence of Calculations.

occurred, the group was terminated with the cycle immediately preceding, so that all cycle sources in the group are properly decayed through this down-time interval. A case in point is cycle 158C in the SSC-2 irradiation (see Table ORNL-1); there was a delay of 289.78 hours after cycle 157E before cycle 158C became active. Thus, if one were to combine the sources from any cycles before 158C with those after 157E, the decay based on the combining procedure illustrated by Eq. (1) would be somewhat over calculated for cycle 158C and any cycles in the group occurring after 158C. Thus, a natural dividing line separating the groups occurs between cycles 157E and 158C. Table ORNL-2 illustrates the grouping of the cycles used in our analysis together with the various weights for each cycle.

The component fluxes calculated in each of the two DOT runs as well as in the ANISN run were synthesized in a manner completely analogous to the procedure followed in the startup experiment analysis:

$$\phi_g(x,y,z) = \phi_g(x,y)\phi_g(y,z)/\phi_g(y) \qquad (2)$$

These synthesized fluxes were calculated as axial profiles for specific values of x and y for each group of cycles appearing in Table ORNL-2. Fluxes were calculated using the same ELXSIR library as was used in the startup analysis, and were followed down only to 0.098 MeV (i.e., only the first 38 groups of the library were used). The fluxes were then multiplied by the total duration of the group, t_L(retracted)-t_1(inserted), which includes the intercycle down times if any, and summed over all the cycle groups to yield the spectral fluences:

$$\phi_g(x,y,z) = 1.039 \sum_G \phi_g^G(x,y,z)\ [t_L(\text{retracted})-t_1(\text{inserted})]_G \quad , \qquad (3)$$

where the factor 1.039 represents the energy- and spatially-dependent bias factor that accounts for the combined effects of the plate and water fuel element geometry and of a slightly inconsistent normalization between the DOT YZ and ANISN Y sources.

These spectral fluence axial profiles appear on tape X13850 in 50 files for possible use in spectral adjustment codes and/or analysis of the metallurgical specimens. A complete description of the contents of this tape is relegated to the appendix.

Calculations of the measured dosimeter activities were made as both saturated activities from each cycle group as well as decayed end of irradiation activities. Since the HEDL measurements still have not all been reduced, some of the comparisons must wait, but there is enough data to compare already to yield a pretty good idea of how well the calculations agree.

Saturated activities for $^{63}Cu(n,\alpha)$, $^{46}Ti(n,p)$, $^{54}Fe(n,p)$, $^{58}Ni(n,p)$ charged particle dosimeters plus $^{238}U(n,f)$ and $^{237}Np(n,f)$ fission dosimeters were calculated for each cycle group by synthesizing the activities calculated in each of the transport runs:

$$RR_S^d(x,y,z) = [RR_S^d(x,y)RR_S^d(y,z)/RR_S^d(y)] \times [Vy/(VxyVyz)] \quad , \qquad (4)$$

TABLE ORNL-2

CYCLE GROUP COMBINATIONS AND REDUCED INDIVIDUAL CYCLE WEIGHTS

Group	Cycles	$\frac{t_L(\text{retracted}) - t_l(\text{inserted})}{\sum_i \Delta tup(i)}$	Source Combination
1	153B+153C	1.124	$0.37352S_{153B}+0.51017S_{153C}$
2	153D	1.0	$0.99471S_{153D}$
3	153F	1.0	$0.97786S_{153F}$
4	153G-154C	1.353	$0.26071S_{153G}+0.21761S_{154A}+0.25271S_{154B}+0.00111S_{154C}$
5	154D-154J	1.159	$0.08626S_{154D}+0.15650S_{154E}+0.18293S_{154F}+0.18073S_{154G}+0.12059S_{154I}+0.14337S_{154J}$*
6	155B-155F	1.075	$0.18977S_{155B}+0.24024S_{155C}+0.23141S_{155E}+0.22383S_{155F}$†
7	155G-156B**	1.192	$0.50812\bar{S}_{155B-155F}+0.46452\bar{S}_{156C-157B}$**
8	156C-157B	1.165	$0.19772S_{156C}+0.24847S_{156D}+0.20416S_{157A}+0.22820S_{157B}$
9	157C-157E	1.165	$0.19695S_{157C}+0.31216S_{157D}+0.37439S_{157E}$
10	158C+158D	1.056	$0.47356S_{158C}+0.39838S_{158D}$
11	158E-158G	1.187	$0.27840S_{158E}+0.17491S_{158F}+0.40036S_{158G}$
12	158H-158K	1.046	$0.34607S_{158H}+0.18532S_{158I}+0.22270S_{158J}+0.21474S_{158K}$
13	159A-159C	1.239	$0.35518S_{159A}+0.20464S_{159B}+0.26202S_{159C}$
14	159D-160C	1.141	$0.17081S_{159D}+0.09227S_{159E}+0.09214S_{160A}+0.28715S_{160B}+0.24989S_{160C}$
15	160D+160E	1.032	$0.45395S_{160D}+0.52416S_{160E}$
16	161B	1.0	$1.0096S_{161B}$
17	161C	1.0	$1.0041S_{161C}$

*S_{154H} assumed to be $(S_{154D}+S_{154E}+S_{154F}+S_{154G}+S_{154I}+S_{154J})/6$

†S_{155D} assumed to be $(S_{155B}+S_{155C}+S_{155E}+S_{155F})/4$

**$S_{155G-156B}$ assumed to be $0.5\ (28.15/27.7)\bar{S}_{155B-155F}+0.5(28.15/30.3)\bar{S}_{156C-157B}$

where the last term represents the inverse of the volumes integrated over in the edit of the saturated activities. These synthesized saturated activities are easily extracted from the zone edits of the transport runs, and agree to within negligible error of the activities calculated using Eq. (2) in conjunction with folding with the reaction cross section:

$$RR_S^d(x,y,z) = \sum_G \phi_g(x,y,z)\sigma_g^d \quad . \tag{5}$$

Thus, synthesizing the activities by using Eq. (4) is an excellent approximation to Eq. (5) and is more easily performed. Hence for a given group of cycles,

$$RR_S^d = 1.039 \; \frac{t_L(\text{retracted}) - t_1(\text{inserted})}{\sum_i \Delta tup(i)} \times [RR_S^d(x,y) RR_S^d(y,z)/RR_S^d(y)] \times [Vy/VxyVyz] \quad , \tag{6}$$

where the time factor represents a correction to the original source combining prescription Eq. (1) to properly renormalize the source to provide a correct saturated activity.
These saturated activities are excellent indicators of the magnitude of any cycle-to-cycle variation, which is one of the most important questions to be answered by this analysis. Table ORNL-3 presents comparison of these saturated activities, corrected to a power of 30 MW.

Table ORNL-3 indicates that the variation is as much as 40%, with cycle groups 158C + 158D and 161C representing the extremes. The spectrum remains unaltered from cycle to cycle, however, at least at T/2, since the last column represents the ratio of two markedly different responses. The very slow, monotonic hardening of the spectrum at T/2, independent of cycle, is very interesting! The rms standard deviation of the intensity at T/2 is about 10%. For comparative purposes, the calculated startup saturated activities at T/2 are 8.84-15, 7.05-17, and 7.04-13, respectively. The straight averages of the two-year activities in Table ORNL-3 are 8.00-15, 6.21-17, and 6.44-13, respectively - about 10% lower than the startup activities. Thus, it seems indicated that the differences in the HEDL and ECN measurements noted earlier for the two-year irradiation experiment and the startup experiment, respectively, are due to source variations and not differences in measurement techniques.

TABLE ORNL-3

CYCLE GROUP-TO-CYCLE GROUP VARIATION OF SOME SATURATED ACTIVITIES AT THE T/2 LOCATION, X = -5.37, Z = 0

Cycles	$^{54}Fe(n,p)$	$^{63}Cu(n,\alpha)$	$^{237}Np(n,f)$	Np/Cu
153B+153C	7.59-15*	5.87-17*	6.17-13*	1.05+4
153D	7.58-15	5.87-17	6.16-13	1.05+4
153F	7.38-15	5.71-17	5.99-13	1.05+4
153G-154C	7.83-15	6.05-17	6.35-13	1.05+4
154D-154J	7.47-15	5.79-17	6.06-13	1.05+4
155B-155F	9.15-15	7.06-17	7.42-13	1.05+4
156C-157B	8.65-15	6.68-17	6.99-13	1.05+4
157C-157E	8.82-15	6.80-17	7.14-13	1.05+4
158C+158D	9.65-15	7.45-17	7.83-13	1.05+4
158E-158G	8.24-15	6.36-17	6.64-13	1.04+4
158H-158K	8.14-15	6.33-17	6.50-13	1.03+4
159A-159C	8.42-15	6.54-17	6.73-13	1.03+4
159D-160C	7.83-15	6.10-17	6.24-13	1.02+4
160D+160E	7.27-15	5.69-17	5.76-13	1.01+4
161B	7.14-15	5.62-17	5.65-13	1.01+4
161C	6.86-15	5.40-17	5.41-13	1.00+4

*Units are reactions per atom per second at 30 MW.

To compare calculated activities with measurement, recourse must be made to decaying the saturated activities to the ends of irradiation, since saturated activities lose much of their significance when the core leakage is a function of time. Thus, for each dosimeter,

$$A_{EOI}(x,y,z) = \sum_G \frac{RR_S^G(x,y,z)\sum_{i\epsilon G}^{L}\Delta tup(i)}{t_L^G(\text{retracted})-t_1^G(\text{inserted})} \times \left[e^{-\frac{0.69315}{\tau_{1/2}}(t_{EOI}-t_L^G)}-e^{-\frac{0.69315}{\tau_{1/2}}(t_{EOI}-t_1^G)}\right], \quad (7)$$

for non-fission reactions, and the above equation multiplied by Y, the yield, for fission reactions. In Eq. (7), $\tau_{1/2}$ is the half life of the decaying reaction product in days and the $(t_{EOI}-t^G)$ values must also be expressed in days. Table ORNL-1 shows the decay factors [i.e., the last bracket in Eq. (7)] calculated for the cycle groups in Table ORNL-4 for the end of SSC-1 irradiation.

TABLE ORNL-4

DECAY FACTORS TO THE END OF SSC-1 IRRADIATION
FOR THE VARIOUS CYCLE GROUPS

	$\tau_{1/2}$(days)*	Y*	153B+153C	153D	153F
$^{63}Cu(n,\alpha)$	1925		.007275	.005549	.004006
$^{46}Ti(n,p)$	83.85		.1184	.1052	.08805
$^{54}Fe(n,p)$	312.5		.04133	.03268	.02443
$^{58}Ni(n,p)$	70.85		.1312	.1200	.1033
$^{238}U(n,f)^{137}Cs$	11023	.06000	.001287	.000976	.000701
$^{238}U(n,f)^{95}Zr$	64.10	.05105	.1387	.1294	.1136
$^{238}U(n,f)^{103}Ru$	39.43	.06229	.1683	.1788	.1780
$^{238}U(n,f)^{140}Ba$	12.79	.05948	.1096	.2323	.4535
$^{237}Np(n,f)^{137}Cs$	11023	.06267	.001287	.000976	.000701
$^{237}Np(n,f)^{95}Zr$	64.10	.05699	.1387	.1294	.1136
$^{237}Np(n,f)^{103}Ru$	39.43	.05584	.1683	.1788	.1780
$^{237}Np(n,f)^{140}Ba$	12.79	.05489	.1096	.2323	.4535

*Values are the ones used by HEDL in their data reduction procedures.

Tables ORNL-5 through -7 present the results of the calculations using Eq. (7) with the measurements as reported by HEDL for the SSC-1 irradiation.

A general conclusion from inspection of Tables ORNL-5 through 7 is that the agreement between calculation and measurement is within about 15%, which is about the same as the comparisons in the startup experiment. Since the SSC-1 measurements averaged about 10% lower than the startup ones, we have verified that this difference is due to source differences over the duration of the two experiments, and not to geometric differences or differences in the measurement techniques between ECN and HEDL. The axial profiles are well calculated, but there is evidence from Table ORNL-5 that the flux synthesis procedure is beginning to overestimate at 10 cm below the z axis (approximately 15 cm below the horizontal midplane). The calculated $^{46}Ti(n,p)$ activities are also generally a little lower, a circumstance noted in previous analyses. Finally, the effect of the decay on the relative importance of each cycle group is clearly indicated in the tables, especially Table ORNL-7. Here it is apparent that the last cycle (153F) is becoming more and more important in its relative contribution to the end of irradiation activities as the half life decreases; indeed, it contributes better than half of the calculated ^{140}Ba activity ($\tau_{1/2}$ = 12.79 days) whereas only about a fourth of the ^{137}Cs activity ($\tau_{1/2}$ = 11,023 days).

TABLE ORNL-5

CONTRIBUTIONS OF THE CYCLE GROUPS TO THE CALCULATED SSC-1 ACTIVITIES AT THE END OF IRRADIATION AND COMPARISON WITH HEDL MEASUREMENTS

		Axial Profiles at x = 0, y = 131.5 mm*					
		E_{EOI}	153B+153C	153D	153F	C_{EOI}	C/E
$^{54}Fe(n,p)$:	z = 96.9 mm	3.70-14†	1.37-14	1.20-14	0.86-14	3.43-14	0.93
	z = 62.0	4.06-14	1.44-14	1.26-14	0.91-14	3.61-14	0.89
	z = -1.5	4.01-14	1.46-14	1.29-14	0.93-14	3.68-14	0.92
	z = -65.0	3.87-14	1.41-14	1.24-14	0.90-14	3.55-14	0.92
	z = -100.0	3.36-14	1.33-14	1.17-14	0.85-14	3.35-14	1.00
$^{58}Ni(n,p)$:	z = 96.9 mm	1.86-13	0.60-13	0.60-13	0.50-13	1.70-13	0.91
	z = 62.0	2.01-13	0.63-13	0.64-13	0.53-13	1.80-13	0.90
	z = -1.5	2.04-13	0.64-13	0.65-13	0.54-13	1.83-13	0.90
	z = -65.0	1.95-13	0.61-13	0.62-13	0.52-13	1.75-13	0.90
	z = -100.0	1.73-13	0.58-13	0.59-13	0.49-13	1.66-13	0.96
$^{46}Ti(n,p)$:	z = 96.9 mm	1.51-14	0.48-14	0.47-14	0.38-14	1.33-14	0.88
	z = 62.0	1.63-14	0.51-14	0.50-14	0.40-14	1.41-14	0.87
	z = -1.5	1.68-14	0.51-14	0.51-14	0.41-14	1.43-14	0.85
	z = -65.0	1.58-14	0.50-14	0.49-14	0.40-14	1.39-14	0.88
	z = -100.0	1.35-14	0.46-14	0.46-14	0.37-14	1.29-14	0.96

*All locations are based on the coordinate system defined by HEDL.

†Units are disintegrations per second per atom. Read 3.70×10^{-14}.

TABLE ORNL-6

CONTRIBUTIONS OF THE CYCLE GROUPS TO THE CALCULATED SSC-1 ACTIVITIES AT THE END OF IRRADIATION AND COMPARISON WITH HEDL MEASUREMENTS AT X = ±50, Y = 133.0, Z = 0 MM AND X = ±50, Y = 139.9, Z = -67.5 MM*

	(x,y,z)	E_{EOI}	153B+153C	153D	153F	C_{EOI}	C/E
$^{54}Fe(n,p)$:	(-50,133,0)	3.92-14†	1.31-14	1.16-14	0.84-14	3.41-14	0.84
	(50,133,0)	3.91-14	1.37-14	1.20-14	0.87-14	3.44-14	0.88
	(50,139.9,-67.5)	3.21-14	1.16-14	1.02-14	0.74-14	2.92-14	0.91
$^{46}Ti(n,p)$:	(-50,133,0)	1.67-14	0.46-14	0.46-14	0.37-14	1.29-14	0.77
	(50,133,0)	1.68-14	0.48-14	0.47-14	0.38-14	1.33-14	0.79
$^{58}Ni(n,p)$:	(-50,133,0)	1.97-13	0.57-13	0.58-13	0.49-13	1.64-13	0.83
	(50,133,0)	1.99-13	0.60-13	0.61-13	0.51-13	1.72-13	0.86
	(-50,139.9,-67.5)	1.62-13	0.48-13	0.49-13	0.41-13	1.38-13	0.85
$^{63}Cu(n,\alpha)$:	(-50,133,0)	4.44-17	1.45-17	1.24-17	0.87-17	3.56-17	0.80
	(50,133,0)	4.47-17	1.52-17	1.29-17	0.90-17	3.71-17	0.83
	(-50,139.9,-6.75)	3.64-17	1.24-17	1.06-17	0.75-17	3.05-17	0.84

*All locations are based on the coordinate system defined by HEDL.
†Units are disintegrations per second per atom. Read 3.92×10^{-14}.

TABLE ORNL-7

CONTRIBUTIONS OF THE CYCLE GROUPS TO THE CALCULATED SSC-1 FISSION PRODUCT ACTIVITIES AT THE END OF IRRADIATION AND COMPARISON WITH HEDL MEASUREMENTS AT X = ±50, Y = 133.0, Z = -7.9 MM AND X = -50, Y = 133.0, Z = 7.9 MM*

	(x,y,z)	E_{EOI}	153B+153C	153D	153F	C_{EOI}	C/E
$^{238}U(n,f)^{137}Cs$:	(-50,133,-7.9)	4.08-16†	1.34-16	1.14-16	0.79-16	3.27-16	0.80
	(50,133,-7.9)	4.00-16	1.40-16	1.18-16	0.82-16	3.40-16	0.85
$^{238}U(n,f)^{95}Zr$:	(-50,133,-7.9)	4.40-14	1.23-14	1.28-14	1.08-14	3.59-14	0.82
	(50,133,-7.9)	4.30-14	1.28-14	1.33-14	1.13-14	3.74-14	0.87
$^{238}U(n,f)^{103}Ru$:	(-50,133,-7.9)	7.79-14	1.82-14	2.21-14	2.07-14	6.10-14	0.78
	(50,133,-7.9)	7.61-14	1.89-14	2.29-14	2.16-14	6.34-14	0.83
$^{238}U(n,f)^{140}Ba$:	(-50,133,-7.9)	1.07-13	0.11-13	0.27-13	0.50-13	8.8-14	0.82
	(50,133,-7.9)	1.04-13	0.12-13	0.28-13	0.53-13	9.3-14	0.89
$^{237}Np(n,f)^{137}Cs$:	(-50,133, 7.9)	3.29-15	1.07-15	0.91-15	0.63-15	2.61-15	0.79
$^{237}Np(n,f)^{95}Zr$:	(-50,133, 7.9)	3.75-13	1.05-13	1.09-13	0.93-13	3.07-13	0.82
$^{237}Np(n,f)^{103}Ru$:	(-50,133, 7.9)	5.18-13	1.25-13	1.48-13	1.42-13	4.15-13	0.80
$^{237}Np(n,f)^{140}Ba$:	(-50,133, 7.9)	8.04-13	0.80-13	1.89-13	3.56-13	6.25-13	0.78

*All locations are based on the coordinate system defined by HEDL.
†Units are disintegrations per second per atom. Read 3.92×10^{-14}.

Following an identical analysis of the end of irradiation measurements for the SSC-2, the next three tables, Tables ORNL-8 through -10, summarize similar results to those in Tables ORNL-4 through 7 for the SSC-1 exposures.

The agreement between calculations and measurements averages about 10% better for the SSC-2 than for either the SSC-1 or startup comparisons. This better agreement (within about 5%) is caused by average increases in the calculations of about 15% and average increases in the measurements of about 5% over the corresponding SSC-1 values. As will be discussed again later, it begins to look like the more cycles that are introduced into the calculation, the better the agreement. So far, we have gone from one cycle (startup) to four cycles (SSC-1) to eight cycles (SSC-2) with improvement in the comparisons with measurement. This suggests either that a calculated VENTURE source for a given cycle requires a bias factor which tends to be uncorrelated with that of other cycles, or that some important geometric dimension is changing with the insertion and retraction of the experiment during each cycle but its average value tends to agree with the value assumed in the calculation.

Using the same analytical procedure as outlined for the analyses of the SSC-1 and SSC-2 exposures, but now extended over the full two-year time span, the following results for calculations with the SPVC and SVBC were obtained and are shown in Tables ORNL-11 through -17.

From an inspection of Tables ORNL-12 through 14, it is evident that the calculations and the measurements agree at "OT," lie within about 5% at T/4, and about 10% at T/2, with the $^{46}Ti(n,p)$ as usual about 5% more discrepant than either the $^{58}Ni(n,p)$ or the $^{54}Fe(n,p)$ comparisons. [Apparently, the $^{46}Ti(n,p)$ cross sections used in the calculations are about 5% too low.] This agreement is about 5% better at both the T/4 and T/2 locations than in the startup comparisons.

Since the two-year measurements average from 10 to 25% lower than the startup in the SPVC on a saturated activity basis, we have shown that this effect is at least partially calculable and is again due to the cycle-to-cycle source variation, expecially near the end of the irradiation. The $^{54}Fe(n,p)$ counting rates reflect truer integrals over the entire irradiation period than either the $^{58}Ni(n,p)$ or $^{46}Ti(n,p)$ counting rates do, again from Tables ORNL-12 through -14. The measured $^{54}Fe(n,p)$ saturated activities averaged about 13% lower in the two common SPVC locations (T/4 and T/2) for the two-year exposure than for the startup experiment. A glance at Table ORNL-3 verifies that the saturated activities over the course of the two-year exposure average about 10% lower than for the startup experiment. For the $^{58}Ni(n,p)$ and $^{46}Ti(n,p)$ saturated activities, the two-year exposure values in the SPVC average about 25% lower. From Tables ORNL-13 and -14, better than 90% of the calculated activities at the end of the two-year irradiation come from cycles 158H-158K and later. From Table ORNL-3, the average saturated activities averaged over these last six cycle groups are about 20% lower than for the startup experiment. This well-known effect of decay can be even more pronounced for some of the fission product activities as is evidenced in Tables ORNL-16 and -17. It will be interesting to validate the calculations in these two tables when HEDL fission dosimetry data finally become available.

The general conclusion from this analysis is that cycle-to-cycle source variations can be important, and that comparisons between calculations and measurements at the PSF seem to improve when more cycles are averaged into the calculation. Whether this is due to VENTURE uncertainties or geometric variations in the exposure procedures is a matter of conjecture at this time.

TABLE ORNL-8

DECAY FACTORS TO THE END OF SSC-2 IRRADIATION
FOR THE VARIOUS CYCLE GROUPS

	157C-157E	158C+158D	158E-158G
$^{63}Cu(n,\alpha)$	.01464	.01014	.01236
$^{46}Ti(n,p)$	.1558	.1565	.2479
$^{54}Fe(n,p)$	.07499	.05667	.07345
$^{58}Ni(n,p)$	.1593	.1717	.2861
$^{237}Np(n,f)^{137}Cs$	.002626	.001792	.002164
$^{237}Np(n,f)^{95}Zr$	.1595	.1804	.3110
$^{237}Np(n,f)^{103}Ru$	.1359	.2101	.4542

Expected Future Accomplishments

A final NUREG report which documents the calculations and analysis of the PSF two-year irradiation experiment is expected this fiscal year.

TABLE ORNL-9

CONTRIBUTION OF THE CYCLE GROUPS TO THE CALCULATED SSC-2 ACTIVITIES
AT THE END OF IRRADIATION AND COMPARISON WITH HEDL MEASUREMENTS
AXIAL PROFILES AT X = 0, Y = 131.5 MM*

		E_{EOI}	157C-157E	158C+158D	158E-158G	C_{EOI}	C/E
$^{54}Fe(n,p)$:	z = 96.9 mm	7.09-14†	2.73-14	2.24-14	2.35-14	7.32-14	1.03
	z = 62.0	7.74-14	2.90-14	2.36-14	2.52-14	7.78-14	1.01
	z = -1.5	7.97-14	2.96-14	2.37-14	2.67-14	8.00-14	1.00
	z = -65.0	7.63-14	2.86-14	2.27-14	2.62-14	7.75-14	1.02
	z = -100.0	6.53-14	2.68-14	2.13-14	2.49-14	7.30-14	1.12
$^{58}Ni(n,p)$:	z = 96.9 mm	2.89-13	0.80-13	0.92-13	1.24-13	2.96-13	1.02
	z = 62.0	3.15-13	0.84-13	0.97-13	1.33-13	3.14-13	1.00
	z = -1.5	3.24-13	0.84-13	0.98-13	1.41-13	3.25-13	1.00
	z = -65.0	3.09-13	0.83-13	0.94-13	1.39-13	3.16-13	1.02
	z = -100.0	2.73-14	0.78-14	0.88-14	1.32-14	2.98-13	1.09
$^{46}Ti(n,p)$:	z = 96.9 mm	2.37-14	0.69-14	0.75-14	0.97-14	2.41-14	1.02
	z = 62.0	2.80-14	0.73-14	0.79-14	1.04-14	2.56-14	0.91
	z = -1.5	2.81-14	0.75-14	0.80-14	1.09-14	2.64-14	0.94
	z = -65.0	2.71-14	0.72-14	0.76-14	1.08-14	2.56-14	0.94
	z = -100.0	2.38-14	0.68-14	0.71-14	1.02-14	2.41-14	1.01

*All locations are based on the coordinate system defined by HEDL.
†Units are disintegrations per second per atom. Read 3.92×10^{-14}.

TABLE ORNL-10

CONTRIBUTIONS OF THE CYCLE GROUPS TO THE CALCULATED SSC-2 ACTIVITIES AT THE END OF IRRADIATION AND COMPARISON WITH HEDL MEASUREMENTS AT X = ±50, Y = 133.0, Z = 0.6 MM AND X = ~±25.3, Y = 139.0, Z = -12.7 mm*

	(x,y,z)	E_{EOI}	157C-157E	158C+158D	158E-158G	C_{EOI}	C/E
$^{54}Fe(n,p)$:	(50,133,-0.6)	7.56-14†	2.69-14	2.14-14	2.41-14	7.24-14	0.96
	(-50,133, 0.6)	7.81-14	2.75-14	2.23-14	2.49-14	7.47-14	0.96
	(25.3,139,-12.7)	7.28-14	2.24-14	1.95-14	2.20-14	6.39-14	0.88
	(-25.3,139,-12.7)	7.52-14	2.48-14	2.00-14	2.23-14	6.71-14	0.89
$^{46}Ti(n,p)$:	(50,133, 0.6)	2.73-14	0.68-14	0.72-14	0.99-14	2.39-14	0.88
	(-50,133, 0.6)	2.80-14	0.70-14	0.75-14	1.02-14	2.47-14	0.88
$^{58}Ni(n,p)$:	(50,133, 0.6)	3.11-13	0.78-13	0.88-13	1.28-13	2.94-13	0.95
	(-50,133, 0.6)	3.20-13	0.80-13	0.92-13	1.32-13	3.04-13	0.95
$^{63}Cu(n,\alpha)$:	(50,133, 0.6)	8.88-17	3.30-17	2.41-17	2.56-17	8.27-17	0.93
	(-50,133, 0.6)	9.13-17	3.38-17	2.51-17	2.63-17	8.52-17	0.93
$^{237}Np(n,f)^{137}Cs$:	(50,133, 0.6)	6.71-15	2.46-15	1.76-15	1.85-15	6.07-15	0.90
	(-50,133, 0.6)	6.91-15	2.50-15	1.84-15	1.91-15	6.25-15	0.91
$^{237}Np(n,f)^{95}Zr$:	(50,133, 0.6)	5.87-13	1.36-13	1.60-13	2.38-13	5.34-13	0.91
	(-50,133, 0.6)	5.96-13	1.38-13	1.67-13	2.45-13	5.50-13	0.92
$^{237}Np(n,f)^{103}Ru$	(50,133, 0.6)	7.20-13	1.14-13	1.84-13	3.44-13	6.42-13	0.89
	(-50,133, 0.6)	7.29-13	1.16-13	1.92-13	3.54-13	6.62-13	0.91

*All locations are based on the coordinate system defined by HEDL.
†Units are disintegrations per second per atom. Read 3.92×10^{-14}.

TABLE ORNL-11

DECAY FACTORS TO THE END OF THE SPVC + SVBC IRRADIATION FOR THE VARIOUS CYCLE GROUPS

Cycle group	$^{63}Cu(n,\alpha)$	$^{46}Ti(n,p)$	$^{54}Fe(n,p)$	$^{58}Ni(n,p)$	$(n,f)^{137}Cs$	$(n,f)^{95}Zr$	$(n,f)^{103}Ru$	$(n,f)^{140}Ba$
153B+153C	0.005606	2.847-4	0.008196	1.043-4	0.001230	5.202-5	4.538-7	7.425-19
153D	0.004268	2.530-4	0.006480	9.55-5	9.325-4	4.855-5	4.822-7	1.574-18
153F	0.003081	2.118-4	0.004844	8.22-5	6.694-4	4.261-5	4.800-7	3.073-18
153G-154C	0.01368	0.001237	0.02295	5.085-4	0.002942	2.736-4	3.956-6	1.120-16
154D-154J	0.02269	0.003592	0.04325	0.001648	0.004769	9.558-4	2.281-5	1.171-14
155B-155F	0.01262	0.003899	0.02821	0.002027	0.002587	0.001280	5.281-5	4.228-13
155G-156B	0.01772	0.008289	0.06198	0.004669	0.003577	0.003115	1.850-4	1.160-11
156C-157B	0.02122	0.1696	0.05926	0.01059	0.004205	0.007575	7.150-4	5.858-10
157C-157E	0.01328	0.01657	0.04116	0.01125	0.002582	0.008521	0.001161	5.943-9
158C+158D	0.009193	0.1664	0.3110	0.1213	0.001762	0.009635	0.001795	4.728-8
158E-158G	0.01121	0.02637	0.04031	0.02020	0.002127	0.01661	0.003881	3.553-7
158H-158K	0.01666	0.05543	0.06495	0.04541	0.003122	0.03909	0.01237	6.333-6
159A-159C	0.01957	0.1016	0.08465	0.04541	0.003122	0.03909	0.01237	6.333-6
159D-160C	0.02159	0.1920	0.1059	0.1899	0.003898	0.1859	0.1374	0.007425
160D-160E	0.007316	0.09073	0.03886	0.09546	0.001304	0.09742	0.09392	0.01761
161B	0.008680	0.1428	0.04925	0.1586	0.001530	0.1680	0.2064	0.1455
161C	0.009366	0.1939	0.05609	0.2251	0.001638	0.2456	0.3676	0.7565

TABLE ORNL-12

CONTRIBUTIONS OF THE CYCLE GROUPS TO THE CALCULATED SPVC AND SVBC ACTIVITIES AT THE END OF IRRADIATION AND COMPARISON WITH HEDL MEASUREMENTS FOR $^{54}Fe(n,p)$

Cycle Group	"OT"*	T/4*	T/2*	VEPCO*
153B+153C	3.65-16†	1.53-16	5.59-17	3.07-18
153D	3.21-16	1.35-16	4.92-17	2.70-18
153F	2.32-16	9.73-17	3.55-17	1.93-18
153G-154C	1.53-16	3.57-16	1.30-16	7.09-18
154D-154J	1.81-15	7.58-16	2.77-16	1.54-17
155B-155F	1.44-15	6.02-16	2.20-16	1.22-17
155G-156B	2.81-15**	1.18-15**	4.29-16**	2.38-17**
156C-157B	2.87-15	1.20-15	4.40-16	2.42-17
157C-157E	2.04-15	8.53-16	3.12-16	1.71-17
158C+158D	1.65-15	6.91-16	2.52-16	1.43-17
158E-158G	1.83-15	7.64-16	2.79-16	1.42-17
158H-158K	3.29-15	1.38-15	5.02-16	1.43-17
159A-159C	3.75-15	1.57-15	5.71-16	3.03-17
159D-160C	4.75-15	1.98-15	7.22-16	3.89-17
160D+160E	1.78-15	7.45-16	2.72-16	1.48-17
161B	2.32-15	9.72-16	3.54-16	1.89-17
161C	2.53-15	1.06-15	3.87-16	2.10-17
SUM, CALC.	3.46-14	1.45-14	5.29-15	2.88-16
MEASURED	3.40-14	1.51-14	5.87-15	
C/E	1.02	0.96	0.90	

*The SPVC locations "OT," T/4, and T/2 have coordinates (x,y,z) of (±53.7, 241.3, -8.5) mm, (±53.7, 286.4, -8.4) mm, and (±53.7, 337.8, -8.5), respectively, based on the HEDL coordinate system; and the SVBC location in the VEPCO capsule has coordinated (-72.6, 765.0, 55.3) mm. Both the measured and calculated activities vary little between the +53.7 and -53.7 locations, so that only the average of the activities at the two x locations appear in this table.

†Read 3.65×10^{-10} disintegrations per second per atom.

**Estimated.

TABLE ORNL-13

CONTRIBUTIONS OF THE CYCLE GROUPS TO THE CALCULATED SPVC AND SVBC ACTIVITIES AT THE END OF IRRADIATION AND COMPARISON WITH HEDL MEASUREMENTS FOR $^{46}Ti(n,p)$

Cycle Group	"OT"*	T/4*	T/2*	VEPCO*
153B+153C	1.73-18†	7.08-19	2.55-19	1.56-20
153D	1.72-18	7.03-19	2.52-19	1.55-20
153F	1.39-18	5.70-19	2.04-19	1.24-20
153G-154C	6.30-18	2.57-18	9.23-19	5.60-20
154D-154J	2.06-17	8.43-18	3.02-18	1.88-19
155B-155F	2.72-17	1.11-17	3.97-18	2.47-19
155G-156B	5.14-17**	2.10-17**	7.51-18**	4.66-19**
156C-157B	1.13-16	4.60-17	1.65-17	1.01-18
157C-157E	1.12-16	4.58-17	1.64-17	1.01-18
158C+158D	1.21-16	4.92-17	1.77-17	1.12-18
158E-158G	1.64-16	6.68-17	2.38-17	1.43-18
158H-158K	3.86-16	1.58-16	5.64-17	3.40-18
159A-159C	6.18-16	2.53-16	8.96-17	5.33-18
159D-160C	1.18-15	4.82-16	1.73-16	1.03-17
160D+160E	5.75-16	2.34-16	8.40-17	5.09-18
161B	9.32-16	3.81-16	1.37-16	8.07-18
161C	1.22-15	4.95-16	1.78-16	1.07-17
SUM, CALC.	5.53-15	2.26-15	8.10-16	4.85-17
MEASURED	5.90-15	2.57-15	9.45-16	
C/E	0.94	0.88	0.86	

*The SPVC locations "OT," T/4, and T/2 have coordinates (x,y,z) of (±53.7, 241.3, -8.5) mm, (±53.7, 286.4, -8.4) mm, and (±53.7, 337.8, -8.5), respectively, based on the HEDL coordinate system; and the SVBC location in the VEPCO has coordinated (-72.6, 765.0, 55.3) mm. Both the measured and calculated activities vary little between the +53.7 and -53.7 locations, so that only the average of the activities at the two x locations appear in this table.

†Read 1.73×10^{-18} disintegrations per second per atom.

**Estimated.

TABLE ORNL-14

CONTRIBUTIONS OF THE CYCLE GROUPS TO THE CALCULATED SPVC AND SVBC ACTIVITIES AT THE END OF IRRADIATION AND COMPARISON WITH HEDL MEASUREMENTS FOR $^{58}Ni(n,p)$

Cycle Group	"OT"*	T/4*	T/2*	VEPCO*
153B+153C	6.29-18†	2.69-18	1.01-18	5.52-20
153D	6.40-18	2.75-18	1.02-18	5.62-20
153F	5.34-18	2.28-18	8.55-19	4.63-20
153G-154C	2.68-17	1.15-17	4.28-18	2.32-19
154D-154J	9.71-17	4.17-17	1.56-17	8.62-19
155B-155F	1.45-16	6.19-17	2.31-17	1.28-18
155G-156B	2.95-16**	1.27-16**	4.74-17**	2.60-18**
156C-157B	7.12-16	3.05-16	1.14-16	6.26-18
157C-157E	7.54-16	3.23-16	1.21-16	6.60-18
158C+158D	8.68-16	3.73-16	1.40-16	7.86-18
158E-158G	1.24-15	5.31-16	1.98-16	1.07-17
158H-158K	3.12-15	1.34-15	4.97-16	2.68-17
159A-159C	5.44-15	2.33-15	8.67-16	4.59-17
159D-160C	1.15-14	4.93-15	1.83-15	9.82-17
160D+160E	5.92-15	2.54-15	9.48-16	5.13-17
161B	1.00-14	4.33-15	1.62-15	8.57-17
161C	1.38-14	5.87-15	2.21-15	1.19-16
SUM, CALC.	5.39-14	2.31-14	8.64-15	4.64-16
MEASURED	5.44-14	2.45-14	9.61-15	
C/E	0.99	0.94	0.90	

*The SPVC locations "OT," T/4, and T/2 have coordinates (x,y,z) of (±53.7, 241.3, -8.5) mm, (±53.7, 286.4, -8.4) mm, and (±53.7, 337.8, -8.5), respectively, based on the HEDL coordinate system; and the SVBC location in the VEPCO capsule has coordinated (-72.6, 765.0, 55.3) mm. Both the measured and calculated activities vary little between the +53.7 and -53.7 locations, so that only the average of the activities at the two x locations appear in this table.

†Read 6.29 x 10^{-18} disintegrations per second per atom.

**Estimated.

TABLE ORNL-15

CONTRIBUTIONS OF THE CYCLE GROUPS TO THE CALCULATED SPVC AND SVBC ACTIVITIES AT THE END OF IRRADIATION FOR $^{63}Cu(n,\alpha)$

Cycle Group	"OT"*	T/4*	T/2*	VEPCO*
153B+153C	1.91-18†	8.00-19	2.95-19	1.96-20
153D	1.62-18	6.78-19	2.51-19	1.66-20
153F	1.13-18	4.73-19	1.75-19	1.15-20
153G-154C	3.90-18	1.63-18	6.01-19	3.94-20
154D-154J	7.26-18	3.04-18	1.13-18	7.55-20
155B-155F	4.90-18	2.05-18	7.57-19	5.07-20
155G-156B	6.13-18**	2.57-18**	9.47-19**	6.33-20**
156C-157B	7.88-18	3.31-18	1.22-18	8.09-20
157C-157E	5.02-18	2.10-18	7.75-19	5.12-20
158C+158D	3.71-18	1.55-18	5.75-19	3.93-20
158E-158G	3.88-18	1.62-18	5.98-19	3.87-20
158H-158K	6.49-18	2.72-18	9.99-19	6.50-20
159A-159C	6.66-18	2.79-18	1.02-18	6.52-20
159D-160C	7.43-18	3.10-18	1.14-18	7.38-20
160D+160E	2.59-18	1.09-18	4.01-19	2.63-20
161B	3.17-18	1.33-18	4.90-19	3.13-20
161C	3.29-18	1.38-18	5.09-19	3.32-20
SUM, CALC.	7.70-17	3.70-17	1.19-17	7.82-19

*The SPVC locations "OT," T/4, and T/2 have coordinates (x,y,z) of (±53.7, 241.3, -8.5) mm, (±53.7, 286.4, -8.4) mm, and (±53.7, 337.8, -8.5), respectively, based on the HEDL coordinate system; and the SVBC location in the VEPCO capsule has coordinated (-72.6, 765.0, 55.3) mm. Both the measured and calculated activities vary little between the +53.7 and -53.7 locations, so that only the average of the activities at the two x locations appear in this table.

†Read 6.91×10^{-18} disintegrations per second per atom.

**Estimated.

TABLE ORNL-16

CONTRIBUTIONS OF THE CYCLE GROUPS TO THE CALCULATED SPVC FISSION PRODUCT ACTIVITIES AT THE END OF IRRADIATION FOR $^{238}U(n,f)$ F.P.

Cycle group	"OT"*				T/4*				T/2*			
	^{137}Cs	^{95}Zr	^{103}Ru	^{140}Ba	^{137}Cs	^{95}Zr	^{103}Ru	^{140}Ba	^{137}Cs	^{95}Zr	^{103}Ru	^{140}Ba
153B+153C	1.67-17†	6.02-19	6.40-21	1.00-32	8.08-18	2.91-19	3.10-21	4.84-33	3.37-18	1.21-19	1.29-21	2.01-33
153D	1.41-17	6.26-19	7.58-21	2.36-32	6.80-18	3.02-19	3.66-21	1.14-32	2.84-18	1.26-19	1.53-21	4.78-33
153F	9.80-18	5.31-19	7.30-21	4.46-32	4.74-18	2.57-19	3.53-21	2.16-32	1.97-18	1.07-19	1.47-21	8.97-33
153G-154C	3.34-17	2.64-18	4.66-20	1.26-30	1.61-17	1.27-18	2.25-20	6.07-31	6.72-18	5.31-19	9.38-21	2.54-31
154D-154J	6.08-17	1.04-17	3.02-19	1.48-28	2.92-17	4.99-18	1.45-19	7.11-29	1.22-17	2.09-18	6.06-20	2.97-29
155B-155F	4.03-17	1.70-17	8.54-19	6.53-27	1.94-17	8.18-18	4.11-19	3.14-27	8.08-18	3.41-18	1.71-19	1.31-27
155G-156B**	4.96-17	3.67-17	2.66-18	1.59-25	2.39-17	1.77-17	1.28-18	7.66-26	9.95-18	7.38-18	5.34-19	3.20-26
156C-157B	6.24-17	9.56-17	1.10-17	8.60-24	3.00-17	4.60-17	5.29-18	4.13-24	1.25-17	1.92-17	2.20-18	1.72-24
157C-157E	3.91-17	1.10-16	1.83-17	8.93-23	1.88-17	5.29-17	8.80-18	4.29-23	7.84-18	2.21-17	3.67-18	1.79-23
158C+158D	2.85-17	1.33-16	3.02-17	7.59-22	1.38-17	6.44-17	1.46-17	3.68-22	5.74-18	2.68-17	6.08-18	1.53-22
158E-158G	2.95-17	1.96-16	5.59-17	4.89-21	1.42-17	9.43-17	2.69-17	2.35-21	5.91-18	3.93-17	1.12-17	9.80-22
158H-158K	4.82-17	5.13-16	1.98-16	9.69-20	2.31-17	2.46-16	9.49-17	4.64-20	9.63-18	1.02-16	3.96-17	1.94-20
159A-159C	4.86-17	9.48-16	5.38-16	2.21-18	2.33-17	4.54-16	2.58-16	1.06-18	9.72-18	1.90-16	1.08-16	4.42-19
159D-160C	5.29-17	2.15-15	1.94-15	9.99-17	2.54-17	1.03-15	9.31-16	4.80-17	1.06-17	4.31-16	3.89-16	2.00-17
160D-160E	1.81-17	1.15-15	1.35-15	2.43-16	8.68-18	5.51-16	6.47-16	1.17-16	3.62-18	2.30-16	2.70-16	4.86-17
161B	2.19-17	2.05-15	3.07-15	2.06-15	1.06-17	9.92-16	1.49-15	9.97-16	4.36-18	4.08-16	6.11-16	4.10-16
161C	2.23-17	2.85-15	5.20-15	1.02-14	1.08-17	1.38-15	2.52-15	4.94-15	4.47-18	5.71-16	1.04-15	2.04-15
SUM, CALC.	5.96-16	1.03-14	1.24-14	1.27-14	2.87-16	4.94-15	6.00-15	6.11-15	1.20-16	2.05-15	2.48-15	2.52-15

*The SPVC locations "OT," T/4, and T/2 have coordinates (x,y,z) of (±53.7, 241.3, -8.5) mm, (±53.7, 286.4, -8.4) mm, and (±53.7, 337.8, -8.5), respectively, based on the HEDL coordinate system; and the SVBC location in the VEPCO capsule has coordinated (-72.6, 765.0, 55.3) mm. Both the measured and calculated activities vary little between the +53.7 and -53.7 locations, so that only the average of the activities at the two x locations appear in this table.

†Read 1.67×10^{-17} disintegrations per second per atom.

**Estimated.

TABLE ORNL-17

CONTRIBUTIONS OF THE CYCLE GROUPS TO THE CALCULATED SPVC FISSION PRODUCT ACTIVITIES AT THE END OF IRRADIATION FOR $^{237}Np(n,f)$ F.P.

Cycle group	"OT"*				T/4*				T/2*			
	^{137}Cs	^{95}Zr	^{103}Ru	^{140}Ba	^{137}Cs	^{95}Zr	^{103}Ru	^{140}Ba	^{137}Cs	^{95}Zr	^{103}Ru	^{140}Ba
153B+153C	1.26-16†	4.83-18	4.13-20	6.64-32	7.78-17	2.98-18	2.55-20	4.10-32	4.26-17	1.63-18	1.40-20	2.25-32
153D	1.07-16	5.02-18	4.89-20	1.57-31	6.58-17	3.09-18	3.01-20	9.66-32	3.60-17	1.70-18	1.66-20	5.35-32
153F	7.37-17	4.26-18	4.71-20	2.96-31	4.55-17	2.63-18	2.90-20	1.83-31	2.49-17	1.44-18	1.60-20	1.00-31
153G-154C	2.51-16	2.12-17	3.01-19	8.37-30	1.55-16	1.30-17	1.85-19	2.49-17	1.44-18	1.60-20	1.02-19	2.84-30
154D-154J	4.58-16	8.34-17	1.95-18	9.83-28	2.83-16	5.11-17	1.19-18	6.02-18	1.55-16	2.82-17	6.58-19	3.32-28
155B-155F	3.03-16	1.36-16	5.51-18	4.34-26	1.88-16	8.38-17	3.38-18	2.66-26	1.02-16	4.59-17	1.86-18	1.47-26
155G-156B**	3.73-16	2.94-16	1.72-17	1.06-24	2.31-16	1.81-16	1.05-17	6.49-25	1.26-16	9.94-17	5.80-18	3.58-25
156C-157B	4.69-16	7.67-16	7.10-17	5.71-23	2.90-16	4.71-16	7.35-17	3.50-23	1.59-16	2.59-17	2.39-17	1.93-23
157C-157E	2.93-16	8.83-16	1.18-16	5.93-22	1.81-16	5.42-16	7.24-17	3.63-22	9.92-17	2.98-16	3.98-17	2.00-22
158C+158D	2.14-16	1.07-15	1.95-16	5.04-21	1.33-16	6.59-16	1.20-16	3.12-21	7.28-17	3.61-16	6.60-17	1.71-21
158E-158G	2.20-16	1.57-15	3.71-16	3.25-20	1.36-16	9.66-16	2.21-16	1.99-20	7.45-17	5.29-16	1.22-16	1.10-20
158H-158K	3.59-16	4.12-15	1.28-15	6.43-19	2.22-16	2.52-15	7.81-16	3.93-19	1.21-16	1.37-15	4.30-16	2.17-19
159A-159C	3.62-16	7.61-15	3.47-15	1.47-17	2.23-16	4.65-15	2.12-15	8.98-18	1.22-16	2.56-15	1.17-15	1.95-18
159D-160C	3.94-16	1.73-14	1.25-14	6.63-16	2.44-16	1.05-14	7.66-15	4.07-16	1.33-16	5.81-15	4.22-15	2.24-16
160D-160E	1.35-16	9.23-15	8.71-15	1.61-15	8.31-17	5.64-15	5.32-15	9.91-16	4.54-17	3.10-15	2.93-15	5.44-16
161B	1.62-16	1.64-14	1.98-14	1.37-14	1.01-16	1.02-14	1.23-14	8.45-15	5.46-17	5.50-15	6.63-15	4.59-15
161C	1.65-16	2.25-14	3.30-14	6.69-14	1.02-16	1.39-14	2.04-14	4.14-14	5.59-17	7.62-15	1.12-14	2.26-14
SUM, CALC.	4.47-15	8.20-14	7.96-14	8.29-14	2.76-15	5.03-14	4.90-14	5.13-14	1.51-15	2.76-15	2.67-14	1.79-14

*The SPVC locations "OT," T/4, and T/2 have coordinates (x,y,z) of (±53.7, 241.3, -8.5) mm, (±53.7, 286.4, -8.4) mm, and (±53.7, 337.8, -8.5), respectively, based on the HEDL coordinate system; and the SVBC location in the VEPCO capsule has coordinated (-72.6, 765.0, 55.3) mm. Both the measured and calculated activities vary little between the +53.7 and -53.7 locations, so that only the average of the activities at the two x locations appear in this table.

†Read 1.67×10^{-17} disintegrations per second per atom.

**Estimated.

APPENDIX

Description of the Contents of Tape X19802

The source data are calculated using the VENTURE code for 46 of the 52 fuel cycles operational during the two-year metallurgical blind test experiment performed at the ORR-PSF. All data for the 46 cycles are in BCD form on a nine-track tape and use a fixed 6E12.5 format for the values of the fission source density. The tape can be read by the following Fortran statements:

```
  DO 4 ICYCLE=1,46
  READ(5,3)ICYCLE,LOG,IXMAX,JYMAX
  DO 1 KZ=1,41
1 READ(5,2)((PSF(IS,JY),IX=1,43),JY=1,36)
4 CONTINUE
2 FORMAT(6E12.5)
3 FORMAT(4I4)
```

where PFS(IX,JY) is the fission source density by interval, in $n \cdot s \cdot cm^3 \cdot 30Mwt$. Each of the 46 sources is identified with the appropriate cycle number in the header record, and the 43 x-intervals (width), 36 y-intervals (height), and 41 z-intervals (depth) include active core with control rods, experiments within the core, beryllium reflector, and a surrounding water medium.

The header record has 4 intergers in it, but only the first one, ICYCLE, is important. The correspondence between ICYCLE and the cycle is the following:

ICYCLE	CYCLE	ICYCLE	CYCLE	ICYCLE	CYCLE	ICYCLE	CYCLE
1	153B	13	154I	25	157E	37	159C
2	153C	14	154J	26	158C	38	159D
3	153D	15	155B	27	158D	39	159E
4	153F	16	155C	28	158E	40	160A
5	153G	17	155E	29	158F	41	160B
6	154A	18	155F	30	158G	42	160C
7	154B	19	156C	31	158H	43	160D
8	154C	20	156E	32	158I	44	160E
9	154D	21	157A	33	158J	45	161B
10	154E	22	157B	34	158K	46	161C
11	154F	23	157C	35	159A		
12	154G	24	157D	36	159B		

Cycles 154H, 155D, 155G, 155H, 156A, and 156B were not calculated.

There is no aluminum window in the VENTURE geometry, but it should be included in any transport calculation. Figure ORNL-2 gives the mesh structure for the calculational model. The 43 x-intervals are "columns," the 36 y-intervals are "rows," and the 41 z-intervals are "planes" in VENTURE notation. The source is confined always to $9 \leq KZ \leq 32$, $6 \leq IX \leq 38$, and $7 \leq JY \leq 34$ and usually to $9 \leq KZ \leq 32$, $9 \leq IX \leq 35$, and $7 \leq JY \leq 30$.

The x-interval boundaries, if they are not clear from the figure, are the following, in cm: 0, 5.9267, 11.8533, 17.78, 20.32, 22.86, 25.4, 27.94, 30.48, 33.02, 35.56, 38.1, 40.64, 43.18, 45.72, 46.55185, 46.90745, 49.53, 52.15255, 52.50815, 53.34, 55.88, 58.42, 60.96, 61.79185, 62.14745, 64.77, 67.39255, 67.74815, 68.58, 71.12, 73.66, 76.2, 78.74, 81.28, 83.82, 86.36, 88.9, 91.44, 93.98, 96.52, 102.4467, 103.3733, and 114.3. The y-interval boundaries are, in cm: 0, 6.35, 12.70, 15.24, 17.78, 20.32, 22.86, 25.4, 27.94, 30.48, 33.02, 35.56, 38.1, 40.64, 43.18, 45.72, 48.26, 50.8, 53.34, 55.88, 58.42, 60.96, 63.5, 66.04, 68.58, 71.12, 73.66, 76.2, 78.72, 81.28, 83.82, 86.36, 88.9, 91.44, 93.98, 100.33, and 106.68. The first 33 z-interval boundaries are the same as the x, 0 - 76.2; then 79.0575, 81.915, 88.265, 94.615, 100.965, 107.315, 113.665, 126.365, and 139.065.

The parameters describing the individual cycles are given in Table ORNL-1.

The final question remains as to how to treat the composition of the core since it is a function of time from cycle to cycle (i.e., a given core location such as C2, for example, might contain fuel in one cycle and an experiment the next, and if the latter, the composition of the experiment must be known). Past experience in this matter is that, as far as the transport is concerned, attention need only be paid to rows A, B, and C, and some sort of approximate cycle weighting of composition and source at these locations is more than adequate. Thus, in any transport calculations, access to some core loading information for the cycles with some idea of the atomic composition of each experiment in rows A, B, and C as well as the atomic composition of a typical fuel assembly and a beryllium block is necessary and can be made available. You will also have to factor in the missing approximate contributions from the six cycles, 154H, 155D, 155G, 155H, 156A, and 156B to obtain the SPVC-SVBC source.

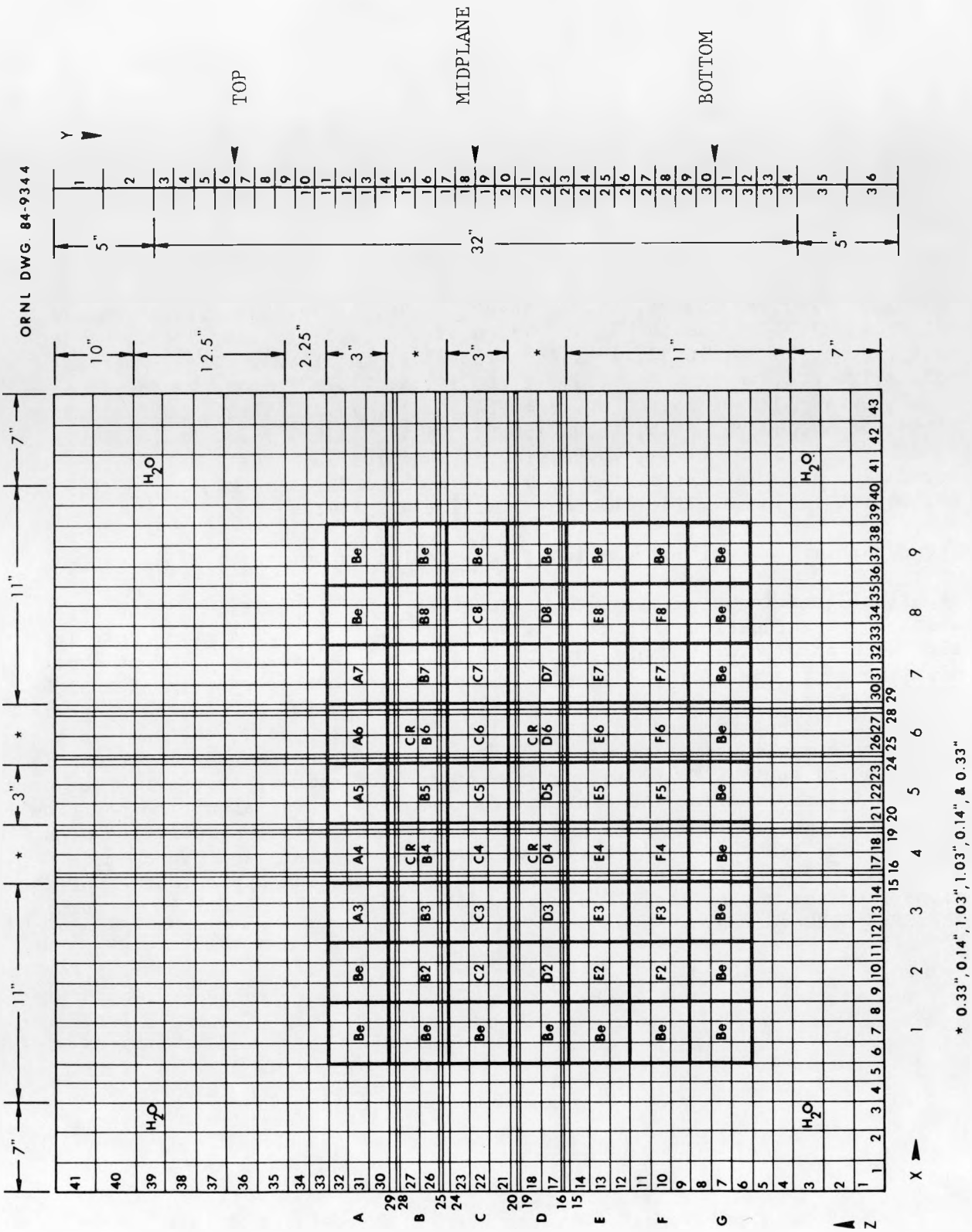

FIGURE ORNL-2. Mesh Structure for the VENTURE Calculational Model.

Description of the Contents of Tape X13850

All 50 files are BCD and use a fixed 6E12.5 format. The tape is non-labeled and has the following general JCL:

```
//GØ.FTXXFOOl DD UNIT=TAPE8,LABEL=(YY,NL,,IN),DISP=(ØLD,KEEP),
//    DCB=(RECFM=FB,LRECL=72,BLKSIZE=7200,DEN=3),VØL=SER=X13850
```

where

XX is the logical tape number for a given file YY to be read,
and
XX can be any number between 01 and 99 except 05, 06, 07, and 53,
and
YY can be any number between 1 and 50.

File 1 contains the upper energy limits of each of the 38 energy groups in eV, and a 39th entry is the lower energy limit of the 38th group. (39 entries)

File 2 contains the midpoint values of the axial mesh that describes all the vertical profiles in files 3-50. These z values may be assumed to be the point axial locations at which the fluences in files 3-50 are accumulated. These coordinates follow the HEDL scheme, i.e., they are relative to a horizontal plane 5.08 cm below the midplane, and are negative below this plane and positive above. These 21 values are expressed in cm, and represent the spatial order in which the fluences appear. These 21 values cover the entire axial range of the locations of all the metallurgical specimens used in the two-year exposure, and are, in order:

```
27.94,   23.02,  20.165,  18.735,  17.465,  16.195,  13.97,
11.43,    9.69,   8.42,    6.20,    3.66,    1.27,   -0.85,
-3.665, -6.625,  -8.56,  -10.0,   -11.6,   -13.97,  -16.195.
```

Files 3-50 each contain spectral fluence profiles, each file representing the spectral fluence profiles for a given x and y location and irradiation history. Thus, files 3-10 contain the spectral fluence axial profiles for the SSC-2 irradiation exposure, files 11-42 the profiles for the SPVC and SVBC full two-year exposure, and files 43-50 the profiles for the SSC-1 irradiation exposure. Both the SSC-1 and SSC-2 files consider the same eight (x,y) locations, file 3 corresponding to the same (x,y) location as file 43, file 4 the same as file 44, and so on up to file 10 and file 50. The SPVC and SVBC two-year exposures appearing in files 11-42 are at 32 (x,y) locations, one (x,y) location for each file. Table ORNL-18 summarizes the contents of each file.

TABLE ORNL-18

CONTENTS OF THE SPECTRAL FLUENCE AXIAL PROFILE TAPE

File No.	Description*
1	Energy grid of the first 38 ELXSIR groups in eV (39 entries)
2	Axial locations at which the profiles are given, in cm. (21)
3	Accumulated fluences in neut/cm2 as a function of energy and axial location for the SSC-2 exposure: (x,y)=(-10.37,12.221)cm. (798)
4	Same as for file 3 except (x,y)=(10.37,12.221)
5	Same as for file 3 except (x,y)=(0.0,12.655)
6	Same as for file 3 except (x,y)=(-4.572,13.290)
7	Same as for file 3 except (x,y)=(4.572,13.290)
8	Same as for file 3 except (x,y)=(0.0,13.925)
9	Same as for file 3 except (x,y)=(-10.37,14.359)
10	Same as for file 3 except (x,y)=(10.37,14.359)
11	Accumulated fluences in neutrons/cm2 as a function of energy and axial location for the full two-year exposure. This is a special point 1/4 in. inside the aluminum window: (x,y)=(0.0,-0.685)cm.
12	Same as for file 11 except (x,y)=(0.0,19.606), another special point 2.264 cm in front of the SPVC
13	Same as for file 11 except (x,y)=(-10.37,22.981) "OT" location
14	Same as for file 11 except (x,y)=(10.37,22.981) "OT" location
15	Same as for file 11 except (x,y)=(0.0,23.415) "OT" location
16	Same as for file 11 except (x,y)=(-4.572,24.050) "OT" location
17	Same as for file 11 except (x,y)=(4.572,24.050) "OT" location
18	Same as for file 11 except (x,y)=(0.0,24.685) "OT" location
19	Same as for file 11 except (x,y)=(-10.37,25.119) "OT" location
20	Same as for file 11 except (x,y)=(10.37,25.119) "OT" location
21	Same as for file 11 except (x,y)=(-10.37,27.491) T/4 location
22	Same as for file 11 except (x,y)=(10.37,27.491) T/4 location
23	Same as for file 11 except (x,y)=(0.0,27.925) T/4 location
24	Same as for file 11 except (x,y)=(-4.572,28.560) T/4 location
25	Same as for file 11 except (x,y)=(4.572,28.560) T/4 location
26	Same as for file 11 except (x,y)=(0.0,29.195) T/4 location
27	Same as for file 11 except (x,y)=(-10.37,29.629) T/4 location
28	Same as for file 11 except (x,y)=(10.37,29.629) T/4 location
29	Same as for file 11 except (x,y)=(-10.37,32.631) T/2 location
30	Same as for file 11 except (x,y)=(10.37,32.631) T/2 location
31	Same as for file 11 except (x,y)=(0.0,33.065) T/2 location
32	Same as for file 11 except (x,y)=(-4.572,33.70) T/2 location
33	Same as for file 11 except (x,y)=(4.572,33.70) T/2 location
34	Same as for file 11 except (x,y)=(0.0,34.335) T/2 location
35	Same as for file 11 except (x,y)=(-10.37,34.769) T/2 location
36	Same as for file 11 except (x,y)=(10.37,34.769) T/2 location
37	Same as for file 11 except (x,y)=(0.0,38.455), a special point 5.945 cm inside the SPVC as measured from the back face; a nominal 3T/4 location

TABLE ORNL-18. CONTINUED

File No.	Description*
38	Same as for file 11 except (x,y)=(0.0,43.925), another special point 0.475 cm inside the SPVC as measured from the back face; a nominal full T location
39	Same as for file 11 except (x,y)=(-10.37,76.709) SVBC(VEPCO) location
40	Same as for file 11 except (x,y)=(-4.872,76.709) SVBC(VEPCO) location
41	Same as for file 11 except (x,y)=(4.872,76.709) SVBC(VEPCO) location
42	Same as for file 11 except (x,y)=(10.37,76.709) SVBC(VEPCO) location
43	Accumulated fluences in neutrons/cm^2 as a function of energy and axial location for the SSC-1 exposure: (x,y)=(-10.37,12.221)cm.
44	Same as for file 43 except (x,y)=(10.37,12.221)
45	Same as for file 43 except (x,y)=(0.0,12.655)
46	Same as for file 43 except (x,y)=(-4.572,13.290)
47	Same as for file 43 except (x,y)=(4.572,13.290)
48	Same as for file 43 except (x,y)=(0.0,13.925)
49	Same as for file 43 except (x,y)=(-10.37,14.359)
50	Same as for file 43 except (x,y)=(10.37,14.359)

*The origin for the x-axis is the same as the HEDL scheme with negative values to the south. The origin for the y-axis also follows the HEDL scheme, but the y-dimensions are based not on the nominal values used by HEDL but actually measured water gap thicknesses, as used by C. A. Baldwin in his description of the absolute notch locations of the metallurgical specimens. The transport calculations assumed the thermal shield to be 6.00 cm. thick instead of 5.99 used by Baldwin and the thickness of the biggest water gap to be 6.17 cm. rather than the 6.13 used by Baldwin. All locations within the SSC, SPVC, and SVBC have been adjusted in the calculations to reflect these slight differences, and no further adjustment of the calculated values to either the HEDL locations for dosimetry or the Baldwin locations for metallurgy are necessary.

The fluences are read from file YY by such statements as:

```
      DØ 1 K=1,21
    1 READ(XX,2)(FLUENS(IG,K),IG=1,38)
    2 FØRMAT(6E12.5)
      REWIND XX
```

where XX is the logical tape number assigned to file YY. Thus, the fluence spectrum at each axial locations constitutes a logical record. The fluences above 1 MeV (groups 1-27) for each of the 21 axial locations in files 6, 16, 24, 32, 40, and 46 appear in Table ORNL-19.

TABLE ORNL- 19

FLUENCE ABOVE 1 MeV AXIAL PROFILES NEAR X = -4.572 FOR TYPICAL SSC-1, "OT," T/4, T/2, SVBC, AND SSC-2 METALLURGICAL SPECIMEN LOCATIONS

z	SSC-1	OT	T/4	T/2	SVBC	SSC-2
27.94	7.02+18*	2.08+19	1.14+19	5.43+18	3.64+17	1.62+19
23.02	9.44+18	2.65+19	1.44+19	6.84+18	4.05+17	2.19+19
20.165	1.37+19	3.01+19	1.63+19	7.82+18	4.14+17	3.21+19
18.735	1.68+19	3.17+19	1.75+19	8.40+18	4.25+17	3.94+19
17.465	1.70+19	3.39+19	1.94+19	9.25+18	4.30+17	3.98+19
16.195	1.68+19	3.33+19	1.83+19	8.71+18	4.40+17	3.94+19
13.97	1.84+19	3.44+19	1.87+19	8.81+18	4.53+17	4.32+19
11.43	1.96+19	3.55+19	1.92+19	8.97+18	4.77+17	4.64+19
9.69	2.02+19	3.61+19	1.94+19	9.08+18	4.98+17	4.79+19
8.42	2.07+19	3.67+19	1.97+19	9.17+18	5.17+17	4.93+19
6.20	2.13+19	3.77+19	2.02+19	9.32+18	5.22+17	5.09+19
3.66	2.17+19	3.83+19	2.04+19	9.42+18	5.18+17	5.20+19
1.27	2.19+19	3.86+19	2.06+19	9.47+18	5.13+17	5.26+19
-0.85	2.18+19	3.86+19	2.05+19	9.44+18	5.07+17	5.25+19
-3.665	2.17+19	3.85+19	2.04+19	9.38+18	5.07+17	5.23+19
-6.625	2.10+19	3.73+19	1.98+19	9.13+18	5.00+17	5.08+19
-8.56	2.04+19	3.63+19	1.93+19	8.91+18	4.93+17	4.93+19
-10.0	1.97+19	3.54+19	1.88+19	8.71+18	4.73+17	4.76+19
-11.6	1.90+19	3.44+19	1.83+19	8.51+18	4.49+17	4.59+19
-13.97	1.76+19	3.26+19	1.75+19	8.19+18	4.26+17	4.26+19
-16.195	1.58+19	3.03+19	1.67+19	7.91+18	4.10+17	3.83+19

*Read 7.02 x 10^{18} neutrons/cm^2.

A.2 POWER DISTRIBUTION CALCULATIONS FOR THE VENUS PWR ENGINEERING MOCKUP

M. L. Williams
P. Morakinyo
F. B. K. Kam

Summary

A 10-group two-dimensional DOT-IV eigenvalue calculation of the VENUS core was performed to obtain space-dependent fission rate distribution for comparison with measurements. The purpose is to validate the transport methodology to predict the source density in the peripheral fuel bundles on a pin-to-pin basis. A slight tilt in the power distribution was reported in the FY 1983 annual report to the NRC Materials Engineering Branch, Division of Engineering Technology. The source of this tilt has been identified and corrected (Fig. ORNL-3). Agreement between calculations and measurements is in most cases within 5%. The worst agreement occurs where it is expected - near the baffles.

Accomplishments and Status

Calculations of the VENUS PWR mockup benchmark experiment being performed in Mol, Belgium have been proceeding since June 1983. The initial calculations have focused on computing the in-core fission density distribution and several ex-core fission chamber results, which were also obtained experimentally by CEN/SCK. Figure ORNL-4 shows a plan view of the VENUS configuration. The computed results have been obtained with two-dimensional transport theory code DOT-IV, using 10-group cross sections. The 10-group cross sections were collapsed from a 218-group set based on ENDF/B-IV data (Fo76). The 218-group structure contains approximately 70 thermal groups. The 218-group cross sections were resonance-shielded using the Nordheim integral method, and were then cell-averaged by applying cell disadvantage factors obtained from 1-D discrete ordinates calculations of the 3 and 4% fuel pins and the borated pyrex rods. The resulting 218 cell-homogenized cross sections were finally collapsed to 10 groups using zone-dependent fluxes obtained for 20 different spatial zones in a 1-D cylindrical representation of the VENUS experiment configuration. In the first set of calculations, two special zones of 2.52 cm (2 pin pitches) were defined in the core region adjacent to the inner and outer baffles, respectively. The average fluxes in these zones were used in order to account for changes in the thermal neutron spectrum which occurs near the boundary of the core and the steel baffle.

The initial comparison between the calculated and experimental results was made in October 1983. At that time, there was some unexplained discrepancies between the calculations and the experimental values -- specifically:

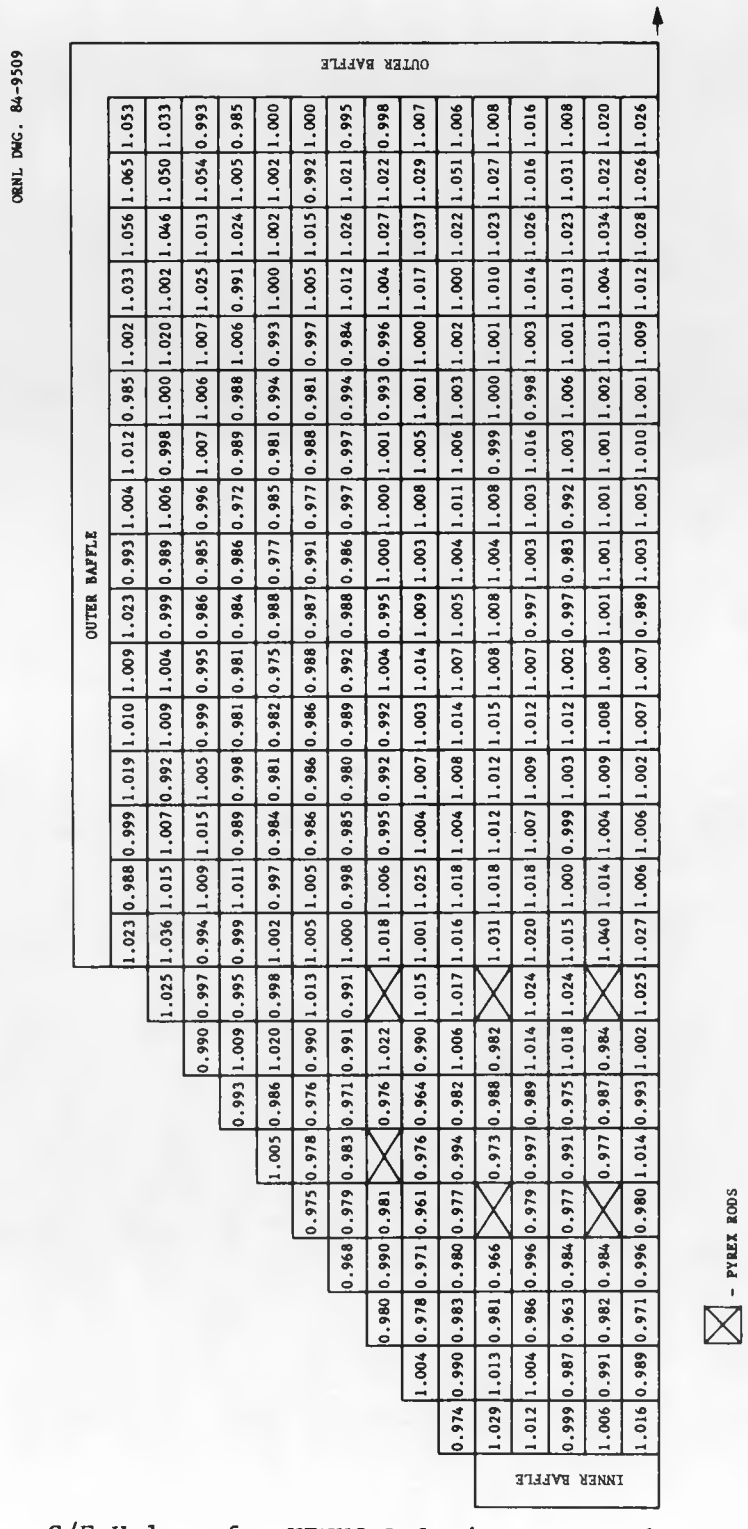

FIGURE ORNL- . C/E Values for VENUS Relative Power Distribution.

FIGURE ORNL-3. C/E Values for VENUS Relative Power Distribution.

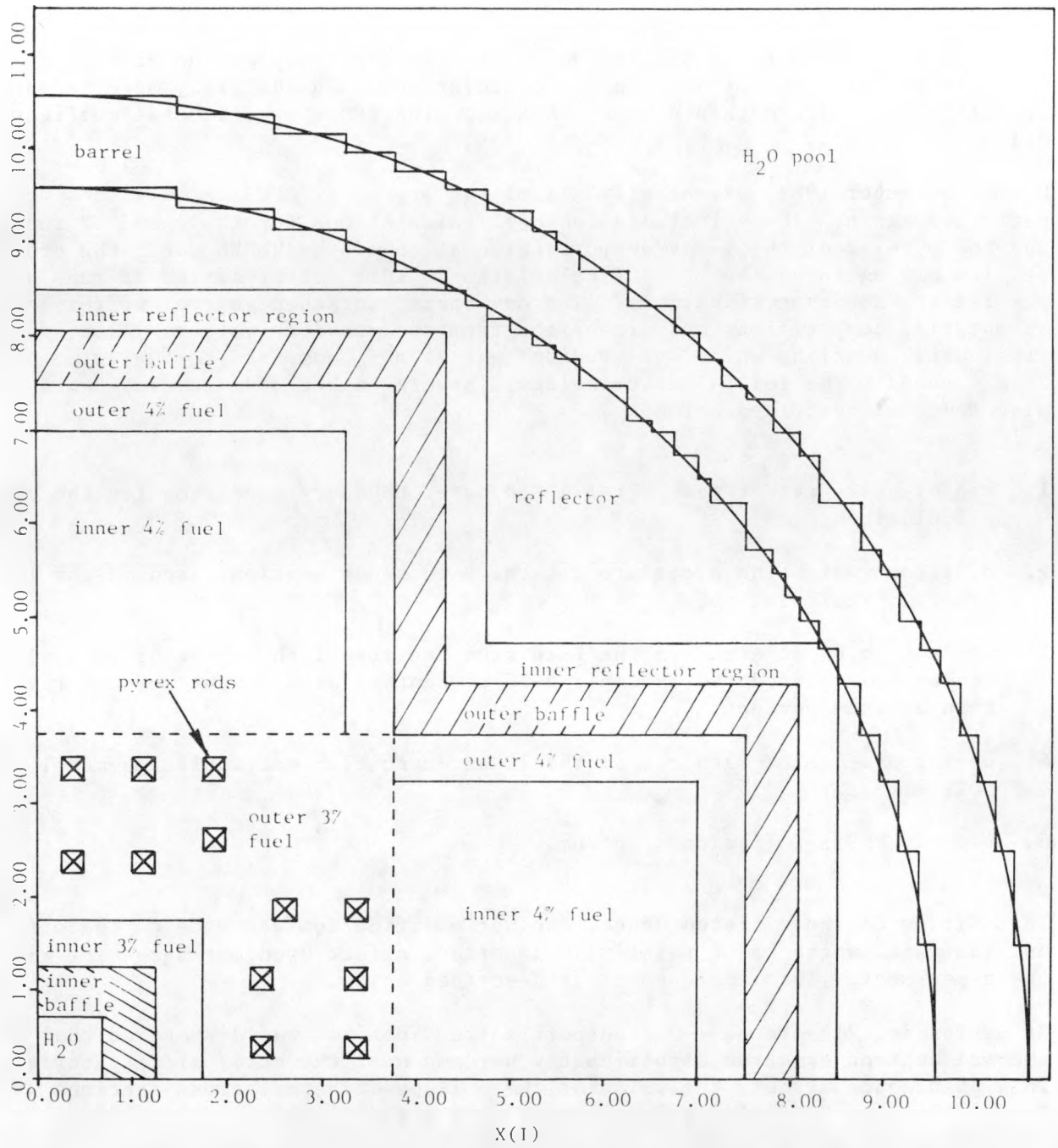

FIGURE ORNL-4. VENUS Plan View (1 Unit = 4 Pitches = 5.04 cm).

1. the computed eigenvalue of 0.986 was about 1 1/2% low, and

2. the computed fission density distribution was tilted toward the outer boundary, compared to the experimental measurements.

In order to resolve these discrepancies, a thorough study was undertaken to identify any problems present in the calculations. In addition, more recent specifications were obtained from CEN/SCK on the VENUS experimental configuration.

During December 1983, essentially all of the previous VENUS calculations were performed again. These included the cell calculations for the 3 and 4% fuels and the pyrex rod, the 1-D transport calculation of the VENUS core, the cross section mixing runs, and the DOT calculation. This latest series of runs used the latest VENUS specifications. The new specs contained several differences in material compositions and dimensions from the previous values. Also, the final axial buckling which was provided was 24 m^{-2}, compared to the value of 26 m^{-2} used in the initial calculations. Several other modifications were also made, as described below:

1. use of white rather than a reflected outer boundary condition for the cell calculations,

2. different weighting procedure for the B-10 cross sections used in the 1-D transport calculation,

3. correction of an error in the B-10 atom density of the pyrex (previously, we had interpreted the isotopic B-10 percentage as a weight percent rather than an atom percent),

4. use of a weighted rather than the linear-zero flux extrapolation model in DOT, and

5. use of ENDF/B-V fission spectrum.

In addition to those listed above, another modification was made to the original analysis, which had a relatively important effect upon our agreement with the experiment. This improvement is described below.

By performing 218-group, 1-D transport calcuations, it was discovered that the thermal neutron spectrum significantly hardens near the core/baffle interface. This phenomenon affects the value of the collapsed thermal cross sections used in the 10-group DOT calculations (which used a single thermal group below 0.625 eV), and changes the calculated power distribution. We were aware, of course, that a transition in the thermal spectrum would occur in the region near the baffle, from an asymptotic core spectrum to one representative of a thermal spectrum in iron; and, as previously discussed, the original model

contained a transition zone of 2.52 cm (2 cell widths) in which specifically weighted cross sections were used. However, it was unexpected that the thermal spectrum would change significantly within the last 2 cm or so of the core boundary - the transition zone of 2.52 cm was simply not fine enough.

It was necessary to obtain a separately weighted set of collapsed cross sections approximately every 1/4 cm in order to properly account for the change in the thermal spectrum near the core/baffle interface. Table ORNL-20 illustrates the effect of the new zone-weighting procedure on the collapsed ^{235}U thermal fission cross section. It can be seen that the thermal cross section varies by 6% over the last 1.26 cm of the core. The cross section weighted next to the baffle is about 10% lower than the value weighted over the 4% fuel region away from the core baffle region. Such a variation is enough to cause our computed power density to be high relative to the experimental values near the baffle. In the latest DOT calculations, a different set of zone-weighted cross sections was used in each of the last six intervals which had widths of 0.252 cm, and in the next two intervals which had widths of 0.504 cm. Therefore, within the last 2.52 cm of the VENUS core, eight different cross section weightings are now used, instead of the single weighting function used in the original analysis.

TABLE ORNL-20

COMPARISON OF ^{235}U THERMAL FISSION CROSS SECTION (FOR 4% FUEL) COLLAPSED AT DIFFERENT LOCATIONS

Distance* from Outer Baffle (cm)	^{235}U-Group 10/10 Fission Cross Section (b)
0.252	250.35
0.504	255.79
0.756	259.64
1.008	262.40
1.26	264.55
1.512	266.28
2.52	269.41
Remaining 4% Fuel	278.80

*Left zone boundary.

TABLE ORNL-21

^{235}U AND ^{237}Np FISSION CHAMBER RESULTS

No.	Position	X(I) cm	Y(J) cm	^{235}U Calc. normalized	^{235}U Exp. normalized	^{235}U C/E	^{237}Np Calc. normalized	^{237}Np Exp. normalized	^{237}Np C/E
1	W.H. (45°)	0.63	0.63	7.25974	--	--	0.62048	0.65680	0.94470
2	I.B. (8.13°)	4.41	0.63	1.0	1.0	1.0	1.0	1.0	1.0
3	I.B. (45°)	4.41	4.41	0.62727	--	--	1.18165	1.18644	0.99596
4	O.B. (40.24°)	24.57	20.79	0.48961	0.50810	0.96361	0.59129	0.59746	0.98967
5	O.B. (24.72°)	39.69	18.27	0.17727	--	--	0.18397	0.18136	1.01429
6	O.B. (16.78°)	39.69	11.97	0.26039	0.26010	1.00111	0.30723	0.31271	0.98248

Figure ORNL-3 shows the C/E values for the VENUS relative power distribution obtained from the latest series of calculations. The power tilt observed earlier has been essentially eliminated, and the C/E values now look very reasonable. The tendancy to overpredict the power density in the last row of pins has been improved considerably by the detailed space-dependent cross section weighting, although C/E values which are 5 to 6% high still occur near the baffle corner where cells are surrounded on two sides by steel. The second and third rows of pins from the outer baffle now seem to show the worst agreement with experiment, but in many cases they are within 3% of the measurements. It is probable that the agreement in these rows also could be improved by using more detailed space-dependent cross section weighting as was done for the last row of pins, but this would take a lot of effort. Overall, the latest calculations of the relative power distribution in the VENUS PWR mockup experiment show good agreement with experiment.

Recall that the earlier calculations were also producing a low critical eigenvalue of 0.986. It is well known that the ENDF/B-IV cross sections being used will tend to underestimate the k_{eff} value for these types of lattices. However, the low value of 0.986 was worse than expected, and in earlier progress reports some concern was expressed about this value, although it did not directly affect the computed power distribution. The latest calculations give an eigenvalue of 0.996. This value is more consistent with expectations, and it is quite reasonable.

A number of fission chamber results for both ^{235}U and ^{237}Np detectors have also been obtained. The computed-versus-measured values at several locations in the core are given in Table ORNL-21. For both calculation and experiment, the value of the fission rate at the 8.13° inner baffle location was normalized to unity. It can be seen that the C/E values are within 4% of unity at all locations, except for the inner water hole, which has a value of 0.94.

The initial phase of the VENUS PWR benmark was mainly concerned with validation of the calculational methods used to determine the fission source distribution near the core/baffle interface in PWR-type configurations. The conclusions of this study are based on results of 2-D transport theory calculations (rather than diffusion theory as used by utilities and vendors) and can be summarized as follows:

1. It is important to have thermal cross sections averaged over relatively fine spatial zones near the core/baffle interface. This places a burden on cross-section collapsing procedures and can result in large data files. The mixed number density (MND) procedure used in some diffusion theory calculations could possibly improve this situation for diffusion theory calculations.

2. For relatively coarse spatially-weighted cross sections, the agreement between the computed and measured power density distribution is better than 5% for interior pins, and from 2 to 7% for pins adjacent to the baffle. There is a tendancy to over-estimate the power production near

the core boundary, due to a high value for the thermal fission cross section near the core/baffle interface. This procedure would tend to overestimate the computed pressure-vessel fluence by 4 to 6%.

3. For fine spatially-weighted cross sections, the agreement between calculation and experiment is better than 3% for interior pins and better than 2% for most pins adjacent to the baffle, except those near the baffle corner. For three pins near the corner, the agreement is 5 to 6%. This region is important for contributing to the peak pressure-vessel fluence.

4. Agreement between the noralized computed and measured ^{235}U fission-chamber results in the inner and outer baffles is within about 6%.

5. Agreement between the normalized computed and measured ^{237}Np fission-chamber results in the inner and outer baffles is within about 2%.

To carry this study one step further and estimate the uncertainty in the pressure-vessel fluence due to uncertainties in the power distribution for a PWR would require much effort to do rigorously. However, the discrepancy in the computed power distribution for this particular experiment should cause less than a 5% error in the computed pressure fluence. If the use of diffusion theory with MND thermal cross sections is a good approximation for transport theory in the core/baffle region, then the 5% uncertainty value is probably appropriate for PWR cores. However, the validity of diffusion theory remains to be proven in the VENUS benchmark experiment.

Expected Future Accomplishments

Neutron transport calculations for the spatial distribution of the VENUS ex-core measurements are in progress. It is expected that the results will be documented in the next reporting period.

A.3 BABCOCK AND WILCOX (B&W) SDMF PERTURBATION EXPERIMENT

F. B. K. Kam
C. A. Baldwin
B. A. Worley

Summary

Three-dimensional fission source densities were calculated for the B&W perturbation experiment using the VENTURE diffusion theory code (Vo77). The results were stored on magnetic tape for easy distribution. A copy of the results was sent to C. L. Whitmarsh who plans to calculate flux perturbation factors and capsule lead factors to benchmark B&W analytical procedures.

Accomplishments and Status

The current report documents the work performed by ORNL in the B&W surveillance capsule perturbation experiment. Two capsules (Figure ORNL-5) that closely simulate existing in-reactor surveillance capsules, including the guide tubes and multiple specimen regions, were fabricated at B&W for the experiment. The experiment assembly suspended between the thermal shield and pressure vessel simulator (Fig. ORNL-6) simulates the positioning in a B&W 177FA reactor.

Extensive dosimetry by B&W, HEDL, AEEH, and CEN/SCK was inserted into each capsule. Microtubes were supplied by HEDL and CEN/SCK to obtain horizontal and vertical flux profiles in the water adjacent to the B&W capsules. In addition, three capsules (Fig. ORNL-7) which were loaded with SSTRs were provided by HEDL and installed behind the void box. The latter three capsules were inserted in support of the TMI-2 recovery program.

The power time history for the experiment is given in Table ORNL-22. The ORR core loading is shown in Fig. ORNL-8.

The three-dimensional fission source distribution for ORR core 162-B was calculated using the VENTURE code. The results were stored on magnetic tape and made available to C. L. Whitmarsh to evaluate B&W's analytical procudures for calculating the flux perturbation caused by the physical presence of surveillance capsules.

Future Accomplishments

ORNL expects to complete the analysis of the B&W SDMF perturbation experiment by the next reporting period. Comparison of calculations and measurements will be made. Final NUREG documentation is expected in early 1985.

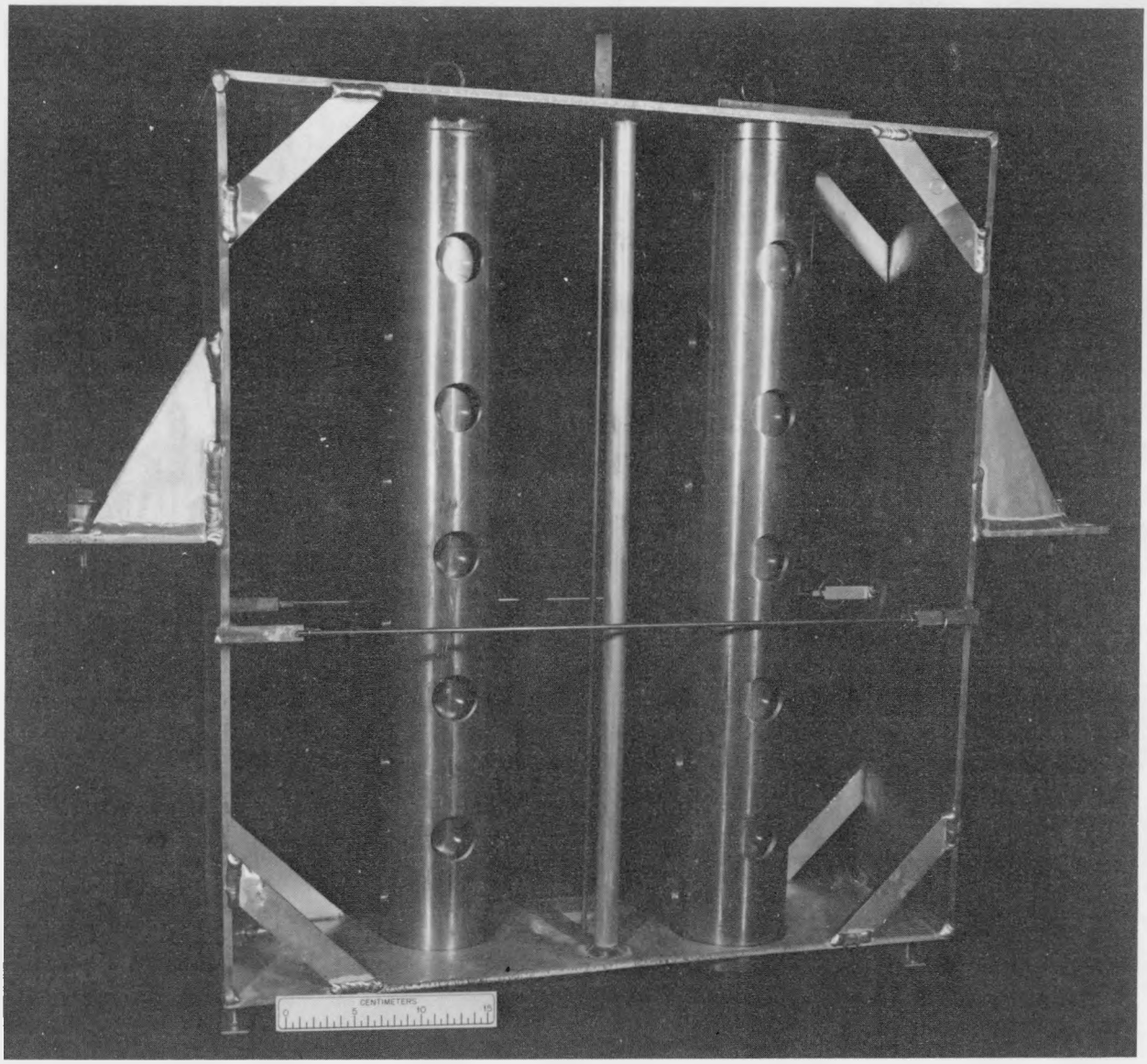

FIGURE ORNL-5. As-Built Experimental Configuration for the Babcock and Wilcox-Type Surveillance Capsules.

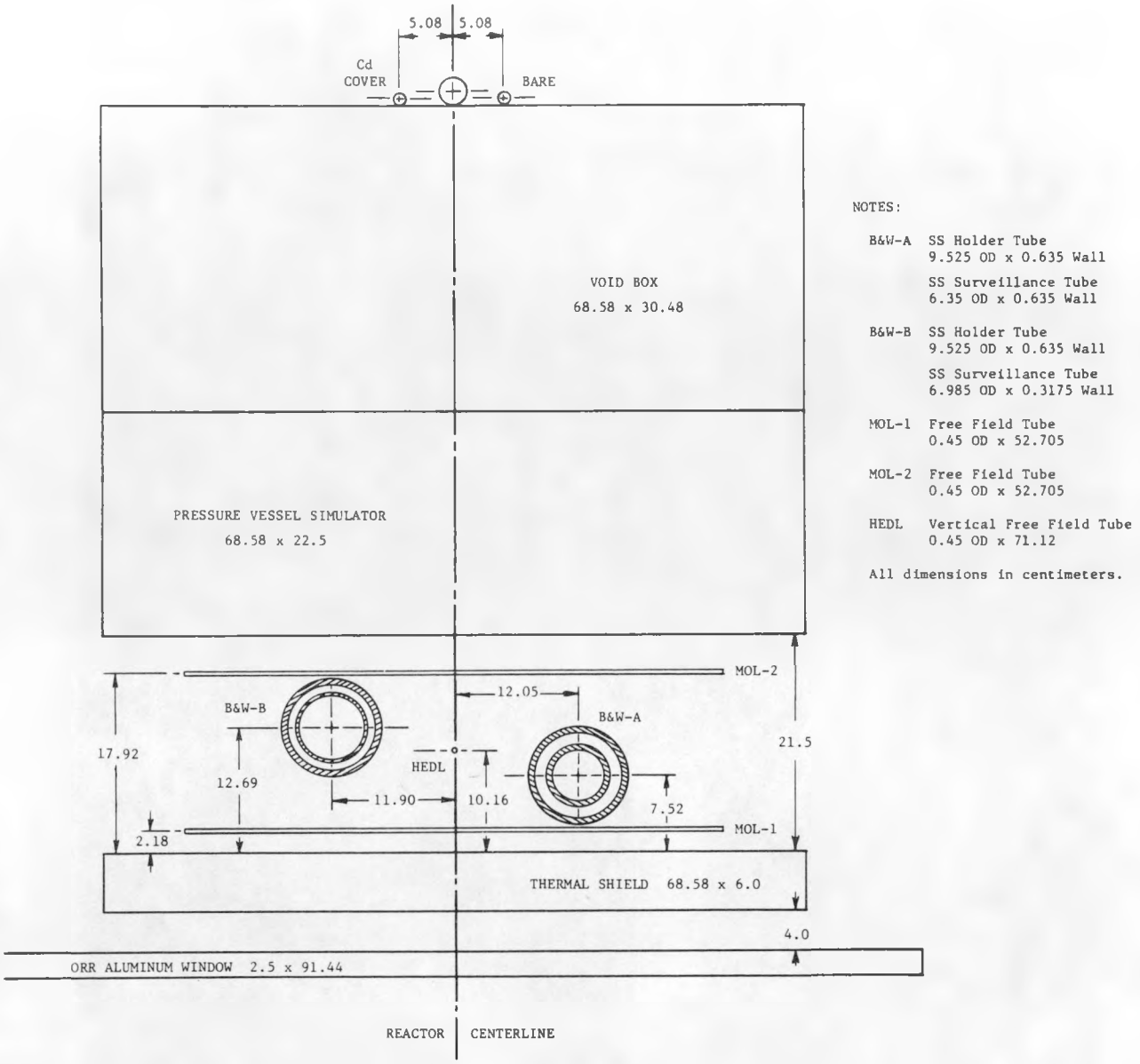

FIGURE ORNL-6. B&W Perturbation Experiment As-Built Dimensions.

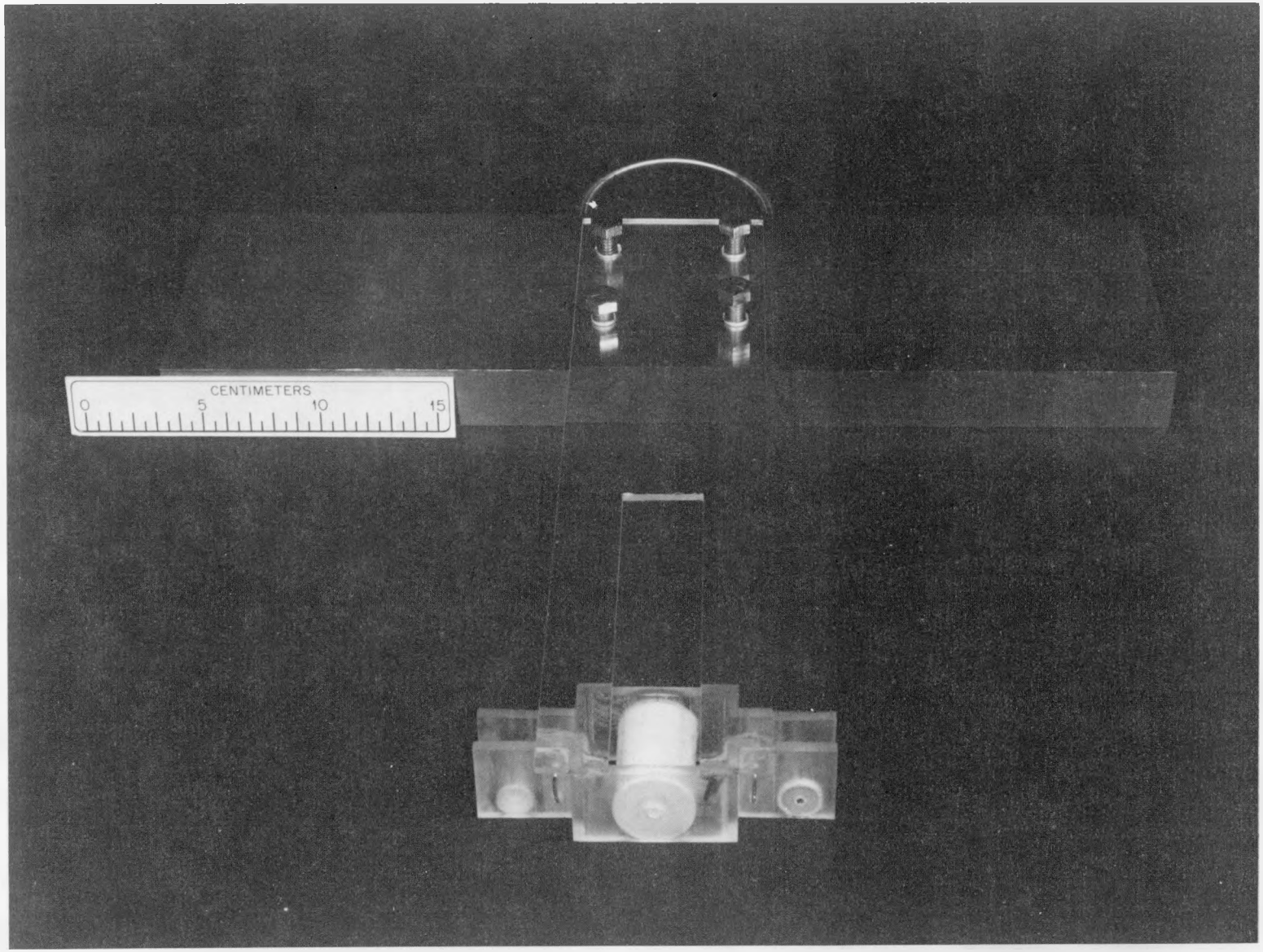

FIGURE ORNL-7. Void Box SSTR Dosimetry in Support of TMI-2 Recovery.

TABLE ORNL-22

ORR B&W PERTURBATION EXPERIMENT IRRADIATION DATA

Core Cycle: 162-B

Facility Insertion Time: August 26, 1982 - 1:55 p.m.

Facility Retraction Time: September 7, 1982 - 8:15 a.m.

Power vs Time History:

August 26, 1982, 1:55 p.m. - August 27, 1982, 1:00 p.m. - 29 MW.

August 27, 1982, 1:00 p.m. - September 7, 1982, 8:15 a.m. - 30 MW.

ORR CORE

Cycle 162-B

Start August 26, 1982

End September 14, 1982

Core location ⟶	A-3
Element identification ⟶	T-365
Initial ^{235}U mass (g) ⟶	285
^{235}U mass (g) at start of cycle ⟶	221

POOL

W

A-1 Be	A-2 Be	A-3 T-342 285 236	A-4 T-331 285 250	A-5 T-332 285 250	A-6 T-346 285 252	A-7 T-347 285 235	A-8 Be	A-9 Be
B-1 Be	B-2 Be	B-3 T-356 285 285	B-4* U-015 167 96	B-5 CLE453 284 204	B-6* U-016 167 104	B-7 T-357 285 285	B-8 Be	B-9 Be
C-1 Be	C-2 T-278 265 209	C-3 HFED	C-4 T-95 300 161	C-5 T-174 265 165	C-6 T-194 265 157	C-7 CLE451 282 90	C-8 Al	C-9 Be
D-1 ISO	D-2 T-250 265 195	D-3 T-271 265 196	D-4* U-017 167 158	D-5 T-293X 280 173	D-6* U-018 167 158	D-7 T-257 265 198	D-8 T-234 265 195	D-9 Be
E-1 Be	E-2 T-352 285 263	E-3 Al	E-4 T-233 265 195	E-5 Al	E-6 T-207 265 195	E-7 MFE 4B	E-8 T-355 285 263	E-9 Be
F-1 Be	F-2 T-247 265 184	F-3 T-252 265 201	F-4* U-010 167 36	F-5 T-201 265 201	F-6* U-014 167 65	F-7 T-235 265 195	F-8 T-255 265 195	F-9 Be
G-1 Be	G-2 Be	G-3 Be	G-4 Be	G-5 Be	G-6 Be	G-7 Be	G-8 Be	G-9 Be

S N

*Control rod location.

FIGURE ORNL-8. ORR B&W Perturbation Experiment Core Loading.

A.4 FOURTH SDMF IRRADIATION EXPERIMENT

C. A. Baldwin
F. B. K. Kam

Summary

The fourth SDMF irradiation experiment was completed in December 1983. E. P. Lippincott of HEDL supervised the recovery of the dosimetry in late February 1984, and the dosimetry was shipped to HEDL and KFA in early March 1984.

Accomplishments and Status

The 18-day irradiations spanned two ORR fuel cycles. Prior to the irradiation, dimensional measurements were made of the SDMF 4/12 SSC configurations to verify that water gap distances did not vary from a previous test (Table ORNL-23). Reactor operation data for the two fuel cycles are given in Table ORNL-24 and Figs. ORNL-9 through ORNL-11. Gang rods are those in the "B" and "D" rows, rods in the "F" row are fully withdrawn from the core.

Expected Accomplishments in the Next Reporting Period

No further work is anticipated.

TABLE ORNL-23

WATER GAP MEASUREMENTS FOR ORR-SDMF EXPERIMENT NO. 4
COMPARED WITH PREVIOUS MEASUREMENTS

APPROXIMATE MEASUREMENT LOCATIONS

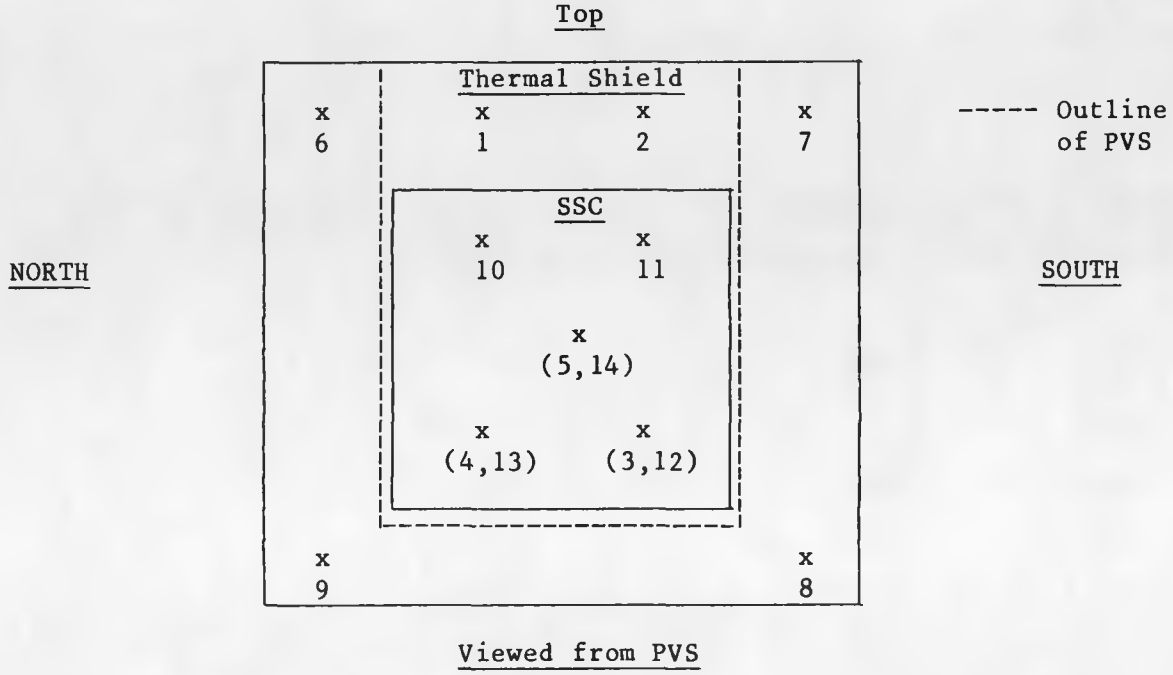

Comment	Location	July 6 and 7, 1983		November 9 and 10, 1983	
PVS to Thermal Shield Distance (mm)	1	120.54		120.23	
	2	119.72		120.02	
	3	120.12		120.00	
	4	119.96		120.02	
	5	120.24		120.06	
PVS Holder to Thermal Shield Distance (mm)	6	119.82	119.86	119.80	
	7	120.10	120.18	120.25	
	8	119.56		119.82	119.58
	9	119.34		119.56	
SSC to PVS Distance (mm)	10	61.48	61.60	62.09	
	11	63.04	63.19	63.04	
	12	63.18	63.14	63.05	
	13	61.24	61.34	61.07	
	14	62.72	62.76		

TABLE ORNL-24

IRRADIATION DATA FOR ORR-SDMF EXPERIMENT NO. 4

Run No. 1

- Core Cycle 166-D (November 23, 1983 to December 7, 1983)
- Experiment inserted with reactor at 30MW - November 23, 1983 at 2:00 p.m.
- Reactor scrammed with experiment inserted - December 7, 1983 at 3:00 a.m.
- Duration of run - 1.170×10^6 sec.
- Average instrument power - 30 MW
- Average heat balance power - 29.79 MW

Run No. 2

- Core Cycle 166-E (December 7, 1983 to December 21, 1983)
- Experiment inserted with reactor at 30MW - December 9, 1983 at 10:23 a.m.
- Experiment retracted with reactor at 30MW - December 14, 1983 at 1:03 p.m.
- Duration of run - 4.416×10^5 sec.
- Average instrument power - 30 MW
- Average heat balance power - 29.60 MW

ORR CORE

Cycle 166-D

Start November 23, 1983

End December 7, 1983

Core location ⟶	A-3
Element identification ⟶	T-365
Initial ^{235}U mass (g) ⟶	285
^{235}U mass (g) at start of cycle ⟶	221

POOL
W

A-1 Be	A-2 Be	A-3 T-361 285 207	A-4 T-418 285 268	A-5 T-430 285 285	A-6 T-431 285 285	A-7 T-382 285 207	A-8 Be	A-9 Be
B-1 Be	B-2 ** NLE 201 340 237	B-3 T-271 265 155	B-4* U-028 167 89	B-5 T-370 285 207	B-6* U-029 167 88	B-7 T-341 285 194	B-8 Xe	B-9 ** CLE 202 336 208
C-1 Be	C-2 ** BSI 201 340 340	C-3 IR	C-4 ** NSI 202 340 134	C-5 IR	C-6 ** CSI 202 339 134	C-7 IR	C-8 ** BSI 202 340 340	C-9 Be
D-1 Be	D-2 T-343 285 211	D-3 T-402 285 211	D-4* U-026 167 160	D-5 T-419 285 269	D-6* U-027 167 160	D-7 T-410 285 247	D-8 T-387 285 211	D-9 Be
E-1 Be	E-2 T-388 285 208	E-3 MFE 4A	E-4 T-404 285 245	E-5 IR	E-6 T-330 285 212	E-7 MFE 4B	E-8 T-432 285 285	E-9 Be
F-1 Be	F-2 Be	F-3 T-344 285 184	F-4* U-021 167 40	F-5 T-408 285 252	F-6* U-022 167 42	F-7 T-324 285 181	F-8 Be	F-9 Be
G-1 Be	G-2 Be	G-3 Be	G-4 Be	G-5 Be	G-6 Be	G-7 Be	G-8 Be	G-9 Be

S N

*Control rod elements.

**LEU 20 w/o; These elements are low-enriched ^{235}U (20 weight percent). All other elements are high-enriched ^{235}U (93 weight percent).

FIGURE ORNL-9. Core Loading for ORR-SDMF Experiment No. 4, Run 1.

ORR CORE

Cycle 166-E

Start December 7, 1983

End December 21, 1983

Core location ⟶	A-3
Element identification ⟶	T-365
Initial ^{235}U mass (g) ⟶	285
^{235}U mass (g) at start of cycle ⟶	221

POOL

W

A-1 Be	A-2 Be	A-3 T-373 285 202	A-4 T-421 285 268	A-5 T-422 285 281	A-6 T-423 285 281	A-7 T-360 285 202	A-8 Be	A-9 Be
B-1 Be	B-2 ** CLE 202 336 202	B-3 ** CLE 203 326 122	B-4* U-028 167 81	B-5 T-391 285 202	B-6* U-029 167 81	B-7 T-340 285 195	B-8 Xe	B-9 ** NLE 201 340 220
C-1 Be	C-2 ** BSI 202 340 318	C-3 IR	C-4 T-139 265 156	C-5 IR	C-6 T-213 265 150	C-7 IR	C-8 ** BSI 201 340 318	C-9 Be
D-1 Be	D-2 T-400 285 215	D-3 T-398 285 213	D-4* U-026 167 146	D-5 T-425 285 281	D-6* U-027 167 146	D-7 T-405 285 251	D-8 T-379 285 203	D-9 Be
E-1 Be	E-2 T-362 285 202	E-3 MFE 4A	E-4 T-399 285 239	E-5 IR	E-6 T-364 285 214	E-7 MFE 4B	E-8 T-424 285 281	E-9 Be
F-1 Be	F-2 ISO	F-3 T-351 285 185	F-4* U-021 167 35	F-5 T-411 285 261	F-6* U-022 167 37	F-7 T-307 285 181	F-8 Be	F-9 Be
G-1 Be	G-2 Be	G-3 Be	G-4 Be	G-5 Be	G-6 Be	G-7 Be	G-8 Be	G-9 Be

S N

*Control rod elements.

**LEU 20 w/o; these elements are low-enriched ^{235}U (20 weight percent). All other elements are high-enriched ^{235}U (93 weight percent).

FIGURE ORNL-10. Core Loading for ORR-SDMF Experiment No. 4, Run 2.

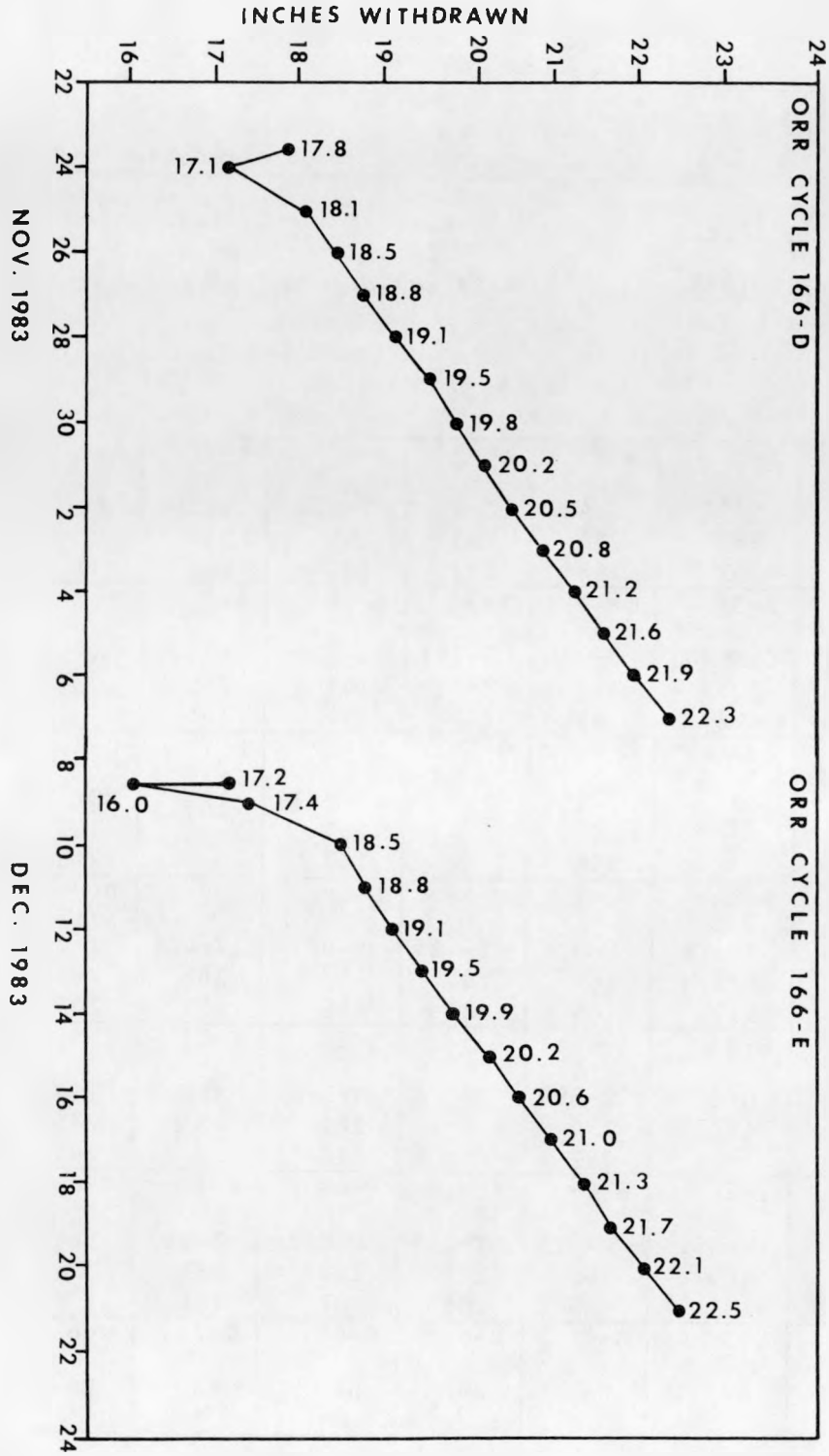

FIGURE ORNL-11. ORR Gang Rod Withdrawal Pattern for SDMF Experiment No. 4.

A.5 DETERMINATION OF DAMAGE EXPOSURE PARAMETER VALUES IN THE PSF METALLURGICAL IRRADIATION EXPERIMENT

F. W. Stallmann

Summary

Damage exposure parameter values in the PSF metallurgical irradiation experiment are determined from the spectral fluences of Section A.1 and the dosimetry data given in reference (Mc84b) using the LSL adjustment procedure. The resulting uncertainties for the damage parameters are 7% for fluence > 1.0 MeV, 12% for fluence > 0.1 MeV, and 9% for dpa. The percentages above represent one standard deviation values.

Accomplishments and Status

Values for the damage exposure parameters ϕt (ϕt = fluence) > 1.0 MeV, ϕt > 0.1 MeV, and displacements per atom (dpa) were estimated with uncertainties for all locations of metallurgical specimen in the test assembly in the ORR-PSF irradiation experiment. The fluence maps can be expressed as cosine functions in the axial (z) and lateral (x) direction and by an exponential attenuation away from the core (y) of the form:

$$P(x,y,z) = P_o \cdot \cos B_x(x-x_o) \cos B_z(z-z_o) e^{-\lambda(y-y_o)} \qquad (1)$$

where P is the damage parameter in question. The coordinates are adapted from the system described in the ORR-PSF Blind Test (see Fig. ORNL-12). The procedures for determining the damage parameters are essentially the same as in NUREG/CR 3333 (St83) (see Fig. ORNL-13).

The dosimetry data are taken from the Blind Test data package distributed February 17, 1984 (Mc84b). Only the activity data were used and the total reaction probabilities (saturated activities) were calculated independently using the reactor history with core leakage correction from the spectral fluence calculations by R. E. Maerker and B. A. Worley (see Section A.1). Nuclear data from ECN-70 and ECN-71 (Zi79) and fission yields in ENDF-292 (1980) (Ri80) were used in the calculation of the reaction probabilities. The fluence spectra by R. E. Maerker and B. A. Worley and the reaction probabilities were used as an input to the LSL-M2 adjustment procedure. This procedure is similar to the one used in NUREG/CR 3333 (St83) but allows more flexible assignment of correlations between fluence spectra at different locations with some restrictions about the number of different spectra to be processed simultaneously.

The calculated 37-energy group spectra were condensed to 17 groups and extended upward by one group to 18 MeV and downward by two groups from 0.098 MeV to 0.1265 eV and from there 10^{-4} eV, respectively (see Table ORNL-25). Group cross sections and covariances were obtained from the ENDF/B-V dosimetry file as presented in the IRDF-83 file (Cu82) through the PUFF (SmXX) processing code. Uncertainties of the calculated group fluences were assumed to be

20% for energies above 1 MeV, 30% for energies between 1.0 and 0.1 MeV and 300% below 0.1 MeV, since these values were simply extrapolated using 1/E and Maxwellian thermal spectra. Auto correlations between fluences in adjacent groups were assumed to be 0.95 diminishing according to a multiplication law for groups farther apart. Fluence correlations between spectra in positions of the same metallurgical capsule were estimated to be 0.95 and in the ranges between 0.90 and 0.70 for positions in different capsules, depending on the distance between the capsules. The non-fission reaction $^{63}Cu(n,\alpha)^{60}Co$, $^{46}Ti(n,p)^{46}Sc$, $^{58}Ni(n,p)^{58}Co$, $^{54}Fe(n,p)^{54}Mn$, $^{59}Co(n,\gamma)^{60}Co$, $^{58}Fe(n,\gamma)^{59}Fe$, $^{45}Sc(n,\gamma)^{46}Sc$, and the fission reactions $^{238}U(n,f)$, $^{237}Np(n,f)$, and $^{235}(n,f)$ were included in the first adjustment runs. [$^{109}Ag(n,\gamma)$ was excluded because the reaction cross section is not listed in the ENDF/B-V dosimetry file and four other non-threshold reactions are available.] The reaction uncertainties were estimated to be 4% for non-fission and 8% for fission reaction (one standard deviation). Averages were calculated whenever more than one reaction was measured at the same location or more than one fission product for the same fission sensor. No photo-fission corrections were made since the measurements and calculations for the PCA 4/12+SSC configuration shows negligible effect of photo-fission (Mc84a).

The first preliminary runs of the adjustment program showed strong inconsistencies with Chi-square per degree of freedom (χ^2/F) in the order of 4-8. The first source of inconsistencies was identified in the $^{238}U(n,f)$ reactions, primarily at the SSC2 and 0-T capsules, requiring adjustment in the order of 30 to 50%. Since these are the locations with the highest fluence, effect of ^{239}Pu production and fission must be suspected. The fluence between 0.1 MeV and the gadolinium cutoff at 0.12 eV contributes most to this effect but this fluence is poorly known, since no calculations were made for this energy range. Comparison with other measured non-threshold reactions at these locations indicate that an effect of the suspected magnitude can reasonably be attributed to plutonium production but no reliable estimate of the needed correction can be made. This effect is also consistent with roughly 30% discrepancies in calculated reaction rates for $^{238}U(n,f)$ based on different fission products. For the stated reasons, it was decided to eliminate the $^{238}U(n,f)$ reaction.

A second source of inconsistencies was found in the $^{58}Fe(n,\gamma)$ and $^{45}Sc(n,\gamma)$ reactions. These reactions need to be increased by about 20 to 40% to be consistent with the $^{59}Co(n,\gamma)$ reaction (bare and gadolinium covered) and $^{235}U(n,f)$ reactions (Gd covered). The reason for this discrepancy is not clear, possibly an effect of large resonances in the epithermal region.

After eliminating these two reactions, the χ^2/F value drops to about 0.2 which indicates a consistency of the remaining measurements and calculations which is much better than the assigned uncertainties. The resulting uncertainties for the damage parameters are as follows:

$\phi t > 1.0$ MeV : 7%
$\phi t > 0.1$ MeV : 12%
dpa : 9%

(one standard deviation). These values are probably too conservative but should be left standing until all discrepancies are cleared up.

The estimated values of the damage parameters are fitted to obtain the buckling and attenuation constants in formula (1). There is a slight decrease of buckling B_x and B_z with increasing distance y indicating decreasing influence of finite core dimensions with increasing distance from the core. There is also some consistent differences of these values for different damage parameters and thus some change of spectrum when going from the center to the periphery of the capsules. The individual fits are excellent and all differences between the formula (1) and measured values are well within measuring uncertainties. Typical cosine fits are shown in Figs. ORNL-14 through ORNL-16.

The constants, P_o, B_x, x_o, B_z, z_o, λ, and y_o, in formula (1) for different capsules and different damage parameters are listed in Table ORNL-26. This formula was used to calculate the damage parameter values at the positions of the metallurgical specimen. The coordinates chosen for this calculation are listed in Table ORNL-27 (see Fig. ORNL-17 for arrangement of specimens). These are the locations at the v-notches of the Charpy specimen and at the crack tips of the CT specimen. The calculated damage parameter values are listed in Tables ORNL-28 through ORNL-32. The uncertainties stemming from the fitting and interpolation procedures are probably negligible so that the uncertainty estimates obtained from the adjustment procedure apply also to the final damage parameter values.

TABLE ORNL-25

ENERGY GROUPS USED FOR THE LSL-M2 ADJUSTMENT PROCEDURE IN THE ORR-PSF METALLURGICAL IRRADIATION EXPERIMENT

Group No.	Upper Energy Boundary (eV)
1	1.800 E+7
2	1.733 E+7
3	1.221 E+7
4	1.000 E+7
5	7.408 E+6
6	6.065 E+6
7	4.066 E+6
8	2.725 E+6
9	2.466 E+6
10	2.123 E+6
11	1.827 E+6
12	1.496 E+6
13	1.353 E+6
14	1.003 E+6
15	8.209 E+5
16	6.081 E+5
17	3.020 E+5
18	1.832 E+5
19	9.804 E+4
20	1.265 E-1
lowest energy	1.000 E-4

TABLE ORNL-26

FITTING PARAMETERS FOR FORMULA (1)

	P_o[a]	B_x[b]	x_o[c]	B_z[b]	Z_o[c]	λ[b]	y_o[c]
SSC1							
$\phi t > 1$	2.64	.052	-0.3	.046	1.1	.139	13.29
$\phi t > .1$	8.17	.052	-0.3	.048	1.1	.080	13.29
dpa	4.09	.052	-0.3	.047	1.1	.109	13.29
SSC2							
$\phi t > 1$	5.50	.052	-0.3	.046	1.1	.139	13.29
$\phi t > .1$	16.84	.052	-0.3	.048	1.1	.080	13.29
dpa	8.46	.052	-0.3	.047	1.1	.109	13.29
0-T							
$\phi t > 1$	4.03	.052	-0.8	.042	1.4	.139	24.05
$\phi t > .1$	12.56	.052	-0.8	.046	1.4	.080	24.05
dpa	6.44	.052	-0.8	.044	1.4	.109	24.05
1/4 T							
$\phi t > 1$	2.21	.049	-0.8	.040	2.4	.139	28.56
$\phi t > .1$	8.95	.049	-0.8	.045	2.4	.080	28.56
dpa	3.94	.049	-0.8	.043	2.4	.109	28.56
1/2 T							
$\phi t > 1$	1.06	.046	-0.8	.038	3.1	.139	33.70
$\phi t > .1$	5.84	.046	-0.8	.044	3.1	.080	33.70
dpa	2.26	.046	-0.8	.042	3.1	.109	33.70

[a] $10^{19}/cm^2$ for $\phi t > 1$, $\phi t > .1$, % for dpa.

[b] cm^{-1}.

[c] cm.

TABLE ORNL-27

COORDINATES OF THE LOCATIONS OF THE METALLURGICAL SPECIMEN
RELATIVE TO THE CAPSULE CENTER
(ALL COORDINATES IN CM)

No.[a]	Z	X (left)	X (right)	$(y-y_o)^b$ (front)	$(y-y_o)^b$ (rear)
			Charpy Specimen		
1	12.20	-10.37	+10.37	-1.07	+1.07
2	11.20	-10.37	+10.37	-1.07	+1.07
3	10.20	-10.37	+10.37	-1.07	+1.07
4	9.20	-10.37	+10.37	-1.07	+1.07
5	8.20	-10.37	+10.37	-1.07	+1.07
6	7.19	-10.37	+10.37	-1.07	+1.07
7	6.19	-10.37	+10.37	-1.07	+1.07
8	5.19	-10.37	+10.37	-1.07	+1.07
9	4.19	-10.37	+10.37	-1.07	+1.07
10	3.19	-10.37	+10.37	-1.07	+1.07
11	2.19	-10.37	+10.37	-1.07	+1.07
12	1.19	-10.37	+10.37	-1.07	+1.07
13	0.19	-10.37	+10.37	-1.07	+1.07
14	-0.81	-10.37	+10.37	-1.07	+1.07
15	-1.81	-10.37	+10.37	-1.07	+1.07
16	-2.82	-10.37	+10.37	-1.07	+1.07
17	-3.82	-10.37	+10.37	-1.07	+1.07
18	-4.82	-10.37	+10.37	-1.07	+1.07
19	-5.82	-10.37	+10.37	-1.07	+1.07
20	-6.82	-10.37	+10.37	-1.07	+1.07
21	-7.82	-10.37	+10.37	-1.07	+1.07
22	-8.82	-10.37	+10.37	-1.07	+1.07
23	-9.82	-10.37	+10.37	-1.07	+1.07
24	-10.82	-10.37	+10.37	-1.07	+1.07
25	-11.82	-10.37	+10.37	-1.07	+1.07
			1/2 CT Specimen		
29	11.39	0.0		-0.64	+0.64
31T[c]	8.22	0.0		-0.64	+0.64
31B[c]	4.48	0.0		-0.64	+0.64
32T	1.87	0.0		-0.64	+0.64
32B	-1.87	0.0		-0.64	+0.64
33T	-4.48	0.0		-0.64	+0.64
33B	-8.22	0.0		-0.64	+0.64
30	-11.39	0.0		-0.64	+0.64

TABLE ORNL-27, CONTINUED

No.[a]	Z	X (left)	X (right)	$(y-y_o)^b$ (front)	$(y-y_o)^b$ (rear)
			1 CT Specimen		
34	10.05	-4.57		0.0	
38T	3.70	-4.57		0.0	
38B	-3.70	-4.57		0.0	
36	-10.05	-4.57		0.0	
35	10.05	4.57		0.0	
39T	3.70	4.57		0.0	
39B	-3.70	4.57		0.0	
37	-10.05	4.57		0.0	

[a]For numbers of specimen, refer to Fig. ORNL-17.

[b]For values of y_o for different capsules, see Table ORNL-26.

[c]31T = specimen on top of hole 31.
31B = specimen below hole 31, etc.

TABLE ORNL-28

DAMAGE PARAMETER VALUES AT THE LOCATION OF METALLURGICAL SPECIMENS
CAPSULE SSC1

Spec. No.	Fluence >1 MeV 10^{19}/cm^2	Fluence >.1 MeV 10^{19}/cm^2	dpa (ASTM) (%)	Spec. No.	Fluence >1 MeV 10^{19}/cm^2	Fluence >.1 MeV 10^{19}/cm^2	dpa (ASTM) (%)	Spec. No.	Fluence >1 MeV 10^{19}/cm^2	Fluence >.1 MeV 10^{19}/cm^2	dpa (ASTM) (%)	Spec. No.	Fluence >1 MeV 10^{19}/cm^2	Fluence >.1 MeV 10^{19}/cm^2	dpa (ASTM) (%)
							Charpy Specimen								
	Left Front				Right Front				Left Rear				Right Rear		
1	2.314	6.600	3.430	1	2.271	6.473	3.364	1	1.719	5.562	2.717	1	1.687	5.455	2.665
2	2.371	6.779	3.519	2	2.328	6.648	3.451	2	1.762	5.713	2.788	2	1.729	5.603	2.734
3	2.424	6.943	3.600	3	2.379	6.809	3.531	3	1.801	5.851	2.852	3	1.767	5.738	2.797
4	2.471	7.090	3.673	4	2.425	6.954	3.602	4	1.835	5.976	2.910	4	1.802	5.860	2.854
5	2.512	7.222	3.738	5	2.466	7.082	3.666	5	1.867	6.086	2.961	5	1.832	5.969	2.904
6	2.549	7.336	3.795	6	2.502	7.195	3.722	6	1.894	6.183	3.006	6	1.859	6.064	2.948
7	2.580	7.434	3.844	7	2.532	7.291	3.769	7	1.917	6.265	3.045	7	1.881	6.144	2.986
8	2.606	7.514	3.883	8	2.557	7.369	3.808	8	1.936	6.333	3.076	8	1.900	6.211	3.017
9	2.626	7.578	3.915	9	2.577	7.431	3.839	9	1.951	6.386	3.101	9	1.915	6.263	3.041
10	2.640	7.623	3.937	10	2.591	7.476	3.861	10	1.961	6.425	3.119	10	1.925	6.301	3.059
11	2.649	7.651	3.951	11	2.600	7.504	3.875	11	1.968	6.448	3.130	11	1.932	6.324	3.069
12	2.652	7.662	3.956	12	2.603	7.514	3.880	12	1.971	6.457	3.134	12	1.934	6.333	3.073
13	2.650	7.654	3.953	13	2.601	7.507	3.876	13	1.969	6.451	3.131	13	1.932	6.327	3.071
14	2.642	7.629	3.940	14	2.593	7.482	3.864	14	1.963	6.430	3.121	14	1.927	6.306	3.061
15	2.629	7.587	3.919	15	2.580	7.441	3.844	15	1.953	9.394	3.105	15	1.917	6.271	3.045
16	2.610	7.527	3.890	16	2.561	7.382	3.815	16	1.939	6.344	3.081	16	1.903	6.221	3.022
17	2.585	7.449	3.851	17	2.537	7.306	3.777	17	1.920	6.278	3.051	17	1.885	6.157	2.992
18	2.555	7.355	3.804	18	2.508	7.213	3.731	18	1.898	6.199	3.013	18	1.863	6.079	2.955
19	2.519	7.243	3.749	19	2.473	7.103	3.677	19	1.872	6.104	2.970	19	1.837	5.987	2.912
20	2.478	7.115	3.685	20	2.433	6.978	3.614	20	1.841	5.996	2.919	20	1.807	5.881	2.863
21	2.432	6.970	3.614	21	2.387	6.836	3.544	21	1.807	5.874	2.862	21	1.774	5.761	2.807
22	2.381	6.809	3.534	22	2.337	6.678	3.466	22	1.769	5.739	2.799	22	1.736	5.628	2.745
23	2.325	6.633	3.446	23	2.282	6.505	3.380	23	1.727	5.590	2.730	23	1.695	5.482	2.677
24	2.263	6.441	3.351	24	2.222	6.317	3.287	24	1.682	5.428	2.655	24	1.650	5.324	2.603
25	2.197	6.234	3.249	25	2.157	6.114	3.186	25	1.632	5.254	2.573	25	1.602	5.153	2.524
							1/2 CT Specimen				1 CT Specimen				
	Front				Rear				Left				Right		
29	2.566	7.567	3.880	29	2.151	6.836	3.378	34	2.360	7.238	3.638	35	2.342	7.182	3.610
31T*	2.730	8.098	4.140	31T	2.288	7.316	3.605	38T	2.557	7.900	3.956	39T	2.538	7.838	3.925
31B	2.848	8.482	4.327	31B	2.387	7.662	3.768	38B	2.513	7.751	3.885	39B	2.494	7.691	3.854
32T	2.881	8.589	4.380	32T	2.415	7.759	3.814	36	2.244	6.849	3.451	37	2.227	6.795	3.424
32B	2.856	8.508	4.340	32B	2.394	7.686	3.779								
33T	2.789	8.288	4.233	33T	2.337	7.487	3.685								
33B	2.622	7.749	3.969	33B	2.198	7.001	3.456								
30	2.420	7.095	3.649	30	2.029	6.410	3.177								

*31T = top of hole 31.
31B = bottom of hole 31.

TABLE ORNL-29

DAMAGE PARAMETER VALUES AT THE LOCATION OF METALLURGICAL SPECIMENS CAPSULE SSC2

Spec. No.	Fluence >1 MeV 10^{19}/cm^2	Fluence >.1 MeV 10^{19}/cm^2	dpa (ASTM) (%)	Spec. No.	Fluence >1 MeV 10^{19}/cm^2	Fluence >.1 MeV 10^{19}/cm^2	dpa (ASTM) (%)	Spec. No.	Fluence >1 MeV 10^{19}/cm^2	Fluence >.1 MeV 10^{19}/cm^2	dpa (ASTM) (%)	Spec. No.	Fluence >1 MeV 10^{19}/cm^2	Fluence >.1 MeV 10^{19}/cm^2	dpa (ASTM) (%)
							Charpy Specimen								
	Left Front				Right Front				Left Rear				Right Rear		
1	4.821	13.604	7.095	1	4.732	13.341	6.958	1	3.582	11.465	5.620	1	3.516	11.244	5.512
2	4.941	13.973	7.279	2	4.849	13.704	7.139	2	3.670	11.777	5.766	2	3.602	11.549	5.655
3	5.049	14.311	7.447	3	4.956	14.035	7.303	3	3.751	12.061	5.899	3	3.682	11.828	5.785
4	5.147	14.615	7.598	4	5.052	14.333	7.452	4	3.824	12.317	6.019	4	3.753	12.080	5.903
5	5.234	14.885	7.733	5	5.138	14.598	7.584	5	3.889	12.545	6.125	5	3.817	12.303	6.007
6	5.310	15.122	7.850	6	5.212	14.830	7.699	6	3.945	12.744	6.218	6	3.872	12.498	6.098
7	5.375	15.323	7.950	7	5.276	15.027	7.797	7	3.993	12.914	6.298	7	3.919	12.665	6.176
8	5.428	15.489	8.033	8	5.328	15.190	7.878	8	4.033	13.054	6.363	8	3.958	12.802	6.240
9	5.470	15.619	9.097	9	5.369	15.318	7.941	9	4.064	13.163	6.414	9	3.989	12.909	6.290
10	5.501	15.713	8.144	10	5.399	15.410	7.987	10	4.086	13.243	6.451	10	4.011	12.987	6.327
11	5.519	15.771	8.173	11	5.417	15.467	8.015	11	4.100	13.291	6.474	11	4.024	13.035	6.349
12	5.526	15.792	8.183	12	5.424	15.488	8.026	12	4.105	13.310	6.482	12	4.029	13.053	6.357
13	5.521	15.777	8.176	13	5.419	15.473	8.018	13	4.102	13.297	6.276	13	4.026	13.040	6.351
14	5.505	15.726	8.150	14	5.403	15.422	7.993	14	4.089	13.254	6.456	14	4.014	12.998	6.332
15	5.476	15.638	8.107	15	5.375	15.336	7.950	15	4.069	13.180	6.422	15	3.993	12.925	6.298
16	5.437	15.514	8.045	16	5.336	15.215	7.890	16	4.039	13.075	6.373	16	3.964	12.823	6.250
17	5.385	15.355	7.966	17	5.286	15.059	7.812	17	4.001	12.941	6.310	17	3.927	12.691	6.188
18	5.323	15.160	7.869	18	5.224	14.867	7.717	18	3.954	12.776	6.233	18	3.881	12.530	6.113
19	5.249	14.930	7.755	19	5.152	14.642	7.605	19	3.899	12.583	6.143	19	3.827	12.340	6.024
20	5.163	14.665	7.623	20	5.068	14.382	7.476	20	3.836	12.360	6.039	20	3.765	12.121	5.922
21	5.067	14.367	7.475	21	4.974	14.090	7.331	21	3.765	12.108	5.921	21	3.695	11.875	5.807
22	4.961	14.035	7.310	22	4.869	13.765	7.169	22	3.685	11.829	5.790	22	3.617	11.601	5.679
23	4.843	13.671	7.129	23	4.754	13.408	6.991	23	3.598	11.522	5.647	23	3.531	11.300	5.538
24	4.716	13.276	6.932	24	4.628	13.020	6.798	24	3.503	11.189	5.491	24	3.438	10.973	5.385
25	4.578	12.850	6.720	25	4.493	12.602	6.590	25	3.401	10.830	5.323	25	3.338	10.621	5.220
							1/2 CT Specimen								
	Front				Rear										
29	5.346	15.597	8.025	29	4.481	14.090	6.988								
31T*	5.688	16.692	8.563	31T	4.767	15.079	7.456								
31B	5.934	17.482	8.951	31B	4.974	15.793	7.794								
32T	6.003	17.703	9.059	32T	5.032	15.993	7.888								
32B	5.951	17.536	8.977	32B	4.988	15.842	7.817								
33T	5.810	17.083	8.755	33T	4.870	15.433	7.623								
33B	5.464	15.973	8.210	33B	4.579	14.430	7.148								
30	5.042	14.625	7.547	30	4.226	13.212	6.571								
							1 CT Specimen								
								Left				Right			
								34	4.917	14.920	7.526	35	4.880	14.803	7.467
								38T	5.327	16.283	8.183	39T	5.286	16.155	8.119
								38B	5.235	15.977	8.035	39B	5.195	15.852	7.972
								36	4.675	14.116	7.138	37	4.640	14.006	7.082

*31T = top of hole 31.
31B = bottom of hole 31.

TABLE ORNL-30

DAMAGE PARAMETER VALUES AT THE LOCATION OF METALLURGICAL SPECIMENS
SPV-CAPSULE 0-T

Spec. No.	Fluence >1 MeV 10^{19}/cm^2	Fluence >.1 MeV 10^{19}/cm^2	dpa (ASTM) (%)	Spec. No.	Fluence >1 MeV 10^{19}/cm^2	Fluence >.1 MeV 10^{19}/cm^2	dpa (ASTM) (%)	Spec. No.	Fluence >1 MeV 10^{19}/cm^2	Fluence >.1 MeV 10^{19}/cm^2	dpa (ASTM) (%)	Spec. No.	Fluence >1 MeV 10^{19}/cm^2	Fluence >.1 MeV 10^{19}/cm^2	dpa (ASTM) (%)
							Charpy Specimen								
	Left Front				Right Front				Left Rear				Right Rear		
1	3.693	10.569	5.654	1	3.514	10.055	5.379	1	2.744	8.907	4.479	1	2.610	8.474	4.261
2	3.766	10.821	5.776	2	3.582	10.295	5.496	2	2.797	9.120	4.576	2	2.661	8.677	4.353
3	3.831	11.051	5.888	3	3.645	10.514	5.602	3	2.846	9.314	4.664	3	2.708	8.861	4.437
4	3.890	11.257	5.988	4	3.701	10.710	5.697	4	2.890	9.487	4.743	4	2.750	9.026	4.513
5	3.942	11.439	6.076	5	3.751	10.883	5.781	5	2.929	9.641	4.813	5	2.786	9.172	4.579
6	3.987	11.598	6.153	6	3.794	11.034	5.854	6	2.962	9.774	4.874	6	2.818	9.299	4.637
7	4.026	11.731	6.217	7	3.830	11.161	5.915	7	2.991	9.887	4.925	7	2.845	9.406	4.686
8	4.057	11.840	6.270	8	3.859	11.264	5.965	8	3.014	9.978	4.967	8	2.867	9.493	4.725
9	4.080	11.923	6.310	9	3.882	11.344	6.004	9	3.031	10.049	4.999	9	2.884	9.560	4.756
10	4.097	11.981	6.339	10	3.898	11.399	6.030	10	3.044	10.098	5.021	10	2.896	9.607	4.777
11	4.106	12.014	6.354	11	3.907	11.430	6.046	11	3.051	10.125	5.033	11	2.902	9.633	4.789
12	4.108	12.021	6.358	12	3.909	11.437	6.049	12	3.052	10.132	5.036	12	2.904	9.639	4.791
13	4.103	12.003	6.349	13	3.904	11.420	6.041	13	3.048	10.116	5.029	13	2.900	9.625	4.785
14	4.091	11.960	6.328	14	3.892	11.378	6.021	14	3.039	10.080	5.013	14	2.891	9.590	4.769
15	54071	11.891	6.295	15	3.873	11.313	5.989	15	3.024	10.021	4.986	15	2.877	9.534	4.744
16	4.044	11.797	6.249	16	3.848	11.223	5.945	16	3.005	9.942	4.950	16	2.859	9.459	4.710
17	4.010	11.678	6.192	17	3.815	11.110	5.891	17	2.979	9.842	4.904	17	2.834	9.363	4.666
18	3.969	11.534	6.122	18	3.776	10.973	5.824	18	2.949	9.720	4.849	18	2.805	9.248	4.614
19	3.921	11.365	6.040	19	3.631	10.813	5.747	19	2.913	9.579	4.785	19	2.771	9.113	4.552
20	3.866	11.173	5.947	20	3.678	10.630	5.658	20	2.872	9.416	4.711	20	2.733	8.959	4.482
21	3.804	10.957	5.842	21	3.619	10.424	5.558	21	2.826	9.234	4.628	21	2.689	8.785	4.403
22	3.736	10.718	5.726	22	3.554	10.197	5.448	22	2.775	9.033	4.536	22	2.640	8.594	4.315
23	3.661	10.455	5.599	23	3.483	9.947	5.327	23	2.719	8.812	4.435	23	2.587	8.383	4.219
24	3.579	10.171	5.461	24	3.405	9.677	5.195	24	2.659	8.572	4.325	24	2.530	8.156	4.115
25	3.491	9.865	5.312	25	3.321	9.386	5.054	25	2.593	8.315	4.208	25	2.467	7.910	4.003

							1/2 CT Specimen				1 CT Specimen				
	Front				Rear				Left				Right		
29	4.016	11.833	6.240	29	3.366	10.690	5.433	34	3.695	11.357	5.865	35	3.621	11.130	5.748
31T*	4.219	12.559	6.588	31T	3.536	11.346	5.736	38T	3.934	12.250	6.284	39T	3.856	12.006	6.159
31B	4.361	13.071	6.832	31B	3.655	11.808	5.949	38B	3.862	11.982	6.158	39B	3.785	11.743	6.035
32T	4.397	13.200	6.894	32T	3.686	11.925	6.003	36	3.505	10.650	5.532	37	3.435	10.437	5.422
32B	4.357	13.054	6.824	32B	3.652	11.793	5.942								
33T	4.264	12.723	6.666	33T	3.574	11.493	5.804								
33B	4.044	11.932	6.287	33B	3.390	10.779	5.475								
30	3.778	10.982	5.832	30	3.167	9.921	5.078								

*31T = top of hole 31.
31B = bottom of hole 31.

TABLE ORNL-31

DAMAGE PARAMETER VALUES AT THE LOCATION OF METALLURGICAL SPECIMENS
SPV-CAPSULE 1/4 T

Spec. No.	Fluence >1 MeV 10^{19}/cm^2	Fluence >.1 MeV 10^{19}/cm^2	dpa (ASTM) (%)	Spec. No.	Fluence >1 MeV 10^{19}/cm^2	Fluence >.1 MeV 10^{19}/cm^2	dpa (ASTM) (%)	Spec. No.	Fluence >1 MeV 10^{19}/cm^2	Fluence >.1 MeV 10^{19}/cm^2	dpa (ASTM) (%)	Spec. No.	Fluence >1 MeV 10^{19}/cm^2	Fluence >.1 MeV 10^{19}/cm^2	dpa (ASTM) (%)
							Charpy Specimen								
	Left Front				Right Front				Left Rear				Right Rear		
1	2.114	7.865	3.604	1	2.023	7.529	3.450	1	1.570	6.628	2.855	1	1.503	6.345	2.732
2	2.147	8.024	3.670	2	2.055	7.681	3.513	2	1.595	6.763	2.907	2	1.527	6.473	2.783
3	2.177	8.167	3.729	3	2.084	7.818	3.570	3	1.617	6.883	2.954	3	1.548	6.589	2.828
4	2.203	8.293	3.782	4	2.109	7.939	3.620	4	1.637	6.989	2.995	4	1.567	6.691	2.867
5	2.226	8.403	3.827	5	2.131	8.043	3.663	5	1.654	7.082	3.031	5	1.583	6.779	2.902
6	2.245	8.495	3.865	6	2.149	8.132	3.700	6	1.668	7.160	3.062	6	1.597	6.854	2.931
7	2.261	8.570	3.897	7	2.164	8.204	3.730	7	1.680	7.223	3.087	7	1.608	6.914	2.955
8	2.273	8.628	3.921	8	2.176	8.259	3.753	8	1.689	7.272	3.106	8	1.616	6.961	2.973
9	2.281	8.668	3.937	9	2.184	8.298	3.769	9	1.695	7.306	3.119	9	1.622	6.993	2.986
10	2.286	8.691	3.947	10	2.188	8.320	3.778	10	1.698	7.325	3.126	10	1.626	7.012	2.993
11	2.287	8.696	3.949	11	2.189	8.325	3.780	11	1.699	7.329	3.128	11	1.627	7.016	2.994
12	2.285	8.684	3.944	12	2.187	8.313	3.775	12	1.697	7.319	3.124	12	1.625	7.006	2.990
13	2.278	8.654	3.931	13	2.181	8.284	3.763	13	1.693	7.293	3.114	13	1.620	6.981	2.981
14	2.268	8.606	3.911	14	2.171	8.238	3.744	14	1.685	7.253	3.098	14	1.613	6.943	2.966
15	2.255	8.541	3.884	15	2.158	8.176	3.718	15	1.675	7.198	3.077	15	1.604	6.890	2.945
16	2.238	8.458	3.850	16	2.142	8.097	3.686	16	1.662	7.129	3.050	16	1.591	6.824	2.919
17	2.217	8.359	3.809	17	2.122	8.001	3.646	17	1.647	7.045	3.017	17	1.577	6.743	2.888
18	2.193	8.242	3.760	18	2.099	7.890	3.600	18	1.629	6.946	2.979	18	1.559	6.649	2.851
19	2.165	8.109	3.705	19	2.972	7.762	3.547	19	1.608	6.834	2.935	19	1.539	6.542	2.809
20	2.133	7.959	3.643	20	2.042	7.619	3.487	20	1.585	6.708	2.886	20	1.517	6.421	2.762
21	2.099	7.793	3.574	21	2.009	7.460	3.421	21	1.559	6.568	2.831	21	1.493	6.287	2.710
22	2.061	7.611	3.498	22	1.973	7.286	3.349	22	1.531	6.415	2.771	22	1.465	6.141	2.653
23	2.019	7.414	3.416	23	1.933	7.097	3.270	23	1.500	6.249	2.706	23	1.436	5.981	2.590
24	1.975	7.202	3.328	24	1.890	6.894	3.185	24	1.467	6.070	2.636	24	1.404	5.810	2.523
25	1.927	6.975	3.233	25	1.845	6.677	3.095	25	1.432	5.879	2.561	25	1.370	5.627	2.452
							1/2 CT Specimen								
	Front				Rear										
29	2.258	8.649	3.908	29	1.892	7.814	3.402								
31T*	2.347	9.089	4.088	31T	1.967	8.211	3.559								
31B	2.404	9.368	4.202	31B	2.015	8.463	3.659								
32T	2.412	9.406	4.218	32T	2.021	8.498	3.673								
32B	2.377	9.236	4.148	32B	1.992	8.344	3.612								
33T	2.321	8.961	4.036	33T	1.946	8.096	3.514								
33B	2.198	8.356	3.787	33B	1.842	7.548	3.297								
30	2.054	7.654	3.499	30	1.722	6.915	3.046								
							1 CT Specimen								
									Left				Right		
								34	2.071	8.282	3.665	35	2.035	8.135	3.600
								38T	2.169	8.783	3.867	39T	2.131	8.627	3.798
								38B	2.108	8.468	3.741	39B	2.071	8.318	3.674
								36	1.909	7.453	3.331	37	1.875	7.321	3.272

*31T = top of hole 31.
31B = bottom of hole 31.

TABLE ORNL-32

DAMAGE PARAMETER VALUES AT THE LOCATION OF METALLURGICAL SPECIMENS
SPV-CAPSULE 1/2 T

Spec. No.	Fluence >1 MeV 10^{19}/cm^2	Fluence >.1 MeV 10^{19}/cm^2	dpa (ASTM) (%)	Spec. No.	Fluence >1 MeV 10^{19}/cm^2	Fluence >.1 MeV 10^{19}/cm^2	dpa (ASTM) (%)	Spec. No.	Fluence >1 MeV 10^{19}/cm^2	Fluence >.1 MeV 10^{19}/cm^2	dpa (ASTM) (%)	Spec. No.	Fluence >1 MeV 10^{19}/cm^2	Fluence >.1 MeV 10^{19}/cm^2	dpa (ASTM) (%)
							Charpy Specimen								
	Left Front				Right Front				Left Rear				Right Rear		
1	1.047	5.300	2.131	1	1.088	5.102	2.052	1	0.778	4.467	1.688	1	0.749	4.300	1.625
2	1.060	5.393	2.166	2	1.021	5.192	2.085	2	0.788	4.546	1.715	2	0.758	4.376	1.651
3	1.072	5.477	2.196	3	1.032	5.272	2.114	3	0.797	4.616	1.739	3	0.767	4.443	1.674
4	1.083	5.549	2.222	4	1.042	5.342	2.139	4	0.804	4.677	1.760	4	0.774	4.502	1.695
5	1.092	5.611	2.245	5	1.051	5.401	2.161	5	0.811	4.729	1.778	5	0.781	4.552	1.712
6	1.099	5.662	2.263	6	1.058	5.450	2.179	6	0.817	4.772	1.793	6	0.786	4.593	1.726
7	1.105	5.702	2.278	7	1.064	5.489	2.193	7	0.821	4.805	1.804	7	0.790	4.626	1.737
8	1.109	5.731	2.288	8	1.068	5.517	2.203	8	0.824	4.830	1.813	8	0.793	4.649	1.745
9	1.112	5.748	2.295	9	1.070	5.534	2.209	9	0.826	4.845	1.818	9	0.795	4.664	1.750
10	1.113	5.755	2.297	10	1.071	5.540	2.211	10	0.827	4.850	1.820	10	0.796	4.669	1.752
11	1.112	5.750	2.296	11	1.070	5.536	2.210	11	0.826	4.846	1.818	11	0.795	4.665	1.750
12	1.110	5.735	2.290	12	1.068	5.520	2.204	12	0.824	4.833	1.814	12	0.794	4.653	1.746
13	1.106	5.708	2.280	13	1.064	5.495	2.195	13	0.821	4.810	1.806	13	0.791	4.631	1.739
14	1.100	5.670	2.266	14	1.059	5.458	2.182	14	0.817	4.778	1.795	14	0.787	4.600	1.728
15	1.093	5.621	2.248	15	1.052	5.411	2.164	15	0.812	4.737	1.781	15	0.782	4.560	1.715
16	1.085	5.561	2.227	16	1.044	5.353	2.144	16	0.806	4.687	1.764	16	0.776	4.512	1.698
17	1.074	5.490	2.201	17	1.034	5.285	2.119	17	0.798	4.627	1.743	17	0.768	4.455	1.678
18	1.063	5.409	2.171	18	1.023	5.207	2.090	18	0.789	4.559	1.720	18	0.760	4.389	1.656
19	1.049	5.318	2.138	19	1.010	5.119	2.058	19	0.780	4.482	1.693	19	0.750	4.314	1.630
20	1.034	5.215	2.101	20	0.996	5.021	2.022	20	0.769	4.396	1.664	20	0.740	4.231	1.602
21	1.018	5.103	2.060	21	0.980	4.913	1.983	21	0.756	4.301	1.632	21	0.728	4.140	1.571
22	1.000	4.981	2.015	22	0.963	4.795	1.940	22	0.743	4.198	1.596	22	0.715	4.041	1.537
23	0.981	4.850	1.967	23	0.944	4.668	1.894	23	0.729	4.087	1.558	23	0.702	3.934	1.500
24	0.960	4.708	1.915	24	0.925	4.533	1.844	24	0.714	3.968	1.517	24	0.687	3.820	1.461
25	0.938	4.558	1.861	25	0.903	4.388	1.791	25	0.697	3.842	1.474	25	0.671	3.698	1.419
							1/2 CT Specimen								1 CT Specimen
	Front				Rear				Left				Right		
29	1.100	5.736	2.275	29	0.922	5.182	1.981	34	1.008	5.486	2.132	35	0.992	5.400	2.099
31T*	1.135	5.985	2.365	31T	0.952	5.407	2.059	38T	1.044	5.750	2.225	39T	1.028	5.661	2.191
31B	1.155	6.129	2.416	31B	0.968	5.537	2.104	38B	1.009	5.497	2.136	39B	0.994	5.411	2.103
32T	1.156	6.131	2.417	32T	0.969	5.539	2.105	36	0.916	4.816	1.895	37	0.902	4.741	1.866
32B	1.136	5.994	2.368	32B	0.953	5.415	2.062								
33T	1.109	5.802	2.299	33T	0.930	5.241	2.001								
33B	1.052	5.395	2.152	33B	0.881	4.873	1.874								
30	0.986	4.934	1.986	30	0.826	4.457	1.729								

*31T = top of hole 31.
31B = bottom of hole 31.

ORNL DWG. 84-9111

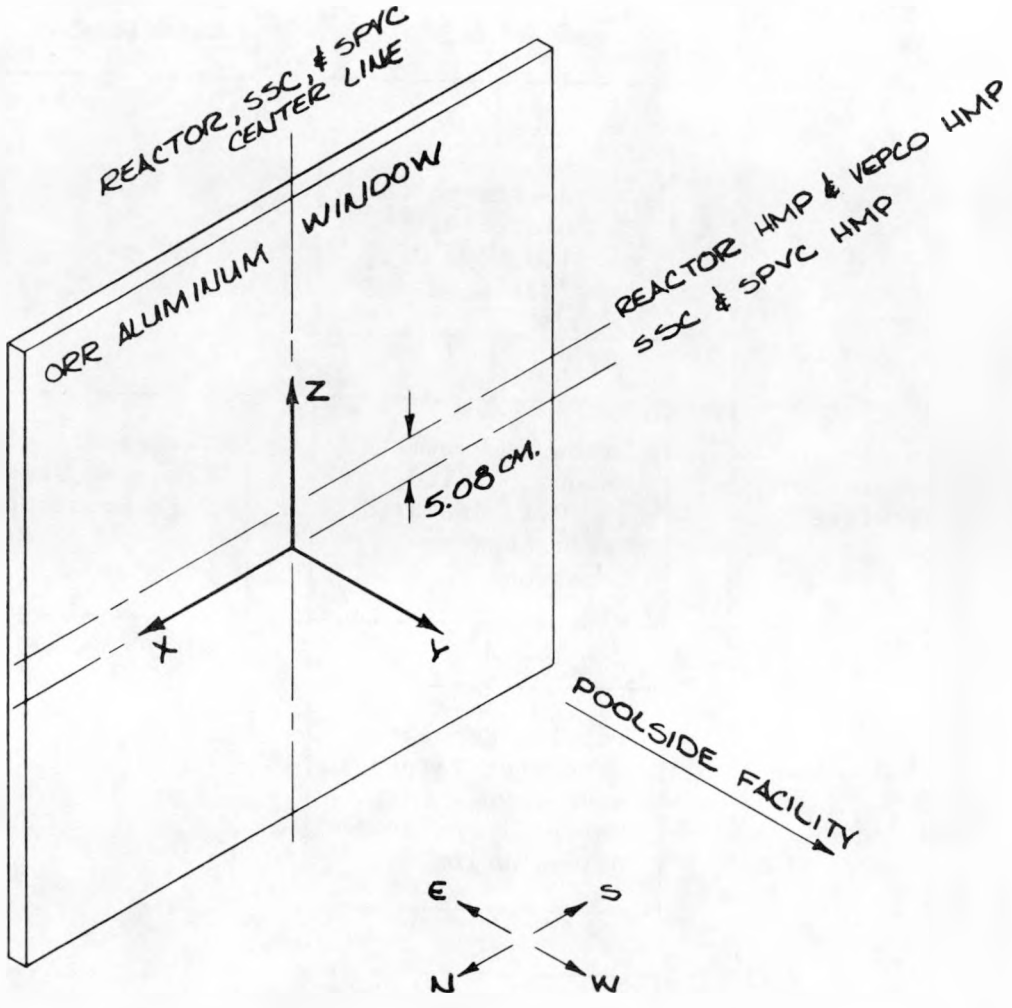

FIGURE ORNL-12. Coordinate System for the ORR-PSF Metallurgical Experiment.

ORNL DWG 83-12862

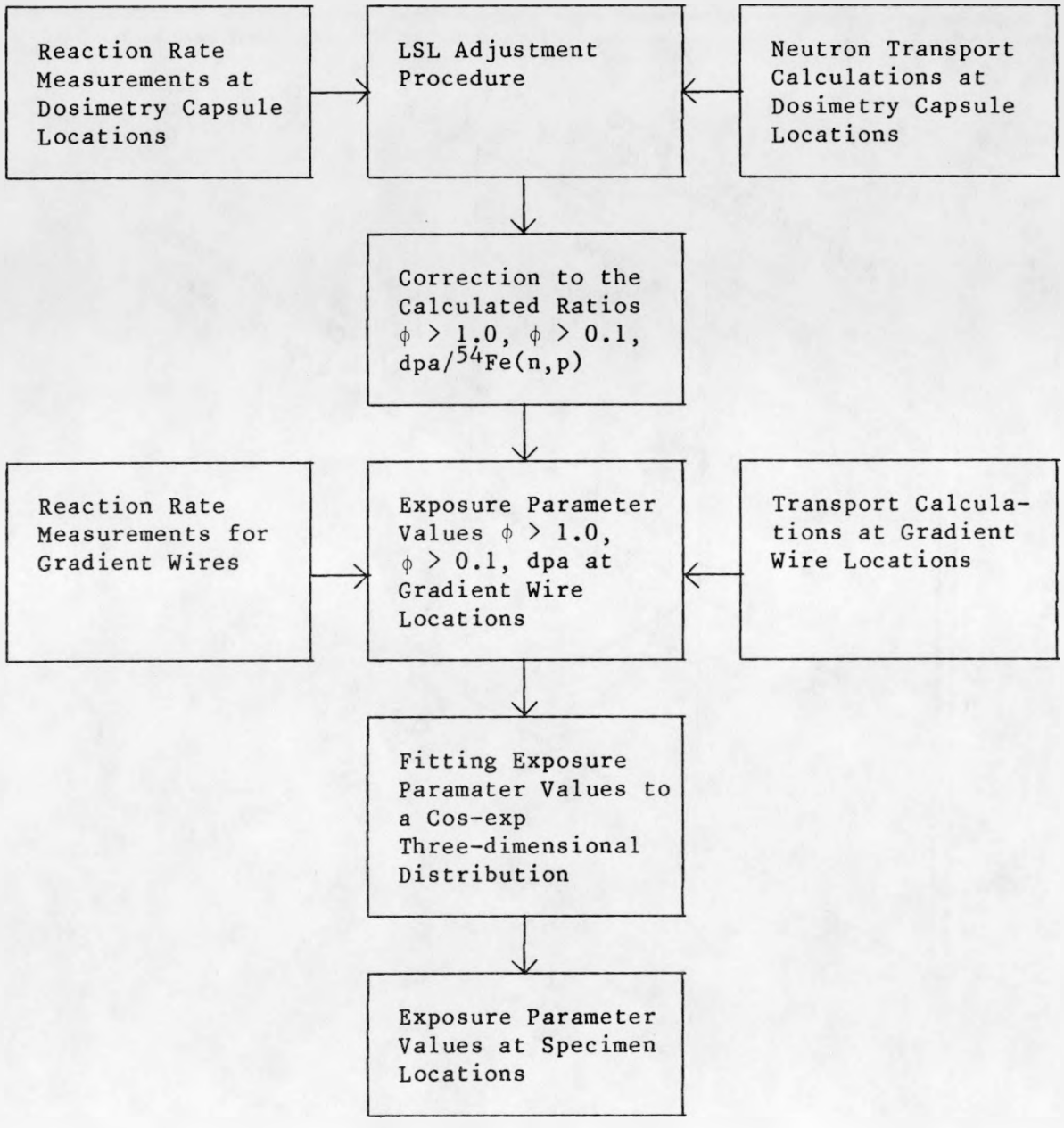

FIGURE ORNL-13. Methodology for the Determination of Exposure Parameter Values and Uncertainties.

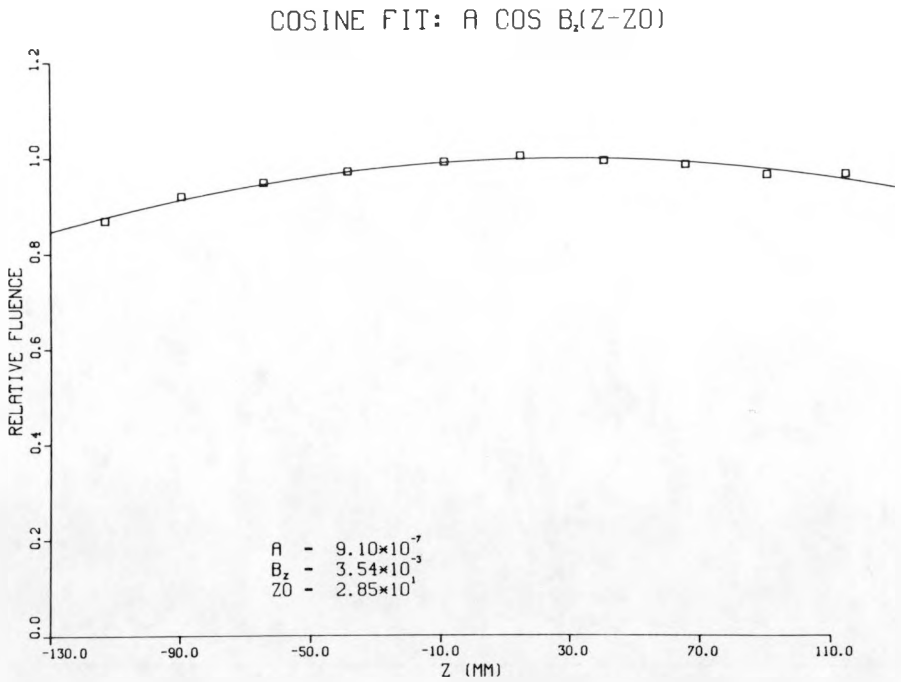

FIGURE ORNL-14. Cosine Fit of the $^{54}Fe(n,p)$ Reaction Along the Gradient Wire Positioned at the Left Rear Row of Charpy Specimen in the 1/4-T Capsule.

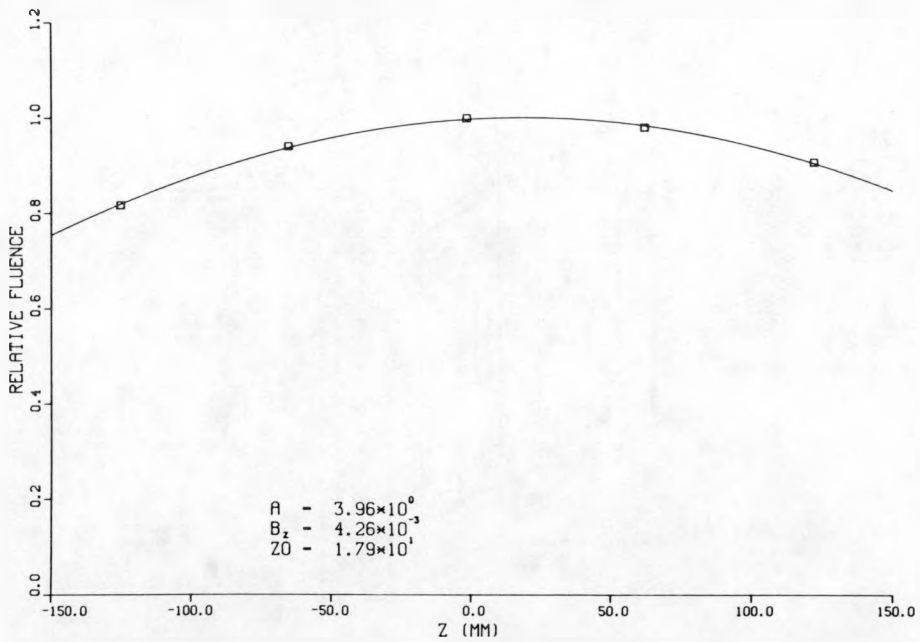

FIGURE ORNL-15. Cosine Fit of dpa Determined from the Gradient Sets H-16 to H-20 at the Axial Centerline of the 1/4-T Capsule.

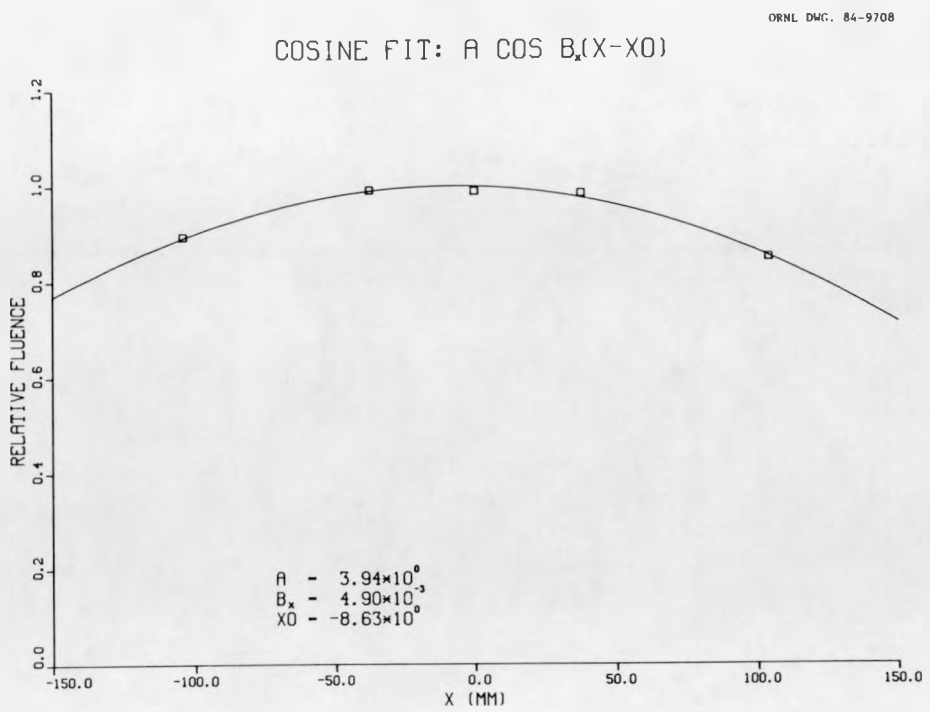

FIGURE ORNL-16. Cosine Fit of dpa in the Lateral Direction Along the Centerline of the 1/4-T Capsule.

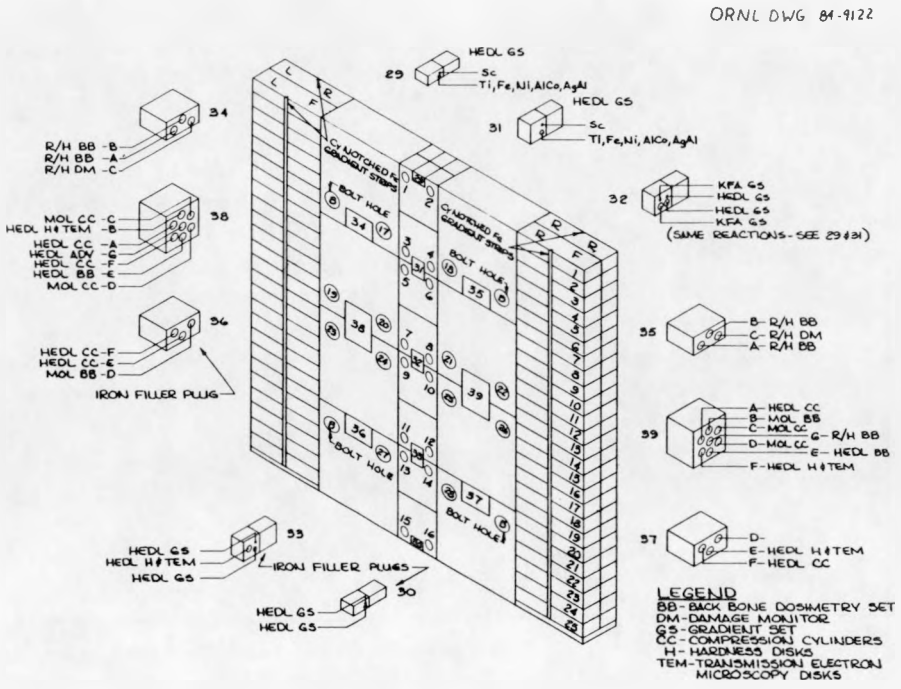

FIGURE ORNL-17. Illustration of Dosimeter and Metallurgical Specimen Location in the Irradiation Capsules.

A.6 NEUTRONICS CALCULATIONS FOR THE POOL CRITICAL ASSEMBLY - 4/12 SSC AND 4/12 CONFIGURATIONS

C. A. Baldwin
L. F. Miller
F. B. K. Kam

Summary

Neutron transport calculations are reported for off-axis locations in the PCA 4/12 SSC and PCA 4/12 configurations. These calculations were made in support of the PSF two-year metallurgical irradiation experiment and have not been reported previously.

Accomplishments and Status

Within the framework of the Light Water Reactor Pressure Vessel Surveillance Dosimetry Improvement Program, a mock-up pressure vessel simulator was designed and constructed at the ORNL Pool Critical Assembly (PCA) (Mc81). The facility consists of the PCA core, a fixed aluminum window, a movable thermal shield and pressure vessel wall, and a void box attached to the back of the pressure vessel wall. The thermal shield and vessel wall move independently and, thus, provide great flexibility in altering the geometry in terms of water gaps between aluminum window and thermal shield and between thermal shield and pressure vessel wall simulator. In describing the facility, one typically refers to a "X/Y" configuration where "X" is the nominal distance in centimeters from the back face of the aluminum window to the front face of the thermal shield and "Y" is the nominal distance from the back face of the thermal shield to the front face of the pressure vessel wall. Access to the vessel wall is provided in the form of removable inserts such that measurements can be made within the wall as well as outside in the water gaps. Extensive measurements and calculations were performed and compared for the 8/7 and 12/13 configurations as part of a PCA benchmark "Blind Test" (Mc81). Other measurements were made in the 4/12 SSC* and 4/12 configurations in support of the PSF metallurgical irradiation experiment. Results from neutronic calculations performed at ORNL for the PCA 4/12 SSC and 4/12 configurations are reported and compared with available experimental results. In addition, the damage correlation parameters fluence rate greater than 1 MeV, fluence rate greater than 0.1 MeV, and displacements per atom have been calculated and tabulated.

The PCA 4/12 SSC configuration is illustrated by Fig. ORNL-18. In the figure, locations where experimental measurements were made are designated by the notations A0 through A7. The 4/12 configuration is the same as the 4/12 SSC configuration except for the absence of the SSC. Discrete ordinates transport theory calculations were performed by ORNL for both configurations to compare

*SSC refers to a simulated surveillance capsule which can be positioned immediately behind the thermal shield.

with experimental results. The calculations involve correcting a two-dimensional DOT (Rh79) midplane calculation with a leakage correction term. The leakage term is derived from a two-dimensional DOT axial calculation normalized by a one-dimensional ANISN (En67) calculation. All calculations use the same group structure, cross sections, and source term. The leakage correction terms are applied to the group flux densities and are, therefore, space and energy dependent. The following equation represents the synthesis technique:

$$\phi_g(x,y,z) \simeq \phi_g(x,y) \left[\frac{\phi_g(y,z)}{\phi_g(y)} \right] , \qquad (1)$$

where $\phi_g(x,y)$, $\phi_g(y,z)$, and $\phi_g(y)$ are the group flux densities from the DOT midplane, DOT axial, and ANISN calculations, respectively. This methodology has been investigated and applied to several similar problems (Ma81e,Ma82e, Wi82,Ba83).

The geometrical models for the two-dimensional DOT midplane and axial calculations for the 4/12 SSC configuration are illustrated by Figs. ORNL-19 and ORNL-20. The model for the one-dimensional ANISN calculation is illustrated by Fig. ORNL-21. The geometrical buckling corrections normally applied by the DOT and ANISN programs are not used in these calculations, so dummy inputs are utilized to simulate infinite slab geometry in the untreated direction(s). Cross sections for the various material compositions were obtained from the VITAMIN-C (Ro82) library and were processed using the AMPX-II (Gr78b) system. Stainless steel and carbon steel cross sections were specially weighted using $1/E\ \Sigma_T^{\text{stainless steel}}$ weighting for the stainless steel and $1/E\ \Sigma_T^{\text{iron}}$ weighting for the carbon steel. All calculations are fixed source calculations which use a measured fission source (Mc81) normalized to one neutron in the core. The exact formulation for the source was taken from R. E. Maerker's work for the PCA-PVF "Blind Test" (Mc81). In this particular formulation, a two-dimensional measured fission rate distribution at the horizontal midplane was coupled with an axial cosine distribution which represented the best fit for several fission rate measurement traverses in the axial direction. The resulting three-dimensional distribution was integrated over the appropriate directions to provide two-dimensional and one-dimensional source distributions for the transport calculations. The source spectral representation used was the Watt ^{235}U thermal neutron-induced fission spectrum from ENDF/B-V. The first 102 groups of the VITAMIN-C structure (17.33 MeV to 0.098 MeV) were calculated using a pointwise flux density convergence criterion of 1×10^{-3}.

Synthesized flux densities, $\phi_g(x,y,z)$, were calculated at several axial elevations for each of the measurement locations A0 through A6. Flux densities were then integrated with group cross sections derived from the ENDF/B-V dosimetry file to produce the calculated reaction rates in Appendix A. The experimental reaction rates which appear in Appendix A were obtained from

three sources. The Ni and Al data for location A0 were taken from Table 8.3.1 of the PCA Blind Test NUREG (Mc81). The Np and U data for locations A4, A5, and A6 were obtained from private communications with E. D. McGarry (NBS). All other experimental data were obtained from a memo from A. Fabry (Mol), F. Cops (Mol), and F. B. K. Kam (ORNL) concerning radiometric fission flux measurements for the ORR-PSF, the PCA-PVF, and the BSR-HSST. Comparison of calculated and experimental results indicate that the trends and accuracy are consistent with the previous results of the PCA Blind Test (Mc81) i.e., the calculations are, in general, lower than the measurements with increasing distance from the source. Absolute comparisons of calculated-to-measured results are in the range of 4 to 20%. Damage correlation parameters were also calculated using the synthesized flux densities. Fluence rate greater than 1 MeV, fluence rate greater than 0.1 MeV, and displacements per atom of iron have all been computed and tabulated in Appendix B for both PCA configurations.

Expected Future Accomplishments

No further work is anticipated.

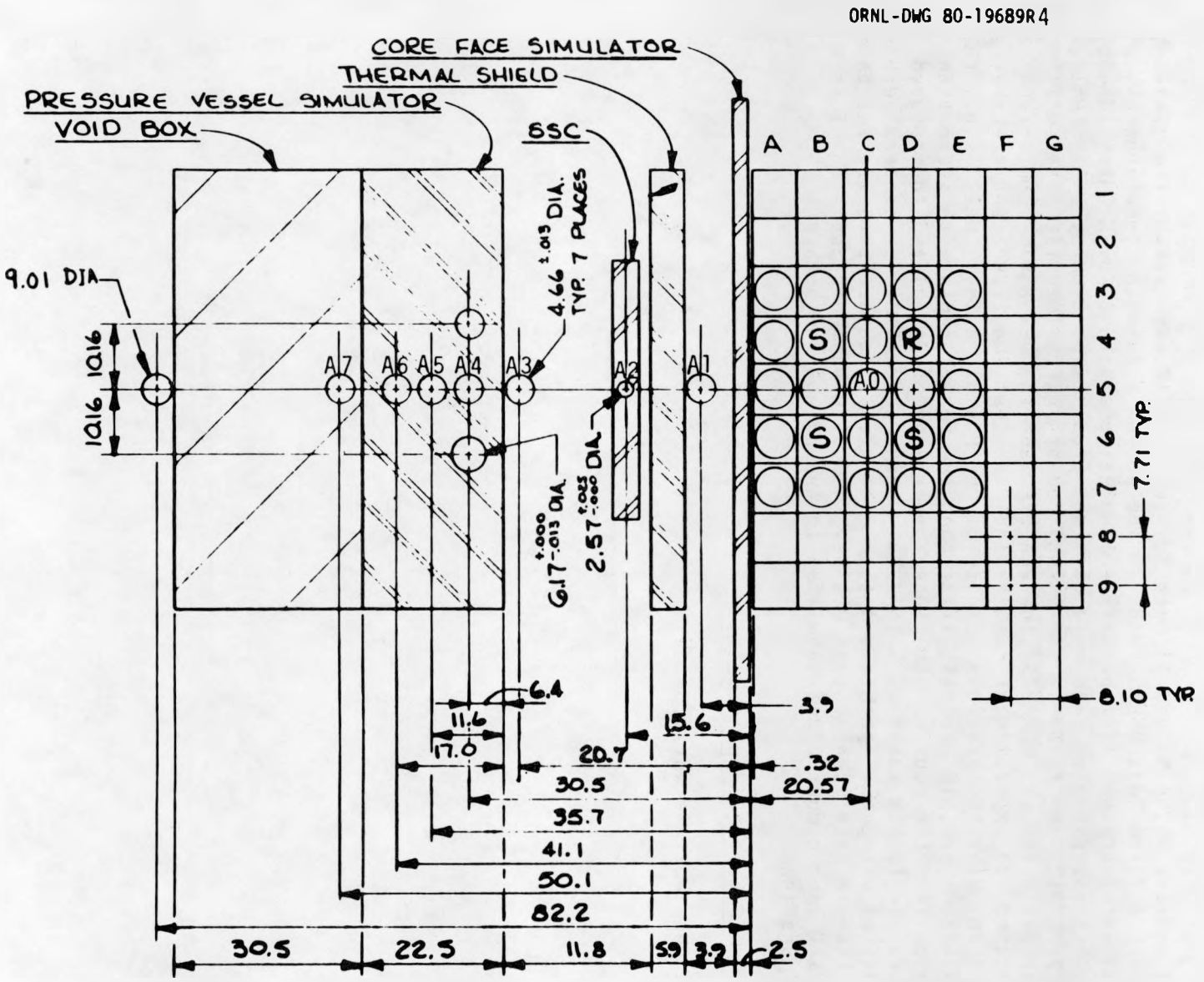

FIGURE ORNL-18. PCA Pressure Vessel Benchmark Facility 4/12 SSC Configuration.

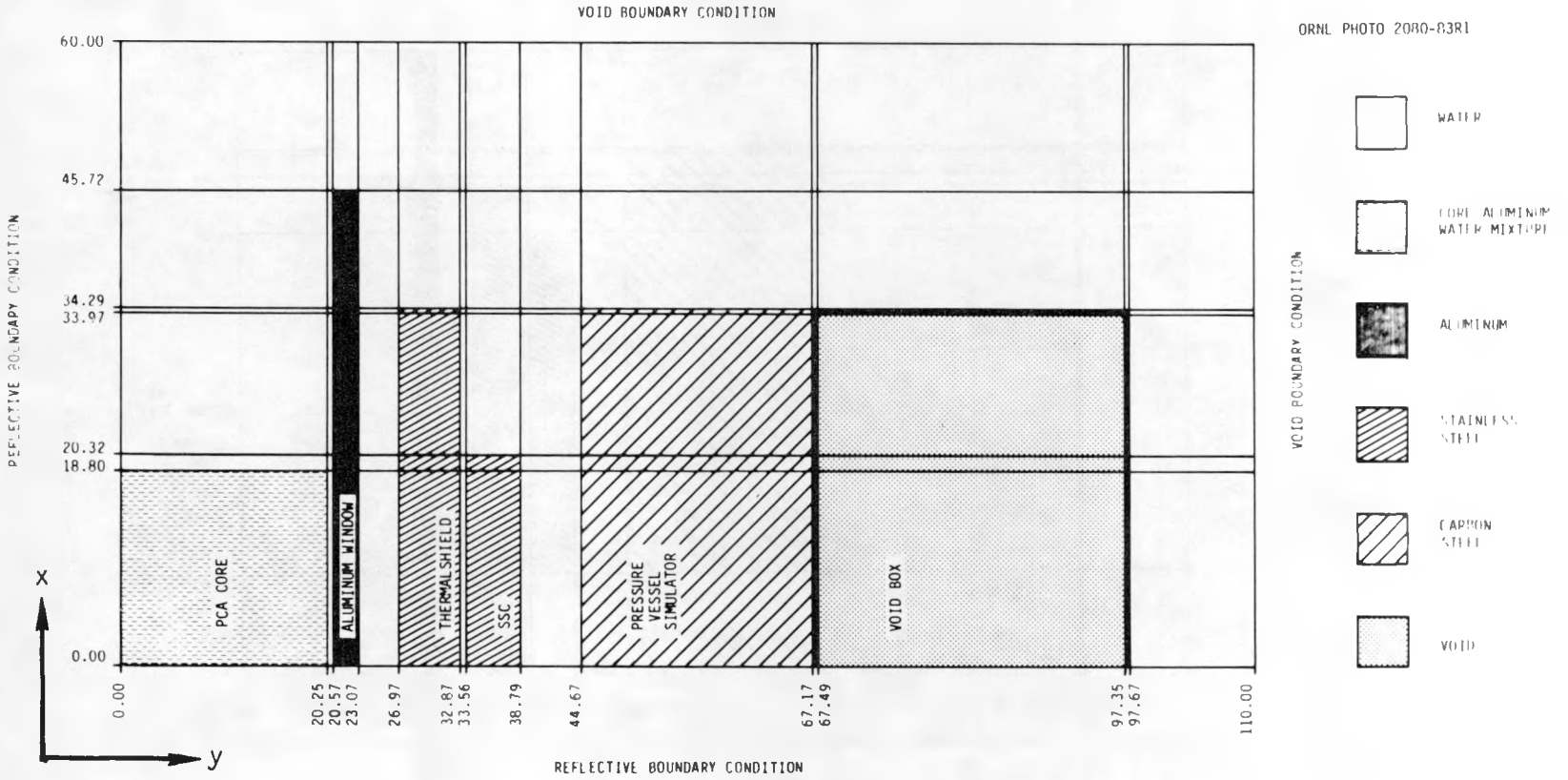

FIGURE ORNL-19. Geometrical Model for ORNL PCA 4/12 SSC Configuration "Midplane" DOT Calculation.

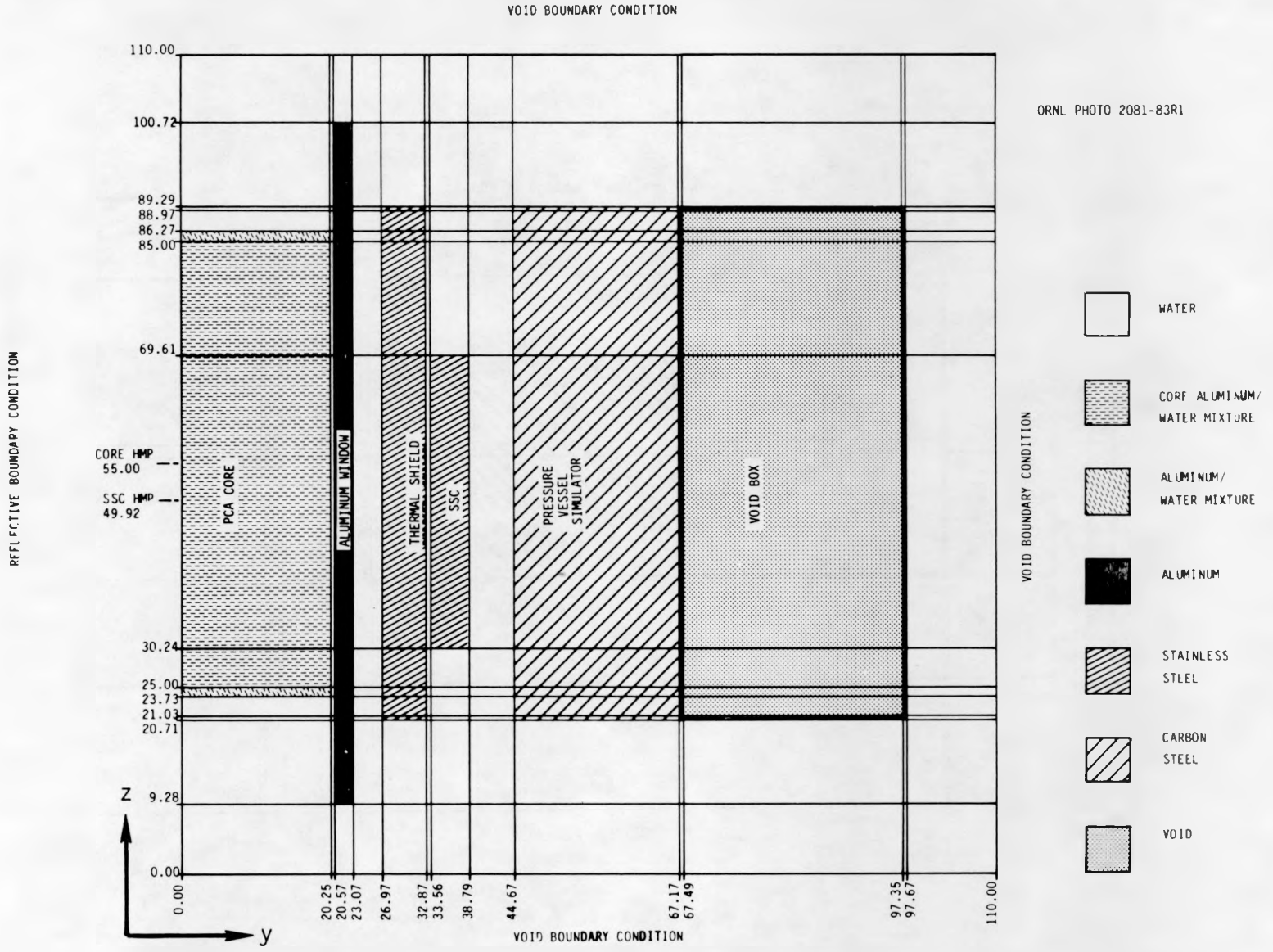

FIGURE ORNL-20. Geometrical Model for ORNL PCA 4/12 SSC Configuration "Axial" DOT Calculation.

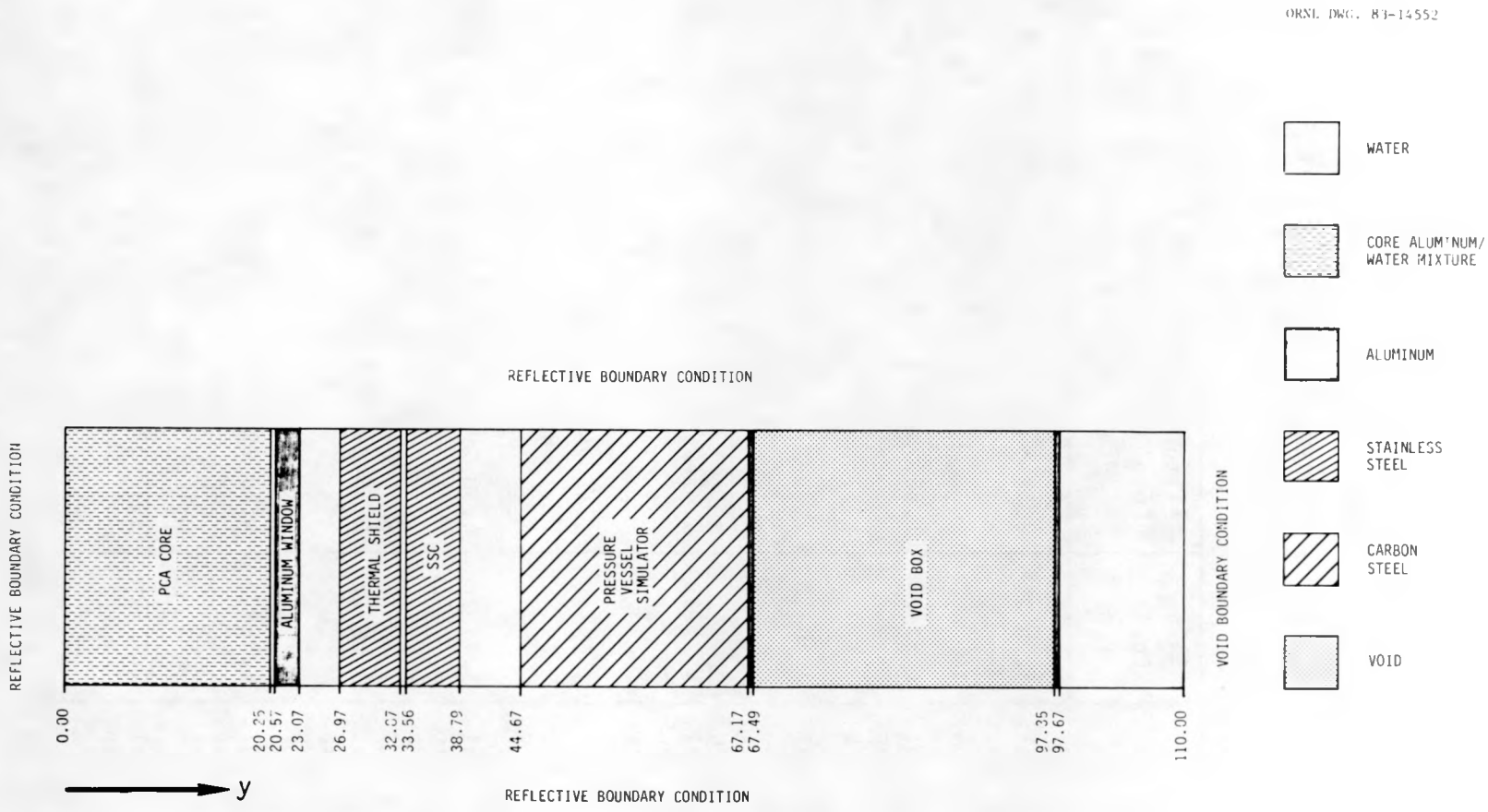

FIGURE ORNL-21. Geometrical Model for ORNL PCA 4/12 SSC Configuration ANISN Calculation.

APPENDIX A

REACTION RATES FOR THE 4/12 SSC AND 4/12 CONFIGURATIONS COMPARED WITH AVAILABLE MEASUREMENTS

TABLE ORNL-33

CALCULATED AND EXPERIMENTAL REACTION RATES[a] FOR THE 4/12 SSC CONFIGURATION A0 LOCATION

Location		^{237}Np (n,f) F.P.	^{115}In (n,n') ^{115m}In	^{103}Rh (n,n') ^{103m}Rh	^{238}U (n,f) F.P.	^{58}Ni (n,p) ^{58}Co	^{27}Al (n,α) ^{24}Na
A0 +28.50[b]	Cal.	6.98-29[c]	8.54-30	3.58-29	1.43-29	4.71-30	3.20-32
	Exp.						
	C/E						
A0 +22.50	Cal.	1.52-28	1.86-29	7.81-29	3.10-29	1.02-29	6.70-32
	Exp.						
	C/E						
A0 +15.00	Cal.	2.50-28	3.05-29	1.28-28	5.08-29	1.66-29	1.09-31
	Exp.						
	C/E						
A0 +7.50	Cal.	3.25-28	3.95-29	1.66-28	6.59-29	2.16-29	1.41-31
	Exp.						
	C/E						
A0 +0.00	Cal.	3.65-28	4.44-29	1.87-28	7.41-29	2.42-29	1.58-31
	Exp.					2.40-29	1.51-31
	C/E					1.01	1.05
A0 -5.08	Cal.	3.71-28	4.50-29	1.90-28	7.51-29	2.46-29	1.60-31
	Exp.						
	C/E						
A0 -7.50	Cal.	3.66-28	4.45-29	1.88-28	7.42-29	2.43-29	1.58-31
	Exp.						
	C/E						
A0 -13.50	Cal.	3.38-28	4.10-29	1.73-28	6.84-29	2.24-29	1.46-31
	Exp.						
	C/E						
A0 -20.50	Cal.	2.72-28	3.31-29	1.39-28	5.52-29	1.81-29	1.18-31
	Exp.						
	C/E						

[a]Reactions per second per target atom per source neutron (multiply by 2.265×10^{18} to normalize to 30 MW).

[b]Read as A0 location, 28.5 cm above core horizontal midplane.

[c]Read as 6.98×10^{-29}.

TABLE ORNL-34

CALCULATED AND EXPERIMENTAL REACTION RATES[a]
FOR THE 4/12 SSC CONFIGURATION Al LOCATION

Location		^{237}Np (n,f) F.P.	^{115}In (n,n') ^{115m}In	^{103}Rh (n,n') ^{103m}Rh	^{238}U (n,f) F.P.	^{58}Ni (n,p) ^{58}Co	^{27}Al (n,α) ^{24}Na
Al +28.50[b]	Cal.	1.30-29[c]	1.57-30	6.65-30	2.62-30	8.66-31	6.36-33
	Exp.						
	C/E						
Al +22.50	Cal.	2.29-29	2.73-30	1.17-29	4.55-30	1.48-30	1.03-32
	Exp.						
	C/E						
Al +15.00	Cal.	3.55-29	4.22-30	1.81-29	7.01-30	2.27-30	1.55-32
	Exp.						
	C/E						
Al +7.50	Cal.	4.55-29	5.39-30	2.32-29	8.95-30	2.88-30	1.95-32
	Exp.						
	C/E						
Al +0.00	Cal.	5.09-29	6.03-30	2.59-29	1.00-29	3.22-30	2.17-32
	Exp.						
	C/E						
Al -5.08	Cal.	5.16-29	6.10-30	2.62-29	1.01-29	3.26-30	2.19-32
	Exp.						
	C/E						
Al -7.50	Cal.	5.09-29	6.03-30	2.59-29	1.00-29	3.22-30	2.16-32
	Exp.						
	C/E						
Al -13.50	Cal.	4.68-29	5.54-30	2.38-29	9.20-30	2.96-30	2.00-32
	Exp.						
	C/E						
Al -20.50	Cal.	3.76-29	4.45-30	1.91-29	7.40-30	2.39-30	1.63-32
	Exp.						
	C/E						

[a]Reactions per second per target atom per source neutron (multiply by 2.265×10^{18} to normalize to 30 MW).

[b]Read as Al location, 28.5 cm above core horizontal midplane.

[c]Read as 1.30×10^{-29}.

TABLE ORNL-35

CALCULATED AND EXPERIMENTAL REACTION RATES[a], FOR THE 4/12 SSC CONFIGURATION A2 LOCATION

Location		^{237}Np (n,f) F.P.	^{115}In (n,n') ^{115m}In	^{103}Rh (n,n') ^{103m}Rh	^{238}U (n,f) F.P.	^{58}Ni (n,p) ^{58}Co	^{27}Al (n,α) ^{24}Na
A2 +12.00[b]	Cal.	6.61-30[c]	5.70-31	3.10-30	8.76-31	2.23-31	1.57-33
	Exp.						
	C/E						
A2 +8.00	Cal.	7.86-30	6.64-31	3.67-30	1.01-30	2.52-31	1.74-33
	Exp.						
	C/E						
A2 +3.90	Cal.	8.65-30	7.24-31	4.03-30	1.10-30	2.73-31	1.86-33
	Exp.		7.25-31	3.91-30		2.79-31	1.97-33
	C/E		1.00	1.03		0.98	0.94
A2 +0.00[d]	Cal.	9.05-30	7.56-31	4.22-30	1.15-30	2.84-31	1.93-33
	Exp.		7.47-31	4.02-30		2.87-31	2.03-33
	C/E		1.01	1.05		0.99	0.95
A2 -3.80	Cal.	9.18-30	7.66-31	4.28-30	1.16-30	2.88-31	1.96-33
	Exp.		7.46-31	4.01-30		2.87-31	2.04-33
	C/E		1.03	1.07		1.00	0.96
A2 -5.08	Cal.	9.16-30	7.64-31	4.27-30	1.16-30	2.87-31	1.95-33
	Exp.						
	C/E						
A2 -11.30	Cal.	8.62-30	7.20-31	4.02-30	1.09-30	2.71-31	1.85-33
	Exp.		6.91-31	3.69-30		2.64-31	1.89-33
	C/E		1.04	1.09		1.02	0.98
A2 -18.80	Cal.	6.96-30	5.88-31	3.25-30	8.98-31	2.24-31	1.56-33
	Exp.		5.51-31	2.96-30		2.16-31	1.55-33
	C/E		1.07	1.10		1.04	1.00
A2 -23.00	Cal.	5.34-30	4.64-31	2.51-30	7.15-31	1.84-31	1.32-33
	Exp.						
	C/E						

[a]Reactions per second per target atom per source neutron (multiply by 2.265×10^{18} to normalize to 30 MW).

[b]Read as A2 location, 12.0 cm above core horizontal midplane.

[c]Read as 6.61×10^{-30}.

[d]Experimental data derived from cosine fits.

TABLE ORNL-36

CALCULATED AND EXPERIMENTAL REACTION RATES[a]
FOR THE 4/12 SSC CONFIGURATION A3 LOCATION

Location		^{237}Np (n,f) F.P.	^{115}In (n,n') ^{115m}In	^{103}Rh (n,n') ^{103m}Rh	^{238}U (n,f) F.P.	^{58}Ni (n,p) ^{58}Co	^{27}Al (n,α) ^{24}Na
A3 +28.50[b]	Cal.	5.31-31[c]	6.56-32	2.74-31	1.12-31	4.01-32	4.44-34
	Exp.						
	C/E						
A3 +22.50	Cal.	8.02-31	9.68-32	4.11-31	1.64-31	5.72-32	6.02-34
	Exp.						
	C/E						
A3 +15.00	Cal.	1.33-30	1.39-31	6.56-31	2.27-31	7.05-32	6.62-34
	Exp.						
	C/E						
A3 +7.50	Cal.	1.93-30	1.82-31	9.28-31	2.89-31	8.21-32	7.17-34
	Exp.						
	C/E						
A3 +0.00	Cal.	2.19-30	2.04-31	1.05-30	3.24-31	9.12-32	7.87-34
	Exp.						
	C/E						
A3 -5.08	Cal.	2.21-30	2.06-31	1.06-30	3.27-31	9.20-32	7.93-34
	Exp.						
	C/E						
A3 -7.50	Cal.	2.18-30	2.03-31	1.05-30	3.22-31	9.08-32	7.83-34
	Exp.						
	C/E						
A3 -13.50	Cal.	1.99-30	1.86-31	9.58-31	2.96-31	8.36-32	7.26-34
	Exp.						
	C/E						
A3 -20.50	Cal.	1.55-30	1.48-31	7.47-31	2.35-31	6.77-32	6.01-34
	Exp.						
	C/E						

[a]Reactions per second per target atom per source neutron (multiply by 2.265×10^{18} to normalize to 30 MW).

[b]Read as A3 location, 28.5 cm above core horizontal midplane.

[c]Read as 5.31×10^{-31}.

TABLE ORNL-37

CALCULATED AND EXPERIMENTAL REACTION RATES[a]
FOR THE 4/12 SSC CONFIGURATION A4 LOCATION

Location		^{237}Np (n,f) F.P.	^{115}In (n,n') ^{115m}In	^{103}Rh (n,n') ^{103m}Rh	^{238}U (n,f) F.P.	^{58}Ni (n,p) ^{58}Co	^{27}Al (n,α) ^{24}Na
A4 +28.50[b]	Cal.	2.29-31[c]	1.91-32	1.07-31	3.00-32	8.29-33	9.24-35
	Exp.					9.55-33	1.04-34
	C/E					0.87	0.89
A4 +22.50	Cal.	3.35-31	2.69-32	1.56-31	4.15-32	1.10-32	1.14-34
	Exp.					1.29-32	1.33-34
	C/E					0.85	0.86
A4 +15.00	Cal.	4.70-31	3.57-32	2.16-31	5.39-32	1.33-32	1.26-34
	Exp.					1.62-32	1.50-34
	C/E					0.82	0.84
A4 +7.50	Cal.	5.89-31	4.32-32	2.69-31	6.44-32	1.52-32	1.39-34
	Exp.		5.34-32	3.05-31		1.79-32	1.60-34
	C/E		0.81	0.88		0.85	0.87
A4 +0.00	Cal.	6.57-31	4.77-32	3.00-31	7.09-32	1.66-32	1.50-34
	Exp.	6.64-31	5.81-32	3.32-31	7.63-32	1.90-32	1.68-34[d]
	C/E	0.99	0.82	0.90	0.93	0.87	0.89
A4 -5.08	Cal.	6.63-31	4.81-32	3.03-31	7.15-32	1.67-32	1.52-34
	Exp.						
	C/E						
A4 -7.50	Cal.	6.54-31	4.74-32	2.98-31	7.05-32	1.65-32	1.50-34
	Exp.		5.55-32	3.24-31		1.82-32	1.67-34
	C/E		0.85	0.92		0.91	0.90
A4 -13.50	Cal.	5.98-31	4.35-32	2.73-31	6.48-32	1.52-32	1.39-34
	Exp.		5.16-32	2.95-31		1.69-32	1.55-34
	C/E		0.84	0.92		0.90	0.90
A4 -20.50	Cal.	4.83-31	3.56-32	2.21-31	5.33-32	1.27-32	1.18-34
	Exp.						
	C/E						

[a]Reactions per second per target atom per source neutron (multiply by 2.265×10^{18} to normalize to 30 MW).

[b]Read as A4 location, 28.5 cm above core horizontal midplane.

[c]Read as 2.29×10^{-31}.

[d]Experimental data derived from cosine fit.

TABLE ORNL-38

CALCULATED AND EXPERIMENTAL REACTION RATES[a]
FOR THE 4/12 SSC CONFIGURATION A5 LOCATION

Location		^{237}Np (n,f) F.P.	^{115}In (n,n') ^{115m}In	^{103}Rh (n,n') ^{103m}Rh	^{238}U (n,f) F.P.	^{58}Ni (n,p) ^{58}Co	^{27}Al (n,α) ^{24}Na
A5 +28.50[b]	Cal.	1.30-31[c]	8.66-33	5.90-32	1.26-32	3.08-33	3.48-35
	Exp.						
	C/E						
A5 +22.50	Cal.	1.90-31	1.21-32	8.58-32	1.74-32	4.04-33	4.27-35
	Exp.						
	C/E						
A5 +15.00	Cal.	2.63-31	1.60-32	1.18-31	2.26-32	4.92-33	4.78-35
	Exp.						
	C/E						
A5 +7.50	Cal.	3.24-31	1.93-32	1.45-31	2.67-32	5.64-33	5.29-35
	Exp.		2.54-32			7.31-33	6.37-35
	C/E		0.76			0.77	0.83
A5 +0.00	Cal.	3.59-31	2.11-32	1.60-31	2.92-32	6.08-33	5.64-35
	Exp.	3.66-31		1.82-31	3.32-32	7.50-33	6.70-35
	C/E	0.98		0.88	0.88	0.81	0.84
A5 -5.08	Cal.	3.61-31	2.12-32	1.61-31	2.93-32	6.11-33	5.67-35
	Exp.						
	C/E						
A5 -7.50	Cal.	3.56-31	2.09-32	1.59-31	2.89-32	6.03-33	5.61-35
	Exp.		2.69-32			7.33-33	6.74-35
	C/E		0.78			0.82	0.83
A5 -13.50	Cal.	3.27-31	1.93-32	1.46-31	2.67-32	5.59-33	5.22-35
	Exp.					6.82-33	6.17-35
	C/E					0.82	0.85
A5 -20.50	Cal.	2.66-31	1.59-32	1.19-31	2.22-32	4.71-33	4.46-35
	Exp.						
	C/E						

[a]Reactions per second per target atom per source neutron (multiply by 2.265×10^{18} to normalize to 30 MW).

[b]Read as A5 location, 28.5 cm above core horizontal midplane.

[c]Read as 1.30×10^{-31}.

TABLE ORNL-39

CALCULATED AND EXPERIMENTAL REACTION RATES[a]
FOR THE 4/12 SSC CONFIGURATION A6 LOCATION

Location		^{237}Np (n,f) F.P.	^{115}In (n,n') ^{115m}In	^{103}Rh (n,n') ^{103m}Rh	^{238}U (n,f) F.P.	^{58}Ni (n,p) ^{58}Co	^{27}Al (n,α) ^{24}Na
A6 +28.50[b]	Cal.	6.92-32[c]	3.72-33	3.08-32	5.02-33	1.10-33	1.27-35
	Exp.						
	C/E						
A6 +22.50	Cal.	1.00-31	5.19-33	4.44-32	6.86-33	1.41-33	1.52-35
	Exp.						
	C/E						
A6 +15.00	Cal.	1.37-31	6.83-33	6.04-32	8.85-33	1.73-33	1.73-35
	Exp.						
	C/E						
A6 +7.50	Cal.	1.67-31	8.14-33	7.33-32	1.04-32	1.98-33	1.93-35
	Exp.						
	C/E						
A6 +0.00	Cal.	1.83-31	8.86-33	8.04-32	1.13-32	2.12-33	2.03-35
	Exp.	1.93-31			1.37-32		
	C/E	0.95			0.82		
A6 -5.08	Cal.	1.84-31	8.90-33	8.09-32	1.13-32	2.13-33	2.03-35
	Exp.						
	C/E						
A6 -7.50	Cal.	1.82-31	8.78-33	7.98-32	1.12-32	2.10-33	2.01-35
	Exp.						
	C/E						
A6 -13.50	Cal.	1.67-31	8.12-33	7.35-32	1.03-32	1.95-33	1.88-35
	Exp.						
	C/E						
A6 -20.50	Cal.	1.37-31	6.74-33	6.03-32	8.66-33	1.66-33	1.62-35
	Exp.						
	C/E						

[a]Reactions per second per target atom per source neutron (multiply by 2.265×10^{18} to normalize to 30 MW).

[b]Read as A6 location, 28.5 cm above core horizontal midplane.

[c]Read as 6.92×10^{-32}.

TABLE ORNL-40

CALCULATED AND EXPERIMENTAL REACTION RATES[a]
FOR THE 4/12 CONFIGURATION A0 LOCATION

Location		^{237}Np (n,f) F.P.	^{115}In (n,n') ^{115m}In	^{103}Rh (n,n') ^{103m}Rh	^{238}U (n,f) F.P.	^{58}Ni (n,p) ^{58}Co	^{27}Al (n,α) ^{24}Na
A0 +28.50[b]	Cal.	6.98-29[c]	8.54-30	3.58-29	1.43-29	4.71-30	3.20-32
	Exp.						
	C/E						
A0 +22.50	Cal.	1.52-28	1.86-29	7.81-29	3.10-29	1.02-29	6.70-32
	Exp.						
	C/E						
A0 +15.00	Cal.	2.50-28	3.05-29	1.28-28	5.08-29	1.66-29	1.09-31
	Exp.						
	C/E						
A0 +7.50	Cal.	3.25-28	3.95-29	1.66-28	6.59-29	2.16-29	1.41-31
	Exp.						
	C/E						
A0 +0.00	Cal.	3.65-28	4.44-29	1.87-28	7.41-29	2.42-29	1.58-31
	Exp.					2.40-29	1.51-31
	C/E					1.01	1.05
A0 -5.08	Cal.	3.71-28	4.50-29	1.90-28	7.51-29	2.46-29	1.60-31
	Exp.						
	C/E						
A0 -7.50	Cal.	3.66-28	4.45-29	1.88-28	7.42-29	2.43-29	1.58-31
	Exp.						
	C/E						
A0 -13.50	Cal.	3.38-28	4.10-29	1.73-28	6.84-29	2.24-29	1.46-31
	Exp.						
	C/E						
A0 -20.50	Cal.	2.72-28	3.31-29	1.39-28	5.52-29	1.81-29	1.18-31
	Exp.						
	C/E						

[a]Reactions per second per target atom per source neutron (multiply by 2.265×10^{18} to normalize to 30 MW).

[b]Read as A0 location, 28.5 cm above core horizontal midplane.

[c]Read as 6.98×10^{-29}.

TABLE ORNL-41

CALCULATED AND EXPERIMENTAL REACTION RATES[a]
FOR THE 4/12 CONFIGURATION Al LOCATION

Location		^{237}Np (n,f) F.P.	^{115}In (n,n') ^{115m}In	^{103}Rh (n,n') ^{103m}Rh	^{238}U (n,f) F.P.	^{58}Ni (n,p) ^{58}Co	^{27}Al (n,α) ^{24}Na
Al +28.50[b]	Cal.	1.30-29[c]	1.57-30	6.65-30	2.62-30	8.66-31	6.36-33
	Exp.						
	C/E						
Al +22.50	Cal.	2.29-29	2.73-30	1.17-29	4.54-30	1.48-30	1.03-32
	Exp.						
	C/E						
Al +15.00	Cal.	3.54-29	4.21-30	1.81-29	7.00-30	2.26-30	1.55-32
	Exp.						
	C/E						
Al +7.50	Cal.	4.53-29	5.38-30	2.31-29	8.93-30	2.88-30	1.95-32
	Exp.						
	C/E						
Al +0.00	Cal.	5.07-29	6.01-30	2.58-29	9.99-30	3.22-30	2.17-32
	Exp.						
	C/E						
Al -5.08	Cal.	5.13-29	6.09-30	2.61-29	1.01-29	3.26-30	2.19-32
	Exp.						
	C/E						
Al -7.50	Cal.	5.07-29	6.01-30	2.58-29	9.99-30	3.22-30	2.16-32
	Exp.						
	C/E						
Al -13.50	Cal.	4.66-29	5.53-30	2.37-29	9.18-30	2.96-30	2.00-32
	Exp.						
	C/E						
Al -20.50	Cal.	3.74-29	4.45-30	1.91-29	7.39-30	2.39-30	1.63-32
	Exp.						
	C/E						

[a]Reactions per second per target atom per source neutron (multiply by 2.265×10^{18} to normalize to 30 MW).

[b]Read as Al location, 28.5 cm above core horizontal midplane.

[c]Read as 1.30×10^{-29}.

TABLE ORNL-42

CALCULATED AND EXPERIMENTAL REACTION RATES[a]
FOR THE 4/12 CONFIGURATION A2 LOCATION

Location		^{237}Np (n,f) F.P.	^{115}In (n,n') ^{115m}In	^{103}Rh (n,n') ^{103m}Rh	^{238}U (n,f) F.P.	^{58}Ni (n,p) ^{58}Co	^{27}Al (n,α) ^{24}Na
A2 +12.00[b]	Cal.	3.63-30[c]	3.99-31	1.81-30	6.59-31	2.09-31	1.78-33
	Exp.						
	C/E						
A2 +8.00	Cal.	4.04-30	4.45-31	2.02-30	7.33-31	2.32-31	1.97-33
	Exp.						
	C/E						
A2 +3.90	Cal.	4.36-30	4.79-31	2.17-30	7.90-31	2.49-31	2.11-33
	Exp.						
	C/E						
A2 +0.00	Cal.	4.54-30	4.99-31	2.26-30	8.22-31	2.59-31	2.19-33
	Exp.						
	C/E						
A2 -3.80	Cal.	4.59-30	5.05-31	2.29-30	8.32-31	2.62-31	2.21-33
	Exp.						
	C/E						
A2 -5.08	Cal.	4.58-30	5.04-31	2.29-30	8.30-31	2.62-31	2.21-33
	Exp.						
	C/E						
A2 -11.30	Cal.	4.32-30	4.75-31	2.16-30	7.83-31	2.47-31	2.09-33
	Exp.						
	C/E						
A2 -18.80	Cal.	3.58-30	3.95-31	1.79-30	6.52-31	2.07-31	1.77-33
	Exp.						
	C/E						
A2 -23.00	Cal.	3.00-30	3.32-31	1.50-30	5.48-31	1.74-31	1.50-33
	Exp.						
	C/E						

[a]Reactions per second per target atom per source neutron (multiply by 2.265×10^{18} to normalize to 30 MW).

[b]Read as A2 location, 12.0 cm above core horizontal midplane.

[c]Read as 3.63×10^{-30}.

TABLE ORNL-43

CALCULATED AND EXPERIMENTAL REACTION RATES[a]
FOR THE 4/12 CONFIGURATION A3 LOCATION

Location		^{237}Np (n,f) F.P.	^{115}In (n,n') ^{115m}In	^{103}Rh (n,n') ^{103m}Rh	^{238}U (n,f) F.P.	^{58}Ni (n,p) ^{58}Co	^{27}Al (n,α) ^{24}Na
A3 +28.50[b]	Cal.	5.20-31[c]	6.41-32	2.69-31	1.10-31	3.92-32	4.30-34
	Exp.						
	C/E						
A3 +22.50	Cal.	7.69-31	9.39-32	3.96-31	1.60-31	5.61-32	5.90-34
	Exp.						
	C/E						
A3 +15.00	Cal.	1.09-30	1.32-31	5.59-31	2.25-31	7.82-32	8.02-34
	Exp.						
	C/E						
A3 +7.50	Cal.	1.34-30	1.63-31	6.91-31	2.77-31	9.60-32	9.72-34
	Exp.						
	C/E						
A3 +0.00	Cal.	1.49-30	1.80-31	7.62-31	3.06-31	1.06-31	1.06-33
	Exp.						
	C/E						
A3 -5.08	Cal.	1.50-30	1.82-31	7.69-31	3.08-31	1.07-31	1.07-33
	Exp.						
	C/E						
A3 -7.50	Cal.	1.48-30	1.79-31	7.59-31	3.04-31	1.05-31	1.06-33
	Exp.						
	C/E						
A3 -13.50	Cal.	1.36-30	1.65-31	6.98-31	2.80-31	9.71-32	9.83-34
	Exp.						
	C/E						
A3 -20.50	Cal.	1.11-30	1.36-31	5.72-31	2.30-31	8.02-32	8.21-34
	Exp.						
	C/E						

[a]Reactions per second per target atom per source neutron (multiply by 2.265×10^{18} to normalize to 30 MW).

[b]Read as A3 location, 28.5 cm above core horizontal midplane.

[c]Read as 5.20×10^{-31}.

TABLE ORNL-44

CALCULATED AND EXPERIMENTAL REACTION RATES[a]
FOR THE 4/12 CONFIGURATION A4 LOCATION

Location		^{237}Np (n,f) F.P.	^{115}In (n,n') ^{115m}In	^{103}Rh (n,n') ^{103m}Rh	^{238}U (n,f) F.P.	^{58}Ni (n,p) ^{58}Co	^{27}Al (n,α) ^{24}Na
A4 +28.50[b]	Cal.	2.17-31[c]	1.89-32	1.02-31	2.98-32	8.35-33	9.37-35
	Exp.						
	C/E						
A4 +22.50	Cal.	3.13-31	2.68-32	1.47-31	4.21-32	1.15-32	1.23-34
	Exp.						
	C/E						
A4 +15.00	Cal.	4.25-31	3.64-32	1.99-31	5.72-32	1.55-32	1.62-34
	Exp.						
	C/E						
A4 +7.50	Cal.	5.13-31	4.41-32	2.41-31	6.93-32	1.88-32	1.93-34
	Exp.						
	C/E						
A4 +0.00	Cal.	5.60-31	4.83-32	2.63-31	7.58-32	2.05-32	2.09-34
	Exp.						
	C/E						
A4 -5.08	Cal.	5.63-31	4.86-32	2.64-31	7.63-32	2.06-32	2.10-34
	Exp.						
	C/E						
A4 -7.50	Cal.	5.56-31	4.79-32	2.61-31	7.53-32	2.04-32	2.08-34
	Exp.						
	C/E						
A4 -13.50	Cal.	5.13-31	4.43-32	2.41-31	6.97-32	1.89-32	1.95-34
	Exp.						
	C/E						
A4 -20.50	Cal.	4.24-31	3.67-32	1.99-31	5.77-32	1.57-32	1.63-34
	Exp.						
	C/E						

[a]Reactions per second per target atom per source neutron (multiply by 2.265×10^{18} to normalize to 30 MW).

[b]Read as A4 location, 28.5 cm above core horizontal midplane.

[c]Read as 2.17×10^{-31}.

TABLE ORNL-45

CALCULATED AND EXPERIMENTAL REACTION RATES[a]
FOR THE 4/12 CONFIGURATION A5 LOCATION

Location		^{237}Np (n,f) F.P.	^{115}In (n,n') ^{115m}In	^{103}Rh (n,n') ^{103m}Rh	^{238}U (n,f) F.P.	^{58}Ni (n,p) ^{58}Co	^{27}Al (n,α) ^{24}Na
A5 +28.50[b]	Cal.	1.22-31[c]	8.59-33	5.55-32	1.28-32	3.18-33	3.67-35
	Exp.						
	C/E						
A5 +22.50	Cal.	1.75-31	1.22-32	7.97-32	1.79-32	4.34-33	4.76-35
	Exp.						
	C/E						
A5 +15.00	Cal.	2.36-31	1.63-32	1.07-31	2.40-32	5.78-33	6.16-35
	Exp.						
	C/E						
A5 +7.50	Cal.	2.82-31	1.96-32	1.28-31	2.89-32	6.93-33	7.31-35
	Exp.						
	C/E						
A5 +0.00	Cal.	3.06-31	2.14-32	1.39-31	3.15-32	7.55-33	7.92-35
	Exp.						
	C/E						
A5 -5.08	Cal.	3.07-31	2.15-32	1.39-31	3.17-32	7.59-33	7.97-35
	Exp.						
	C/E						
A5 -7.50	Cal.	3.03-31	2.12-32	1.38-31	3.13-32	7.50-33	7.89-35
	Exp.						
	C/E						
A5 -13.50	Cal.	2.80-31	1.96-32	1.27-31	2.90-32	6.96-33	7.37-35
	Exp.						
	C/E						
A5 -20.50	Cal.	2.32-31	1.63-32	1.06-31	2.41-32	5.81-33	6.18-35
	Exp.						
	C/E						

[a]Reactions per second per target atom per source neutron (multiply by 2.265×10^{18} to normalize to 30 MW).

[b]Read as A5 location, 28.5 cm above core horizontal midplane.

[c]Read as 1.22×10^{-31}.

TABLE ORNL-46

CALCULATED AND EXPERIMENTAL REACTION RATES[a]
FOR THE 4/12 CONFIGURATION A6 LOCATION

Location		^{237}Np (n,f) F.P.	^{115}In (n,n') ^{115m}In	^{103}Rh (n,n') ^{103m}Rh	^{238}U (n,f) F.P.	^{58}Ni (n,p) ^{58}Co	^{27}Al (n,α) ^{24}Na
A6 +28.50[b]	Cal.	6.39-32[c]	3.70-33	2.85-32	5.11-33	1.15-33	1.36-35
	Exp.						
	C/E						
A6 +22.50	Cal.	9.13-32	5.19-33	4.06-32	7.12-33	1.55-33	1.75-35
	Exp.						
	C/E						
A6 +15.00	Cal.	1.21-31	6.89-33	5.39-32	9.44-33	2.03-33	2.24-35
	Exp.						
	C/E						
A6 +7.50	Cal.	1.44-31	8.21-33	6.39-32	1.13-32	2.42-33	2.64-35
	Exp.						
	C/E						
A6 +0.00	Cal.	1.56-31	8.91-33	6.91-32	1.22-32	2.63-33	2.85-35
	Exp.						
	C/E						
A6 -5.08	Cal.	1.56-31	8.95-33	6.93-32	1.23-32	2.64-33	2.87-35
	Exp.						
	C/E						
A6 -7.50	Cal.	1.54-31	8.83-33	6.83-32	1.21-32	2.61-33	2.84-35
	Exp.						
	C/E						
A6 -13.50	Cal.	1.42-31	8.18-33	6.32-32	1.12-32	2.42-33	2.64-35
	Exp.						
	C/E						
A6 -20.50	Cal.	1.18-31	6.84-33	5.26-32	9.41-33	2.04-33	2.24-35
	Exp.						
	C/E						

[a]Reactions per second per target atom per source neutron (multiply by 2.265×10^{18} to normalize to 30 MW).

[b]Read as A6 location, 28.5 cm above core horizontal midplane.

[c]Read as 6.39×10^{-32}.

APPENDIX B

DAMAGE CORRELATION PARAMETERS FOR THE 4/12 SSC AND 4/12 CONFIGURATIONS

TABLE ORNL-47

DAMAGE CORRELATION PARAMETERS FOR THE 4/12 SSC CONFIGURATION A0 LOCATION

Location	Fluence Rate[b] ϕ (E >1 Mev)	Fluence Rate[b] ϕ (E >.1 Mev)	dpa[d] (ASTM)
A0 +28.50[a]	3.36-5[c]	6.23-5	4.50-26
A0 +22.50	7.32-5	1.35-4	9.76-26
A0 +15.00	1.20-4	2.23-4	1.60-25
A0 +7.50	1.56-4	2.89-4	2.08-25
A0 +0.00	1.75-4	3.25-4	2.34-25
A0 -5.08	1.78-4	3.30-4	2.37-25
A0 -7.50	1.76-4	3.26-4	2.34-25
A0 -13.50	1.62-4	3.00-4	2.16-25
A0 -20.50	1.31-4	2.42-4	1.74-25

TABLE ORNL-48

DAMAGE CORRELATION PARAMETERS FOR THE 4/12 SSC CONFIGURATION A1 LOCATION

Location	Fluence Rate[b] ϕ (E >1 Mev)	Fluence Rate[b] ϕ (E >.1 Mev)	dpa[d] (ASTM)
A1 +28.50	6.15-6	1.20-5	8.39-27
A1 +22.50	1.08-5	2.14-5	1.47-26
A1 +15.00	1.67-5	3.34-5	2.27-26
A1 +7.50	2.14-5	4.28-5	2.91-26
A1 +0.00	2.39-5	4.80-5	3.26-26
A1 -5.08	2.42-5	4.86-5	3.30-26
A1 -7.50	2.39-5	4.80-5	3.26-26
A1 -13.50	2.20-5	4.41-5	2.99-26
A1 -20.50	1.76-5	3.53-5	2.40-26

TABLE ORNL-49

DAMAGE CORRELATION PARAMETERS FOR THE 4/12 SSC
CONFIGURATION A2 LOCATION

Location	Fluence Rate[b] ϕ (E >1 Mev)	Fluence Rate[b] ϕ (E >.1 Mev)	dpa[d] (ASTM)
A2 +12.00	2.52-6	7.64-6	3.80-27
A2 +8.00	2.95-6	9.25-6	4.51-27
A2 +3.90	3.23-6	1.02-5	4.95-27
A2 +0.00	3.37-6	1.08-5	5.19-27
A2 -3.80	3.42-6	1.09-5	5.26-27
A2 -5.08	3.41-6	1.09-5	5.25-27
A2 -11.30	3.21-6	1.02-5	4.94-27
A2 -18.80	2.62-6	8.18-6	3.99-27
A2 -23.00	2.04-6	6.15-6	3.08-27

TABLE ORNL-50

DAMAGE CORRELATION PARAMETERS FOR THE 4/12 SSC
CONFIGURATION A3 LOCATION

Location	Fluence Rate[b] ϕ (E >1 Mev)	Fluence Rate[b] ϕ (E >.1 Mev)	dpa[d] (ASTM)
A3 +28.50	2.54-7	4.87-7	3.52-28
A3 +22.50	3.78-7	7.54-7	5.27-28
A3 +15.00	5.68-7	1.43-6	8.29-28
A3 +7.50	7.68-7	2.24-6	1.17-27
A3 +0.00	8.66-7	2.56-6	1.32-27
A3 -5.08	8.75-7	2.59-6	1.33-27
A3 -7.50	8.63-7	2.56-6	1.32-27
A3 -13.50	7.90-7	2.33-6	1.20-27
A3 -20.50	6.21-7	1.78-6	9.38-28

TABLE ORNL-51

DAMAGE CORRELATION PARAMETERS FOR THE 4/12 SSC
CONFIGURATION A4 LOCATION

Location	Fluence Rate[b] ϕ (E >1 Mev)	Fluence Rate[b] ϕ (E >.1 Mev)	dpa[d] (ASTM)
A4 +28.50	8.26-8	2.89-7	1.36-28
A4 +22.50	1.18-7	4.35-7	1.98-28
A4 +15.00	1.59-7	6.30-7	2.75-28
A4 +7.50	1.94-7	8.04-7	3.43-28
A4 +0.00	2.14-7	9.02-7	3.82-28
A4 -5.08	2.16-7	9.11-7	3.85-28
A4 -7.50	2.13-7	8.98-7	3.80-28
A4 -13.50	1.96-7	8.20-7	3.48-28
A4 -20.50	1.60-7	6.55-7	2.81-28

TABLE ORNL-52

DAMAGE CORRELATION PARAMETERS FOR THE 4/12 SSC
CONFIGURATION A5 LOCATION

Location	Fluence Rate[b] ϕ (E >1 Mev)	Fluence Rate[b] ϕ (E >.1 Mev)	dpa[d] (ASTM)
A5 +28.50	3.88-8	1.96-7	7.69-29
A5 +22.50	5.50-8	2.94-7	1.12-28
A5 +15.00	7.36-8	4.14-7	1.55-28
A5 +7.50	8.88-8	5.16-7	1.90-28
A5 +0.00	9.75-8	5.73-7	2.10-28
A5 -5.08	9.82-8	5.78-7	2.12-28
A5 -7.50	9.68-8	5.69-7	2.09-28
A5 -13.50	8.92-8	5.21-7	1.91-28
A5 -20.50	7.33-8	4.21-7	1.56-28

TABLE ORNL-53

DAMAGE CORRELATION PARAMETERS FOR THE 4/12 SSC CONFIGURATION A6 LOCATION

Location	Fluence Rate[b] ϕ (E >1 Mev)	Fluence Rate[b] ϕ (E >.1 Mev)	dpa[d] (ASTM)
A6 +28.50	1.70-8	1.20-7	4.13-29
A6 +22.50	2.39-8	1.77-7	6.00-29
A6 +15.00	3.17-8	2.45-7	8.18-29
A6 +7.50	3.80-8	3.00-7	9.94-29
A6 +0.00	4.14-8	3.30-7	1.09-28
A6 -5.08	4.16-8	3.32-7	1.10-28
A6 -7.50	4.10-8	3.28-7	1.08-28
A6 -13.50	3.80-8	3.01-7	9.96-29
A6 -20.50	3.14-8	2.45-7	8.16-29

[a]Read as A0 location, 28.5 cm above core horizontal midplane.

[b]Neutrons per square centimeter per source neutron (multiply by 2.265×10^{18} to normalize to 30 MW).

[c]Read as 6.98×10^{-29}.

[d]Displacements per atom per source neutron (multiply by 2.265×10^{18} to normalize to 30 MW).

TABLE ORNL-54

DAMAGE CORRELATION PARAMETERS FOR THE 4/12 CONFIGURATION
A0 LOCATION

Location	Fluence Rate[b] ϕ (E >1 Mev)	Fluence Rate[b] ϕ (E >.1 Mev)	dpa[d] (ASTM)
A0 +28.50[a]	3.36-5[c]	6.23-5	4.50-26
A0 +22.50	7.32-5	1.35-4	9.76-26
A0 +15.00	1.20-4	2.23-4	1.60-25
A0 +7.50	1.56-4	2.89-4	2.08-25
A0 +0.00	1.75-4	3.25-4	2.34-25
A0 -5.08	1.78-4	3.30-4	2.37-25
A0 -7.50	1.76-4	3.26-4	2.34-25
A0 -13.50	1.62-4	3.00-4	2.16-25
A0 -20.50	1.31-4	2.42-4	1.74-25

TABLE ORNL-55

DAMAGE CORRELATION PARAMETERS FOR THE 4/12 CONFIGURATION
A1 LOCATION

Location	Fluence Rate[b] ϕ (E >1 Mev)	Fluence Rate[b] ϕ (E >.1 Mev)	dpa[d] (ASTM)
A1 +28.50	6.15-6	1.21-5	8.39-27
A1 +22.50	1.08-5	2.14-5	1.47-26
A1 +15.00	1.67-5	3.32-5	2.27-26
A1 +7.50	2.13-5	4.25-5	2.90-26
A1 +0.00	2.38-5	4.76-5	3.24-26
A1 -5.08	2.41-5	4.82-5	3.28-26
A1 -7.50	2.38-5	4.76-5	3.24-26
A1 -13.50	2.19-5	4.37-5	2.98-26
A1 -20.50	1.76-5	3.50-5	2.39-26

TABLE ORNL-56

DAMAGE CORRELATION PARAMETERS FOR THE 4/12 CONFIGURATION
A2 LOCATION

Location	Fluence Rate[b] ϕ (E >1 Mev)	Fluence Rate[b] ϕ (E >.1 Mev)	dpa[d] (ASTM)
A2 +12.00	1.61-6	3.67-6	2.28-27
A2 +8.00	1.79-6	4.10-6	2.54-27
A2 +3.90	1.93-6	4.42-6	2.74-27
A2 +0.00	2.01-6	4.60-6	2.85-27
A2 -3.80	2.04-6	4.66-6	2.88-27
A2 -5.08	2.03-6	4.65-6	2.88-27
A2 -11.30	1.92-6	4.38-6	2.72-27
A2 -18.80	1.59-6	3.63-6	2.25-27
A2 -23.00	1.34-6	3.03-6	1.89-27

TABLE ORNL-57

DAMAGE CORRELATION PARAMETERS FOR THE 4/12 CONFIGURATION
A3 LOCATION

Location	Fluence Rate[b] ϕ (E >1 Mev)	Fluence Rate[b] ϕ (E >.1 Mev)	dpa[d] (ASTM)
A3 +28.50	2.48-7	4.77-7	3.45-28
A3 +22.50	3.65-7	7.12-7	5.07-28
A3 +15.00	5.16-7	1.01-6	7.15-28
A3 +7.50	6.37-7	1.25-6	8.82-28
A3 +0.00	7.03-7	1.38-6	9.73-28
A3 -5.08	7.09-7	1.39-6	9.81-28
A3 -7.50	7.00-7	1.37-6	9.69-28
A3 -13.50	6.44-7	1.26-6	8.92-28
A3 -20.50	5.28-7	1.03-6	7.31-28

TABLE ORNL-58

DAMAGE CORRELATION PARAMETERS FOR THE 4/12 CONFIGURATION
A4 LOCATION

Location	Fluence Rate[b] ϕ (E >1 Mev)	Fluence Rate[b] ϕ (E >.1 Mev)	dpa[d] (ASTM)
A4 +28.50	8.13-8	2.59-7	1.29-28
A4 +22.50	1.16-7	3.76-7	1.85-28
A4 +15.00	1.58-7	5.10-7	2.50-28
A4 +7.50	1.92-7	6.13-7	3.02-28
A4 +0.00	2.10-7	6.66-7	3.30-28
A4 -5.08	2.11-7	6.69-7	3.31-28
A4 -7.50	2.08-7	6.59-7	3.27-28
A4 -13.50	1.92-7	6.08-7	3.02-28
A4 -20.50	1.59-7	5.02-7	2.50-28

TABLE ORNL-59

DAMAGE CORRELATION PARAMETERS FOR THE 4/12 CONFIGURATION
A5 LOCATION

Location	Fluence Rate[b] ϕ (E >1 Mev)	Fluence Rate[b] ϕ (E >.1 Mev)	dpa[d] (ASTM)
A5 +28.50	3.85-8	1.72-7	7.12-29
A5 +22.50	5.48-8	2.49-7	1.02-28
A5 +15.00	7.37-8	3.33-7	1.37-28
A5 +7.50	8.86-8	3.97-7	1.64-28
A5 +0.00	9.65-8	4.29-7	1.78-28
A5 -5.08	9.70-8	4.30-7	1.78-28
A5 -7.50	9.57-8	4.24-7	1.76-28
A5 -13.50	8.86-8	3.91-7	1.63-28
A5 -20.50	7.36-8	3.24-7	1.35-28

TABLE ORNL-60

DAMAGE CORRELATION PARAMETERS FOR THE 4/12 CONFIGURATION
A6 LOCATION

Location	Fluence Rate[b] ϕ (E >1 Mev)	Fluence Rate[b] ϕ (E >.1 Mev)	dpa[d] (ASTM)
A6 +28.50	1.69-8	1.03-7	3.74-29
A6 +22.50	2.39-8	1.48-7	5.34-29
A6 +15.00	3.18-8	1.96-7	7.09-29
A6 +7.50	3.80-8	2.32-7	8.40-29
A6 +0.00	4.12-8	2.50-7	9.07-29
A6 -5.08	4.13-8	2.50-7	9.09-29
A6 -7.50	4.08-8	2.46-7	8.96-29
A6 -13.50	3.78-8	2.27-7	8.29-29
A6 -20.50	3.16-8	1.89-7	6.89-29

[a]Read as A0 location, 28.5 cm above core horizontal midplane.

[b]Neutrons per square centimeter per second per source neutron (multiply by 2.265×10^{18} to normalize to 30 MW).

[c]Read as 3.36×10^{-5}.

[d]Displacements per atom per second per source neutron (multiply by 2.265×10^{18} to normalize to 30 MW).

A.7 STATISTICAL EVALUATION OF THE CHARPY TEST RESULTS IN THE ORR-PSF METALLURGICAL IRRADIATION EXPERIMENT USING THE CV81 PROCEDURE - PRELIMINARY RESULTS

F. W. Stallmann

Summary

The preliminary results of the individual 41-J transition temperature values obtained using the CV81 procedure agree with the values reported by Materials Engineering Associates (MEA) within the statistical uncertainty bounds given in the form of standard deviations.

Correlations relating the NDT shift to a power of a damage parameter such as $\phi t > 1.0$ MeV, $\phi t > 0.1$ MeV, and dpa did not indicate an exponent that was clearly superior to all others.

Initial investigations have not indicated any difference in damage in the SSC and SPVC capsules dut to either fluence rate or spectral effects.

Accomplishments and Status

A preliminary investigation was made of the metallurgical test results in the ORR-PSF experiment as reported in NUREG/CR-3457, MEA-2026. The CV81 code was used which has been developed earlier to analyze results from HSST experiments. This code selects suitable Charpy tests for determining NDT and upper shelf energy separately and can combine results obtained under different irradiation conditions, thereby reducing uncertainties. The values of Chi-square per degree of freedom and standard deviation for the fitting parameters are included in the output. The values of the damage parameters $\phi t > 1.0$ MeV, $\phi t > 0.1$ MeV, and dpa were obtained from the LSL-M2 adjustment procedure and are given in a separate report (St84).

The reported results are preliminary since time did not permit the careful review necessary to establish final conclusions. For the same reason, only the 41-J transition temperature was investigated. Other aspects of the Charpy tests such as upper shelf, 68-J, and lateral expansion will be reported in the near future.

Individual 41-J transition temperature values were determined first (Table ORNL-61). These values agree, as expected, with the values reported by MEA within statistical uncertainty bounds, given in the form of standard deviations. These uncertainties are based on a $\pm$15-J standard deviation for the Charpy energy. This value includes not only the instrument precision but also, and primarily, the variability in toughness property from one specimen to the next. The reasonableness of this assumption is tested in the Chi-square test, which shows smaller than expected values and thus conservative uncertainty estimates. Some material has larger Chi-square values and thus larger scatter, but the values are well within the statistical bounds for small sample sizes.

The combined results were fitted to a variety of damage correlation functions relating the NDT shift to a power of a damage parameter value such as $\phi t > 1.0$ MeV, $\phi t > 0.1$ MeV, and dpa with powers of 0.5, 0.3, and 0.8 (Table ORNL-62). None of the correlations appears to be clearly superior and all agree with each other within uncertainties. However, $[\phi t > 1]^{0.3}$ appears to be closest to the individual fits. More detailed investigations are planned.

One goal of the experiment has been to find out whether there is a difference in damage in the SSC capsule and the SPVC capsules due to either fluence rate effects or spectral effects. None of such effects could be detected so far; fits made for SSC and SPVC separately agree with each other and with combined fits within uncertainties (Table ORNL-63).

No attempt was made to correlate the chemical composition with irradiation sensitivity. The material under investigation differs primarily in Ni content, but its influence on radiation damage is complex and other factors such as heat treatment may be of even greater importance. It appears doubtful that any conclusions can be drawn from the small selection of materials at hand.

Expected Future Accomplishments

Statistical evaluation of the Charpy test results for the ORR-PSF metallurgical irradiation experiment are scheduled for completion by the next report period.

TABLE ORNL-61

41-J TRANSITION TEMPERATURE AS DETERMINED THROUGH THE CV81 CODE AND BY MEA

	$\phi t > 1.0$*	$\phi t > 0.1$*	dpa*	χ^2/F	41-J-NDT CV81	Std.	41-J-NDT MEA
A302-B							
Unirr.	0	0	0	0.11	-6	±9	-4
SSC1	2.59	7.46	3.85	0.64	83	±29	78
SSC2	5.37	15.33	7.95	1.13	83	±20	90
0-T	3.91	11.31	5.99	0.15	71	±7	77
1/4 T	2.15	8.07	3.67	0.77	44	±30	63
1/2 T	1.03	5.29	2.12	04	46	±9	46
A533-B							
Unirr.	0	0	0	0.11	-1	±9	-1
SSC1	2.34	6.69	3.47	0.69	68	±11	60
SSC2	4.88	13.79	7.18	0.04	80	±18	80
0-T	3.61	10.27	5.49	0.23	66	±13	74
1/4 T	1.95	7.12	3.28	0.47	64	±7	68
1/2 T	0.94	4.60	1.87	0.02	48	±10	52
22NIMOCR37							
Unirr.	0	0	0	0.72	-65	±3	-65
SSC1	1.71	5.54	2.71	0.20	-25	±47	-4
SSC2	3.60	11.55	5.66	2.46	+29	±17	29
0-T	2.74	8.90	4.46	0.56	-13	±36	7
1/4 T	1.45	6.01	2.60	1.02	-7	±10	13
1/2 T	0.69	3.87	1.47	0.48	-19	±17	-9
A508-3							
Unirr.	0	0	0	0.62	-56	±4	-54
SSC1	1.94	6.34	3.08	2.54	-42	±7	-34
SSC2	3.97	12.85	6.26	1.35	-15	±4	-15
0-T	2.94	9.68	4.82	0.04	-30	±3	-29
1/4 T	1.61	6.90	2.95	1.04	-35	±7	-34
1/2 T	0.78	4.53	1.70	2.77	-31	±12	-40
Submerged Arc Weld (EC)							
Unirr.	0	0	0	0.20	-21	±8	-18
SSC1	1.87	6.09	2.96	0.21	87	±21	90
SSC2	3.90	12.59	6.14	0.27	118	±38	101
0-T	2.90	3.51	4.74	0.36	104	±33	96
1/4 T	1.61	6.86	2.93	0.29	75	±23	76
1/2 T	0.77	4.48	1.68	0.14	82	±25	71
Submerged Arc Weld (R)							
Unirr.	0	0	0	0.88	-82	±4	-79
SSC1	2.46	7.06	3.66	0.05	141	±11	143
SSC2	5.15	14.64	7.61	0.06	218	±14	210
0-T	3.83	11.04	5.87	0.09	208	±15	207
1/4 T	2.12	7.95	3.62	0.34	171	±14	177
1/2 T	1.02	5.20	2.08	0.29	153	±12	160

*Average values for the specimen selected. $10^{19}/cm^2$ for ϕt and % for dpa.

TABLE ORNL-62

41-J TRANSITION TEMPERATURE INCREASE FOR INDIVIDUAL FITS AND FOR VARIOUS FLUENCE-DEPENDENT FUNCTIONS

	Individual Fits						
	CV81	MEA	$[\phi t>1]\cdot^{5}$	$[\phi t>1]\cdot^{3}$	$[\phi t>1]\cdot^{8}$	$[\phi t>.1]\cdot^{5}$	$[dpa]\cdot^{5}$
A302-B							
SSC1	89	82	64	67	55	61	62
SSC2	89	94	92	84	97	87	89
0-T	77	81	78	76	75	74	77
1/4 T	50	67	58	63	47	63	60
1/2 T	52	50	40	51	26	51	46
A533-B							
SSC1	69	61	61	65	53	59	60
SSC2	81	81	88	81	95	85	86
0-T	67	75	76	73	75	73	75
1/4 T	65	69	56	61	45	61	59
1/2 T	49	53	38	49	25	49	44
22NIMOCR37							
SSC1	40	61	55	57	43	56	55
SSC2	94	94	79	72	78	80	80
0-T	52	72	69	66	63	71	71
1/4 T	58	78	50	54	38	58	54
1/2 T	46	56	34	43	21	47	41
A508-3							
SSC1	14	20	22	23	21	22	22
SSC2	41	39	33	28	37	32	32
0-T	26	25	28	26	29	27	28
1/4 T	21	20	21	22	18	23	22
1/2 T	25	14	14	18	10	19	17
Submerged Arc Weld (EC)							
SSC1	108	108	102	111	89	102	102
SSC2	139	129	147	138	160	147	146
0-T	125	114	127	126	126	128	129
1/4 T	96	94	95	106	79	108	101
1/2 T	103	89	66	85	44	87	77
Submerged Arc Weld (R)							
SSC1	223	222	229	250	---*	227	228
SSC2	300	289	330	311	---	327	329
0-T	290	286	285	285	---	284	288
1/4 T	253	256	212	238	---	240	226
1/2 T	235	239	147	191	---	194	171

*Analysis failed.

TABLE ORNL-63

COEFFICIENTS DETERMINED BY FITTING THE DAMAGE CORRELATION
$\Delta NDT = A(\phi t)^a$ USING THE RESULTS FROM SSC AND SPVC

SEPARATELY AND COMBINED

			SSC		SPVC		Combined	
	Ni*	Cu*	Value	Std.	Value	Std.	Value	Std.
			$[\phi t > 1.0]^{0.5}$					
A302-B	0.18	0.20	40	±8	39	±7	40	±5
A533-B	0.56	0.12	40	±5	40	±4	40	±3
22NIMOCR37	0.96	0.12	49	±4	36	±11	42	±6
A508-3	0.75	0.05	15	±3	19	±6	16	±2
Subm. Arc Weld (EC)	0.64	0.24	78	±10	81	±12	75	±9
Subm. Arc Weld (R)	1.58	0.23	134	±5	157	±9	146	±6
			$[\phi t > 1.0]^{0.3}$					
A302-B	0.18	0.20	55	±11	47	±9	51	±7
A533-B	0.56	0.12	52	±6	49	±4	50	±3
22NIMOCR37	0.96	0.12	50	±20	46	±10	49	±8
A508-3	0.75	0.005	18	±4	22	±6	19	±3
Subm. Arc Weld (EC)	0.64	0.24	96	±13	94	±13	92	±10
Subm. Arc Weld (R)	1.58	0.23	179	±6	202	±7	191	±6

*Wt-%.

B. ASTM STANDARDS ACTIVITIES

F. W. Stallmann

Objective

The objective of this task is to prepare ASTM Standards and Reference NUREG Documents which will support recommendations for proposed modifications, data bases, and methodologies related to Codes and Regulatory Guides.

Accomplishment and Status

Due to the reorganization of the Task Groups of the E10.05 Subcommittee on Nuclear Metrology, the three ASTM Standards of the PV-SDIP which originated at ORNL are now under the jurisdiction of the E10.05.01 Task Group for Uncertainty Analysis and Computational Procedures. The scope of the Task Group is presented in the Appendix. This scope was discussed and adopted at the January 1984 meeting in San Diego. The next Task Group meeting will be held in connection with the 5th ASTM-EURATOM Symposium on Reactor Dosimetry, September 1984 in Geesthacht, Germany, to coordinate efforts with the European counterparts.

The status of the three standards under the jurisdiction of the E10.05.01 Task Group is as follows:

- E706(IID), E483-82, Application of Neutron Transport Methods for Reactor Vessel Surveillance, needs to be reviewed for updating and additional procedures for estimation of uncertainties in transport calculation.

- E706(IIA), E944-83, Application of Neutron Spectrum Adjustment for Methods in Reactor Surveillance, has appeared in the 1983 Book of Standards, Section 12.2. No major revisions are planned in the near future.

- E706(II), Analysis and Interpretation of Physics-Dosimetry Results for Test Reactors, is being ballotted at Society level and is expected to appear in the 1984 Book of Standards.

Further details can be found in the minutes of the ASTM E10.05 Meeting held in January 1984 in San Diego.

APPENDIX

SCOPE OF THE E10.05.01 TASK GROUP FOR UNCERTAINTY ANALYSIS AND COMPUTATIONAL PROCEDURES

1. To write and update ASTM Standards under the jurisdiction of the ASTM E10.05 Subcommittee which are primarily concerned with mathematics/statistics procedures and/or the determination of uncertainties related to nuclear radiation metrology.

2. To identify and to provide consultation in matters of uncertainties and mathematics/statistics procedures contained in other Standards from the area of nuclear radiation metrology which are not directly assigned to the Task Group.

3. To identify those areas in nuclear radiation metrology where present methods for uncertainty analysis are controversial or deficient and to encourage research in these areas in order to improve or replace present methods and to make recommendation for new or updated ASTM Standards concerning such methods.

4. To consult and coordinate efforts with other standard committees, regulatory agencies, and research institutions, not restricted to the ASTM or the U.S., for the purpose of establishing uniform and generally acceptable methods in uncertainty analysis and related mathematics/statistics procedures in the area of nuclear radiation metrology.

ROCKWELL INTERNATIONAL

(RI)

ROCKWELL INTERNATIONAL

APPLICATION OF HELIUM ACCUMULATION FLUENCE MONITORS TO LIGHT WATER REACTOR SURVEILLANCE

B. M. Oliver
Harry Farrar IV

Objectives

1. Apply helium accumulation fluence monitors (HAFMs) to the surveillance dosimetry of light water reactor systems.

2. Fabricate and test selected sets of HAFMs in LWR and benchmark neutron environments.

3. Examine the feasibility of using helium buildup in pressure vessel (PV) materials as a surveillance monitoring procedure.

4. Formulate ASTM recommended practices and procedures for HAFMs in light water reactor systems.

Summary

Very low boron concentration levels in candidate HAFM sensor materials are crucial to their application for LWR neutron dosimetry. This is because helium generation from thermal neutron reactions with the boron can mask that generated by the sensor material itself. Depending on the sensor, boron levels of from ~1 ppb to ~5 ppm by weight can be tolerated. For this reason, boron impurity concentrations have been measured in approximately 40 different materials proposed as potential HAFM dosimetry sensors. These measurements were accomplished by thermal neutron irradiation of the materials, followed by high sensitivity gas mass spectrometric analysis of the helium generated by the $^{10}B(n,\alpha)^{7}Li$ reaction.

The results of these measurements give boron levels in the various materials ranging from <0.2 ppb up to ~25 ppm by weight. The results indicate that, although boron levels in some materials lots are unacceptably high, other material lots are on hand with sufficiently low boron levels such that helium generation from the boron will be low or negligible for typical LWR pressure vessel surveillance environments. It follows, however, that careful characterization of potential HAFM sensor materials for boron content is required prior to their use in LWR dosimetry.

Accomplishments and Status

Boron concentration levels are of critical importance in the application of helium accumulation for neutron dosimetry in LWR environments. This is because the high levels of helium generated in the boron by low energy neutrons, may mask the helium generated by high energy neutrons in the sensor element or isotope itself. To address this subject, approximately 100 samples

of various materials proposed as HAFM sensors for LWR-PV surveillance dosimetry were irradiated in the High Flux Beam Reactor (HFBR) at Brookhaven National Laboratory. Included in the irradiation were 47 samples individually encapsulated in miniature Au-Pt alloy capsules (70% Au-30% Pt) and 50 unencapsulated "bare" samples. The sample package was irradiated in a water-cooled aluminum rabbit in the V-11 assembly of HFBR for 24 hours. Details of the irradiation are given in Table 1.

TABLE 1

HFBR IRRADIATION DETAILS

Parameter	Data
Irradiation date	June 29, 1983
Irradiation location	V-11 rabbit assembly
Irradiation time	24 h
Reactor power	60 MW
Thermal fluence*	1.06×10^{19} n/cm^2
Fast fluence ($\gtrsim$1 MeV)†	~8×10^{15} n/cm^2

*Average thermal neutron fluence at the center of the rabbit determined from helium analyses of Al-0.7% Li samples, and radiometric analyses of Fe and Al-0.116% Co samples (see text).

†Approximate fast neutron fluence at the center of the rabbit determined from radiometric analyses of Fe samples (see text).

To accommodate the samples, an aluminum holder was fabricated to locate the samples in the center of the rabbit assembly. Figure 1 shows the aluminum rabbit, holder, and loading arrangement of samples inside the rabbit. The Au-Pt capsules and solid Au-Pt material were arranged in a ring located next to the inside wall of the rabbit. A few additional samples of Au-Pt material were also loaded in individual holes near this ring. The remaining bare samples were loaded in the central region. The reason for this arrangement was to space the Au-Pt material as far apart as possible, and in a symmetric pattern, to reduce neutron perturbation effects from the gold. Although gamma heating was expected to be minimal, the rabbit was filled with ~1 atm of neon gas to provide thermal coupling for the samples. Additional details on the samples irradiated in HFBR are listed in Columns 1-4 of Tables 2 and 3.

Following irradiation, the samples were returned to Rockwell for unloading and subsequent helium analysis. The results of the helium analyses, listed as helium concentrations in atomic parts per billion (10^{-9} atom fraction), are given in Column 5 of Tables 2 and 3. Generally, two samples for each material type were analyzed. The number following the helium concentration is the standard deviation for the two (or more) analyses. All of the

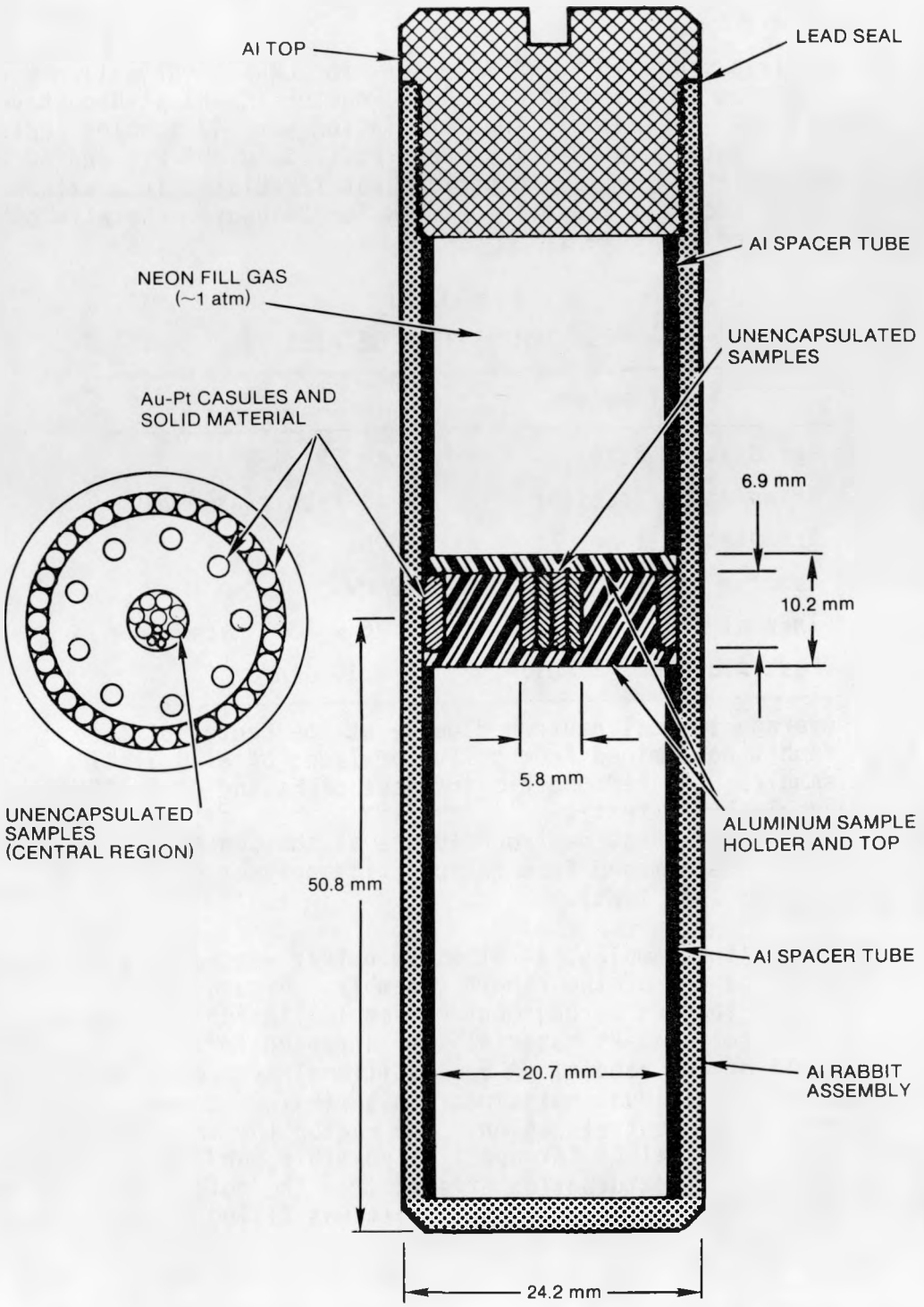

Figure 1. Aluminum Rabbit Assembly, and Sample Loading Arrangement for the HFBR Irradiation.

TABLE 2

BORON CONCENTRATIONS IN ENCAPSULATED HAFM MATERIALS

Sensor Element	Material	Lot No.	No. of Samples	Measured ^4He Concentration (appb)*	Calculated Boron Concentration (wt. ppm)†	Estimated Boron Helium Generation Contribution (%)§
Be	Be	RI-6	2	30 ± 4	5.6	1.5
		RI-7	3	48 ± 11	8.9	2.4
N	TiN	RI-1	2	56 ± 7	1.5	9.6
		RI-2	2	516 ± 19	14.	50
N	ZrN	RI-1	2	49 ± 4	0.77	15
		RI-2	2	127 ± 42	2.0	19
		RI-3	2	635 ± 2	10.	51
O	GeO_2	RI-2	2	46 ± 4	0.74	20
O	Nb_2O_5	RI-1	2	98 ± 34	0.62	17
F	PbF_2	RI-1	2	2 ± 4	0.015	0.7
F	NaF	RI-1	2	2 ± 2	0.08	1.2
S	PbS	RI-1	2	10 ± 5	0.07	1.5
		RI-2	2	3600 ± 400	25.	84
		RI-3	2	550 ± 50	3.9	45
Cl	PbCl	RI-1	2	<6	<0.04	<3.4
Cl	NaCl	RI-1	2	<3	<0.08	<2.9
K	KI	RI-1	2	6 ± 6	0.06	5.9
		RI-2	2	<6	<0.06	<5.9
Ca	CaF_2	RI-1	2	120 ± 30	2.6	15
		RI-2	2	<3	0.06	<0.4
-	Au-Pt	RI-2	6	0.06 ± 0.03	0.0006	<1.5**

*Mean measured ^4He concentration in atomic parts per billion (10^{-9} atom fraction) and standard deviation.

†Boron concentration calculated from Column 5 data and measured thermal neutron fluence (see text).

§Estimated boron contribution to the total helium generation in a typical LWR surveillance environment (assumes no Cd or Gd shields - see text).

**HAFM encapsulating material. The effect of the boron will depend on the sensor material being encapsulated. For KI, which has a low (n,α) cross section, the helium contribution from the capsule itself will be <1.5% of that generated by the KI.

TABLE 3

BORON CONCENTRATIONS IN UNENCAPSULATED HAFM MATERIALS

Sensor Element	Material	Lot No.	No. of Samples	Measured ^4He Concentration (appb)*	Calculated Boron Concentration (wt. ppm)†	Estimated Boron Helium Generation Contribution (%)§
Al	Al	HEDL-19045	3	1.48 ± 0.00	0.075	19
		RI-14A	2	4.23 ± 0.17	0.22	41
Al	Al-Co	SRM-952	2	24.1 ± 0.2	1.23	80
Fe	Fe	HEDL-07448	3	0.59 ± 0.01	0.015	19
		RI-11A	2	0.19 ± 0.01	0.0046	6.6
Ni	Ni	HEDL-SE(II)	3	2.7 ± 0.4	0.015**	1.5
		RI-8A	2	3.38 ± 0.07	0.031**	3.1
		RI-4	2	2.20 ± 0.14	0.004**	0.4
Cu	Cu	HEDL-3054	3	<0.01	<0.0002	<0.2
		HEDL-20414	1	<0.01	<0.0002	<0.2
		RI-8A	2	<0.01	<0.0002	<0.2
Fe	Steel	EPRI-2bE	1	27.1 ± 1.7	0.67	91
		EPRI-EP24	1	28.8 ± 0.3	0.71	92
		EPRI-1b4	1	22.6 ± 0.5	0.56	90
		EPRI-NP	1	18.0 ± 0.7	0.45	87
		EPRI-1bA	1	21.9 ± 0.8	0.54	90
		EPRI-4bA	1	22.7 ± 0.2	0.56	90
		EPRI-7bB	1	53.6 ± 0.3	1.33	95

*Mean measured ^4He concentration in atomic parts per billion (10^{-9} atom fraction) and standard deviation.

†Boron concentration calculated from Column 5 data and measured thermal neutron fluence (see text).

§Estimated boron contribution to the total helium generation in a typical LWR surveillance environment (assumes no Cd or Gd shields - see text).

**Boron concentration determined after subtraction of a calculated helium generation value for the nickel two-stage reaction of 2.05 appb (see text).

samples were etched ~0.01 mm prior to analysis to remove surface material which could have been affected by α-recoil from adjacent materials. Negligible residual helium in the various materials was verified by separate helium analyses of unirradiated samples.

For the encapsulated materials (Table 2), a correction was made to account for helium generation in the Au-Pt capsule. The measurement of this background was accomplished by analyzing three empty Au-Pt HAFM capsules irradiated adjacent to the other materials. Unexpectedly, the results of this measurement yielded a larger helium concentration in the empty Au-Pt capsules (~1 appb) than that measured in solid Au-Pt material from the same Rockwell lot (~0.06 appb). Further investigation resulted in the conclusion that small amounts of helium from a low-level helium impurity (~100 ppm) in the neon cover gas used for thermal coupling had diffused into the empty capsules through the welded tops. The effect of this apparent diffusion of helium into the Au-Pt HAFM capsules is seen in the higher variability (and therefore uncertainty) in the helium data given in Table 2, as compared to Table 3 for the unencapsulated samples which were not influenced by this diffusion.

The tops of all the HAFM capsules were sealed by fusing under vacuum with an electron beam--a procedure which has been used in the past routinely, and successfully, for other pure HAFM encapsulating materials, including V, Nb, Pt, Au, and stainless steel. The reason for using an alloy of Au and Pt as an encapsulating material, rather than pure Au or Pt themselves, is that the lower thermal conductivity of the alloy results in reduced heating of the remaining capsule material and contents during electron beam closure. Because of the apparent porosity of this alloy after vacuum melting, however, other methods for capsule sealing, such as vacuum brazing using pure Au or Ag, are being investigated.

Boron content in each material, calculated from the measured helium concentration data in Column 5, is listed in Column 6 of Tables 2 and 3. For these calculations, a derived thermal neutron fluence at the center of the rabbit of 1.06×10^{19} n/cm^2 was used and a correction was applied for boron burnup (~2%). The thermal fluence was obtained from helium analyses of Al-0.7% ^{6}Li wire and from radiometric analyses (conducted at HEDL) of Fe and Al-0.116% Co wire, irradiated in the central region of the sample assembly (see Figure 1). For the Al-Li samples, corrections were made for ^{6}Li burnup (~0.5%) and neutron self-shielding (~6%). The standard deviation between the thermal fluence values determined from the helium and radiometric measurements was ~7%. This uncertainty is not unexpected in view of the various experimental uncertainties involved (e.g., isotopic abundances, Li content) and flux gradients.

Additional helium analyses were also conducted on three separate Au-Pt encapsulated wire samples of Al-Li alloy, irradiated in the outer ring section of the sample holder, to determine neutron absorption from the Au-Pt capsule material. These measurements indicated an absorption factor for the Au-Pt capsules of 0.83 (i.e., ~17% reduction in the thermal neutron fluence inside the capsules). This absorption factor was used in the calculation of the boron concentrations for the encapsulated HAFM materials in Table 2.

In converting the measured helium concentrations to boron concentrations, helium generation from ^{6}Li impurities was assumed to be negligible. This assumption is valid for most thermally processed materials because of the relatively high volatility of lithium. In any event, for LWR applications, it is not important whether the helium generation occurs from boron or lithium, since only the helium generation itself is of interest. Helium generation from fast neutron threshold reactions was negligible except for beryllium (~2 appb) and nitrogen (~0.2 appb) where a correction has been applied. Helium generation from the nickel two-stage reaction, $^{58}Ni(n,\gamma)^{59}Ni(n,\alpha)^{56}Fe$, which is significant for thermal fluences $>10^{19}$ n/cm^2, was calculated to be 2.05 appb based on cross-section data from Wiffen et al. (Wi84).

The boron concentration results in Tables 2 and 3 indicate boron impurity levels ranging from <0.2 appb to ~25 appm. Uncertainty in the measured boron concentrations can be estimated by combining (in quadrature) the uncertainty in the measured helium concentrations (Column 5) and the uncertainty in the derived thermal neutron fluence (~7%).

The impact of these boron results on the effectiveness of the various HAFM materials for LWR surveillance dosimetry can be estimated by calculating the helium generation from the boron relative to that expected in the material itself for a typical LWR surveillance neutron environment. The results of this calculation are given in the last column of Tables 2 and 3. Here, a thermal-to-fast neutron flux ratio of 1.5, and an ambient temperature of 280°C, have been assumed. Fission spectrum-averaged cross sections (As83) have been used to calculate the fast neutron contribution to the total helium generation for each sensor material.

For the encapsulated HAFM materials in Table 2, the boron contribution ranges from ~0.4% for the RI-2 lot of CaF_2 to ~84% for the RI-2 lot of PbS. The boron contribution data in Table 3 for the unencapsulated samples, show similar results. Here, the data range from $\lesssim$0.2% for the three Cu lots, to ~95% for the EPRI-7bB pressure-vessel steel material. Preliminary boron concentration data for the EPRI steel materials were reported and discussed earlier (Ol84). The important result from Table 3 is that the boron contribution in both lots of Al and in the HEDL lots of Fe, and Al-Co alloy, are relatively high. These materials, which can perform a dual dosimetry function--serving as both radiometric and HAFM sensors, are particularly sensitive to even very low boron levels because of their relatively low fast-neutron helium generation cross sections (~0.3 to 0.7 mb).

It should be noted, however, that the boron contribution levels given in both Tables 2 and 3 are estimates only, and that the actual boron contributions to the total helium generation in these materials will depend on the irradiation environment. Further, the results do not take into account any reduction in the low energy neutron flux from encapsulation in either Cd or Gd. Approximate calculations performed at HEDL, using a cavity neutron spectrum from the power reactor McGuire (~2.8:1 thermal-to-fast neutron ratio) indicate an order of magnitude reduction in the boron helium production cross section when thermally shielded. Such a reduction in the boron cross section would reduce the helium generation contributions in Tables 2 and 3 by a similar amount.

In conclusion, the results indicate that with thermal neutron shielding, material lots of each of the sensor elements of interest (in Tables 2 and 3) are available which have boron (or lithium) contents sufficient low such that helium generation from the boron will be either negligible or small enough to permit accurate correction. For the Al-Co alloy (SRM-952), however, the data indicate that even with thermal shielding, additional pure aluminum wires will be required to be included in dosimetry sets for helium accumulation measurements.

Expected Accomplishments in the Next Reporting Period

Preliminary results from selected HAFMs irradiated in the fourth SDMF test at ORNL will be reported.

A P P E N D I X

BIBLIOGRAPHY

BIBLIOGRAPHY

(Ca81) K. Carlson, G. Guthrie and G. R. Odette, "Embrittlement of Compression Specimens in the PSF," LWR-PV-SDIP, Quarterly Progress Report, NUREG/CR-2345, Vol. 1, HEDL-TME 81-33, Hanford Engineering Development Laboratory, Richland, WA, October 1981.

(Fa81) A. Fabry, R. Gold, F. H. Ruddy, J. H. Roberts, E. D. McGarry and F. W. Stallman, "Comparison Between Solid State Track Recorder and Fission Chamber Measurements," LWR-PV-SDIP: PCA Experiments and Blind Test, W. N. McElroy, Ed., NUREG/CR-1861, HEDL-TME 80-87, NRC, Washington, DC, pp. 4.3-1 - 4.3-8, July 1981.

(Fa81a) A. Fabry, F. Cops and L. S. Kellogg, "Radiometric Measurements," LWR-PV-SDIP: PCA Experiments and Blind Test, W. N. McElroy, Ed., NUREG/CR-1861, HEDL-TME 80-87, NRC, Washington, DC, p. 2.4-1 - 2.4-31, July 1981.

(Fa81b) A. Fabry, N. Maene, R. Menil, G. Mensart and J. Tissot, "Validation of Gamma-Ray Field Calculations by TLD Measurements," LWR-PV-SDIP: PCA Experiments and Blind Test, NUREG/CR-1861, HEDL-TME 80-87, NRC, Washington, DC, Sec. 5.4, July 1981.

(Go68a) R. Gold, "Compton Continuum Measurements for Continuous Gamma-Ray Spectroscopy," Bull. Am. Phys. Soc. 13, p. 1405, 1968.

(Go70) R. Gold and I. K. Olson, Analysis of Compton Continuum Measurements, ANL-7611, Argonne National Laboratory, Argonne, IL, 1970.

(Go70a) R. Gold, "Compton Recoil Gamma-Ray Spectroscopy," Nucl. Instrum. Methods 84, p. 173, 1970.

(Go70b) R. Gold, "Compton Recoil Measurements of Continuous Gamma-Ray Spectra," Trans. Am. Nucl. Soc. 13, p. 421, 1970.

(Go70d) R. Gold and A. M. Strash, "Gamma-Ray Dosimetry for the Natural Environment," Trans. Am. Nucl. Soc. 13, p. 502, 1970.

(Go71a) R. Gold, "Gamma-Continuum at the Air-Land Interface," Health Phys. 21, p. 79, 1971.

(Go71c) R. Gold and A. M. Strash, "Preoperational Measurement of Environmental Gamma Rays at the Monticello Site with a Continuum Spectrometer," Trans. Am. Nucl. Soc. 14, p. 31, 1971.

(Go72a) R. Gold, F. J. Congel, J. H. Roberts and A. M. Strash, "Gamma Continuum at a Fossile-Fuel Site," Trans. Am. Nucl. Soc. 15, p. 639, 1972.

(Go73) R. Gold, A. M. Strash, F. J. Congel and J. H. Roberts, "Continuous Gamma-Ray Spectroscopy in the Natural Environment," Trans. IEEE NS-20, (1), p. 48, February 1973.

(Go74) R. Gold, B. G. Oltman, K. F. Eckerman and A. M. Strash, "Environmental Radiation at the EBR-II Site," Trans. IEEE NS-21, (1), pp. 596-601, February 1974.

(Go78a) R. Gold, "Overview of Gamma-Ray Energy Deposition and Spectra in Fast Reactor Environments," Proc. of the 2nd ASTM-EURATOM Symposium on Reactor Dosimetry, Palo Alto, CA, October 3-7, 1977, NUREG/CP-0004, NRC, Washington, DC, Vol. 1, pp. 101-140, 1978.

(Go78b) R. Gold, "Estimates of High-Energy Gamma and Neutron Flux from Continuous Gamma-Ray Spectrometry," LWR-PV-SDIP Quarterly Progress Report - July-September 1983, NUREG/CR-0551, HEDL-TME 78-8, NRC, Washington, DC, December 1978.

(Go80b) R. Gold, R. B. Kaiser, F. S. Moore Jr, W. L. Bunch, W. N. McElroy and E. M. Sheen, "Continuous Gamma-Ray Spectrometry in the Fast Flux Test Facility," HEDL-SA-2166, Proc. of the ANS Topical Meeting on 1980 Advances in Reactor Physics and Shielding, Sun Valley, ID, September 14-17, 1980, ISDN 0-89448-107-X, p. 803, 1980.

(Go80d) R. Gold and B. J. Kaiser, "Reactor Gamma-Ray Spectrometry: Status," Proc. of the 3rd ASTM-EURATOM Symposium on Reactor Dosimetry, Ispra, Italy, October 1-5, 1979, EUR 6813, Commission of the European Communities, Vol. II, pp. 1160-1171, 1980.

(Go81c) R. Gold and B. J. Kaiser, Gamma-Ray Spectrometry, LWR-PV-SDIP: PCA Experiments and Blind Test, NUREG/CR-1861, HEDL-TME 80-87, NRC, Washington, DC, Sec. 5.3, July 1981.

(Go82b) R. Gold, B. J. Kaiser and J. P. McNeece, "Gamma-Ray Spectrometry in Light Water Reactor Environments," Proc. of the 4th ASTM-EURATOM Symposium on Reactor Dosimetry, Gaithersburg, MD, March 22-26, 1982, NUREG/CP-0029, NRC, Washington, DC, Vol. 1, pp. 267-279, July 1982.

(Go83b) R. Gold, J. H. Roberts, J. P. McNeece, B. J. Kaiser, F. H. Ruddy, C. C. Preston, J. A. Ulseth and W. N. McElroy, "Fuel Debris Assessment for Three Mile Island Unit 2 (TMI-2) Reactor Recovery by Gamma-Ray and Neutron Dosimetry," HEDL-SA-2867, 6th International Conf. on Nondestructive Evaluation in the Nuclear Industry, Zurich, Switzerland, November 27-December 2, 1983.

(Gr84) S. P. Grant and S. L. Earp, "Methods for Extending Life of a PWR Reactor Vessel After Long-Term Exposure to Fast Neutron Radiation," 12th Symposium on Effects of Radiation on Materials, Williamsburg, VA, June 1984.

(Gu82c) G. L. Guthrie, "Development of Trend Curve Formulas Using Surveillance Data-II," LWR-PV-SDIP Quarterly Progress Report, April - June 1982, NUREG/CR-2805, Vol. 2, HEDL-TME 82-19, Hanford Engineering Development Laboratory, Richland, WA, pp. HEDL-3 - HEDL-13, December 1982.

(Gu83) G. L. Guthrie, "Charpy Trend Curve Formulas Derived from an Expanded Surveillance Data Base," LWR-PV-SDIP Quarterly Progress Report, October 1982 - December 1982, NUREG/CR-2805, Vol. 4, HEDL-TME 82-21, Hanford Engineering Development Laboratory, Richland, WA, pp. HEDL-3 - HEDL-13, July 1983.

(Ji78) S. H. Jiang and H. Werle, "Fission Neutron-Induced Gamma Fields in Iron," Nucl. Sci. Eng. 66, p. 354, 1978.

(Ka81) B. J. Kaiser, R. Gold and J. P. McNeece, "Si(Li) Gamma-Ray Dosimetry," LWR-PV-SDIP: PCA Experiments and Blind Test, NUREG/CR-1861, HEDL-TME 80-87, NRC, Washington, DC, pp. 5.3-1 - 5.3-8, July 1981.

(Ko75) H. E. Korn, Measurement of the Energy Distribution of the Gamma Field in a Fast Reactor, KFK 2211, Karlsruhe Nuclear Research Center, Karlsruhe, Federal Republic of Germany, 1975.

(Le83) T. A. Lewis, "Use of Beryllium Oxide Thermoluminescence Dosimeters for Measuring Gamma Exposure Rates in Graphite-Moderated Reactors," TPRD/B/0349/N83, Berkeley, UK, October 1983.

(Ma82) N. Maene, R. Menil, G. Minsart and L. Ghoos, "Gamma Dosimetry and Calculations," Proc. of the 4th ASTM-EURATOM Symposium on Reactor Dosimetry, Gaithersburg, MD, March 22-26, 1982, NUREG/CP-0029, NRC, Washington, DC, Vol. 1, pp. 355-363, July 1982.

(Ma84) R. E. Maerker et al., "Neutron and Gamma Transport Results for 12/13 Configurations," PCA Dosimetry in Support of the PSF Physics-Dosimetry-Metallurgy Experiments, NUREG/CR-3318, HEDL-TME 84-1, NRC, Washington, DC, January 1984.

(Mc80a) W. M. McElroy et al., "NRC Metallurgy and Materials Research Branch LWR-PV-SDIP Review Graphics," HEDL-SA-2225 and Proc. of the 8th WRSR Research Information Meeting, Gaithersburg, MD, October 27-31, 1980.

(Mc81) W. N. McElroy, Ed., LWR-PV-SDIP: PCA Experiments and Blind Test, NUREG/CR-1861, HEDL-TME 80-87, NRC, Washington, DC, July 1981.

(Mc81a) W. N. McElroy et al., LWR-PV-SDIP: 1980 Annual Report, NUREG/CR-1747, HEDL-TME 80-73, NRC, Washington, DC, April 1981.

(Mc81b) E. D. McGarry and A. Fabry, "Fission Chamber Measurements," LWR-PV-SDIP: PCA Experiments and Blind Test, W. N. McElroy, Ed., NUREG/CR-1861, HEDL-TME 80-87, NRC, Washington, DC, pp. 2.3-1 - 2.3-38, July 1981.

(Mc82a) W. N. McElroy et al., LWR-PV-SDIP: 1982 Annual Report, NUREG/CR-2805, Vol. 3, HEDL-TME 82-20, NRC, Washington, DC, December 1982.

(Mc83c) J. P. McNeece, B. J. Kaiser, R. Gold and W. W. Jenkins, Fuel Content of the Three Mile Island Unit 2 Makeup Demineralizers, HEDL-7285, Hanford Engineering Development Laboratory, Richland, WA, February 1983.

(Mc84) W. N. McElroy et al., LWR-PV-SDIP: 1983 Annual Report, NUREG/CR-3391, Vol. 3, HEDL-TME 83-23, NRC, Washington, DC, June 1984.

(Od83a) G. R. Odette, "On the Dominant Mechanism of Irradiation Embrittlement of Reactor Pressure Vessel Streels," Scripta Met. 17, pp. 1183-1188, 1983.

(Ra82a) P. N. Randall, "Status of Regulatory Demands in the U.S. on the Application of Pressure Vessel Dosimetry," Proc. of the 4th ASTM-EURATOM Symposium on Reactor Dosimetry, Gaithersburg, MD, March 22-26, 1982, NUREG/CP-0029, NRC, Washington, DC, Vol. 2, pp. 1011-1022, July 1982.

(Ro83a) J. H. Roberts, F. H. Ruddy and R. Gold, "Optical Efficiency for Fission Fragment Track Counting in Muscovite Solid State Track Recorders," HEDL-SA-2864, Proc. of the 12th International Conference on Solid State Nuclear Track Detectors, Acapulco, Mexico, September 1983.

(Ru81) F. H. Ruddy, R. Gold and J. H. Roberts, "Solid State Track Recorder Measurements," LWR-PV-SDIP: PCA Experiments and Blind Test, W. N. McElroy, Ed., NUREG/CR-1861, HEDL-TME 80-87, NRC, Washington, DC, pp. 2.5-1 - 2.5-13, July 1981.

(Si68) M. G. Silk, Iterative Unfolding of Compton Spectra, AERE-R-5653, Atomic Energy Research Establishment, Harwell, UK, 1968.

(Si69) M. G. Silk, "Energy Spectrum of the Gamma Radiation in the DAPHINE Core," J. Nucl. Energy 23, p. 308, 1969.

(St71) A. M. Strash and R. Gold, "Absolute Gamma-Ray Dosimetry by Recoil Electron Spectroscopy," Nature 234, p. 260, 1971.

(Zi79) W. L. Zijp and J. H. Baard, Nuclear Data Guide for Reactor Neutron Metrology, Parts I and II, EUR 7167, Energieonderzoek Centrum Nederland, Petten, Netherlands, August 1979.

DISTRIBUTION

R5

DOE-HQ/Office of Converter
Reactor Deployment
Nuclear Regulation & Safety Division
NE-12
Washington, DC 20545

JD Griffith, Deputy Director

DOE-HQ/Office of Breeder
Technology Projects (8)
NE-53
Washington, DC 20545

H. Alter, Asst Director, Safety
DF Bunch, Director, Office of Breeder Technology Projects
PB Hemmig, Asst Director, Reactor Physics Technology
JW Lewellen, Manager, Core Analysis Technology
DK Magnus, Director, Fuels & Core Materials
RJ Neuhold, Director, Safety & Physics
CM Purdy, Asst Director, Materials & Structures Tech
A. Van Echo, Manager, Metallurgy, Absorbers & Standards

DOE-RL/AME
Breeder Technology Division
Technology Development Branch
P.O. Box 550, FED/210
Richland, WA 99352

KR Absher, Chief

Arizona State University (2)
College of Eng & Appl Sciences
Tempe, AZ 85287

JW McKlveen
B. Stewart

Argonne National Laboratory (2)
9700 South Cass Avenue
Argonne, IL 60439

RJ Armani
RR Heinrich, Bldg 316

Babcock & Wilcox Co
Lynchburg Research Center (4)
P.O. Box 1260
Lynchburg, VA 24505

LB Gross AA Lowe Jr
RH Lewis CL Whitmarsh

Battelle
Pacific Northwest Laboratory
P.O. Box 999
Richland, WA 99352

EP Simonen

Battelle Memorial Institute
505 King Avenue
Columbus, OH 43201

MP Manahan

Bechtel Power Corporation
15740 Shady Grove Road
Gaithersburg, MD 20760

WC Hopkins

Brookhaven National Laboratory (3)
National Neutron Cross-Section Center
Upton, Long Island, NY 11973

JF Carew BA Magurno
S. Pearlstein, Bldg T-197

Burns & Roe Inc
633 Industrial Avenue
Paramus, NJ 07672

J. Celnik

DISTRIBUTION (Cont'd)

Carolina Power & Light Co
P.O. Box 1551
Raleigh, SC 27602

SP Grant

Centre d'Etude de l'Energie Nucléaire
Studiecentrum voor Kernenergie (6)
Boeretang 200
B-2400 Mol, Belgium

J. Debrue
G. DeLeeuw
S. DeLeeuw
A. Fabry
G. Minsart
Ph Van Asbroeck

Combustion Engineering Inc (5)
1000 Prospect Hill Road
Windsor, CT 06095

S. Byrne
G. Cavanaugh
JJ Koziol
RG Shimko
D. Stephen

Comitato Nazional per Energia Nucléare
Centro di Studi Nucleari della Casaccia
Casella Postale 2400
Santa Maria di Galeria
I-00060 Rome, Italy

U. Farinelli

Commissariat a l'Energie Atomique
Centre d'Etudes Nucleaires de Saclay (6)
Boite Postale 2
91190 Gif-sur-Yvette, France

AA Alberman
C. Buchalet (Framatome)
JM Cerles
JP Genthon
P. Mas (Grenoble)
P. Petrequin

Commonwealth Edison
P.O. Box 767
Chicago, IL 60690

E. Steeve

EG&G Idaho Inc (3)
P.O. Box 1625
Idaho Falls, ID 83415

RC Greenwood
Y. Harker
JW Rogers

EG&G Ortec Inc
100 Midland Road
Oak Ridge, TN 37830

W. Zimmer

Electric Power Research Institute (7)
3412 Hillview Avenue
P.O. Box 10412
Palo Alto, CA 94304

TU Marston
O. Ozer
T. Passell
AD Rossin
R. Shaw
K. Stahlkopf
JJ Taylor

Energieonderzoek Centrum Nederland
Westerduinweg 3
Postfach 1
NL-1755 ZG, Petten, The Netherlands

WL Zijp

Engineering Services Associates
3320 Bailey
Buffalo, NY 14215

M. Haas

EURATOM
Joint Research Center Ispra (2)
I-21020 Ispra, Varese, Italy

R. Dierckx
H. Rief

DISTRIBUTION (Cont'd)

Fracture Control Corporation
5951 Encina Road, No. 105
Goleta, CA 93117

P. McConnell

Fracture Control Corporation
2041 Willowick Drive
Columbus, OH 43229

JS Perrin

General Electric Co
Vallecitos Nuclear Center
P.O. Box 460
Pleasanton, CA 94566

GC Martin

IKE-Stüttgart (2)
Institüt für Kernenergetik
und Energiesysteme
Pfaffenwaldring 31, Postfach 801140
D-7000, Stüttgart 80 (Vaihingen)
Federal Republic of Germany

G. Hehn
G. Prillinger

International Atomic Energy Agency (2)
Wagramerstrasse 5
Postfach 100
A-1400 Vienna, Austria

A. Sinev
JJ Schmidt

IRT Corporation (3)
P.O. Box 80817
San Diego, CA 92183

NA Lurie WE Selph
C. Preskitt

Italian Atomic Power Authority
National Electric Energy Agency (2)
Viale Regina Margherita 137
Rome, Italy

M. Galliani
F. Remondino

Japan Atomic Energy Research Institute (2)
Tokai Research Establishment
Tokai-mura, Naka-gun
Ibaraki-ken, Japan

S. Mizazono
K. Sakurai

Kernforschungsanlage Jülich GmbH (3)
Postfach 1913
D-517 Jülich 1,
Federal Republic of Germany

D. Pachur L. Weise
W. Schneider

Kraftwerk Union Aktiengesellschaft (5)
Postfach 3220
D-8520 Erlangen,
Federal Republic of Germany

A. Gerscha J. Koban
U. Groschel C. Leitz
W. Hofmann

Los Alamos National Laboratory (2)
P.O. Box 1663
Los Alamos, NM 87545

GE Hansen, Group N-2
L. Stewart

Louisiana State University
Nuclear Science Center
Baton Rouge, LA 70803

ML Williams

DISTRIBUTION (Cont'd)

Maine Yankee Atomic Power Co
Edison Drive
Augusta, MA 04336

HF Jones Jr

Materials Engineering Associates Inc
111 Mel-Mara Drive
Oxen Hill, MD 20021

JR Hawthorne

Max-Planck-Institüt
für Plasma Physik
The NET Team
D-8046 Garching bei München,
Federal Republic of Germany

DR Harries, Technology

National Bureau of Standards
Center of Radiation Research (6)
Washington, DC 20234

RS Caswell
CM Eisenhauer
DM Gilliam
JA Grundl
G. Lamaze
ED McGarry

Naval Research Laboratory
Engineering Materials Division
Thermostructural Materials Branch
Code 6390
Washington, DC 20375

LE Steele

Oak Ridge National Laboratory (8)
P.O. Box X
Oak Ridge, TN 37830

CA Baldwin, Bldg 3001
RG Berggren
FBK Kam
AL Lotts
RE Maerker
LS Miller
R. Nanstad
FW Stallmann

Radiation Research Associates (2)
3550 Hulen Street
Fort Worth, TX 76107

RM Rubin
MB Wells

Rockwell International Corp
Rocketdyne Division (2)
6633 Canoga Avenue
Canoga Park, CA 91304

H. Farrar IV
BM Oliver

Rolls-Royce & Associates Ltd (4)
P.O. Box 31
Derby DE2 8BJ, UK

M. Austin
P. Burch
AF Thomas
TJ Williams

S.A. Cockerill-Ougree
Recherches et Developments
Division de la Construction Mecanique
B-4100 Seraing, Belgium

J. Widart

Science Applications Inc (3)
P.O. Box 2325
La Jolla, CA 92037

W. Hagan
GL Simmons
VV Verbinski

Ship Research Institute
Tokai Branch Office
Tokai-mura, Naka-gun
Ibaraki-ken, Japan

K. Takeuchi

DISTRIBUTION (Cont'd)

Southwest Research Institute
8500 Calebra Road
P.O. Box 28510
San Antonio, TX 78284

EB Norris

Swiss Federal Institute
for Reactor Research
CH-5303 Würenlingen, Switzerland

F. Hegedus

United Kingdom Atomic Energy Authority
Atomic Energy Research Establishment (2)
Harwell, Oxon OX11 ORA, UK

LM Davies
AJ Fudge

United Kingdom Atomic Energy Authority
Atomic Energy Establishment (4)
Winfrith, Dorchester, Dorset, UK

J. Butler
CG Campbell
AK McCracken
J. Sanders

University of Arkansas (2)
Dept of Mechanical Engineering
Fayetteville, AR 72701

CO Cogburn
L. West

University of California
at Santa Barbara (2)
Dept of Chem & Nucl Engineering
Santa Barbara, CA 93106

G. Lucas
GR Odette

Univ of London Reactor Center
Silwood Park, Sunnyhill,
Ascot, Berkshire SL5 7PY, UK

JA Mason

University of Tokyo (2)
Dept of Nuclear Engineering
7-3-1, Hongo
Bunkyo-ku, Tokyo, 113 Japan

M. Nakazawa
J. Sekiguchi

Westinghouse
Nuclear Energy Systems (4)
P.O. Box 355
Pittsburgh, PA 15230

SL Anderson
TR Mager
RC Shank
SE Yanichko

Westinghouse
Research and Development Center
1310 Beulah Road
Pittsburgh, PA 15235

JA Spitznagel

University of Missouri at Rolla (2)
Dept of Nucl Engineering
Building C
Rolla, MO 65401

DR Edwards
N. Tsoulfanidis

DISTRIBUTION (Cont'd)

Nuclear Regulatory Commission (17)
Office of Nuclear Regulatory Research
Division of Engineering Technology
Materials Engineering Branch
NL-5650
Gaithersburg, MD 20899

Chief	L. Lois
Public Doc Rm (3)	S. Pawlicki
M. Bolotski	PN Randall
M. Dunenseld	CZ Serpan
R. Gamble	D. Sieno
W. Hazelton	A. Taboada
KG Hoge	M. Vagin
RE Johnson	

HEDL (46)
c/o Supervisor, Documentation
P.O. Box 1970, W/C-123
Richland, WA 99352

HJ Anderson	W/C-28	JP McNeece	W/A-56
RA Bennett	W/D-3	JE Nolan	W/B-65
LD Blackburn	W/A-40	RE Peterson	W/B-66
DG Doran	W/A-57	CC Preston	W/C-39
EA Evans	W/C-23	JH Roberts	W/C-39
DS Gelles	W/A-65	FH Ruddy	W/C-39
R. Gold	W/C-39	JM Ruggles	W/C-33
GL Guthrie	W/A-40	RE Schenter	W/A-58
BR Hayward	W/C-44	FA Schmittroth	W/A-58
LA James	W/A-40	WF Sheely	W/C-44
LS Kellogg	W/C-39	FR Shober	W/E-3
NE Kenny	W/C-115	RL Simons	W/A-65
RL Knecht	W/A-40	HH Yoshikawa	W/C-44
JJ Laidler	W/B-107	Program Files (10)	W/C-39
EP Lippincott (2)	W/C-39	Central Files (2)	W/C-110
WY Matsumoto	W/C-33	Documentation (3)	W/C-123
WN McElroy (2)	W/C-39		

NRC FORM 335 (2-84) NRCM 1102, 3201, 3202

U.S. NUCLEAR REGULATORY COMMISSION

BIBLIOGRAPHIC DATA SHEET

SEE INSTRUCTIONS ON THE REVERSE

1. REPORT NUMBER (Assigned by TIDC, add Vol. No., if any)
NUREG/CR-3746, Vol. 1
HEDL-TME 84-20

2. TITLE AND SUBTITLE
LWR Pressure Vessel Surveillance Dosimetry Improvement Program
Semiannual Progress Report
October 1983 - March 1984

3. LEAVE BLANK

4. DATE REPORT COMPLETED
MONTH: May YEAR: 1984

5. AUTHOR(S)
E.P. Lippincott, W.N. McElroy

6. DATE REPORT ISSUED
MONTH: November YEAR: 1984

7. PERFORMING ORGANIZATION NAME AND MAILING ADDRESS (Include Zip Code)
Hanford Engineering Development Laboratory
P.O. Box 1970,
Richland, WA 99352

8. PROJECT/TASK/WORK UNIT NUMBER

9. FIN OR GRANT NUMBER
B5988

10. SPONSORING ORGANIZATION NAME AND MAILING ADDRESS (Include Zip Code)
Division of Engineering Technology
Office of Nuclear Regulatory Research
U.S. Nuclear Regulatory Commission
Washington, DC 20555

11a. TYPE OF REPORT
Semiannual

b. PERIOD COVERED (Inclusive dates)
October 1983 - March 1984

12. SUPPLEMENTARY NOTES

13. ABSTRACT (200 words or less)

The Light Water Reactor Pressure Vessel Surveillance Dosimetry Improvement Program (LWR-PV-SDIP) has been established by NRC to improve, test, verify, and standardize the physics-dosimetry-metallurgy, damage correlation, and associated reactor analysis methods, procedures and data used to predict the integrated effect of neutron exposure to LWR pressure vessels and their support structures. A vigorous research effort attacking the same measurement and analysis problems exists worldwide, and strong cooperative links between the US NRC-supported activities at HEDL, ORNL, NBS, and MEA-ENSA and those supported by CEN/SCK (Mol, Belgium), EPRI (Palo Alto, USA), KFA (Jülich, Germany), and several UK laboratories have been extended to a number of other countries and laboratories. These cooperative links are strengthened by the active membership of the scientific staff from many participating countries and laboratories in the ASTM E10 Committee on Nuclear Technology and Applications. Several subcommittees of ASTM E10 are responsible for the preparation of LWR surveillance standards.

14. DOCUMENT ANALYSIS - a. KEYWORDS/DESCRIPTORS
light water reactor pressure vessel surveillance dosimetry improvement program (LWR-PV-SDIP)

b. IDENTIFIERS/OPEN-ENDED TERMS

15. AVAILABILITY STATEMENT
Unlimited

16. SECURITY CLASSIFICATION
(This page) Unclassified
(This report) Unclassified

17. NUMBER OF PAGES

18. PRICE